Pontifícia Universidade Católica
do Rio de Janeiro

**Roberto Brauer Di Renna**

# Channel Estimation and Multiuser Detection Techniques for Machine-Type Communications

**Tese de Doutorado**

Thesis presented to the Programa de Pós–graduação em Engenharia Elétrica of PUC-Rio in partial fulfillment of the requirements for the degree of Doutor em Engenharia Elétrica.

Advisor: Prof. Rodrigo Caiado de Lamare

Rio de Janeiro
July 2021

Pontifícia Universidade Católica
do Rio de Janeiro

**Roberto Brauer Di Renna**

# Channel Estimation and Multiuser Detection Techniques for Machine-Type Communications

Thesis presented to the Programa de Pós–graduação em Engenharia Elétrica of PUC-Rio in partial fulfillment of the requirements for the degree of Doutor em Engenharia Elétrica. Approved by the Examination Committee.

**Prof. Rodrigo Caiado de Lamare**
Advisor
Departamento de Engenharia Elétrica – PUC-Rio

**Prof. Lukas Tobias Nepomuk Landau**
Departmento de Engenharia Elétrica – PUC-Rio

**Prof. Marco Antonio Grivet Mattoso Maia**
Departmento de Engenharia Elétrica – PUC-Rio

**Dr. Silvio Fernando Bernardes Pinto**
Departmento de Engenharia Elétrica – PUC-Rio

**Prof. Armin Dekorsy**
Universität Bremen – Uni Bremen

**Prof. Danilo Silva**
Universidade Federal de Santa Catarina – UFSC

**Prof. Marcelo Gomes da Silva Bruno**
Instituto Tecnológico de Aeronáutica – ITA

Rio de Janeiro, July the 2nd, 2021

**Roberto Brauer Di Renna**

The author received the diploma degree and the M.Sc. degrees in telecommunications engineering from the Fluminense Federal University, Niterói, Rio de Janeiro, Brazil, in 2015 and 2017, respectively. He was a visiting researcher with the Department of Communications Engineering, Universität Bremen, Germany between 2019 and 2020.

Bibliographic data

Di Renna, Roberto Brauer

Channel Estimation and Multiuser Detection Techniques for Machine-Type Communications / Roberto Brauer Di Renna; advisor: Rodrigo Caiado de Lamare. – 2021.
204 f: il. color. ; 30 cm

Tese (doutorado) - Pontifícia Universidade Católica do Rio de Janeiro, Departamento de Engenharia Elétrica, 2021.
Inclui bibliografia

1. Engenharia Elétrica – Teses. 2. Engenharia de Telecomunicações – Teses. 3. Comunicação massiva entre máquinas. 4. Acesso aleatório. 5. Mitigação de propagação de erro. 6. Detecção. 7. Decodificação. I. de Lamare, Rodrigo Caiado. II. Pontifícia Universidade Católica do Rio de Janeiro. Departamento de Engenharia Elétrica. III. Título.

CDD: 621.3

To my family, for their support
and encouragement.

## Acknowledgments

First, I would like to thank God for giving me strength and focus to successfully complete the Ph.D. degree in Electrical Engineering at one of the most respected Brazilian universities, the Pontifícia Universidade Católica do Rio de Janeiro (PUC-Rio).

I would like to thank my mother, my brother and my father (in memoriam), for their support and encouragement, not only during my PhD but since I have started my undergraduate course.

I am grateful to have Prof. Rodrigo C. de Lamare as my advisor. During these four years, Prof. de Lamare have been always hard-working, enthusiastic, fair and sincere. Always available to help, Prof. de Lamare contributed incessantly to the construction of this thesis and my training as a researcher, for which I am immensely grateful.

I also would like to thank Prof. Tadeu Ferreira, who helped me since my undergraduate course, with ideas, suggestions and advice. I would like to thank all my colleagues and professors in the Centro de Estudos de Telecomunicações (CETUC/ PUC-Rio), but especially Prof. Landau, which always helped with new ideas and my friends Thiago Cunha, Alireza Danaee, Ana Beatriz Brito, Laisa Carvalho and Robert Mota who contributed to a friendly environment at CETUC. I also would like to thank my friends Gustavo Araújo, Isabel Camerini, Vitor Eboli, Joana Chissini and other colleagues who turned the traffic on the Rio-Niterói bridge into an amusing time.

I would like to thank Prof. Armin Dekorsy, who kindly received me in my research visit, in Uni Bremen. The determination, enthusiasm and sensibility of Prof. Dekorsy are inspiring characteristics that I wish to carry throughout my career. I immensely thank my ANT colleagues and employees of Uni Bremen, especially Carsten Bockelmann for the technical discussions and my friends Edgar, Johannes, Shayan, Matthias, Maik, Shengdi and Christopher. Also from Bremen, I would like to thank my Brazilian friends Satie and Ícaro and my roomates Amina, Carlo, Hala and Lan for the great moments and support.

Moreover, I am pleased for Prof. Lukas Landau, Prof. Marco Grivet, Dr. Silvio Pinto, Prof. Armin Dekorsy, Prof. Danilo Silva and Prof. Marcelo Bruno for having agreed to participate in the Examination Committee of this Thesis.

Finally, this study was financed in part by the Coordenação de Aperfeiçoamento de Pessoal de Nível Superior - Brasil (CAPES) - Finance Code 001 and in part by the Conselho Nacional de Desenvolvimento Científico e Tecnológico (CNPq).

## Abstract

Di Renna, Roberto Brauer; de Lamare, Rodrigo Caiado (Advisor). **Channel Estimation and Multiuser Detection Techniques for Machine-Type Communications**. Rio de Janeiro, 2021. 204p. Tese de doutorado – Departamento de Engenharia Elétrica, Pontifícia Universidade Católica do Rio de Janeiro.

Machine-type communications supports a plenty new applications, as environment sensing, vigilance surveillance, remote manufacturing, among others. Due to unique traffic and medium access characteristics, new estimation, detection and decoding techniques are required.

This work, presents an extensive literature review that highlights innovation opportunities and presents novel solutions for the main uplink mMTC problems. Based on the adaptive Recursive Least Squares (RLS) algorithm, the proposed regularized techniques jointly performs activity detection and signal decoding, without the need to perform explicit channel estimation. In order to improve the detection performance, a list detection technique that uses two candidate-list schemes is developed. Rewriting the problem with factor-graphs, novel message-passing algorithms with dynamic scheduling that jointly estimates the channels and detects devices activity are proposed. Lastly, a complete message-passing solution is presented, where LDPC decoding beliefs are introduced in the system, in a way that the algorithm besides the channel estimation and activity detection, also jointly decodes the signals.

In order to evaluate the proposed techniques, numerical results are provided as well as a computational complexity, state-evolution, convergence and a diversity analysis. Uplink sum-rate expressions that take into account metadata collisions, interference and a variable activity probability for each user are also derived. Finally, conclusions and future directions are discussed.

## Keywords

massive Machine-Type Communication  Grant-free random access  Error propagation mitigation  Detection  Decoding

## Resumo

Di Renna, Roberto Brauer; de Lamare, Rodrigo Caiado. **Estimação de Canal e Técnicas de Detecção para Comunicações entre Máquinas**. Rio de Janeiro, 2021. 204p. Tese de Doutorado – Departamento de Engenharia Elétrica, Pontifícia Universidade Católica do Rio de Janeiro.

As comunicações massivas do tipo máquina-a-máquina (mMTC) cobrem diversas novas aplicações, como sensoriamento ambiental, segurança pública, cidades inteligentes, entre outras. Devido à características únicas de tráfego e acesso, novas técnicas são necessárias para resolver os problemas de estimação de canal, de detecção de atividade e decodificação de sinais.
Esse trabalho realiza uma extensa revisão bibliográfica da literatura, onde pontos de inovação são observados e novas soluções para os principais problemas no *uplink* são propostas. Baseados no algoritmo adaptativo *Recursive Least Squares* (RLS), são apresentadas duas variações regularizadas que conjuntamente detectam a atividade e decodificam os sinais dos dispositivos, sem a necessidade de estimação explícita do canal. Além disso, duas técnicas de detecção por listas são desenvolvidas de modo a refinar o processo de ajuste dos pesos do algoritmo RLS e assim mitigar possíveis propagações de erros. Dividindo o problema em grafos fatoriais, são propostos algoritmos baseados em troca de mensagens de modo a realizar conjuntamente a estimação de canal e detecção de atividade. Além de uma nova derivação das mensagens, são exploradas técnicas de agendamento dinâmico, com base na convergência do algoritmo. Por fim, é apresentada uma solução completa baseada na troca de mensagens, que realiza conjuntamente a estimação de canal, detecção de atividade e decodificação dos dados transmitidos.
Resultados numéricos são fornecidos com o objetivo de comparar o desempenho dos algoritmos propostos aos existentes na literatura. Análises de complexidade computacional, evolução dos estados, convergência e ordem de diversidade também são realizadas, assim como a derivação da soma das taxas para o *uplink*. Por fim, são apresentadas as conclusões obtidas dos trabalhos realizados e discutidas direções para trabalhos futuros.

## Palavras-chave

Comunicação massiva entre máquinas  Acesso aleatório  Mitigação de propagação de erro  Detecção  Decodificação

# Table of contents

# List of figures

# List of tables

## List of Abreviations

| | | |
|---|---|---|
| AER | – | Activity Error Rate |
| AMP | – | Approximate Message-Passing |
| AWGN | – | Additive White Gaussian Noise |
| BER | – | Bit Error Rate |
| BP | – | Belief Propagation |
| BS | – | Base Station |
| CDMA | – | Code-Division Multiple Access |
| CP | – | Cyclic Prefix |
| CS | – | Compressive Sensing |
| CS-MUD | – | Compressive Sensing Multiuser Detection |
| CSI | – | Channel State Information |
| DFTs | – | Direct Fourier Transform spread OFDM |
| FAR | – | False Alarm Rate |
| FER | – | Frame Error Rate |
| GAMP | – | Generalized Approximate Message-Passing |
| GFRA | – | Grant-Free Random Access |
| GOMP | – | Group Orthogonal Matching Pursuit |
| i.i.d | – | Identically Independently Distributed |
| IoE | – | Internet of Everything |
| IoT | – | Internet of the Things |
| ISI | – | Inter-Symbol-Interference |
| LDPC | – | Low-Density Parity-Check |
| LLR | – | Log-Likelihood Ratio |

MIMO – Multiple Input Multiple Output

MMSE – Minimum Mean Square Error

MP – Matching Pursuit

MDR – Missed Detection Rate

MSE – Mean Squared Error

MTC – Machine-type Communications

mMTC – massive Machine-type Communications

MTCD – Machine-Type Device

MUD – Multi-User Detector

NMSE – Normalized Mean Squared Error

OFDM – Orthogonal Frequency Division Multiplexing

OLS – Orthogonal Least Squares

OMP – Orthogonal Matching Pursuit

PDF – Probability Density Function

QAM – Quadrature Amplitude Modulation

RA – Random Access

RLS – Recursive Least Squares

QAM – Quadrature Amplitude Modulation

# 1
# Introduction

The application focus of mobile communication systems in the past decades was on the human interaction. Starting from the beginning of the nineties, mobile communication systems progressed from supporting voice calls only to data packets transmitted from and to the internet. The introduction of the smart phones in the market can be seen as the key to the ever-increasing demand for higher data rates and coverage. To this end, the current communication standard 3GPP Long Term Evolution (LTE) has been developed to exactly target the requirements of human-based communication. However, the rise of new applications that demand communication between autonomous entities without human communication in mind, known as machine-type communications (MTC), brought new requirements. Covering different industries as healthcare, logistics, manufacturing, process automation and utilities, the growth of MTC applications is huge and it is believed that MTC connections will be half of the global connected devices and connections by 2023 [4]. The share of MTC connections will grow from 33% in 2018 to 50% by 2023. There will be 14.7 billion MTC connections by 2023 [5, 6]. Despite the fact that the traffic caused by these MTC devices (MTCD) only represent 7% of the total traffic nowadays, it is also believed that the amount of traffic will be higher. It is due to the increase of deployment of video applications on MTC connections and the increased use of applications, such as telemedicine and smart car navigation systems, which require greater bandwidth and lower latency.

The characteristics of MTC fundamentally differ from the well-known human-type communications (HTC). While HTC often requires high datarates for transmission of large packets, MTC traffic is characterized by small

packets ($\sim$ 100 bits) transmitted sporadically, generally with low data-rate and loose delay constraints. On the other hand, there are also some MTC applications that are less delay tolerant as video surveillance and healthcare monitoring. Besides that, MTC traffic is characterized to be concentrated on the uplink, whereas HTC is mainly driven by large downlink packages. In spite of the sporadic transmission pattern of each device, future mobile communication systems will have to support a massive number of MTCDs, as it is expected up to $300,000$ devices per cell [7, 8].

Given the MTC features described, it is possible to notice that MTC leads a paradigm shift in the evolution of mobile communication systems. Thus, upcoming generations of communication systems have to handle a diverse traffic originating from different type of sources. In this way, discussions regarding the standardization of the fifth generation of mobile communications (5G) were, among others, also driven by the challenge of aggregating MTC. It is also possible to divide MTC in two areas: massive MTC (mMTC) and ultra reliable MTC [9, 10]. Applications that consist of a large number of devices as smart cities, home automation or road and environmental monitoring are categorized as mMTC. Ultra reliable MTC summarizes critical applications with strict requirements on latency and packet error rates, such as autonomous vehicle control, factory automation and smart grid.

Therefore, this chapter presents the research background, motivations and objectives of this thesis. Moreover, the main contributions are described along with the structure of the thesis. In order to make reading this thesis easier, there is a section with the notation used throughout the work. The last section lists the publications and the papers under preparation that refers to this thesis.

## 1.1 Motivation and State of the Art

The inclusion of MTC in communication systems is not recent. Even the second generation of mobile communications systems has a few statements regarding MTC, as the Extended Coverage GSM for IoT [11]. Recently, the 3GPP have been considering to schedule a separate narrow frequency band to aggregate MTCDs, as described in the technical report TS 36.888 [7] and under the name Narrowband Internet of Things (NB-IoT), as a LTE extension [12]. Although it is possible to make extensions in the current mobile communication systems, in order for the network to support all the features of MTC and the expected growth of the number of MTCDs, it requires improvements made by the ongoing standardization of 5G and future communication systems.

The main challenges for aggregating MTC traffic lies in the aggregation of a massive number of MTCDs that sporadically transmit small packets to the base station (BS). One of the major issues is the design of the medium access. The current communication system LTE uses an orthogonal medium access with access reservation, that is, the BS allocates time and frequency resources prior to any transmission of payload data. As depicted in Fig. 1.1a, after a BS (or eNodeB, access point) broadcasts the system information to the devices, the access reservation procedure follows a four-stage message handshake [13], which mainly involves the following four stages: (i) Random Access (RA) preamble transmission from the device to the BS (Message 1), (ii) RA Response (RAR) from the BS to the device (Message 2), (iii) connection request message from the device to the BS (Message 3) and (iv) connection resolution message from the BS to the device (Message 4). Message 1 is the randomly selected preamble previously broadcast by the BS during the initial network synchronization phase. The next step is the BS answer with the preamble index being acknowledged, instructions for the timing alignment and the command for the resource blocks allocation. In the third message, after the device recognizes its response by the preamble index, it requests the connection.

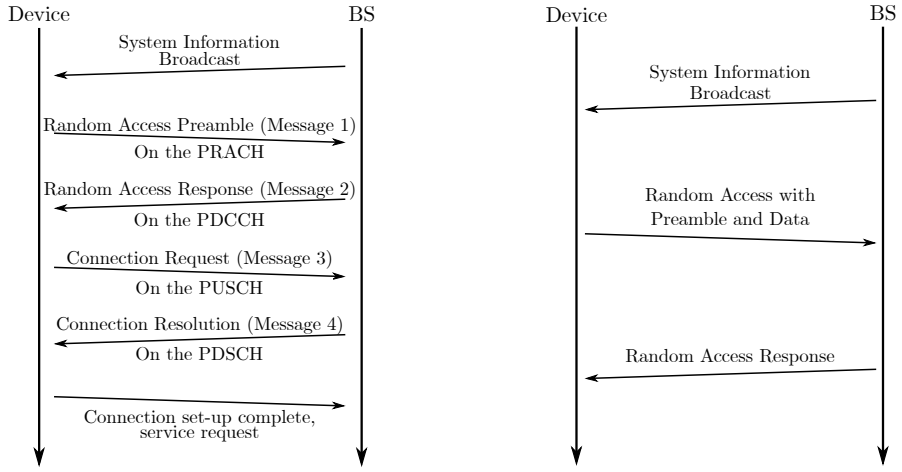


(a) Access reservation. (b) Grant-Free Random Access.

Figure 1.1: Comparison of medium access schemes. Access reservation as employed in LTE (a) and Grant-Free Random Access as candidate technology for mMTC (b).

Subsequently, for the devices which Message 3 are successfully decoded, the BS sends a connection resolution message (Message 4). In the case that more than one device chooses the same preamble, such transmissions will go through collisions.

Despite the fact that this random access procedure is used in LTE, it is not suitable for mMTC. Due to the aforementioned MTC characteristics, the limited number of available preambles for the access reservation procedure, the massive number of concurrent transmissions of the same preambles would cause the overload of the RA procedure both in the uplink and the downlink, resulting in a high collision probability, access failure rate and the access delay. Another point to be highlighted is that additional downlink resources would need to be allocated since each RAR message for one MTC device consists of 56 bits. Beyond that, the signalling overhead degrades the overall system efficiency since the size of the upload data payload from the MTC device is significantly smaller than the traditional HTC [14]. In this way, an approach that does not require orthogonal preambles with reduced signalling would fit better.

One promising approach is the Grant-Free Random Access (GFRA) [15, 16]. This mechanism allows the MTCDs to simply transmit their packages to

the BS directly, without the need to wait for a specific uplink grant from the BS. Fig. 1.1b shows the procedure, in order to be compared to the one used in LTE. The main advantages of this scheme are the reduced transmission latency, smaller signalling overhead due to the simplification of the scheduling procedure and improved energy efficiency (battery life) of MTCDs with the reduction in signalling. As all MTCDs simply transmit, the work of the BS is increased, since it should deal with the reception of many packets of multiple MTCDs at the same time and has to resolve the multiuser interference caused. Furthermore, the BS has no knowledge which MTCD was active at the given time instance such that the physical layer task is to jointly estimate the channels and detect the activity and the data of the devices [10, 17].

Therefore, it has been shown that the physical layer aspects of random access can be optimized. The research problem to be solved consists of how to allocate resources as time, frequency or code to devices that are known to be only sporadically active. Due to the intermittent traffic, the orthogonal resource allocation leads to a waste of resources. Thus, recent works have focused on the use of non-orthogonal resource allocation in the GFRA [18–24].

Although detection techniques have been investigated for more than 50 years, at each new emerging application, novel schemes are required. In a scenario as mMTC, with an accurate CSI, it is possible to deal with the sparse pattern of transmissions in order to detect the data. Therefore, in recent years many recent works have studied multiuser detection (MUD) in this scenario. First, solutions which considered perfect channel state information (CSI) at the BS have been reported. Originally from the compressed sensing (CS) field [25], techniques based on regularization that exploits the sparsity of the scenario have been studied. In this way, several works which perform regularized versions of the Maximum a Posteriori Probability (MAP) [26], Sphere Detection (SD) [27], K-Best [28], MMSE-SIC [29, 30] detectors have been studied and an algorithm based on the direction method of multipliers

(ADMM) has been reported in [31]. There are also iterative solutions to the class of Bayesian inference algorithms, as the works in [32] and [33]. Solutions based on approximate message passing (AMP) [34] have also been discussed in the literature, as in [35–37]. As envisaged, mMTC networks support a massive number of devices, where a common assumption is that the system is underdetermined. That is, the number of devices capable of accessing the BS at the same time instant is much higher than the number of resources at the BS. Owing to the sporadic traffic pattern, greedy algorithms emerged as CS-MUD schemes. The well-known orthogonal matching pursuit (OMP) [38] and orthogonal least squares (OLS) [39] were first applied in the mMTC context in [40] and then some improvements have appeared in [41–47]. Employing channel coding, the schemes in [48–51] propose adaptive and iterative solutions that exchange extrinsic information between activity and symbol detectors. Moreover, prior work on activity detection and channel estimation, [52–55] has focused on the AMP, verifying the missed device detection and false alarm performance. There are other works, as in [56–63] that use the factor graph approach. There are also works as in [64–68] that use the machine-learning as a tool to estimate the channels. Recently, there are a few solutions that jointly perform the activity and data detection and channel estimation. Due to the computational cost, most of them are message-passing solutions, as [69–74].

## 1.2 Objectives of this thesis

The objectives of this thesis are to present and discuss novel channel estimation, activity detection and signal decoding techniques for mMTC. As in this scenario the BS has no knowledge which device is active, besides having data-errors only mMTC techniques also suffer from activity errors known as false alarm and missed detection. The analysis of data and activity errors show that each type of error has a fundamental impact on the underlying communication. As long as false alarm rates may be identified by higher layers,

missed detection errors lead to a loss of data that can not be recovered. In order to address the challenge of joint channel estimation, activity detection and data decoding, this thesis focuses on four main goals. With this in mind, this thesis presents novel algorithms that seek to optimize the mean squared error (MSE), false alarm (FAR), missed detection (MDR) and bit error rates (BER).

## 1.3 Contributions and Structure of this Thesis

The goal of this thesis is to address the challenges of channel estimation, activity detection and data decoding in the mMTC scenario. Throughout the thesis, different solutions based on receive filter estimation, regularized recursive least squares (RLS) and message-passing strategies are presented. Thus, the main contributions are:

1. A review of the main detection techniques for mMTC scenarios and a performance comparison of the literature approaches in the same evaluation framework in terms of the key performance indicators.

2. Development of a regularized version of the adaptive RLS algorithm, that jointly detects the activity and signals of devices without the need to perform explicit channel estimation. Iterative detection and decoding (IDD) schemes that exploit the sparse scenario are also developed for mMTC to mitigate the interference from other devices. A list detection technique is then designed that uses two candidate-list schemes that improves detection performance.

3. The development of novel message-passing algorithms that jointly estimates the channels and detects devices activity is carried out along with a bilinear solution that also performs signal decoding. Dynamic scheduling techniques are then developed that aim to find the best sequence of message updates, reducing the computational cost. A comparison and

discussion of two uplink scenarios is then conducted with the devices transmitting in synchronous and asynchronous patterns.

4. A comparison of the proposed algorithms with the state-of-the art, in terms of NMSE, FAR, MDR and BER is carried out. The derivation of uplink sum-rate expressions, steady-state, convergence and computational cost analyses is also presented.

The next chapters of this thesis include the following content:

- Chapter 2 gives some technical background on this thesis. Firstly, basic concepts of multiuser MIMO are presented, which includes channel estimation, multiuser detection and channel capacity. In order to introduce the mMTC scenario, its unique features are described, as traffic, medium access, challenges and the general assumptions. The rest of the chapter categorizes and provide a comprehensive overview of the main detection techniques designed specifically for mMTC, presenting a performance evaluation of the main state-of-the-art approaches in the same evaluation framework.
- Chapter 3 presents the regularized version of the adaptive RLS algorithm, that jointly detects the activity and signal of devices without the need to perform explicit channel estimation. The IDD scheme is also explained, describing how it is incorporated in the proposed scheme. Simulation results of Symbol Error Rate (SER), FAR, MDR and the comparison of computational complexity between this solution and the state-of-the-art are also described in this chapter.
- Chapter 4 presents two candidate-list detection schemes for mMTC that employ the regularized version of the adaptive RLS algorithm to adjust the receive filter parameters. Moreover, a diversity analysis and uplink sum-rate expressions are presented. Numerical results show the excellent performance of the proposed detection schemes as compared to existing approaches.

- Chapter 5 introduces a joint active device detection and channel estimation framework based on factor graphs. Given the aforementioned mMTC characteristics, the chapter consider the problem under two different scenarios, uplink synchronous and asynchronous transmissions. A message-scheduling GAMP (MSGAMP) algorithm that uses a factor graph approach is devised with three different message-scheduling techniques. Simulation results of NMSE, AER and a convergence analysis that compares MSGAMP performance and the state-of-the-art are also shown in this chapter.
- Chapter 6 presents the bilinear message-scheduling GAMP (BiMSGAMP) scheme, that jointly performs active device detection, channel estimation and data decoding. BiMSGAMP uses the channel decoder beliefs to refine the activity detection and data decoding. This chapter also presents a convergence and computational cost analyses, in addition to a comparison of BiGAMP's efficiency over other approaches in terms of NMSE, FAR, MDR, FER and BER.
- Chapter 7 presents the conclusions of this thesis, discussing the obtained results, future directions and research opportunities.

## 1.4 Notation

The following notation is used throughout the work. Matrices and vectors are denoted by boldfaced capital letters and lower-case letters, respectively. The space of complex (real) $N$-dimensional vectors is denoted by $\mathbb{C}^N$ $\left(\mathbb{R}^N\right)$. The $i$-th column of a matrix $\mathbf{A} \in \mathbb{C}^{M\times N}$ is denoted by $\mathbf{a}_i \in \mathbb{C}^M$. The superscripts $(\cdot)^T$ and $(\cdot)^H$ stand for the transpose and conjugate transpose, respectively. For a given vector $\mathbf{x} \in \mathbb{C}^N$, $||\mathbf{x}||$ denotes its Euclidean norm. $\mathbb{E}[\cdot]$ stands for expected value, $\mathbf{I}$ is the identity matrix and diag $[\cdot]$ is to reshape a vector in the main diagonal of a matrix.

## 1.5 Publication List

Some of the results in this thesis have been published, or are under review for publications.

- Journal papers:

1. **R. B. Di Renna** and R. C. de Lamare, "Informed Dynamic Message Scheduling Strategies for mMTC," in *IEEE Transactions on Communications*, 2021. Under review.

2. **R. B. Di Renna** and R. C. de Lamare, "Dynamic Message Scheduling Based on Activity-Aware Residual Belief Propagation for Asynchronous mMTC," in *IEEE Wireless Communications Letters*, accepted for publication, 2021, doi: 10.1109/LWC.2021.3064304.

3. **R. B. Di Renna**, C. Bockelmann, R. C. de Lamare, and A. Dekorsy, "Detection Techniques for Massive Machine-Type Communications: Challenges and Solutions," in *IEEE Access*, vol. 8, pp. 180928-180954, 2020, doi: 10.1109/ACCESS.2020.3027523.

4. **R. B. Di Renna** and R. C. de Lamare, "Iterative List Detection and Decoding for Massive Machine-Type Communications," in *IEEE Transactions on Communications*, vol. 68, no. 10, pp. 6276-6288, Oct. 2020, doi: 10.1109/TCOMM.2020.3007525.

5. **R. B. Di Renna** and R. C. de Lamare, "Adaptive Activity-Aware Iterative Detection for Massive Machine-Type Communications," in *IEEE Wireless Communications Letters*, vol. 8, no. 6, pp. 1631-1634, Dec. 2019, doi: 10.1109/LWC.2019.2932674.

- Conference papers:

1. **R. B. Di Renna** and R. C. de Lamare, "Joint Activity Detection and Data Decoding for Grant-Free MIMO," *ISWCS 2021; 17th International Symposium on Wireless Communication Systems*, Berlin, Germany, 2021.

2. **R. B. Di Renna** and R. C. de Lamare, "Joint Activity Detection and Channel Estimation Based on Dynamic Message Passing Scheduling for MTC," *SSP 2021; IEEE Statistical Signal Processing Workshop 2021*, Rio de Janeiro, RJ, Brazil, 2021.

3. **R. B. Di Renna** and R. C. de Lamare, "Adaptive Activity-Aware Constellation List-Based Decision Feedback Detection for Massive Machine-Type Communications," *2019 53rd Asilomar Conference on Signals, Systems, and Computers*, Pacific Grove, CA, USA, 2019, pp. 2111-2115, doi: 10.1109/IEEECONF44664.2019.9049081.

4. **R. B. Di Renna** and R. C. de Lamare, "Activity-Aware Multiple Feedback SIC for Massive Machine-Type Communications," *SCC 2019; 12th International ITG Conference on Systems, Communications and Coding,* Rostock, Germany, 2019, pp. 1-6, doi: 10.30420/454862040.

# 2
# Technical Background and Literature Review

## 2.1
## Chapter Overview

This chapter starts with a review of some basic concepts related to this thesis and then proceeds to introduce the massive Machine Type-Communications (mMTC) scenario. The first section briefly introduces topics related to MU-MIMO systems, including sum-rate capacity, channel estimation and multiuser detection. The second section presents the mMTC scenario, describing its unique features as traffic, medium access, challenges and the general assumptions. The rest of the chapter categorizes and provides a comprehensive overview of the main detection techniques designed specifically for mMTC, presenting a performance evaluation of the main state-of-the-art approaches in the same evaluation framework.

## 2.2
## MIMO Wireless Communication Systems

Wireless systems continue to strive for ever higher data rates. This goal is particularly challenging for systems that are power, bandwidth, and complexity constrained. The first studies [75, 76] that indicated high spectral efficiencies for wireless systems with multiple antennas attracted attention of worldwide researchers, that aimed to characterize the theoretical and practical issues associated with multiple-input multiple-output (MIMO) wireless channels and to extend these concepts to multiuser systems. Now in the core of many existing and emerging wireless standards as IEEE 802.11, IEEE 802.16 and IEEE 802.20, the usage of multiple antennas either at the transmitter or at

the receiver side provides a number of benefits that enable the system to face the impairments in the wireless channel as well as resource constraints [77,78].

One of the main advantages of using multiple antennas is the increase in spatial diversity. Spatial diversity relies on the use of multiple antennas at one end of the communication link, either at the transmitter or at the receiver side. The idea is that the receiver has multiple (ideally independent) copies of the transmitted signal in space, frequency or time. Therefore, the more copies are available on the receiver, the more likely it is that at least one of the copies is not experiencing strong channel and noise effects, thereby improving the quality and reliability of reception. Thus, the spatial diversity gain mitigates fading.

In addition to that, a communication system with multiple antennas also benefits from spatial multiplexing [75,79]. Spatial multiplexing is the ability to send several independent data streams simultaneously within the bandwidth of operation. The linear increase in data rate observed in MIMO systems is due to the fact that each data stream experiences at least the same channel quality that would be experienced by a system with only one antenna at the receiver and at the transmitter (SISO), thus increasing the capacity by a multiplicative factor equal to the number of streams.

Besides the above advantages, interference mitigation and array gain are also key features. Although the interference in wireless networks is due to the sharing of resources (time and frequency) from multiple users, it can be mitigated by exploiting the spatial dimension to increase the separation between users. The increase of the receive SNR due to the coherent combining effect of the received signals is the array gain. This increase of receive SNR naturally improves resistance to noise, thereby improving the coverage and the range of a wireless network [77].

With the advantage of using multiple-antennas in the transmitter and the receiver briefly explained, a MIMO communication system is presented. The

first operation is the encoding of the information bits to be transmitted and its interleaving. The codeword is modulated in the symbol mapping block and then encoded on one or more spatial data streams, by a space-time encoder. Lastly, those streams are mapped to the transmitting antennas by the space-time precoding block. After that, the signals are transmitted through the channel and, after being received by the multiple antennas, the signal suffers the inverse operations on the receiver side. Since this thesis focuses on a special case of MIMO systems, the next subsection is devoted to explaining the channel and signal models of massive MIMO [80].

### 2.2.1 Massive MIMO

In order to maximize the gains described in the previous subsection, Thomas Marzetta introduced the idea of using a huge number of antennas in the base station (receiver) in his seminal work [1]. The main idea is that a multiplicity of physically small, individually controlled antennas could perform an aggressive multiplexing/demultiplexing for all active users, utilizing directly measured channel characteristics. Taking advantage of time-division duplexing (TDD), massive MIMO is scalable to any desired degree with respect to the number of BS antennas. Adding more antennas is always beneficial for increased throughput, reduced radiated power, uniformly great service everywhere in the cell, and greater simplicity in signal processing.

It is possible to define massive MIMO network as a multi-carrier cellular network with $L$ cells that operate according to a synchronous TDD protocol, that is, uplink and downlink transmissions within different cells are synchronized. A BS is equipped with $M >> 1$ antennas and communicate with $N$ single-antenna[1] users simultaneously on each time/frequency sample, with the ratio $M/N > 1$. Each BS operates individually ans processes its signals using linear receive combining and linear transmit precoding [1, 81].

[1]Each user can be equipped with more than one antenna, but the simplification of the model is a common assumption in wireless communication systems [1].

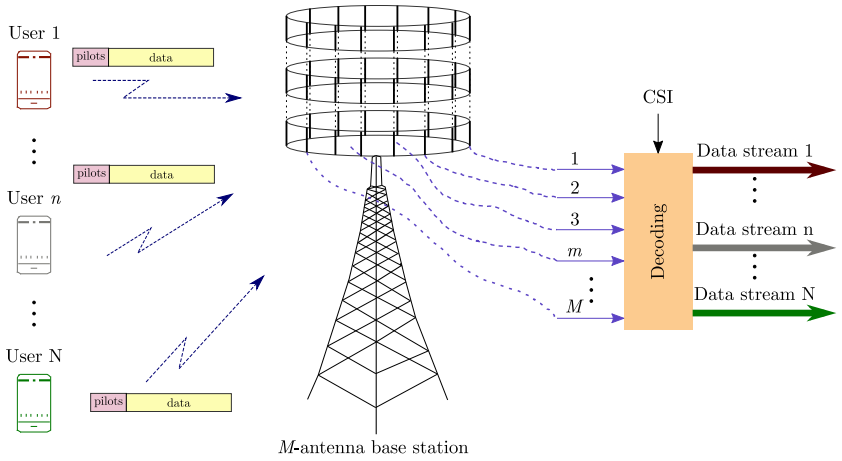


Figure 2.1: Uplink operation of a massive MIMO link. Each user transmits data stream that occupy the same time/frequency resources, and the signals received by the elements of the antenna array are processed to recover the individual data streams [1, 2].

In general, multiuser MIMO systems can be divided in two categories, uplink (or multiple access channel, MAC) and downlink (or broadcast channel, BC). Since the machine-type communications traffic, which is the main topic of this work, is concentrated on the uplink, the next subsection will focus only on the MAC case.

### 2.2.2 System Model

The considered uplink massive MIMO system [1, 2] model is depicted in Fig. 2.1, where a single BS with $M$ antennas communicates with $N$ single-antenna users. Each user has the coherence interval[2] to transmit its frames and receive the downlink data. Assuming the block fading assumption, the channel realizations are independent between any pair of blocks. Since it is a massive MIMO system, $M >> N$. The received signal vector $\mathbf{y} \in \mathbb{C}^{M\times 1}$ of each sample, at the BS is given by

$$\mathbf{y} = \sum_{n=1}^{N} \mathbf{h}_n x_n + \mathbf{v} = \mathbf{H}\mathbf{x} + \mathbf{v}, \tag{2-1}$$

where the $\mathbb{C}^{N\times 1}$ vector $\mathbf{x}$ represents the transmitted symbols of each device in the observed time instant and $\mathbf{v} \in \mathbb{C}^{M\times 1}$ is the independent additive

[2]Time interval over which the channel responses are approximately constant.

receiver noise vector with zero mean and variance $\sigma_n^2$. The matrix $\mathbf{H} \in \mathbb{C}^{M \times N}$ represents the channel response between each user and BS antenna. The channels are constant within a coherence interval, while signals and noise take new realization at every sample. A fading channel $\mathbf{h} \in \mathbb{C}^{M \times 1}$ is spatially uncorrelated if the channel gain $\|\mathbf{h}\|^2$ and the channel $\mathbf{h}/\|\mathbf{h}\|$ are independent random variables, and it is uniformly distributed over the unit-sphere in $\mathbb{C}^M$. Otherwise, the channel is spatially correlated. Practical channels are, in general, spatially correlated. The spatial correlation is important for large arrays since these have good spatial resolution [81,82]. Thus, in massive MIMO, the common channel model is the correlated Rayleigh fading, as given by

$$\mathbf{H} = \begin{bmatrix} h_{1,1} & h_{1,2} & \cdots & h_{1,N} \\ h_{2,1} & h_{2,2} & \cdots & h_{2,N} \\ \vdots & \vdots & \ddots & \vdots \\ h_{M,1} & h_{M,2} & \cdots & h_{M,N} \end{bmatrix}, \tag{2-2}$$

where $h_{M,N}$ is the single-input single output channel gain between the $m$-th receive antenna and $n$-th user. The $n$-th column of $\mathbf{H}$ is often referred to as the spatial signature of the $n$-th transmit antenna across the receive antenna array. Thus, each channel response is given by

$$\mathbf{h}_n \sim \mathcal{N}_c \left( \mathbf{0}_M, \mathbf{R}_n \right), \tag{2-3}$$

where $\mathbf{R}_n \in \mathbb{C}^{M \times M}$ is the positive semi-definite spatial correlation matrix. The Gaussian distribution is used to model the small-scale fading variations. In a new coherence interval, the matrix $\mathbf{H}$ is assumed to take new realizations from this distribution. The spatial correlation matrix represents the large-scale effects, as antenna gains and environment scattering [77]. In this model, the normalized trace determined the average channel gain from one of the antennas at the BS to the user and is given by

$$\beta_n = \frac{1}{M} \mathrm{tr} \left( \mathbf{R}_n \right). \tag{2-4}$$

As an special case, we have the uncorrelated Rayleigh fading, where $\mathbf{R}_n = \beta_n \mathbf{I}_M$ and the classical, independent, identically distributed (i.i.d.) Rayleigh fading model. Under ideal conditions, when the channel elements are perfectly decorrelated, $h_{nm} \sim$ i.i.d. $\mathcal{N}_c(0,1)$. After defining the channel model and the basics of massive MIMO, the next subsection details the channel estimation.

### 2.2.3 Channel Estimation

Channel estimation is a key factor in order to equip the BS with the capability to correctly detect the transmitted data. In this scenario each user transmits, as depicted in Fig. 2.1, a pilot sequence from a list of sequences previously broadcast by the BS. In general, the pilot sequence is assumed to have unit-magnitude elements, to obtain a constant power level. Thus, dividing the transmitted block in $X = [X_p, X_d]$ and rewriting (2-1), we have

$$\underbrace{\mathbf{Y}_p}_{M\times\tau_p} = \underbrace{\mathbf{H}}_{M\times N}\underbrace{\mathbf{X}_p}_{N\times\tau_p} + \underbrace{\mathbf{V}_p}_{M\times\tau_p}, \tag{2-5}$$

where $\tau_p$ is the number of pilots. Ideally, the pilot sequences of all users would be orthogonal. In order for the BS to estimate the channel of the $n$-th user, it can multiply/correlate the received $\mathbf{Y}_p$ with the pilot sequence of this user, thus

$$\mathbf{y}_p = \mathbf{Y}_p\, {\mathbf{x}_{p_n}}^H = \sum_{n=1}^{N} \mathbf{h}_n\, {\mathbf{x}_{p_n}}^T\, {\mathbf{x}_{p_n}}^H + \mathbf{V}_p\, {\mathbf{x}_{p_n}}^H, \tag{2-6}$$

and then, separating the desired pilot from the other users pilots,

$$\mathbf{y}_p = \mathbf{Y}_p\, {\mathbf{x}_{p_n}}^H = \underbrace{\mathbf{h}_n\, {\mathbf{x}_{p_n}}^T\, {\mathbf{x}_{p_n}}^H}_{\text{desired pilot}} + \underbrace{\sum_{i\neq n}^{N} \mathbf{h}_i\, {\mathbf{x}_{p_i}}^T\, {\mathbf{x}_{p_n}}^H}_{\text{other users pilots}} + \underbrace{\mathbf{V}_p\, {\mathbf{x}_{p_n}}^H}_{\text{noise}}. \tag{2-7}$$

It is possible to notice that due to the pilot inner products, if the pilot sequences are orthogonal, they will not act as an interference. However, since the number of orthogonal pilot sequences are finite it is a constraint for a massive MIMO scenario and, as will be detailed in the next sections, for

mMTC.

As an example of channel estimation approach, the linear minimum mean squared (MMSE) is shown. We firstly rewrite (2-5) as given by

$$\underbrace{\mathbf{y}_p}_{M\tau_p\times 1} = \left(\mathbf{X}_p^T \otimes \mathbf{I}_M\right)\mathbf{h} + \mathbf{v}_p = \underbrace{\text{vec}\left\{\mathbf{X}_p\right\}}_{M\tau_p\times MN}\underbrace{\mathbf{h}}_{MN\times 1} + \underbrace{\mathbf{v}_p}_{M\tau_p\times 1}. \tag{2-8}$$

Exploiting the knowledge of covariance matrices, the linear MMSE is widely used for channel estimation in MIMO systems, despite its high computational cost. In a nutshell, the linear filter is given by

$$\mathbf{W}_{\text{MMSE}} = \arg\min_{\mathbf{W}} \mathbb{E}\left\{\|\mathbf{h} - \mathbf{W}\mathbf{y}_p\|^2\right\} = \mathbf{C}_{\mathbf{h}\mathbf{y}_p}\mathbf{C}_{\mathbf{y}_p}^{-1}, \tag{2-9}$$

where $\mathbb{E}\left\{\mathbf{h}\mathbf{y}_p^H\right\} = \mathbf{C}_{\mathbf{h}\mathbf{y}_p}$ and $\mathbb{E}\left\{\mathbf{y}_p\mathbf{y}_p^H\right\} = \mathbf{C}_{\mathbf{y}_p}^{-1}$. Then, the linear MMSE channel estimator is given by

$$\hat{\mathbf{h}}_{\text{MMSE}} = \mathbf{W}_{\text{MMSE}}\,\mathbf{y}_p = \mathbf{C}_{\mathbf{h}\mathbf{y}_p}\mathbf{C}_{\mathbf{y}_p}^{-1}\,\mathbf{y}_p. \tag{2-10}$$

Therefore, the next subsection introduce one of the main advantages of massive MIMO, the channel capacity.

### 2.2.4 Channel Capacity

Firstly presented in Claude Shannon's pioneering work [83], the channel capacity refers to the maximum data rates that can be transmitted over wireless channels under certain conditions. Considering a scenario of wireless channels with asymptotically small error probability and without any constraints on transmitter and receiver complexity, the theory is based on the notion of mutual information between the input and the output of a channel. Shannon defined channel capacity as the channel's mutual information maximized over all possible input distributions [82]. Considering a random input $X$ and random output $Y$, the mutual information of a single-user channel is defined as

$$I(X;Y) = \int_{S_X,S_Y} f(x,y) \log_2 \left( \frac{f(x,y)}{f(x) f(y)} \right) \mathrm{d}x \, \mathrm{d}y, \tag{2-11}$$

where the integral is taken over the supports $S_x$, $S_y$ of the random variables $X$ and $Y$, respectively, and $f(x)$, $f(y)$, and $f(x,y)$ denote the probability density functions of the random variables. Since the mutual information unit is bits per channel use, the base of the log is 2. As Shannon's definition, the channel capacity is the maximization of the channel mutual information. Thus, we have

$$C = \max_{f(x)} I(X;Y) = \max_{f(x)} \int_{S_x,S_y} f(x,y) \log_2 \left( \frac{f(x,y)}{f(x) f(y)} \right). \tag{2-12}$$

For the MIMO channel case, the definition above stands for entropy and mutual information. Considering a constant MIMO channel perfectly known at the transmitter and the receiver, the capacity in the uplink is given by

$$C = \max_{\mathbf{Q}:\mathrm{tr}(\mathbf{Q})=P} \log\det\left(\mathbf{I}_M + \mathbf{H}\mathbf{Q}\mathbf{H}^H\right) \tag{2-13}$$

where the optimization is over the input covariance matrix $\mathbf{Q}$, which is $N \times N$ and must be positive semi-definite by definition and $P$ is the power of the MIMO parallel channels. For a time-invariant AWGN channel with bandwidth $B$ and received SNR $\gamma$, the input distribution that maximizes the mutual information is Gaussian, which results in the following

$$C = B \log_2(1+\gamma) \text{ bps}. \tag{2-14}$$

The advantage of massive MIMO regarding the channel capacity is due to the fact that even without transmitter CSI, random matrix theory dictates that the singular values of the channel matrix converge to the same constant. Hence, the capacity of each spatial dimension is the same, and the total system capacity is given by

$$C = \min(N,M)\ B \log_2(1+\gamma). \tag{2-15}$$

Thus, capacity grows linearly with the size of the antenna arrays in massive MIMO systems [1]. After presenting the basic concepts of MIMO systems and the massive MIMO advantages, the next subsection will briefly comment on the classic detectors.

### 2.2.5 Classic Multiuser Detectors

The study of the MIMO detection problem dates to the 1960s. The first work [84] proposes a solution inspired by the Nyquist's problem [85], which faces the intersymbol interference (ISI) over a SISO channel. Through the years, the MIMO detection problem has been studied in different contexts and can be categorized from various perspectives, such as optimum, linear, adaptive, blind, iterative, among others [86]. Considered an optimal detector, the ***maximum a posteriori* (MAP)** minimizes the error probability based only on the observed signals and a given set of hypotheses $\mathcal{A}^N$, that is

$$\hat{\mathbf{x}}_{\text{MAP}} = \underset{\mathbf{x}\in\mathcal{A}^N}{\arg\max}\, \Pr(\mathbf{x}|\mathbf{y}) = \underset{\mathbf{x}\in\mathcal{A}^N}{\arg\max}\, \frac{p(\mathbf{y}|\mathbf{x})\Pr(\mathbf{x})}{\sum_{\mathbf{x}'\in\mathcal{A}^N} p(\mathbf{y}|\mathbf{x}')\Pr(\mathbf{x}')}, \quad (2\text{-}16)$$

using Bayes' rule. $\Pr(\mathbf{x})$ is the *a priori* probability of $\mathbf{x}$, $p(\mathbf{y}|\mathbf{x})$ is the conditional probability density function (PDF) of the received vector $\mathbf{y}$ given $\mathbf{x}$ and $\hat{\mathbf{x}}$ is the detected transmitted vector. Under the assumption that $p(\mathbf{y})$ is independent of $\mathbf{x}$ and considering that the receiver does not have knowledge of $\Pr(\mathbf{x})$, the MAP detector becomes equivalent to the **maximum likelihood (ML)** detector [86], as given by

$$\hat{\mathbf{x}}_{\text{ML}} = \underset{\mathbf{x}\in\mathcal{A}^N}{\arg\min}\, \|\mathbf{y} - \mathbf{H}\mathbf{x}\|_2^2. \quad (2\text{-}17)$$

Since the MAP and ML detectors have a tremendous computational cost, other solutions have emerged over the years. Considering $\mathbf{W}$ as a filter matrix computed in each detector, the **matched filter (MF)** detector is given by

$$\hat{\mathbf{x}}_{\mathrm{MF}} = \underbrace{\mathbf{H}^H}_{\mathbf{W}_{\mathrm{MF}}} \mathbf{y}. \tag{2-18}$$

The linear **matched filter (MF)** is optimal for maximizing the received SNR in the presence of additive noise. Since it is essentially based on single-user detection, it normally exhibits poor performance in MIMO systems. The **zero-forcing (ZF)** receiver is optimal in terms of maximizing the received signal-to-interference ratio (SIR). By contrast, the linear **minimum mean squared error (MMSE)** criterion based detector takes into account the received signal-to-interference-plus-noise ratio (SINR), which makes it possible to surpass all linear detectors in performance. Thus, the ZF and MMSE filters are given by

$$\hat{\mathbf{x}}_{\mathrm{ZF}} = \underbrace{\left(\mathbf{H}^H\mathbf{H}\right)^{-1}\mathbf{H}^H}_{\mathbf{W}_{\mathrm{ZF}}} \mathbf{y}, \tag{2-19}$$

$$\hat{\mathbf{x}}_{\mathrm{MMSE}} = \underbrace{\left(\mathbf{H}^H\mathbf{H} + 2\sigma^2\mathbf{I}\right)^{-1}\mathbf{H}^H}_{\mathbf{W}_{\mathrm{MMSE}}} \mathbf{y}. \tag{2-20}$$

The class of detectors that focus on the multiuser interference problem, generally outperforms the linear ones. On the other hand, this efficiency occurs with the increase of the computational cost. The classic approaches are the **parallel interference cancellation (SIC)** and the **successive interference cancellation (SIC)**, that perform better in scenarios in which the interfering users have a much stronger signal strength than the desired user.

Initiating with the most popular interference cancellation detector, SIC detects a single symbol at a time. Then the interference imposed by this particular symbol on the other symbols yet to be detected is subtracted after recreating the interference upon generating the modulated signal corresponding to this symbol. In this way, if a wrong detection is performed, SIC suffers from error propagation. Another point to highlight is that it is very important to cancel the effect of the strongest interfering signal before detecting the weaker signals. Therefore, a specific symbol detection ordering is crucial for a good performance [87–89]. One well-known alternative to avoid the need to find the strongest interfering signal is the PIC based MIMO detector. In this algorithm,

all symbols are detected simultaneously, that is, for each symbol, the initial estimate of the interfering symbols is used to reconstruct the interference and then to subtract it from each of the composite received signals. In order to refine the detection, this process is repeated for several iterations [90–92]. Despite that, the PIC detector exhibits a lower processing delay than SIC, but is worse in a scenario of different-power streams [86, 93].

With the basic concepts of MIMO systems and classic detectors presented, the next section introduces the mMTC scenario and provides a comprehensive literature review of main detection approaches, presenting performance and complexity cost comparisons.

## 2.3 Massive Machine-Type Communications Scenario

While the existing data aggregation technologies support various applications, there are still open problems to be investigated. How to deal with the massive access of hundreds of billion devices with small-sized transmission payloads and sporadic features is one of the main challenges of this kind of network [15, 16]. Indeed, promising techniques such as compressed sensing (CS), non-orthogonal multiple access (NOMA) and massive MIMO based random access that can effectively address the lack of spectrum resources and enhance spectrum usage efficiency have been proposed.

MTC devices can be applied to various scenarios, enabling real-time monitoring and control of any physical environment. The major application scenarios are [94], [95]:

1. E-health: Applications as tracking or monitoring a patient, identification and authentication of patients, diagnosing patient conditions and providing real-time information on patients' health related data to the remote monitoring center;

2. Smart-environment: This category encompasses all forms of automation, whether in home/office, agriculture, environmental monitoring, lighting;

3. Intelligent transportation: This field is related to services as smart parking, smart car counting, M2M assisted driving and e-ticketing;

4. Security and public safety: Remote surveillance, personal tracking and public infrastructure alarm protection from disasters such as fire, earthquakes, hazardous spills or crimes. Collaboration among relevant organizations, including medical support, police, military and fire department;

5. Smart-grid: Mainly related to power monitoring, this category also includes applications as meter reading, electricity distribution and transmission tower protection;

6. Industrial automation: Productivity enhancement possible by communications among machines and supply chain automation applications. Other example of applications are production on demand, quality control, optimization of packaging and inventory tracking.

In general, MTC devices access the network sporadically to transmit frames with a few bits. Despite that, mMTC traffic comprises specific patterns due to diversity in the application scenarios. For instance, an agriculture sensor network sends few bits of data periodically while a smart-grid application consumes high bandwidth and requires connection with a higher frequency. In case of a catastrophe event, the network must be prepared to receive simultaneous transmissions of emergency data. Unlike HTC communications, mMTC traffic is mainly in the uplink and can be generated any time of the day. While the human-type communication traffic follows a certain data volume, session length, and interaction frequency during daytime and evening, mMTC should have an infrastructure that handles different traffic patterns. A few works as [96] and [97] investigate the difference between HTC and mMTC and the competition for resources. The study in [51] considers different traffic patterns and their impact with detection algorithms. Therefore, mMTC have challenging traffic aspects such as scalability, periodic, low frame size and data

rates, no mobility and deals mostly with the uplink, which requires special attention to design the infrastructure and coexist with the established cellular networks [94], [96]. 3G and LTE networks can support a few MTC applications but not all of them. Thus, it is expected that 5G handles the massive number of MTCD and the services already available. In the following, we mostly focus on the challenges on the PHY and MAC layers but shortly discuss other issues.

One of the open problems is the limitation of available pilot sequences. Due to the huge number of devices, the reuse of pilots significantly increases the frame collision probability. In addition, as each transmitted frame has a few bits, very high signalling overhead per data frame becomes another critical issue. Thus, an efficient signalling reduction technique is required.

Many MTC devices can be coined low-cost and will have batteries as the main source of power. Therefore, energy efficiency is a concern for mMTC. Since it is required that MTCD operate autonomously for a few years, the communication design should be power efficient. Since long distance communications to the BS is challenging the use of relays could help. Another issue related to energy efficiency is the geographic positions of MTCDs. As they can be located anywhere in the cell, at edges or shadow areas, it would be hard for the BS to serve all devices at any time.

In higher layers, there are also open challenges. For instance, a new transport protocol is required for mMTC, as the Transmission Control Protocol (TCP) is not efficient for mMTC traffic features. The connection setup of TCP is unnecessary and the congestion control would probably degrade the performance as mMTC uses a wireless medium and the amount of data is very small. As it was not designed for it, real-time applications would not work properly with TCP as it requires data to be stored in a memory buffer. Furthermore, low-cost MTCDs have limited capabilities to implement security algorithms. In this way, authentication and data integrity may be a security concern in mMTC.

Some detection techniques take into consideration most of those challenges and propose solutions to deal with them. The next subsection details the general system model assumptions in order to present the main schemes in the literature.

### 2.3.1 MMTC System model

In order to reduce signalling overhead, grant-free random access (GFRA) has been proposed [17]. In the uplink of such systems, each device transmits metadata[3] along with data. This massive uplink connectivity scenario is illustrated in Fig. 2.2, where $N$ devices with a single antenna each access a single base station (BS), equipped with $M$ antennas.

In general, there are two types of metadata considered in GFRA, namely orthogonal [23, 24] and non-orthogonal metadata [36, 52]. Compared with the non-orthogonal counterpart, orthogonal metadata detection is much simpler and effective and channel estimation is more accurate thanks to the orthogonality of metadata. Nevertheless, frame collision restricts its performance due to the limited number of orthogonal-metadata sequences. On the other hand, non-orthogonal metadata can alleviate metadata collisions since it has a larger number of sequences, but its channel estimation would be affected due to non-orthogonality of metadata. Since it is expected to MTC handle a massive number of connections, the insufficient number of resources in a orthogonal metadata approach implies the usage of non-orthogonal metadata in GFRA. In the literature, there are works that address the GFRA in different ways. In [20], sparse sequences were used instead of binary sequences for data signal spreading in order to increase the number of MTC devices and allow device identification. With the aim to reduce the metadata collision and improve the GFRA throughput, the work in [21] suggests the usage of multiple resource blocks. In [22], another GFRA scheme was proposed where each device's chan-

[3]In the mMTC context, pilot sequences are also referred as "metadata". This thesis will use both nomenclatures.

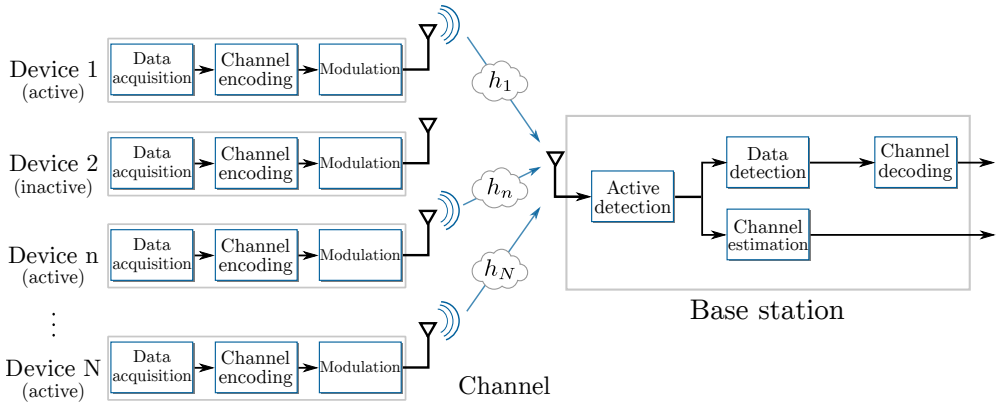


Figure 2.2: System model represented by a block diagram.

nel impulse response is used as a unique signature to differentiate signals that are simultaneously transmitted and the works in [18, 19] studies where the wireless signal of each device is spread by a unique sequence.

Using GFRA with non-orthogonal sequences, we have established a common system model to compare the performance of the detection algorithms. We define that when a device has data to transmit, it splits the codeword in multiple frames and transmit them in multiple transmission slots. In each time slot, each active device selects randomly a non-orthogonal metadata sequence from a predetermined codebook and sends the rest of the codeword. Since in practice the BS would have a list of devices that are associated with it, and their unique identifiers, we assume that the metadata sequences are known at the BS. Since these unique identifiers are known to the BS, the metadata sequence is also known at the BS. Given the sporadic activity of devices, they will communicate to the BS only when it is needed, so not all of them will be active during the same coherence time.

As illustrated in Fig. 2.2, in this chapter, it is considered that devices are synchronized in time[4], i.e., devices are turned on or turned off in the same transmission slot. This assumption is valid since the frame size of mMTC is typically very small (between 10 and 100 bytes) [16]. Thus, it is considered that the whole transmitted frame experience the same channel in such a way that

[4]Although this assumption implies an overhead increase, regarding the frame synchronization, it is commonly used in the literature.

the duration of a transmission slot ($\tau = \tau_\phi + \tau_x$) is smaller than the coherence time and coherence bandwidth of the channel. The time index $t$ indicates each transmitted vector in the same transmission slot. As we consider a grant-free random access model, each frame has metadata and data. Thus, the time index indicates how each frame is divided.

In a given coherence time, at the $t$-th symbol interval, the received signal $\mathbf{y}[t]$ is organized in a $M \times 1$ vector that contains the transmitted metadata ($\boldsymbol{\phi}[t]$) or the data ($\mathbf{x}[t]$), as

$$\mathbf{y}[t] = \begin{cases} \mathbf{H}\sqrt{\tau_\phi}\,\mathbf{B}\,\boldsymbol{\phi}[t] + \mathbf{v}[t], & \text{if} \quad 1 \leq t \leq \tau_\phi \\ \mathbf{H}\sqrt{\tau_x}\,\mathbf{B}\,\mathbf{x}[t] + \mathbf{v}[t], & \text{if} \quad \tau_\phi < t \leq \tau \end{cases} \tag{2-21}$$

where $\mathbf{H}$ is the $M \times N$ channel matrix, $\mathbf{B}$ is the $N \times N$ transmission power matrix, $\mathbf{v}$ is the $M \times 1$ noise vector, while $\tau_\phi$ and $\tau_x$ are the number of metadata and data symbols, respectively. For each time instant $t$, the metadata and data are represented by the $N \times 1$ vectors

$$\boldsymbol{\phi}[t] = \boldsymbol{\Delta}\,\boldsymbol{\varphi}[t] = [\delta_1\,\varphi_1[t], \ldots, \delta_N\,\varphi_N[t]]^T \text{ and} \tag{2-22}$$

$$\mathbf{x}[t] = \boldsymbol{\Delta}\,\mathbf{s}[t] = [\delta_1\,s_1[t], \ldots, \delta_N\,s_N[t]]^T, \tag{2-23}$$

where $\boldsymbol{\varphi}[t]$ and $\mathbf{s}[t]$ are $N \times 1$ vectors of symbols from a regular modulation scheme denoted by $\mathcal{A}$, as quadrature phase-shift keying (QPSK). The $N \times N$ diagonal matrix $\boldsymbol{\Delta}$ controls the activity of each device in the specific transmission slot with

$$\begin{cases} \Pr(\delta_n = 1) &= \rho_n, \\ \Pr(\delta_n = 0) &= 1 - \rho_n, \end{cases} \tag{2-24}$$

where $\rho_n$ is the probability of being active of the $n$-th device. Thus, each transmitted vector ($\boldsymbol{\phi}[t]$ or $\mathbf{x}[t]$) is composed by the augmented alphabet $\mathcal{A}_0$, where $\mathcal{A}_0 = \mathcal{A} \cup \{0\}$. The $N \times N$ diagonal $\mathbf{B}$ matrix gathers the transmission power component of each device, as in mMTC systems each MTCD has a

different power level [5, 16]. The noise vector $\mathbf{v}$ is modelled as an independent zero-mean complex-Gaussian $M \times 1$ vector with variance $\sigma_v^2$.

The block fading model is adopted, where the values change independently from slot to slot, that is, the channel is constant over a transmission slot duration. The $M \times N$ channel matrix $\mathbf{H}$ corresponds to the channel realizations between the BS and devices as modeled by

$$\mathbf{H} = \mathbf{A}\,\boldsymbol{\Upsilon}^{1/2}, \tag{2-25}$$

where $\mathbf{H}$ gathers independent fast fading, geometric attenuation and log-normal shadow fading. $\mathbf{A}$ is the $M \times N$ matrix of fast fading coefficients circularly symmetric complex Gaussian distributed, with zero mean and unit variance. It is also considered the effects of path loss and shadowing experienced by each MTCD, modelling them in the $N \times N$ diagonal matrix $\boldsymbol{\Upsilon}$, where each component is given by $\beta = 10\log_{10}(\chi) + \omega$, where $\chi$ is the signal-to-noise ratio (SNR) and $\omega$ is a Gaussian random variable with zero mean and variance $\sigma_\omega^2$ [98]. Thus, each vector $\mathbf{h}_n$ can be written as

$$\mathbf{h}_n = \mathbf{a}_n\sqrt{\beta_n}, \quad \forall n = 1, \ldots, N. \tag{2-26}$$

The $\beta_n$ coefficients are assumed to be known at the BS and changes very slowly, reaching a new value just in a new transmission slot. Given the features of mMTC scenarios, the number of devices $N$ is larger than that of antennas $M$ at the base station, in a way that it consists of an underdetermined system. All signal model parameters are described in Table 2.1.

### 2.3.2 Key Performance Indicators

To evaluate the performance of detection techniques, we consider three key performance indicators (KPI):

- The **Frame Error Rate** (FER) denotes the total number of frames incorrectly detected by the BS;

- The **Missed Detection Rate** (MDR) denotes the total number of symbols that have been transmitted in a specific time instant that the detector judged as zero, divided by the number of active devices;
- The **False Alarm Rate** (FAR) is the number of symbols detected as different from zero, divided by the difference between the total number of devices and the number of active devices at a time instant;

Considering $S_{\mathbf{x}}$ as the true support set, that is, the list of active devices in $\mathbf{x}$, a Venn diagram in Fig. 2.3 represents the key performance indicators. For the techniques that perform channel estimation, we evaluate the efficiency by the normalized mean-squared error (NMSE).

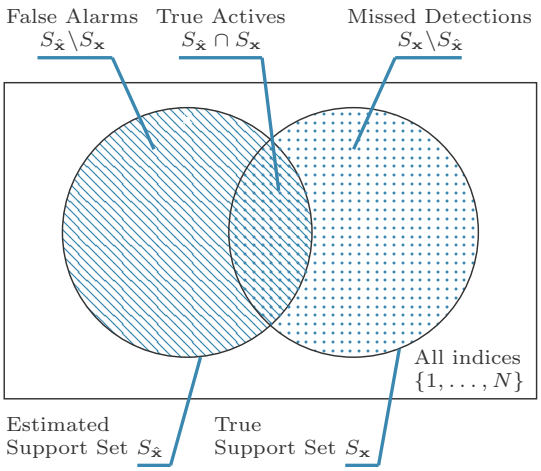


Figure 2.3: Venn Diagram of False Alarm and Missed Detection Errors.

### 2.3.3 General Simulation Parameters

In order to evaluate the performance of the cited algorithms, we consider $N = 128$ MTCDs connected to a single base-station equipped with $M = 64$ antennas. The evaluated solutions experience an independent and identically-distributed (i.i.d.) random flat-fading channel model and the values $a_{m,n}$ of (2-26) are taken from complex Gaussian distribution of $\mathcal{N}_c(0, 1)$. When the device is active, it radiates QPSK symbols with power values drawn uniformly at random in 0.1 W to 0.3 W and the probability of being active of each device

$\rho_n$ is drawn uniformly at random in $[0.1, 0.3]$. Each frame has 256 symbols, split into 128 pilots and 128 data symbols. This balance between pilots and data is suggested in [52].

Table 2.1: Description of mMTC signal model parameters.

| Parameter | Description |
|---|---|
| $M$ | Number of base station antennas; |
| $N$ | Number of devices; |
| $K$ | Number of active devices; |
| $\tau$ | Number of transmitted symbols per trans. slot, given by $\tau = \tau_x + \tau_\phi$, where $\tau_x$ represents the data and $\tau_\phi$ the metadata; |
| $\rho_n$ | Random variable with a beta distribution that represents the probability of being active of the $n$-device; |
| $\mathbf{y}[t]$ | $M \times 1$ received symbol vector of the time instant $t$; |
| $\boldsymbol{\phi}[t]$ | $N \times 1$ metadata vector of the time instant $t$ composed by the augmented alphabet $\mathcal{A}_0$; |
| $\mathbf{x}[t]$ | $N \times 1$ data vector of the time instant $t$ composed by the augmented alphabet $\mathcal{A}_0$; |
| $\boldsymbol{\Delta}$ | $N \times N$ diagonal matrix that controls each device activity in the specific transmission slot; |
| $\mathbf{B}$ | $N \times N$ diagonal matrix that gathers the transmission power of each device; |
| $\mathbf{v}[t]$ | noise component, modelled as a independent zero-mean complex-Gaussian $M \times 1$ vector with variance $\sigma_v^2$; |
| $\mathbf{H}$ | $M \times N$ channel matrix, where $\mathbf{H} = \mathbf{A}\,\boldsymbol{\Upsilon}^{1/2}$; |
| $\mathbf{A}$ | $M \times N$ matrix of fast fading coefficients; |
| $\boldsymbol{\Upsilon}$ | $N \times N$ diagonal matrix that gathers the path loss and shadowing experienced by each device; |

### 2.3.4 Joint Activity and Data Detection Techniques

In this section we present and compare relevant state-of-the-art algorithms divided in four different classes of detectors: regularized, greedy, message-passing and machine learning based. First, we start with the algorithms that aim to perform activity and data detection, discussing the results based on the KPIs.

#### 2.3.4.1 Regularized Detectors

In order to perform MAP detection of the mMTC sparse problem, the Sparse Maximum a Posteriori Probability (S-MAP) detection was proposed in [26]. This work was the first that applied a regularization parameter into the cost function, inspiring the following works to propose suboptimal algorithms. The authors of [26] considered a simplified version of (2-21), that ignores the number of symbols, transmission power and time instant, as given by

$$\mathbf{y} = \mathbf{H}\mathbf{x} + \mathbf{v}. \tag{2-27}$$

Recalling that $\mathcal{A}_0$ is the augmented modulation alphabet and $\rho_n$ the activity probability for the $n$-device, [26] described the prior distribution of $\mathbf{x}$ as

$$\Pr(\mathbf{x}) = \prod_{n=1}^{N} \Pr(x_n) = \prod_{n=1}^{N} (1-\rho_n)^{1-|x_n|_0} \left(\frac{\rho_n}{|\mathcal{A}|}\right)^{|x_n|_0}, \tag{2-28}$$

where $|\mathcal{A}|$ is the cardinality of the modulation alphabet and $|x_n|_0$ is the element-wise $l_0$-norm that is equal to 1 if $x_n$ is a non-zero value, otherwise it is zero. The output of the S-MAP detector maximizing the *a posteriori* probability $\Pr(\mathbf{x}|\mathbf{y})$ is given by Bayes' rule as

$$\hat{\mathbf{x}} = \underset{\mathbf{x}\in\mathcal{A}_0^N}{\arg\max} \Pr(\mathbf{x}|\mathbf{y}) = \underset{\mathbf{x}\in\mathcal{A}_0^N}{\arg\min} \; -\ln\Pr(\mathbf{y}|\mathbf{x}) - \ln\Pr(\mathbf{x}), \tag{2-29}$$

which leads to

$$\hat{\mathbf{x}} = \underset{\mathbf{x}\in\mathcal{A}_0^N}{\arg\min} \frac{1}{2}\|\mathbf{y}-\mathbf{H}\mathbf{x}\|_2^2 + \sigma_v^2 \sum_{n=1}^{N} \lambda_n |x_n|_0, \tag{2-30}$$

where $\lambda_n = \ln\left[(1-\rho_n)/(\rho_n/|\mathcal{A}|)\right]$ is the regularization parameter for the $n$-th symbol detection.

As the main objective of the S-MAP detection is to find a vector in $\mathcal{A}_0^N$ that maximizes the cost function in (2-30), naturally, the complexity of S-MAP is tremendous. In [26] itself the authors propose two relaxing approaches, called Ridge detector (RD) and Lasso detector. RD regularizes

the least squares (LS) solution using the $l_2$-norm, while LD uses the $l_1$-norm.

*SA-SIC*

For the sake of achieving an acceptable detection performance with much lower complexity compared to other optimal but complex S-MAP detectors, the work in [27] proposed the sparsity-aware successive interference cancellation (SA-SIC). Considering that the BS has the perfect knowledge of probability of being active of each device and perfect CSI, SA-SIC recovers transmitted symbols in a sequential manner, incorporating the regularization into the problem. As SA-SIC uses the QR decomposition of $\mathbf{H} = \mathbf{QR}$, we have

$$\hat{\mathbf{x}} = \underset{\mathbf{x} \in \mathcal{A}_0^N}{\arg\min} \frac{1}{2} \sum_{n=1}^{N} \left[ \left| \tilde{y}_n - \sum_{l=n}^{N} R_{nl} x_l \right|^2 + \sigma_v^2 \lambda_n |x_n|_0 \right], \tag{2-31}$$

where $\tilde{\mathbf{y}} = \mathbf{Q}^H \mathbf{y}$. Like any SIC technique, SA-SIC is sensitive to the error propagation from the early layers. Therefore, ordering techniques should be applied to mitigate the error propagation.

*SA-SIC with A-SQRD*

Considering the same assumptions of the SA-SIC, the authors of [29] proposed a permutation of columns of channel matrix $\mathbf{H}$ based on channel gains. The idea of SA-SIC with A-SQRD is to replace the $l_0$-norm with the $l_2$-norm in (2-30), incorporate the regularization factor into the channel matrix $\mathbf{H}$, as

$$\hat{\mathbf{x}} = \underset{\mathbf{x} \in \mathcal{A}_0^N}{\arg\min} \frac{1}{2} \left\| \begin{bmatrix} \mathbf{y} \\ \mathbf{0}_N \end{bmatrix} - \underbrace{\begin{bmatrix} \mathbf{H} \\ \sigma_v \operatorname{diag}\left(\sqrt{\boldsymbol{\lambda}}\right) \end{bmatrix}}_{\mathbf{H}'} \mathbf{x} \right\|_2^2, \tag{2-32}$$

find the QR decomposition of the augmented $\mathbf{H}'$, employ the modified Gram-Schmidt algorithm [99] and reorder the columns of $\mathbf{H}'$ before each orthogonalization step.

*AA-MF-SIC*

Focusing on the filter refinement, we incorporated an $l_1$-norm regularization in the linear MMSE filter ($\mathbf{W}$) and a constellation-list scheme to increase the detection performance [30]. The main idea of the AA-MF-SIC algorithm is to iteratively update the regularized linear MMSE filter at each new symbol detection $n$, as

$$\mathbf{w}_n = \left(\overline{\mathbf{H}}_n \overline{\mathbf{H}}_n^H + \frac{\sigma_v^2}{\sigma_x^2}\mathbf{I} + \frac{2\lambda_n}{\sigma_x^2}\Lambda\right)^{-1} \overline{\mathbf{H}}_n \boldsymbol{\delta}_n, \tag{2-33}$$

where $\Lambda = \text{diag}\left\{\frac{1}{|w_{n,1}|+\epsilon}, \frac{1}{|w_{n,2}|+\epsilon}, \ldots, \frac{1}{|w_{n,M}|+\epsilon}\right\}$, $\boldsymbol{\delta}_n$ is a $N \times 1$ zero column vector with 1 at the $n$-th position and $\lambda_n$ is the regularization parameter defined by [26]. As this algorithm also performs the successive interference cancellation, $\overline{\mathbf{H}}_n$ denotes the matrix obtained by taking the columns $n, n+1, \ldots, N$ of the channel.

As it is precisely described in the next chapter, we included in order to avoid the error propagation a constellation-list scheme to evaluate the reliability of each soft symbol estimate. In a nutshell, the constellation-list consists of a shadow area constraint with the augmented alphabet of a modulation scheme, that compares the distance between the soft estimate and all the possible constellation symbols. If the soft estimate is considered reliable, it is just quantized ($\mathcal{Q}[\cdot]$) to the nearest symbol of $\mathcal{A}_0$, as $\tilde{x}_n = \mathcal{Q}\left[\mathbf{w}_n^H \mathbf{y}_n\right]$. Otherwise, $\tilde{x}_n$ proceeds to the list scheme as given by

$$\kappa_{\text{opt}} = \underset{i \in 1,\cdots,|\mathcal{A}_0|}{\arg\min} \|\mathbf{y}_n - \mathbf{h}_n \mathcal{A}_{0_i}\|^2, \tag{2-34}$$

where $\mathbf{y}_n$ is the received vector after the SIC operation and the vector $\mathbf{h}_n$ contains the estimate of the channel between the device that performs symbol detection and the BS. The index $\kappa_{\text{opt}}$ indicates which candidate of the list $\mathcal{A}_{0_i}$ will replace the quantized version of the unreliable soft symbol estimate $\tilde{x}_n$. After the detection, the algorithm proceeds with SIC.

*AA-RLS-DF*

Since prior techniques do not perform channel estimation, our work in [50] builds on previous decision feedback techniques [93,100] and proposes a scheme with implicit channel estimation. Since this solution is detailed in Chapter 3, here it is just introduced in order to be compared in this technical background chapter.

The AA-RLS-DF uses a regularized recursive least squares (RLS) adaptive algorithm that relies on the metadata to update the weights. The detection order is updated at each new layer, using the least squares estimation (LSE) criterion. The adaptive receive filter is decomposed into feedforward and feedback filters, where the feedforward one is updated at every new received vector by the $l_0$-norm regularized RLS algorithm and the feedback filter is a component that is concatenated to the feedforward filter in order to cancel the interference of the previously detected symbols.

In order to exploit the sparsity scenario, the detection order is updated with the minimum argument of the $l_0$-norm regularized cost function. After a few steps, the $l_0$-norm regularized RLS adaptive expression becomes

$$\mathbf{w}_j[t] = \mathbf{w}_j[t-1] + \mathbf{k}[t]\,\epsilon_n^*[t] - \gamma\,\xi\,\mathrm{sgn}\left(w_{j,p}[t]\right) f_\xi\left(w_{j,p}[t]\right), \tag{2-35}$$

where $\mathbf{k}$ is the gain vector, $\xi$ is a positive parameter that regulates the range of the attraction to zero on small coefficients of the filter and $\gamma$ is a non-zero positive constant to balance the regularization and, consequently, the estimation error. After the filters weights are computed with the metadata symbols, the algorithm uses the same procedure to compute the data soft estimates.

*Performance evaluation*

Fig. 2.4, shows the Frame Error Rate (FER) performance averaged over $10^5$ runs. Considering the average SNR as $10\log\left(N\,\sigma_x^2/\sigma_v^2\right)$, the linear mean

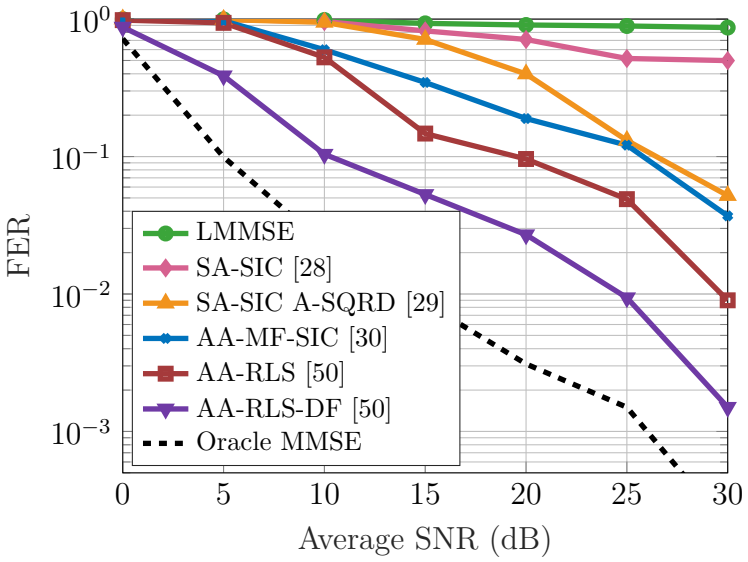


Figure 2.4: Frame error rate vs. Average SNR. Comparison of regularized algorithms for $N = 128$, $M = 64$ with $\rho_n$ drawn uniformly at random in $[0.1, 0.3]$. $10^5$ Monte Carlo trials.

squared error (LMMSE), unsorted SA-SIC [28], SA-SIC with A-SQRD [29], AA-MF-SIC [30], AA-RLS [50] and AA-RLS-DF [50] are compared under the general simulation parameters described in Subsection 2.3.3. As a lower bound, the Oracle LMMSE detector, which has the knowledge of the index of nonzero entries, is considered. Since the schemes of [50] do not require explicit channel state information, in order to perform a fair comparison, we take into account an imperfect channel estimation to the other approaches. We considered $\hat{\mathbf{H}} = \mathbf{H} + \mathbf{E}$, where $\mathbf{H}$ represents the channel estimate and $\mathbf{E}$ is a random matrix corresponding to the error for each link. Each coefficient of the error matrix follows a Gaussian distribution, i.e., $\sum \mathcal{N}_c(0, \sigma_e^2)$ where $\sigma_e^2 = \sigma_v^2/5$.

As the linear MMSE is not designed for the sparse scenario, it presents a poor performance. The unsorted SA-SIC is susceptible to error propagation, thus it does not perform well. A-SQRD and AA-MF-SIC are effective since both consider the activity probabilities, but under imperfect CSI conditions, their performance strongly degrades. On the other hand, as AA-RLS and AA-RLS-DF do not need an explicit channel estimation, they are more efficient. The

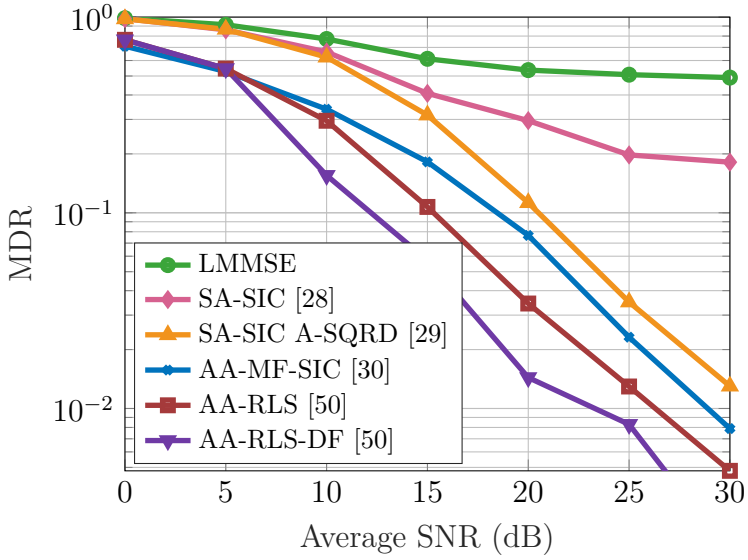


(a) Missed detection rate vs. Average SNR.

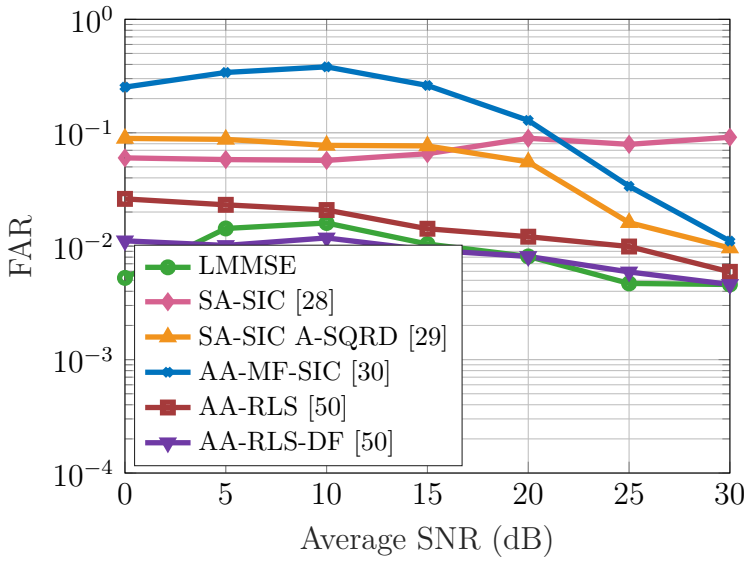


(b) False alarms rate vs. Average SNR.

Figure 2.5: Activity error rates for comparison of regularized algorithms. Simulation parameters: $N = 128$, $M = 64$ with $\rho_n$ drawn uniformly at random in $[0.1, 0.3]$. $10^5$ Monte Carlo trials.

interference cancellation performed by the decision-feedback scheme leads to an evident FER gain. The activity error rates are shown in Figs. 2.5a and 2.5b, much of the FER gain of the schemes of [50] is due to the high activity detection accuracy of the regularized RLS filters illustrated by the MDR performance.

#### 2.3.4.2 Greedy Detectors

Widely studied in the compressive sensing field, greedy algorithms have been applied as potential solutions to mMTC activity and data detection. As this approach has low complexity and generally only requires termination tuning, that is, the termination of the transmitted vector has to be adapted for the specific problem instance in order to avoid inaccurate results. The pioneering work [40] applied the well-known OLS and OMP algorithms to an uplink sparse scenario as mMTC. As OMP has a better performance, a lot of improvements of it are available in the literature and some of them were specifically designed for mMTC.

*wGOMP*

Drawing inspiration from the block-sparse variant of OMP, the GOMP [44], the authors in [42] propose an improvement where they refine the activity detection, exploiting the channel code. Considering perfect CSI and that the BS has the knowledge of the number of active devices, structuring the receiver in an iterative feedback approach, the main idea of wGOMP is to pass weights $\mathbf{w}$ based on the channel decoding output to the multiuser detection. Repeating iterations until $\mathbf{w}$ values no longer change and the feedback process has converged, at each new step, the weights give the likelihood of activity for each node, improving the activity decision. The weights are introduced in each correlation in the block selection step of GOMP, as

$$\tilde{k} = \underset{k \in \overline{\mathcal{B}}^{(u-1)}}{\arg\max} \frac{1}{|\gamma(k)|} \sum_{j \in \gamma(k)} \mathbf{w}_{\{j\}} \frac{|\mathbf{H}_{\{j\}}^{H} \mathbf{r}^{(u-1)}|}{\|\mathbf{H}_{\{j\}}\|_2}, \tag{2-36}$$

where $k$ is the index of the block, $\mathbf{r}$ is the residual, $u$ the iteration index and $\mathbf{H}$ is the channel matrix. The list of inactive devices given by $\mathcal{B}$ and $\gamma$ is the part of the channel matrix that should be considered. These weights allow the choice of devices which are likely active, due to information from channel coding. If no weights are applied, ($\mathbf{w} = 1$), the wGOMP and GOMP are identical.

In order to reduce the complexity of the problem, the work in [42] also considers independent subproblems. The main idea is to apply parallel CS-MUD detectors to each subproblem, detecting each part of the transmitted vector separately. Once all parts have been detected, the estimated symbols can be sorted per node, resulting in the node-specific data vectors, later decoded by the channel decoder.

*bcSIC*

In order to improve the last approach, the authors in [43] incorporate the most likely codeword in the iterative feedback scheme. Known as block-correlation SIC (bcSIC), the idea is to compute the activity estimation as in wGOMP and performs the LS estimation for the chosen node $\tilde{k}$ followed by the channel decoding for this node. Subsequently, the residual is updated with the most likely codeword of node $\tilde{k}$ for interference cancellation, as

$$\mathbf{r}^{(u)} = \mathbf{r}^{(u-1)} - \mathbf{H}_{\{\gamma(\tilde{k})\}}\hat{\mathbf{d}}_{\tilde{k}} \tag{2-37}$$

where, due to this modification, the estimates $\tilde{\mathbf{d}}_k = \mathbf{H}^{\dagger}_{\{\gamma(k)\}}\mathbf{r}^{(u-1)}$ are never re-evaluated, unlike wGOMP that performs an LS estimation for all active nodes $\mathcal{B}^{(u)}$ in each iteration.

*mSOMP-EXT*

Drawing inspiration in other modification of the OMP, the simultaneous orthogonal matching pursuit (SOMP) [101] with extrinsic information transfer (SOMP-EXT) [102], the work in [103] developed an algorithm that performs the joint activity and data detection with no prior knowledge of sparsity and noise levels, just the channel gains. Named mSOMP-EXT [103], this algorithm computes the average LLR of each $n$-th device, where $\mathcal{L}\left(z_{l,n}^{(t)}\right) = \log\left(\Pr\left[z_{l,n}^{(t)} \,|\, n \in \mathcal{S}\right] / \Pr\left[z_{l,n}^{(t)} \,|\, n \notin \mathcal{S}\right]\right)$. $\mathcal{S}$ indicates the list of active devices, $\tau$ is the number of symbols in the frame and $t$ is the time index. The scheme

repeats until $l$ is an iteration marker surpasses the number of subcarriers $M$. As part of the essence of SOMP-EXT, the LLR creates and transfers the extrinsic information through iterations to support detection as, $\forall n \in \{1,\ldots,2N\}\backslash\hat{\mathcal{S}}_{l-1}$,

$$Z_{l,n} = \frac{1}{\tau}\sum_{t=1}^{\tau}\mathcal{L}\left(z_{l,n}^{(t)}\right), \quad (2\text{-}38) \qquad A_{l,n} = \begin{cases} 0 & ,\text{if } l=1, \\ \frac{(\tau-1)}{l-1}\sum_{l'=1}^{l-1} Z_{l',n} & ,\text{if } l \geq 2 \end{cases}, \quad (2\text{-}39)$$

and $\Lambda_{l,n} = Z_{l,n} + (\tau-1)\, Z_{l,n} + A_{l,n}$. As this scheme works with real values, the estimated support list $\hat{\mathcal{S}}_l$ has $2N$ elements, which is updated as follows

$$\hat{\mathcal{S}} = \quad (2\text{-}40)$$
$$\hat{\mathcal{S}}_{l-1} \bigcup \left\{ \underset{n\,\in\,\{1,\cdots,N\}\backslash\hat{\mathcal{S}}_{l-1}}{\arg\max} \left(\Lambda_{l,n} + \Lambda_{l,n+N}\right), \underset{n\,\in\,\{1,\cdots,N\}\backslash\hat{\mathcal{S}}_{l-1}}{\arg\max} \left(\Lambda_{l,n} + \Lambda_{l,n+N}\right) + N \right\}.$$

Using the estimated list of active devices, the soft estimation and the residual are computed as $\tilde{\mathbf{x}}_{\hat{\mathcal{S}}_l}^{(t)} = (\mathbf{H}_{\hat{\mathcal{S}}_l}^{(t)})^{\dagger}\mathbf{y}^{(t)}$ and $\mathbf{r}_l^{(t)} = \mathbf{y}^{(t)} - \mathbf{H}_{\hat{\mathcal{S}}_l}^{(t)}\tilde{\mathbf{x}}_{\hat{\mathcal{S}}_l}^{(t)}$. In the next iteration, the vector $z_{l,n}^{(t)}$ is computed using the last residual and the procedure repeats.

The authors in [103] used an LLR approximation in order to not require the knowledge of the sparsity level $K$ and the noise variance $\sigma_v^2$. As in the work [103] was considered $\Upsilon$-ary QAM symbols, the following LLR approximation is taken into account:

$$\mathcal{L}\left(z_{l,n}^{(t)}\right) \quad (2\text{-}41)$$
$$= \log\left(\frac{1}{\sqrt{\Upsilon}}\sum_{\upsilon=0}^{\sqrt{\Upsilon}-1}\frac{1}{\sqrt{2\pi}\sigma_{l,1}}\exp\left(-\frac{\left(z_{l,n}^{(t)}-q_\upsilon\right)^2}{2\sigma_{l,1}^2}\right)\Big/\frac{1}{\sqrt{2\pi}\sigma_{l,0}}\exp\left(-\frac{\left(z_{l,n}^{(t)}\right)^2}{2\sigma_{l,0}^2}\right)\right),$$

where $q_\upsilon = \frac{2\upsilon-\sqrt{\Upsilon}+1}{\sqrt{2}}$, $\upsilon = (0,1,\ldots,\sqrt{\Upsilon}-1)$, is the in-phase component of an $\Upsilon$-ary QAM symbol that corresponds to a nonzero element of $\tilde{\mathbf{x}}^{(t)}$. For a sufficiently large number of subcarriers $M$, $\sigma_{l,0}^2$ and $\sigma_{l,1}^2$ are approximated as $\sigma_{l,0}^2 \approx \sigma_{l,1}^2 \approx \sigma_x^2$, where $\sigma_x^2 = \frac{1}{\sqrt{\Upsilon}}\sum_{\upsilon=0}^{\sqrt{\Upsilon}-1} q_h^2 = \frac{\Upsilon-1}{6}$ is the average power of nonzero elements of $\mathbf{x}^{(t)}$. This LLR approximation and a threshold parameter

empirically obtained for a stopping criterion, composes the modification of mSOMP-EXT.

*TA-BSASP*

An improvement of the classical subspace pursuit (SP) algorithm is presented in [46]. The threshold aided block sparsity adaptive subspace pursuit (TA-BSASP) reconstructs the sparse vector by exploiting the inherent block sparsity, as the authors vectorized all data transmitted in different time slots. TA-BSASP uses a stopping criterion based on the AWGN noise, given by

$$\min \left\{ \left\| \tilde{\mathbf{c}}^{(l)} [m] \right\|_2^2 \right\} \leq \tau \, P_{th}, \tag{2-42}$$

where $\tilde{\mathbf{c}}^{(t)}$ is the estimated solution of the vectorized transmitted vector, $m$ is an index of the support set, $\tau$ is the number of elements in the same block and $P_{th}$ is the AWGN noise floor, selected experimentally. Until the stopping criterion is met, TA-BSASP updates the support estimate list, with the time index $t$, as

$$\Lambda = \Gamma^{(t-1)} \bigcup \Xi \left( \| \mathbf{D}^H [n] \, \mathbf{r}^{(t-1)} \|_2, s \right), \quad \forall \, n = 1, 2, \ldots, N \tag{2-43}$$

where $\Xi$ is a set, whose elements are the indices of the largest $s$ elements of its argument. $s$ is initialized as one and determines how many devices the algorithm will deal per iteration. $\mathbf{D}$ is a sparse version of the channel matrix $\mathbf{H}$, given by

$$\mathbf{D} = \begin{bmatrix} H(1,1)\,\mathbf{I}_\tau & H(1,2)\,\mathbf{I}_\tau & \ldots & H(1,\tau N)\,\mathbf{I}_\tau \\ H(2,1)\,\mathbf{I}_\tau & H(2,2)\,\mathbf{I}_\tau & \ldots & H(2,\tau N)\,\mathbf{I}_\tau \\ \vdots & \vdots & \ddots & \vdots \\ H(N,1)\,\mathbf{I}_\tau & H(N,2)\,\mathbf{I}_\tau & \ldots & H(N,\tau N)\,\mathbf{I}_\tau \end{bmatrix} = \mathbf{H} \otimes \mathbf{I}_\tau. \tag{2-44}$$

Following this step, TA-BSASP computes the LS estimate $\mathbf{w}$ of the set $\Lambda$ and performs support pruning, as

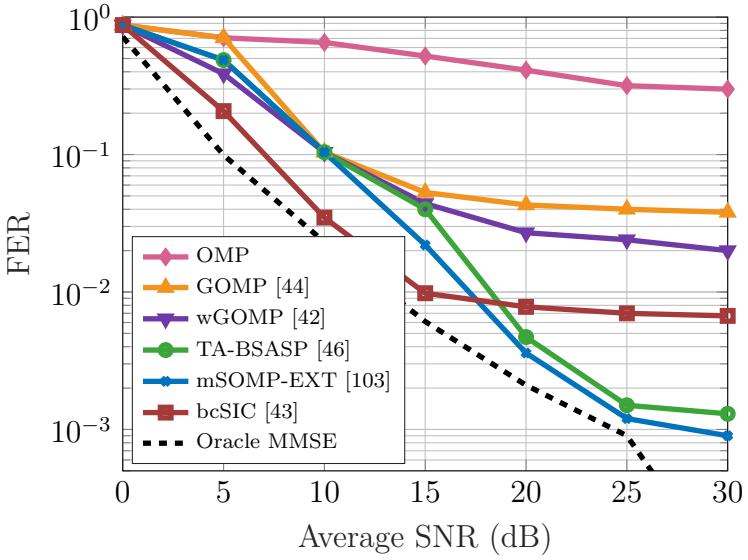


Figure 2.6: Frame error rate vs. Average SNR. Comparison of greedy algorithms for $N = 128$, $M = 64$ with $\rho_n$ drawn uniformly at random in $[0.1, 0.3]$. $10^5$ Monte Carlo trials.

$$\hat{\Gamma}^{(t)} = \Xi\left(\|\mathbf{w}\left[n\right]\|_2, s\right), \quad \forall\, n = 1, 2, \ldots, N. \tag{2-45}$$

Then, the algorithm proceeds with the signal estimate $\tilde{\mathbf{c}}^{(t)}\left[\hat{\Gamma^{(t)}}\right]$, update of residual $\mathbf{r}^{(t)}$ and if $\|\mathbf{r}^{(t)}\|_2 < \|\mathbf{r}^{(t-1)}\|_2 <$, the support pruning is updated $(\Gamma^{(t)} = \hat{\Gamma}^{(t)})$ as the iterative index $(t = t + 1)$. Otherwise, the sparsity level is updated, with $s = s + 1$. When the stopping criteria in (2-42) is met, the algorithm stops and the data are recovered.

*Performance evaluation*

In order to verify the efficiency of the greedy algorithms, we modify the system model of (2-21), as the schemes do not consider the metadata, but include in the signal model spreading sequences. In this way, the general received vector for this performance analysis is given by

$$\mathbf{y}^{(t)} = \sum_{n=1}^{N} \mathrm{diag}\left(\mathbf{h}_n^{(t)}\right)\mathbf{s}_n x_n^{(t)} + \mathbf{v}^{(t)} = \mathbf{G}^{(t)}\mathbf{x}^{(t)} + \mathbf{v}^{(t)}, \tag{2-46}$$

where at a time slot $l$ $(1 \leq l \leq \tau)$, a transmitted symbol $x_n^{(t)}$ of active user $n$ is spread onto $M$ subcarriers using a unique spreading sequence $\mathbf{s}_n \in \mathbb{C}^M$. The channel gain $h_{m,n}$ and noise vector are computed as described in Subsection

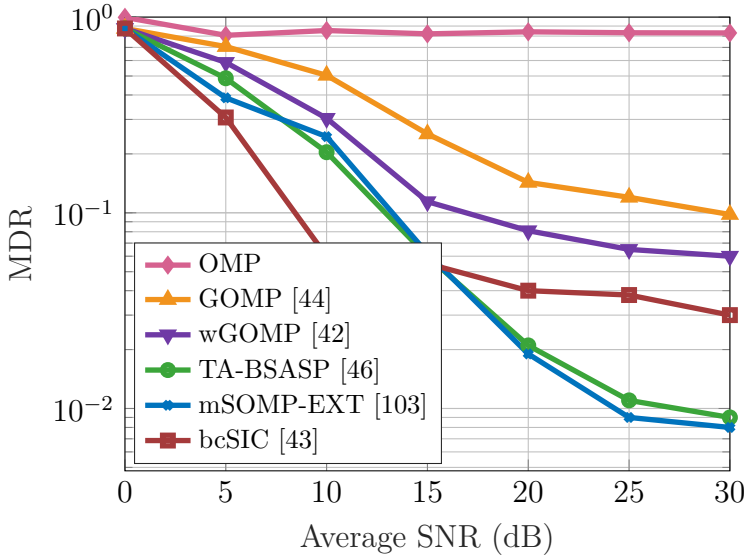


(a) Missed detection rate vs. Average SNR.

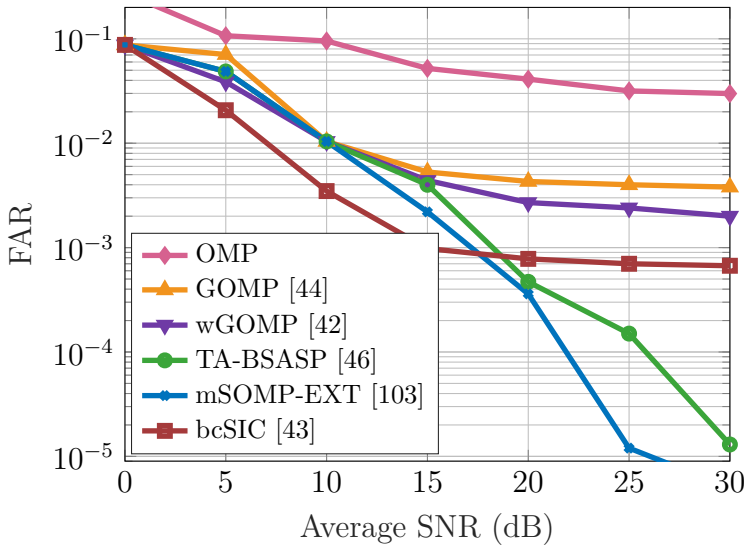


(b) False alarms rate vs. Average SNR.

Figure 2.7: Activity error rates for comparison of greedy algorithms. Simulation parameters: $N = 128$, $M = 64$ with $\rho_n$ drawn uniformly at random in $[0.1, 0.3]$. $10^5$ Monte Carlo trials.

2.3.3, as the other simulation parameters.

For simplicity, we assume as a stopping criterion for wGOMP and bcSIC the number of active devices, even if this is unrealistic. For mSOMP-EXT we choose $v_{th} = -0.4$, as in [103]. In TA-BSASP, the $P_{th}$ used for the stopping criterion is the same as in [46], $0.68, 0.51, 0.48, 0.38,$ and $0.28$, respectively, at

the SNR of 0 dB, 2 dB, 4 dB, 6 dB, 8 dB.

As none of the greedy solutions perform channel estimation, for this comparison we considered perfect CSI. The Frame Error Rate (SER) performance averaged over $10^5$ runs is depicted in Fig. 2.6. Although wGOMP and bcSIC originally use channel coding, we do not use it so that the comparison with other techniques is fair. As each frame has 128 data symbols, we divided wGOMP in $N_{\text{subp}} = 16$ subproblems, thus considering 8 symbols for each device ($\tau_{\text{seg}} = 128/N_{\text{subp}} = 8$).

It is possible to observe that the well-known OMP has the worst performance, as it does not include any refined activity detection scheme. As wGOMP exploits block-sparsity across all subproblems via the feedback of activity estimation based on the output of the channel decoding (or quantization of the soft estimation) wGOMP has a lower FER than GOMP for high SNRs. Since each subproblem only considers changed partial block-sparsity, it enables the correction of some activity errors in the feedback process. The interference cancellation incorporated in bcSIC algorithm reduces its FER comparing to wGOMP and reaches the error floor, due to error propagation, in a low SNR value, approaching the curve to the lower bound. Showing better results in high SNRs, mSOMP-EXT and TA-BSASP have worse performance than bcSIC for low SNR due to poor activity detection compared to the bcSIC as seen in Figs. 2.7a and 2.7b. We can also conclude that the FER performance of OMP, GOMP and wGOMP are primarly limited by activity errors, while bcSIC is primarily limited by error propagation.

#### 2.3.4.3 Message-Passing Detectors

Initially proposed by Donoho, Maleki and Montanari [34, 104, 105], the application of factor graphs to CS problems inspired many other works. As this class of iterative thresholding algorithms considers the posteriori distribution of the signal to be reconstructed, the usage of factor graphs to marginalize the

joint probability distribution of the received vector enabled its application in the communications area.

*Non-coherent scenario*

The works in [36] and [55] propose a modification in the AMP in a non-coherent transmission scenario. The main idea of the non-coherent approach is that the transmitted data bits are embedded in the index of the transmitted pilot sequence of each active device. Therefore, if the algorithm correctly detects the active devices, consequently it will detect the data. The disadvantage of this method is that the BS is required to allocate for each device not just one metadata sequence per frame, but a set of $2^J$ sequences when $J$ bits are transmitted by each device. Due to the massive number of devices requiring connection at the same time and non-orthogonal metadata sequences, the probability of two devices having identical sequences is seen as the probability of frame collisions, which should be taken account in the performance. Considering a system model similar to (2-21), both works [36] and [55], incorporate the sparsity not only in the transmitted vector, but in the channel matrix. In this way, the sparse structure of $\mathbf{H}$ has the rows corresponding to inactive users are zero. Thus, the activity detection problem reduces to finding the non-zero rows of the channel matrix $\mathbf{H}$. In this way, the signal model in this case is given by

$$\mathbf{Y} = \sqrt{\tau_\phi}\mathbf{\Phi}\mathbf{H} + \mathbf{V}, \tag{2-47}$$

where the metadata $\mathbf{\Phi}$ and channel $\mathbf{H}$ matrices are

$$\mathbf{\Phi} = [\mathbf{\Phi}_1, \ldots, \mathbf{\Phi}_N] \in \mathbb{C}^{\tau \times N2^J} \text{ and } \mathbf{H} = [\mathbf{H}_1, \ldots, \mathbf{H}_N]^T,$$

in which the channel matrix between the $n$-th device and the BS is $\mathbf{H}_k = \left[\delta_{k,1}\mathbf{h}_k, \ldots, \delta_{k,2^J}\mathbf{h}_k\right] \in \mathbb{C}^{M \times 2^J}$ and $\delta$ is the parameter that defines if the $n-$th device is active or inactive, as in (2-22). Due to the rewritten

signal model, the channel matrix now has $2^J$ more rows than the previous one but with the same number of active devices, which increases the sparsity level of the system. In order to exploit these properties, the works in [36] and [55] proposes a modified AMP algorithm.

*M-AMP*

The authors in [36] presents the M-AMP where, for the active device $n$, the estimate of the row of $\overline{\mathbf{H}} = \left[\overline{\mathbf{h}}_{k,1}, \ldots, \overline{\mathbf{h}}_{k,2^J}\right] \in \mathbb{C}^{M\times 2^J}$ corresponding to the $i$-th metadata sequence is $\hat{\overline{\mathbf{h}}}_{k,i}$, with $\overline{\mathbf{h}}_{k,i} = \delta_{k,i}\mathbf{h}_k$. Then, with the $k$-th device transmitting the pilot sequence $i'$, the estimate is

$$\overline{\mathbf{h}}_{k,i}^{l} = \begin{cases} \left(\mathbf{h}_k + \left(\boldsymbol{\Sigma}^{l}\right)^{\frac{1}{2}}\mathbf{w}\right) \sim \mathcal{N}_c\left(0, \eta_k\mathbf{I} + \boldsymbol{\Sigma}^{l}\right), & i = i', \\ \left(\left(\boldsymbol{\Sigma}^{l}\right)^{\frac{1}{2}}\mathbf{w}\right) \sim \mathcal{N}_c\left(0, \boldsymbol{\Sigma}^{l}\right), & i \neq i'. \end{cases} \tag{2-48}$$

where the update of the state evolution is given by $\boldsymbol{\Sigma}^{l+1} = \frac{\sigma_v^2}{\tau_\phi}\mathbf{I} + \frac{N}{\tau_\phi}\mathbb{E}\{\mathbf{e}\mathbf{e}^H\}$, $\mathbf{e} = \eta(\mathbf{h}_\beta - (\boldsymbol{\Sigma}^{l})^{\frac{1}{2}}\mathbf{w}) - \mathbf{h}_\beta$ and $\mathbf{w}$ is a complex Gaussian vector with unit variance and $t$ is the iteration index. $\mathbf{h}_\beta$ has the following distribution:

$$p_{\mathbf{h}_\beta} = (1-\rho)\,\delta + \rho\mathcal{N}_c(0, \beta\mathbf{I}), \tag{2-49}$$

$\mathcal{N}_c(0, \beta\mathbf{I})$ is the distribution of the channel vector of the active device and $\delta$ is the dirac Delta at zero corresponding to the inactive device channel distribution. The expectation in the update of the state evolution expression is taken with respect to $\beta$, parameter of (2-26). Thereby, the resulting modified denoiser is

$$\tilde{\eta}_{l,n}\left(\hat{\overline{\mathbf{h}}}_n^{l}\right) = f\left(\psi\left(\hat{\overline{\mathbf{h}}}_k^{l}\right)\right)\eta_{l,n}\left(\hat{\overline{\mathbf{h}}}_n^{l}\right), \tag{2-50}$$

where $\eta_{l,n}$ is the denoising function equivalent for the MMSE [36]. The idea of the modification is to design a denoiser capable to suppress the metadata sequences that do not belong to the evaluated device. For this, a soft-thresholding function is used, the sigmoid function, defined by

$$f\left(\psi\left(\hat{\bar{\mathbf{h}}}_{k,i}^{l}\right)\right)=\frac{1}{1+\exp\left(-c\left(\psi\left(\hat{\bar{\mathbf{h}}}_{k,i}^{l}\right)-\frac{1}{2}\right)\right)}, \tag{2-51}$$

where $c$ is a parameter that determines the sharpness of the sigmoidal transition, the coefficient $\psi\left(\hat{\bar{\mathbf{x}}}_{k,i}^{l}\right)$ is seen as a measure of the proportional likelihood of a given sequence allocated to device $k$ and is given by

$$\psi\left(\hat{\bar{\mathbf{h}}}_{k,i}^{l}\right)=\frac{\Lambda\left(\hat{\bar{\mathbf{h}}}_{k,i}^{l}\right)}{\sum_{i'=1}^{2J}\Lambda\left(\hat{\bar{\mathbf{h}}}_{k,i}^{l}\right)}, \tag{2-52}$$

where the likelihood function is

$$\Lambda\left(\hat{\bar{\mathbf{h}}}_{k,i}^{l}\right)=\frac{\left|\Sigma^{l}\right|}{\left|\beta_{k}\mathbf{I}+\Sigma^{l}\right|}q\left(\hat{\bar{\mathbf{h}}}_{k,i}^{l};\Sigma^{l}\right)^{-1}, \tag{2-53}$$

and

$$q\left(\hat{\bar{\mathbf{h}}}_{k,i}^{l};\Sigma^{l}\right)=\exp\left(-\left(\hat{\bar{\mathbf{h}}}_{k,i}^{l}\right)^{H}\left(\left(\Sigma^{l}\right)^{-1}-\left(\Sigma^{l}+\beta_{n}\mathbf{I}\right)^{-1}\right)\hat{\bar{\mathbf{h}}}_{k,i}^{l}\right). \tag{2-54}$$

As the main idea is that only a single row corresponding to a device may be non-zero as it is impossible for a device to transmit both metadata sequences concurrently, the authors of [36] proposed M-AMP.

*NSD-AMP*

Also focusing on the non-coherent transmission, the work in [55] proposes another modification to the AMP. The idea is to develop a section-wise equivalent model, that decouples the estimation in different sections, in this way allowing the design of the section-wise Bayes-optimal denoiser for the AMP, minimizing the MSE section by section. Starting from the classical AMP,

$$\mathbf{H}_{n}^{l+1}=\eta_{l,n}\left(\left(\mathbf{\Phi}_{n}\right)^{H}\mathbf{R}^{l}+\mathbf{H}_{n}^{l}\right),\quad n=1,\cdots,N, \tag{2-55}$$

$$\mathbf{R}^{l+1}=\mathbf{Y}-\mathbf{\Phi}\mathbf{H}^{l+1}+\frac{\mathbf{R}^{l}}{\tau}\sum_{n=1}^{N}\eta_{l,n}'\left(\left(\mathbf{\Phi}_{n}\right)^{H}\mathbf{R}^{l}+\mathbf{H}_{n}^{l}\right), \tag{2-56}$$

and using the analysis presented in [106], the authors argue that the output of

the denoiser applied to the residual $(\mathbf{\Phi}_n)^H \mathbf{R}^l + \mathbf{H}_n^l$, as in (2-55), is statistically equivalent to the output of applying the denoiser to

$$\hat{\mathbf{H}}_n = \mathbf{H}_n + \mathbf{V}_n \mathbf{\Sigma}_l^{\frac{1}{2}}, \tag{2-57}$$

which is called section-wise equivalent model. Based on the equivalent model in (2-57), the section-wise MMSE denoiser, in other words, the equivalent of (2-55) and (2-56) is given by

$$\eta_{l_n}\left(\hat{\mathbf{H}}_n^l\right) = \left[\overline{\omega}_{n,1}\mathbf{\Theta}_n\hat{\mathbf{h}}_{n,1}^l, \cdots, \overline{\omega}_{n,1}\mathbf{\Theta}_n\hat{\mathbf{h}}_{n,1}^l\right]^T \tag{2-58}$$

in which

$$\mathbf{\Theta}_n = \beta_n \left(\beta_n \mathbf{I} + \mathbf{\Sigma}_l\right)^{-1}, \tag{2-59}$$

$$\overline{\omega}_{n,i} = \frac{\exp\left(M\left(\pi_{n,i} - \phi_n\right)\right)}{\sum_{j=1}^{2^J} \exp\left(M\left(\pi_{n,j} - \phi_n\right)\right) + 2^J\left(\frac{1-\rho}{\rho}\right)}, \tag{2-60}$$

$$\pi_{n,i} = \frac{\left(\hat{\mathbf{h}}_{n,i}^l\right)^H \left(\mathbf{\Sigma}_l^{-1} - \left(\mathbf{\Sigma}^{-1} + \beta_n \mathbf{I}\right)^{-1}\right) \hat{\mathbf{h}}_{n,i}^l}{M}, \tag{2-61}$$

$$\phi_n = \frac{\log\left(|\mathbf{I} + \beta_n \mathbf{\Sigma}_l^{-1}|\right)}{M}. \tag{2-62}$$

where $\rho$ refers to the probability of being active of each device (equal for all) and $\beta_n$ are the large scale coefficients given by (2-26). Besides the section-wise MMSE denoiser, the authors of [55] describe how to decode the embedded data. After $t$ iterations with (2-55) and (2-56) the following threshold is computed

$$\mathcal{M}_{n,i} = \left(\frac{1}{\varkappa_t^2}\frac{1}{\beta_n + \varkappa_l^2}\right)\frac{\boldsymbol{\zeta}_{n,i}^H \boldsymbol{\zeta}_{n,i}}{M} - \phi_n, \qquad \forall i, n \tag{2-63}$$

$$\phi_n = \log\left(1 + \frac{\beta_n}{\varkappa_l^2}\right) \tag{2-64}$$

where $\boldsymbol{\zeta}_{n,i}$ denotes the $i$-th row of the matrix $(\mathbf{\Phi}_n)^H \mathbf{R}^l + \mathbf{H}_n^l$, as in (2-55) and $\varkappa_t^2$ is iteratively obtained using the scalar form of state evolution equations

given by

$$\varkappa_0^2 = \frac{1}{\text{SNR}} + \frac{\rho}{\epsilon}\,\mathbb{E}\left[\beta\right] \tag{2-65}$$

$$\varkappa_{l+1}^2 = \frac{1}{\text{SNR}} + \frac{1}{\epsilon}\sum_{i=1}^{2^J}\mathbb{E}\left[\overline{\omega}_{\beta,i}\theta_\beta\varkappa_l^2\right] + \frac{1}{\epsilon}\sum_{i=1}^{2^J}\mathbb{E}\left[\Upsilon_{\beta,i}^l\right] \tag{2-66}$$

with all expectations with respect to $\beta$, $\mathbf{H}_\beta$ and $\mathbf{V}$ and

$$\theta_\beta = \frac{\beta}{\beta + \varkappa_l^2}, \tag{2-67}$$

$$\Upsilon_{\beta,i}^l = \overline{\omega}_{\beta,i}\left(1 - \overline{\omega}_{\beta,i}\right)\left(\frac{\beta}{\beta + \varkappa_l^2}\right)^2 \frac{\left(\hat{\mathbf{h}}_{\beta,i}^l\right)^H \hat{\mathbf{h}}_{\beta,i}^l}{M}, \tag{2-68}$$

$$\hat{\mathbf{H}}_\beta^l = \left[\hat{\mathbf{h}}_{\beta,1}^l, \cdots, \hat{\mathbf{h}}_{\beta,2^J}^l\right]^T + \varkappa_l\mathbf{V}, \tag{2-69}$$

where $\epsilon = \tau/N$ is a positive value when $(\tau, N) \to \infty$. Thus, $\mathcal{M}_{n,i}$ is evaluated as $i_n^* = \arg\max_i \mathcal{M}_{n,i}, \forall i, n$. Then the support vector $\boldsymbol{\delta}_n = \left[\delta_{n,1}, \cdots, \delta_{n,2^J}\right]^T$ of the $n$-th device is a vector of zeros if $\mathcal{M}_{n,i_n^*} \geq 0$ or a vector of zeros with an 1 in the $i_n^*$ element, otherwise.

*Performance evaluation*

As in this section we have two different approaches to deal with the problem, we have also two simulation scenarios, in order to have the fairest possible comparison. Firstly, we compare the activity detection performance of the non-coherent algorithms. As the goal of these algorithms is to improve the denoiser, we simulated a scenario with 100 devices, 50 receive antennas and 200 metadata sequences for M-AMP and NSD-AMP, while the well-known AMP has 100 metadata sequences, as suggested in [36] and [55]. If the detector determines that one of the metadata sequences corresponds to one assigned to a device, then that device is detected as active, independently of whether an information bit is transmitted. In all algorithms, the number of iterations is fixed in 30, the number of embedded data bits transmitted by each active device is 4($J = 2$) and each device has a activity probability drawn uniformly

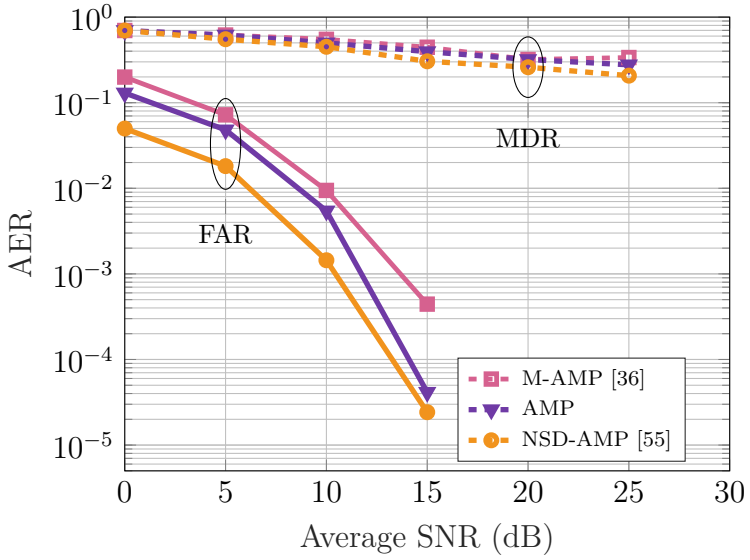


Figure 2.8: Activity error rate vs. Average SNR. Comparison of message-passing algorithms for $N = 100$, $M = 50$ with $\rho_n$ drawn uniformly at random in $[0.1, 0.3]$ which M-AMP and NSD-AMP consider 200 metadata sequences and detect devices along with a single embedded information bit. $10^5$ Monte Carlo trials.

at random in $[0.1, 0.3]$. As shown in Fig. 2.8, AMP has a better performance than the M-AMP, as expected. Besides deal with more metadata sequences, the modification of the denoiser is a function outside of the standard denoiser, which carries less information than the scheme of NSD-AMP, that incorporates the system statistics in the new denoiser. Another important point is that the NSD-AMP has the information of the probability of being active of each device, which is not available for M-AMP and AMP. Since the setup to include the bits of each algorithm is different and this is not the main goal of the paper, the evaluation of the non-coherent boils down to the activity detection performance.

*Coherent scenario*

Returning to the coherent scenario, the works in [32], [37] and [41] uses the message-passing approach to achieve the activity and signal detection.

*Joint-EM-AMP*

The authors of [37] proposes the Joint-EM-AMP, solution that uses the expectation maximization (EM) algorithm to estimate the activity of devices. As EM is an iterative algorithm that increases the likelihood probability of each iteration, it guarantees convergence to at least a local maximum of the likelihood function $f\left(\mathbf{y}_j|\lambda_{n,j}\right)$. Thus, this approach updates the activity estimate with the detection of each $j$ symbol of the received frame. Considering a system model similar to (2-27) with $r_{n,j}$ being the estimated mean of $x_{n,j}$ by decoupling of AMP and $\phi_{n,j}$ the effective noise variance, the posterior probability of $x_{n,j}$ is expressed as

$$f\left(x_{n,j}|r_{n,j},\lambda_{n,j}\right)=\frac{f\left(r_{n,j}|x_{n,j}\right)p\left(x_{n,j}|\lambda_{n,j}\right)}{f\left(r_{n,j}|\lambda_{n,j}\right)} \tag{2-70}$$

where

$$f\left(r_{n,j}|\lambda_{n,j}\right)=\sum_{x_{n,j},\in\mathcal{A}}f\left(r_{n,j}|x_{n,j}\right)p\left(x_{n,j}|\lambda_{n,j}\right), \tag{2-71}$$

$$f\left(r_{n,j}|x_{n,j}\right)=\mathcal{N}_c\left(r_{n,j}-x_{n,j},\phi_{n,j}\right), \tag{2-72}$$

$$p\left(x_{n,j}|\lambda_{n,j}\right)=\left(1-\lambda_{n,j}\right)\delta\left(x_{n,j}\right)+\lambda_{n,j}\sum_{i=1}^{|\mathcal{A}|}p_{\mathcal{A}}^{i}\delta\left(x_{n,j}-d_i\right). \tag{2-73}$$

Here, $\delta\left(\cdot\right)$ is the Dirac delta function and (2-73) is the prior information of the transmitted discrete symbols conditioned on user activity parameter $\lambda_{n,j}$, obtained iteratively by the expectation maximization algorithm. $p_{\mathcal{A}}$ is the a *priori* probability of each $d_i$, that is the $i$-th symbol of the modulation constellation $\mathcal{A}$. The estimates of the posterior mean and variance of $x_{n,j}$ are given by

$$\hat{x}_{n,j}=\sum_{x_{n,j}\in\mathcal{A}}x_{n,j}f\left(x_{n,j}|r_{n,j},\lambda_{n,j}\right), \tag{2-74}$$

$$v_{n,j}=\sum_{x_{n,j}\in\mathcal{A}}|x_{n,j}|^2f\left(x_{n,j}|r_{n,j},\lambda_{n,j}\right)-|\hat{x}_{n,j}|^2. \tag{2-75}$$

Thus, the updated $\lambda_{n,j}$ is then obtained as

$$\lambda_n^{t+1} = \frac{1}{\tau} \sum_{j=1}^{\tau} \sum_{x_{n,j} \in \mathcal{A}} f\left(x_{n,j} | \mathbf{y}_{n,j}, \lambda_{n,j}^t\right) \tag{2-76}$$

where

$$f\left(x_{n,j} | \mathbf{y}_{n,j}, \lambda_{n,j}^t\right) = \frac{\sum_{i=1}^{\mathcal{A}} p_{\mathcal{A}}^i \delta\left(x_{n,j} - d_i\right) - \delta\left(x_{n,j}\right)}{p\left(x_{n,j} | \lambda_{n,j}\right)}. \tag{2-77}$$

Thus, the Joint-EM-AMP performs the classical AMP algorithm and iteratively estimates the activity of devices with the expectation propagation approach. After $t$ predefined iterations, if $\lambda_n$ is greater than 0.5 the $k$-th device is considered active and inactive, otherwise. The data of active devices are recovered from the estimated values of $x_{n,j}$ in this approach.

*EM-BSBL*

The work in [32] applies the expectation maximization in a different way. Without requiring the priori knowledge of the activity factor, the work in [32] modifies the block sparse Bayesian learning (BSBL) [107] that considers the prior of the row sparsity property and the column coherence of each device. This Bayesian inference method make use of reasonable priors and a set of hyperparameters to control the estimated signals which can be learned from the training progress via expectation maximization.

This method vectorizes the transmitted frame, from the simplified signal model of (2-27). In order to estimate the vectorized transmitted frame $\overline{\mathbf{x}} = \text{vec}\left(\mathbf{X}\right)$, two hyperparameters are included in the system, $\boldsymbol{\gamma}$ and $\mathbf{C}$. The first one, $\boldsymbol{\gamma} = \left(\gamma_1, \cdots, \gamma_N\right)$ is a non-negative hyperparameter that controls the row sparsity property of $\mathbf{X}$ and $\mathbf{C}$ is a positive definite matrix that controls the column coherence of $\mathbf{X}$. The likelihood of the received signal $\mathbf{y}$ is

$$p\left(\mathbf{y} | \mathbf{x}; \sigma_v^2\right) = \mathcal{N}_c\left(\mathbf{y} | \mathbf{H}\mathbf{x}, \sigma_v^2 \mathbf{I}\right). \tag{2-78}$$

The authors assume zero-mean Gaussian *prior* for the transmitted signals $\mathbf{x}$, and the variance is composed of $\boldsymbol{\gamma}$ and $\mathbf{C}$, therefore $p\left(\mathbf{x}; \gamma_n, \mathbf{C}_n\right) = \mathcal{N}_c\left(\mathbf{x} | 0, \boldsymbol{\Sigma}_0\right), \forall n$, where the variance $\boldsymbol{\Sigma}_0 = \text{diag}\left(\gamma_1 \mathbf{C}_1, \cdots, \gamma_N \mathbf{C}_N\right)$. Then, the

posterior distribution of $\mathbf{x}$ is computed as

$$p\left(\mathbf{x}|\mathbf{y};\sigma_v^2,\gamma,\mathbf{C}\right)=\frac{p\left(\mathbf{y}|\mathbf{x};\sigma_v^2\right)p\left(\mathbf{x};\gamma,\mathbf{C}\right)}{\int p\left(\mathbf{y}|\mathbf{x};\sigma_v^2\right)p\left(\mathbf{x};\gamma,\mathbf{C}\right)d\mathbf{x}}=\mathcal{N}_c\left(\mathbf{x}|\boldsymbol{\mu},\boldsymbol{\Sigma}\right), \tag{2-79}$$

where the posterior mean ($\hat{\mathbf{x}}=\boldsymbol{\mu}$) and covariance are respectively

$$\hat{\mathbf{x}}=\boldsymbol{\Sigma}\mathbf{H}^H\mathbf{y}(\sigma_v^2)^{-1} \quad \text{and} \quad \boldsymbol{\Sigma}=\left(\boldsymbol{\Sigma}_0^{-1}+\sigma_v^2\mathbf{H}^H\mathbf{H}\right)^{-1}. \tag{2-80}$$

Knowing that $\boldsymbol{\mu}_x^i$ is a $\tau\times 1$ vector and denotes the $i$-th block of $\boldsymbol{\mu}$, and $\boldsymbol{\Sigma}_x^i$ is a $\tau\times\tau$ matrix and denotes the $i$-th block of $\boldsymbol{\Sigma}$, the hyperparameters $\boldsymbol{\gamma}$, $\mathbf{C}$, and $\sigma_v^2$ estimation via the iterative EM method are summarized as follows

$$\begin{aligned}
\gamma_i &= \frac{1}{\tau}\mathrm{tr}\left(\mathbf{C}^{-1}\boldsymbol{\Sigma}_x^i+\boldsymbol{\mu}_x^i(\boldsymbol{\mu}_x^i)^H\right),\\
\mathbf{C} &= \frac{1}{N}\sum_{i=1}^{N}\frac{\boldsymbol{\Sigma}_{\boldsymbol{x}}^{\boldsymbol{i}}+\boldsymbol{\mu}_{\boldsymbol{x}}^{\boldsymbol{i}}(\boldsymbol{\mu}_{\boldsymbol{x}}^{\boldsymbol{i}})^{\boldsymbol{H}}}{\gamma_i}\\
\sigma_v^2 &= \frac{\|\mathbf{y}-\mathbf{D}\boldsymbol{\mu}\|_2^2+\sigma_2^v\left(N\tau-\mathrm{tr}\left(\boldsymbol{\Sigma}\boldsymbol{\Sigma}_0^{-1}\right)\right)}{M\tau},
\end{aligned} \tag{2-81}$$

As a stopping criterion, if the mean $\|\boldsymbol{\mu}^t-\boldsymbol{\mu}^{t-1}\|_2$ is lower than a prescribed threshold, as $10^{-6}$, the algorithm stops.

*CS-MPA*

The work in [41] proposed a mixture of techniques, a CS approach to realize the user activity and a message-passing method to the data detection. Named CS-MPA detector, the algorithm is divided in two parts. Initially, the signal model considered is similar to (2-47) in terms of the channel matrix contains the sparsity of the system. The compressive sampling matching pursuit (CoSaMP) [108] algorithm is used to estimate the number of active users and the maximum iteration number. Thereby, the algorithm perform a least squares approach and computes a residual in order to aid in the next iteration. After all iterations, the estimated channel columns different from zero are considered to be related to an active device.

For the data detection, CS-MPA considers a simple factor graph in which transmitted symbols for all devices are variable nodes $\{x_n\}_{n=1}^{N}$ and the observations are factor nodes $\{y_m\}_{m=1}^{M}$. In the factor graph, there exists an edge between a variable node and a factor node if and only if the device is active. In MPA, the marginal distribution of a variable node can be regarded as the product of the messages received by that node as it is represented by

$$\mu_{m\to n}^{t}(x_n) \propto \sum_{x_i|i\in M(m)\backslash n} \frac{1}{\sqrt{2\pi}\sigma_v} \exp\left\{-\frac{1}{2\sigma_v^2}\|y_m - h_{m,n}x_n - \sum_{i\in M(m)\backslash n} h_{m,i}x_i\|^2\right\} \prod_{i\in M(m)\backslash n} \mu_{i\to m}^{t-1}(x_i), \tag{2-82}$$

$$\mu_{n\to m}^{t}(x_n) \propto \prod_{i\in M(n)\backslash m} \mu_{i\to n}^{t-1}(x_n), \tag{2-83}$$

where $\mu_{m\to n}^{t}(x_n)$ denotes the message passed from factor node $y_m$ to variable node $x_n$ in the $i$-th iteration, $\mu_{n\to m}^{t}(x_n)$ is the message passed from the other direction and and $M(m)\backslash n$ presents all elements in $M(m)$ except for $n$. After all iterations, the (approximate) marginal probability distribution of $x_n$ is computed by

$$p(x_n) \propto \prod_{i\in M(n)} \mu_{i\to n}^{T}(x_n). \tag{2-84}$$

Therefore, each estimated symbol of active users is taken from the modulation alphabet with the maximum marginal probability.

*Performance evaluation*

For the coherent scenario, AMP, CS-MPA, EM-BSBL and Joint-EM-AMP are evaluated. Considering 128 devices transmitting frames with 128 QPSK symbols to a single base station equipped with 64 antennas, its is possible to notice that EM-BSBL and Joint-EM-AMP shows better performance than other schemes. Due to the expectation-maximization procedure, the activity estimation of each algorithm is more refined. Despite being based on AMP, the consideration of posterior probability of the transmitted symbols to reach the update equation of the activity parameter improves considerably the

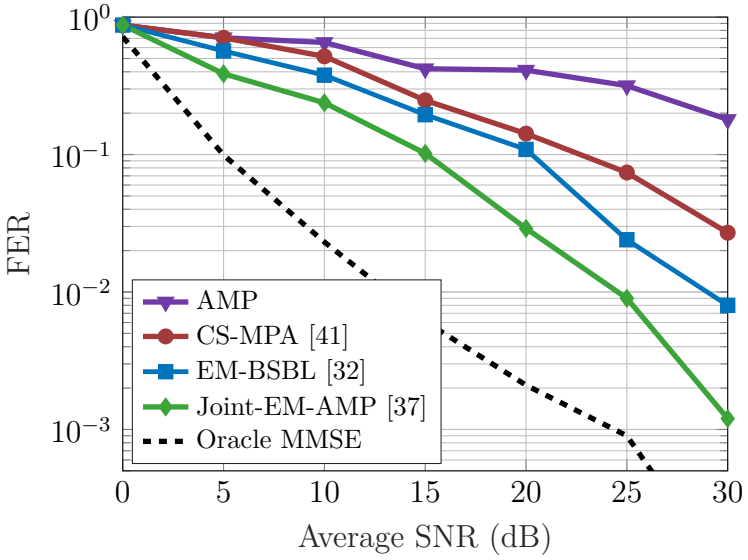


Figure 2.9: Frame error rate vs. Average SNR. Comparison of message-passing algorithms for $N = 128$, $M = 64$ with $\rho_n$ drawn uniformly at random in $[0.1, 0.3]$. $10^5$ Monte Carlo trials.

estimation performance. On the other hand, CS-MPA uses a simple scheme to estimate the activity and the classical message-passing algorithm to detect the transmitted symbols, which results in intermediate performance.

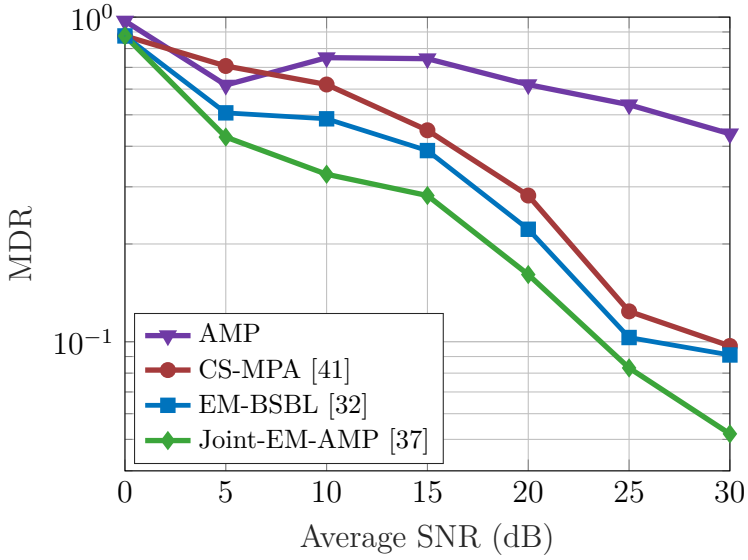


(a) Missed detection rate vs. Average SNR.

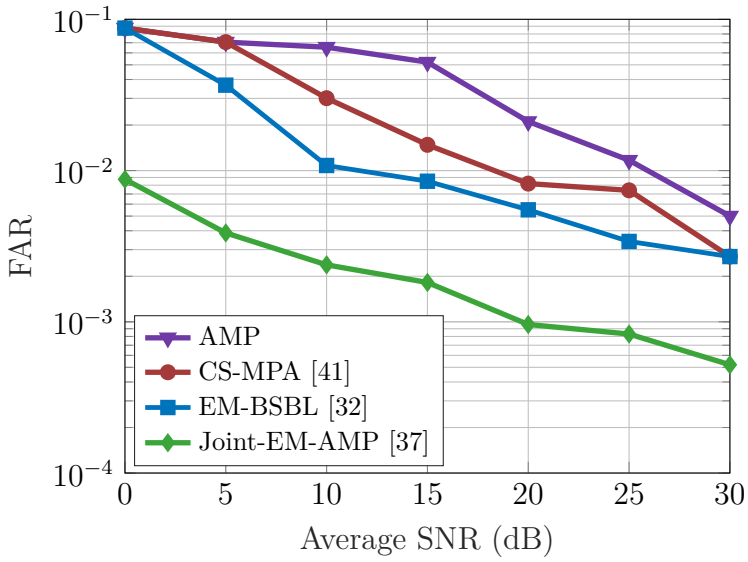


(b) False alarms rate vs. Average SNR.

Figure 2.10: Activity error rates for comparison of message-passing algorithms in a coherent scenario. Simulation parameters: $N = 128$, $M = 64$ with $\rho_n$ drawn uniformly at random in $[0.1, 0.3]$. $10^5$ Monte Carlo trials.

### 2.3.5 Joint Activity Detection and Channel Estimation Techniques

In this subsection we present and compare relevant state-of-the-art algorithms divided in two different classes of detectors: message-passing and machine learning based. Each approach is compared under the NMSE and AER KPIs.

#### 2.3.5.1 Message-Passing Solutions

Message-passing approaches, besides singal detection, have been also applied to obtain accurate channel estimation with a low computational complexity. As most of channel models consider Gaussian approximations, the use of message passing approaches is attractive.

*AMP with MMSE denoiser*

One of the first works [52] consists of a robust technique, where a minimum mean-squared error (MMSE) denoiser in the vector AMP algorithm is designed for user activity detection and channel estimation based on statistical channel information. Considering a signal model similar to (2-47), the main difference between the MMSE denoiser in (2-58) is the component of (2-60), which is given by

$$\overline{\omega}_n = 1 \Big/ \left(1 + \left(\frac{1-\epsilon}{\epsilon}\right) \exp\left(-M\left(\pi_n - \phi_n\right)\right)\right), \tag{2-85}$$

being updated in each state. For the device activity detection, a threshold strategy is adopted as

$$\begin{cases} 1, \text{ if } \left(\left(\mathbf{R}^t\right)^H \mathbf{\Phi}_n + \hat{\mathbf{h}}_n^t\right)^H \left(\left(\mathbf{R}^t\right)^H \mathbf{\Phi}_n + \hat{\mathbf{h}}_n^t\right) > \theta_{t,n}, \\ 0, \text{ if } \left(\left(\mathbf{R}^t\right)^H \mathbf{\Phi}_n + \hat{\mathbf{h}}_n^t\right)^H \left(\left(\mathbf{R}^t\right)^H \mathbf{\Phi}_n + \hat{\mathbf{h}}_n^t\right) < \theta_{t,n}, \end{cases} \tag{2-86}$$

with the threshold as $\theta_{t,n} = M \log\left(1 + \frac{\beta_n}{\varkappa_t^2}\right) \Big/ \left(\frac{1}{\varkappa_t^2} - \frac{1}{\varkappa_t^2 + \beta_n}\right)$ where $\varkappa_t$ is iteratively obtained as in (2-65) and (2-66). Thus, if the device is considered active then the estimated channel is given by the corresponding $\hat{\mathbf{h}}$.

*MP-BSBL*

Based on Bayesian learning, the work in [57] uses a block sparse approach with belief propagation (BP) and mean field (MF), to achieve low complexity. Considering a vector version of (2-47) and that the metadata of each device is composed by Zadoff-Chu sequences, in the signal model of [57], both the

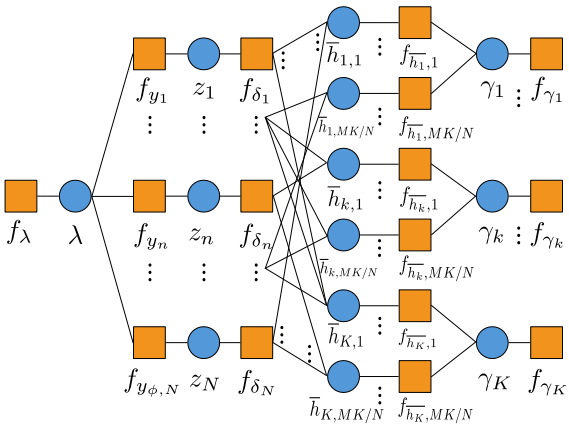


Figure 2.11: Factor graph of MP-BSBL, where the auxiliary variable $z_n$ and extra constrains $\delta$, denoted by $f_{\delta_n}$ and $f_{y_n}$ are introduced. This auxiliary variables are function of the channel, metadata vector and $\lambda$.

metadata and channel matrices are sparse. Based on the idea of separating the problem in blocks as the well-known block orthogonal matching pursuit (BOMP) [109], a two-layer hierarchical structure, shown in Fig. 2.11, factorizes the joint a posteriori pdf of the block sparse channel vector $\overline{\mathbf{h}}$:

$$\begin{aligned} p\left(\overline{\mathbf{h}}, \boldsymbol{\gamma}, \lambda | \mathbf{y}\right) &\propto p\left(\mathbf{y}|\overline{\mathbf{h}}, \boldsymbol{\lambda}\right) p\left(\overline{\mathbf{h}}|\boldsymbol{\gamma}\right) p\left(\boldsymbol{\gamma}\right) p\left(\lambda\right) \\ &= p\left(\lambda\right) \prod_{m=1}^{\tau_\phi M} p\left(y_m|\overline{\mathbf{h}}, \boldsymbol{\lambda}\right) \prod_{n=1}^{M} \prod_{i=1}^{(M/N)K} p\left(\overline{h}_{n,i}|\gamma_n\right) p\left(\gamma_n\right), \end{aligned} \tag{2-87}$$

where $p(\overline{\mathbf{h}}) = \int_\gamma p\left(\overline{\mathbf{h}}|\boldsymbol{\gamma}\right) p\left(\boldsymbol{\gamma}\right) \, \mathrm{d}\boldsymbol{\gamma}$ is the prior pdf of $\overline{\mathbf{h}}$ given by the product of a conditional prior pdf $p\left(\overline{\mathbf{h}}|\boldsymbol{\gamma}\right)$ and a hyperprior pdf $p\left(\boldsymbol{\gamma}\right)$. Since the parameter $\lambda$ here is the noise precision $1/\sigma_w^2$ and the joint a posteriori pdf is composed of complex Gaussian pdfs, a Gamma distribution ($p\left(\gamma_n\right)$), the factor graph in Fig. 2.11 can be build. The BP rule is used at the function nodes and MF rule is used at other function nodes. After a predetermined number of iterations, the channel is estimated with the mean $m_{\overline{h}_{n,i}}$ computed by the exchange of messages, most of them approximated by complex Gaussian pdfs between the factor and variable nodes. The activity detection is performed by the evaluation of the inverse of the estimated hiperprior $\gamma$ with a predefined threshold.

*Iterative EP*

With a different approach, the work in [59] proposes an iterative algorithm that uses expectation propagation (EP) to perform active user detection and channel estimation. Considering the signal model as (2-47):

$$\mathbf{y} = \mathbf{\Phi}\mathbf{h} + \mathbf{v}, \tag{2-88}$$

where $\mathbf{\Phi}$ is the metadata matrix and the prior distribution of the channel vector $\mathbf{h}$ is given by

$$p(\mathbf{h}) = \prod_{n=1}^{N} \left[(1-\rho_n)\,\delta(h_n) + \rho_n \mathcal{N}_c\left(h_n|0,\beta_n\right)\right], \tag{2-89}$$

where $\delta(\cdot)$ is the dirac function. With this, the idea of the algorithm is to approximate the target distribution $f(\mathbf{h}) = p(\mathbf{y}|\mathbf{h})p(\mathbf{h})$ to the Gaussian distribution $q(\mathbf{h}) = \mathcal{N}_c(\mathbf{h}|\tilde{\mathbf{m}}, \tilde{\mathbf{V}})$. After that, the algorithm proceeds in order to match the mean vector true target $\tilde{\mathbf{m}}$ and covariance matrix $\tilde{\mathbf{V}}$ to those of the true target distribution $f(\mathbf{h})$ based on the iterative EP algorithm.

Thus, using the Kullback-Leibler (KL) divergence criterion and approximating the target distribution as

$$\begin{aligned} f(\mathbf{h}) &= f_1(\mathbf{h}) f_2(\mathbf{h}) = p(\mathbf{y}|\mathbf{h})p(\mathbf{h}), \\ f_1(\mathbf{h}) &= p(\mathbf{y}|\mathbf{h}) \approx q_1(\mathbf{h}) = \mathcal{N}_c(\mathbf{h}|\tilde{\mathbf{m}}_1, \tilde{\mathbf{V}}_1), \qquad (2\text{-}90) \\ f_2(\mathbf{h}) &= p(\mathbf{h}) \approx q_2(\mathbf{h}) = \mathcal{N}_c(\mathbf{h}|\tilde{\mathbf{m}}_2, \tilde{\mathbf{V}}_2), \qquad (2\text{-}91) \end{aligned}$$

where, after reconstructing the unnormalized global Gaussian approximation as $f(\mathbf{h}) \approx q(\mathbf{h}) = q_1(\mathbf{h})q_2(\mathbf{h}) = \mathcal{N}_c(\mathbf{h}|\tilde{\mathbf{m}}, \tilde{\mathbf{V}})$, the mean vector $\tilde{\mathbf{m}}$ and the covariance matrix $\tilde{\mathbf{V}}$ are given by

$$\tilde{\mathbf{V}} = \left(\sigma_w^{-2}\mathbf{\Phi}^H\mathbf{\Phi} + \tilde{\mathbf{V}}_2^{-1}\right)^{-1} \tag{2-92}$$

$$\tilde{\mathbf{m}} = \tilde{\mathbf{V}}\left(\sigma_w^{-2}\mathbf{\Phi}^H\mathbf{y} + \tilde{\mathbf{V}}_2^{-1}\tilde{\mathbf{m}}_2\right), \tag{2-93}$$

where $\tilde{\mathbf{m}}_1$ and $\tilde{\mathbf{V}}_1$ where approximated. Then, the task of the iterative EP is

to compute the $\tilde{\mathbf{m}}_2$ and $\tilde{\mathbf{V}}_2$ parameters. The update equations are given by

$$\tilde{v}_{2,n}^{t+1} = \left[V_q^t[h_n]^{-1} - (\tilde{v}_{\setminus 2,n}^t)^{-1}\right]^{-1}, \tag{2-94}$$

$$\tilde{m}_{2,n}^{t+1} = \left[V_q^t[h_n]^{-1} E_q^t[h_n] - (\tilde{v}_{\setminus 2,n}^t)^{-1} \tilde{m}_{\setminus 2,n}^t\right], \tag{2-95}$$

where $\tilde{v}_{\setminus 2,n}^t$ corresponds to the contribution of the $n$-th marginal of $q^t(\mathbf{h})$ and $E_q^t[h_n]$ and $V_q^t[h_n]$ are the mean and variance of the distribution to be match and are computed by method of moments. The algorithm proceeds until a predefined number of iterations is reached and the mean vector $\tilde{\mathbf{m}}$ is the estimated channel $\hat{\mathbf{h}}$. Once $\hat{\mathbf{h}}$ is obtained, by performing the likelihood test on $\hat{\mathbf{h}}$, the active devices are detected. Considering $H_1$ as the hypothesis for the active device and $H_0$ as inactive, the log-likelihood ratio test is obtained after the threshold of each element of $\hat{\mathbf{h}}$ as

$$\begin{cases} H_1 & \text{if } |\hat{h}_n|^2 \geq \theta_n, \\ H_0 & \text{if } |\hat{h}_n|^2 < \theta_n, \end{cases} \tag{2-96}$$

where $\theta_n = \log(1 + \frac{\beta_n}{\tilde{V}_{nn}})/(\frac{1}{\tilde{V}_{nn}} - \frac{1}{\beta_n + \tilde{V}_{nn}})$ and $\tilde{V}_{nn}$ is the $n$-th diagonal of $\tilde{\mathbf{V}}$.

*Performance evaluation*

With the same framework of the previous simulations, the message-passing algorithms are evaluated in the scenario of $N = 128$ MTCDs connected to a single base-station equipped with $M = 64$ antennas. Each frame is composed of 128 metadata symbols in order to estimate the channels, considered as the same of (2-26). Initially, Fig. 2.12, shows the Frame Error Rate (SER) performance averaged over $10^5$ runs. Considering the average SNR as $10\log(N\sigma_x^2/\sigma_v^2)$, the AMP with MMSE denoiser in [52] outperfoms the traditional AMP [34]. On the other hand, the techniques in [57] and [59] consider the prior distribution of the channel vector and show better performance, as shown in Figs.2.13a and 2.13b referred to as the activity detection performance. Using the method of moments, the Iterative EP [59] has a much better NMSE performance com-

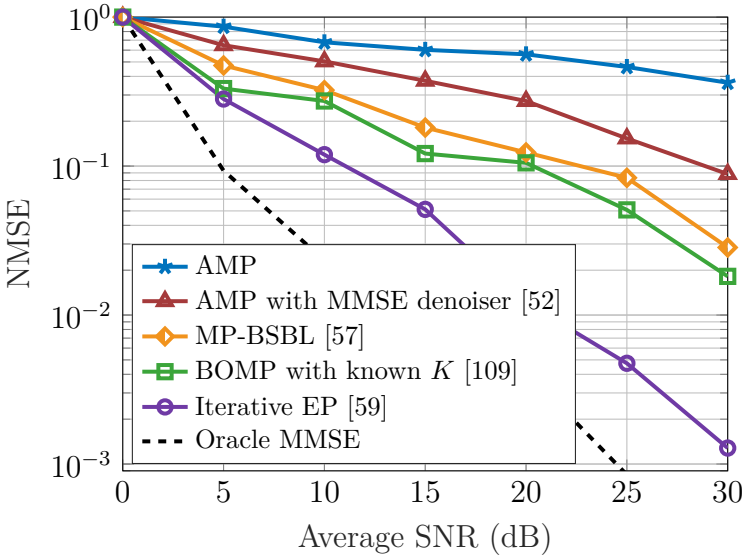


Figure 2.12: Normalized mean squared error vs. Average SNR. Comparison of message-passing algorithms for $N = 128, M = 64$ with $\rho_n$ drawn uniformly at random in $[0.1, 0.3]$ and active devices transmitting frames with 128 QPSK symbols. $10^5$ Monte Carlo trials.

pared to the other schemes, while its computational complexity is quadratic and that of MP-BSBL [57] is linear. The well-known BOMP [109] algorithm with knowledge of the the number of active devices is used as a lower bound for MP-BSBL, as done in the original paper.

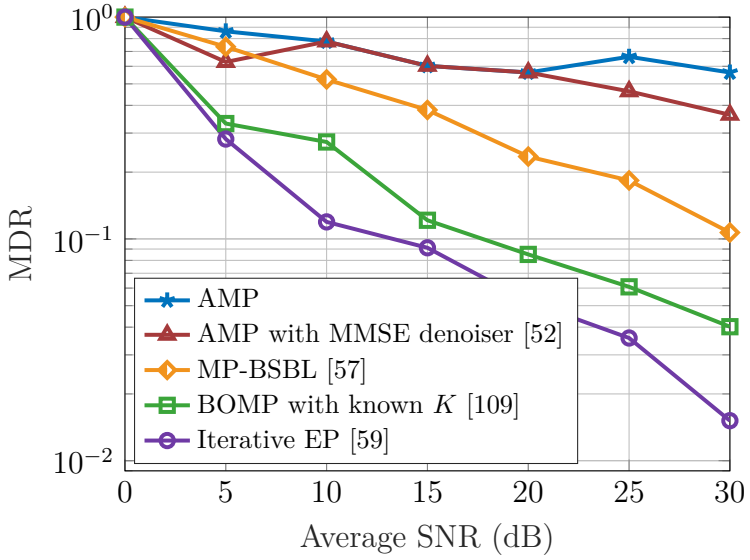


(a) Missed detection rate vs. Average SNR.

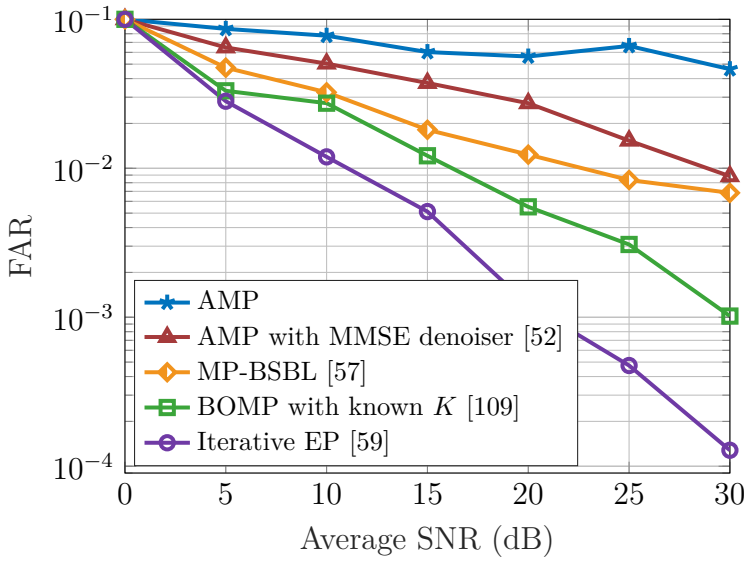


(b) False alarms rate vs. Average SNR.

Figure 2.13: Activity error rates for comparison of message-passing algorithms for channel estimation. Simulation parameters: $N = 128$, $M = 64$ with $\rho_n$ drawn uniformly at random in $[0.1, 0.3]$. Each frame is composed by 128 QPSK symbols. $10^5$ Monte Carlo trials.

#### 2.3.5.2 Machine-Learning Solutions

Recently, some works investigated the use of machine-learning approaches to channel estimation. Deep Learning (DL) [110] is a branch of machine-learning which is also referred to as deep neural networks (DNNs), uses a large amount of training data to learn parameters in a neural network.

In order to analyze the complex channel characteristics, the work in [65] uses a typical branch of DNN, the long short-term memory (LSTM). By implicitly reproducing the behavior of the channel with the LSTM algorithm, this approach considers the greedy SISD algorithm [111] to perform activity and data detection. On the other hand, the works in [64] and [66] uses the DL approach to explicitly estimate the channels. Using the metadata vectors as the training set, both works map each received vector $\mathbf{y}$ as an input and considers as the loss function the mean square error (MSE) $\|\hat{\mathbf{h}}_{\text{DNN}} - \mathbf{h}\|_2^2$, where $\hat{\mathbf{h}}_{\text{DNN}}$ is the estimated channel gain and $\mathbf{h}$ is the known channel gain in the training set.

*BRNN*

The work in [64] consists of a feedforward neural network with interleaved fully connected layers and non-linear transformation layers. A batch normalization is added for initialization and residual connection is used to avoid vanishing/exploding gradients. The $t$-th layer of the network can be expressed as

$$\mathbf{h}^{t+1} = f\left(\mathbf{W}^t \mathbf{h}^t + \mathbf{b}^t\right), \tag{2-97}$$

where the parameters to be learned $\mathbf{W}^t$ and $\mathbf{b}^t$ are the weight matrix and the bias vector, respectively, while $f(\cdot)$ denotes the non-linear operator given by

$$f\left(h_1, \ldots, h_M\right) = \text{sign}\left(0, h_1, \ldots, h_M\right) \cdot \left[h_1, \ldots, h_M\right], \tag{2-98}$$

where sign$(\cdot)$ denotes the sign function. In the back propagation, the gradient of (2-98) is 1 if $f(h) = h$ and 0 if $f(h) = 0$. The main goal of this approach is to detect the active devices and estimate the channel using an MMSE estimator. Thus, the loss function of the designed network is the cross entropy loss function given by

$$\mathcal{L}(\hat{\mathbf{z}}) = -\sum_{n=1}^{N} z_n \log(\hat{z}_n), \tag{2-99}$$

where $\hat{z}_n$ is the $n$-th element of the activation vector $\mathbf{z}$ with $z_n = 1$ if $\|x_n\|_2 > 0$ and $z_n = 0$ otherwise. This network uses 6 nodes for training

and test phases, while the optimizer adopted for training neural networks is a stochastic gradient algorithm with a momentum 0.9 and a learning rate 0.01.

*DNN-MP-BSBL*

The work in [66] transfers the iterative message-passing process of MP-BSBL [57], depicted in the last section, to a neural network. Motivated by the convergence speed of MP-BSBL, the authors of [66] impose weights on the Gaussian messages represented on the factor graph depicted in Fig. 2.11. The idea is to simultaneously use the weights on the MF message update and further train it to improve the activity detection accuracy. Under the argument that the training of the network is conducted offline, just a small computational complexity is added to the online process, the authors argue that it is possible to use the network even though it is necessary to use $10^5$ training sequences. With 9 layers within each iteration block, the received vector is primarily used as the input and then, at each layer, the quantities present in the joint a posteriori pdf in (2-87) are updated, as its weights. After a predefined number of iterations, the activity detection decision is made by comparing the variable $\gamma$ with a threshold. If the device is detected as active, the estimated channel gain is attributed to the device.

*Performance evaluation*

Differently from the other simulation scenarios, the networks need an offline training, before the real transmissions. Although the scenario matches with the previous ones, with $N = 128$, $M = 64$, MTCDs sporadically active with an activity probability drawn uniformly at random in $[0.1, 0.3]$ and the channel modelled as in (2-26), for both simulations, was necessary a training set with the size of $10^5$. The rest of the parameters considered specifically for each algorithm, are consistent with those cited in the original works, as for DNN-MP-BSBL [66], the threshold to decide the activity of the device

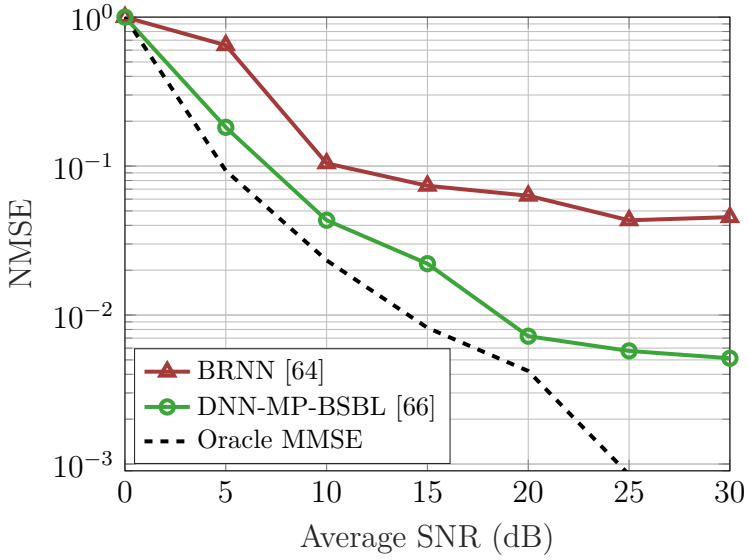


(a) Normalized mean squared error vs Average SNR.

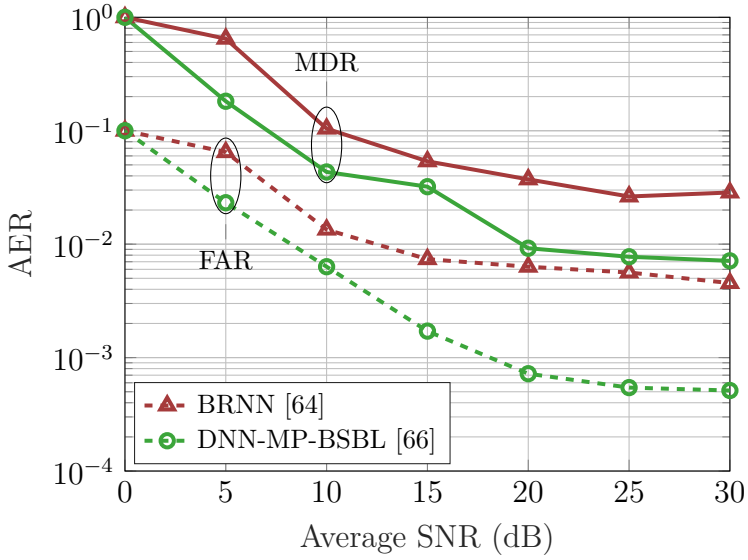


(b) Activity error rate vs. Average SNR.

Figure 2.14: KPI results of machine-learning algorithms. Simulation parameters: $N = 128$, $M = 64$ with $\rho_n$ drawn uniformly at random in $[0.1, 0.3]$. $10^5$ Monte Carlo trials.

is 0.1, the epoch number is 20, the learning rate is $10^{-3}$ and 20 iterations. For BRNN, we used $10^6$ samples for training, and the rest of the parameters followed the description in the section and the original paper. To evaluate the channel estimates, we used the normalized mean square error (NMSE), $\text{NMSE} = \|\hat{\mathbf{h}} - \mathbf{h}\|_2^2 / \|\mathbf{h}\|_2^2$.

Only the channels associated with active devices were considered. Fig. 2.14a shows the simulation results of the NMSE performance of BRNN

and DNN-MP-BSBL under different SNR scenarios. With the results averaged under $10^5$ runs, it is possible to realize that DNN-MP-BSBL achieves an efficiency closer to the lower bound, the oracle linear MMSE. The weight update scheme and the joint a posteriori pdf of the model, considerably outperforms BRNN, since that network only estimates the activity of devices. The superiority of the DNN-MP-BSBL scheme is even more evident in Fig. 2.14b, where the activity detection is shown.

## 2.4 Discussions and Complexity Analysis

The results demonstrate that each solution provides a direct relation between activity detection rates and data detection. In order to verify the best approach, Fig. 2.15 compares the schemes with the best performance in each family of algorithms. Considering the unified evaluation framework and perfect channel estimation, we notice that the regularized and greedy detectors show better performance with a few techniques being as efficient as the lower bound.

As part of the performance analysis, each technique should have their computational cost evaluated. Concerning the channel estimation algorithms, as shown in Fig. 2.16, Iterative EP shows the best performance, but requires a cubic complexity order. As for machine learning schemes, even though BRNN has high complexity due to the use of the linear MMSE channel estimator, DNN-MP-BSBL has linear complexity at least in the online process. Compared with message-passing schemes, machine learning approaches present better performance but require the offline process, which consumes a large amount of training data to learn parameters in the neural network.

Figs. 2.17 and 2.18 depicts the detailed complexity analysis of simulated approaches based on required floating-point operations (FLOPs). Fig. 2.17a shows that the regularization approaches exhibits a competitive performance as compared to the greedy techniques (Fig. 2.17b) exhibit a high computational complexity as those schemes require matrix inversions. Since the expected

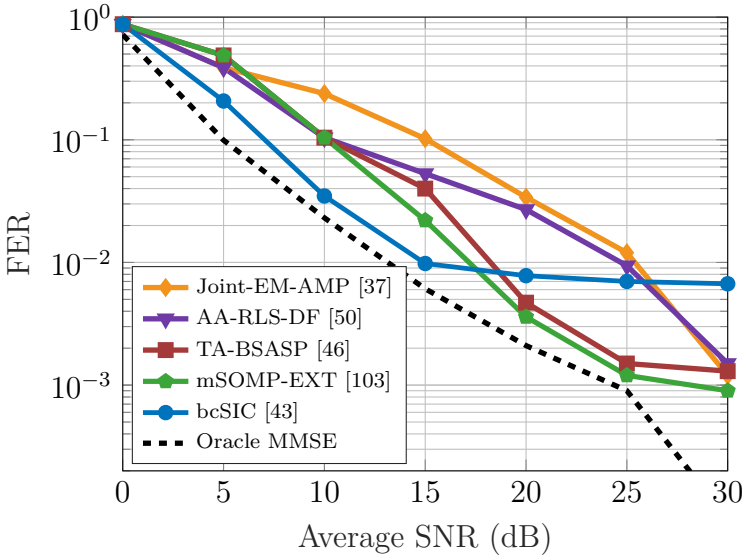


Figure 2.15: Frame error rate vs Average SNR. Comparison between better performance algorithms.

number of devices is huge, a cubic computational complexity order would be an issue to be dealt with at the BS. As for the message-passing techniques, Fig 2.18a shows a competitive performance as the number of iterations have greater influence on the computational cost. In particular, the algorithms that exhibit lower computational cost are compared in Fig. 2.18b. One can see that there is a trade-off between computational cost and data detection performance as the algorithms with lowest computational cost are not those with lowest frame error rates. Table 2.2 details the FLOPs counting of the analyzed techniques, for each detected vector. Parameters that have not been previously presented, such as $T_1, T_2, c$, and $c'$, are constants determined in the original papers.

In addition to the techniques analyzed here, it is important to highlight that recent relevant papers were published that jointly perform all the three tasks in the same scheme, channel estimation and activity and data detection. Given the performance and computational cost shown before, it is no surprise that those works are message-passing schemes that employ a factor graph representation for the problem. The work in [69] considers the uplink SCMA scenario and uses the expectation propagation to project the intractable

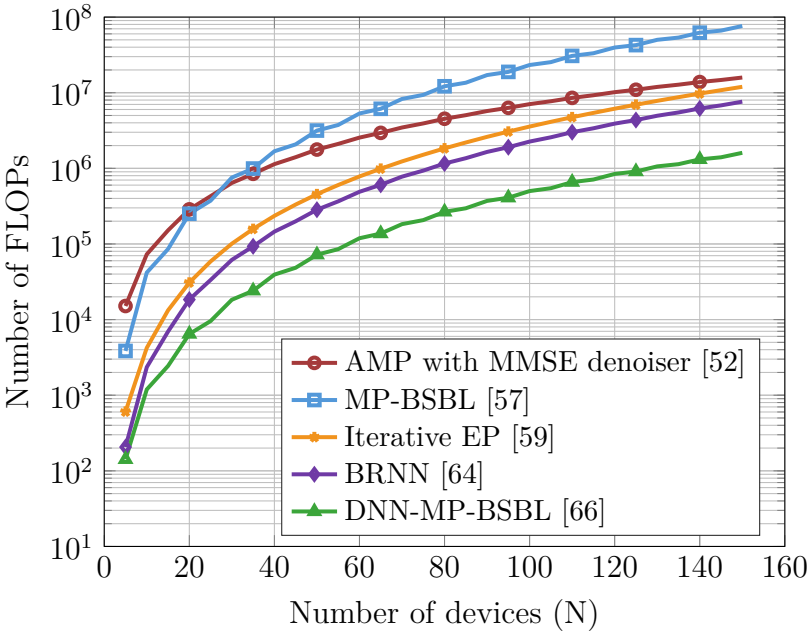


Figure 2.16: Floating-point operations vs. Number of devices of activity detection and channel estimation algorithms.

distributions into Gaussian families in order to obtain a linear complexity decoder. With the aim of investigating the time-slotted and non-time-slotted grant-free NOMA, the work in [70] applies the bilinear generalized approximate message passing (BiG-AMP) [112] algorithm to mMTC. In order to address the overhead problem, the work in [74] proposes a Bayesian receiver design for grant-free low density signature orthogonal frequency division multiplexing (LDS-OFDM). This approach is composed by the belief propagation (BP), expectation propagation (EP) and mean field (MF) techniques, so that the scheme jointly estimates the channels and performs activity and data detection, avoiding the use of metadata signals.

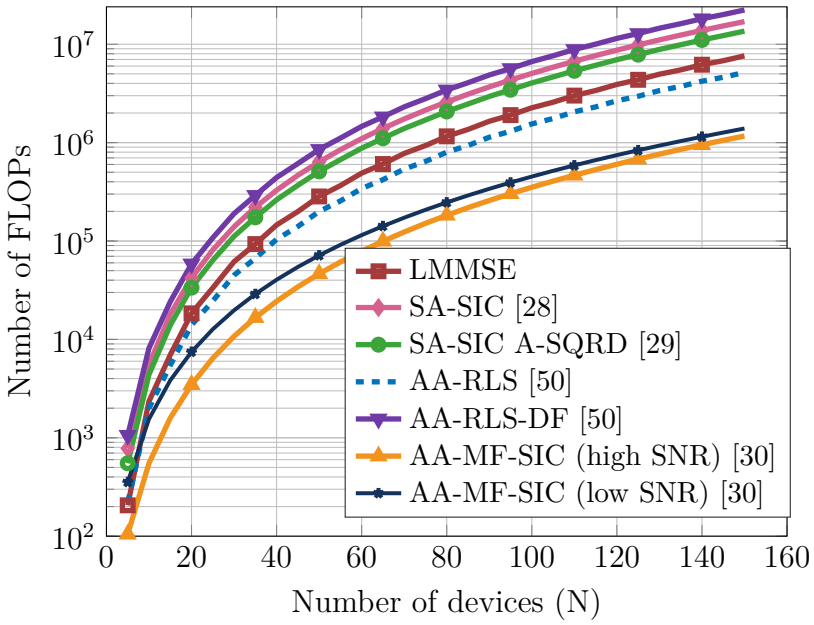


(a) Regularized algorithms for activity and data detection.

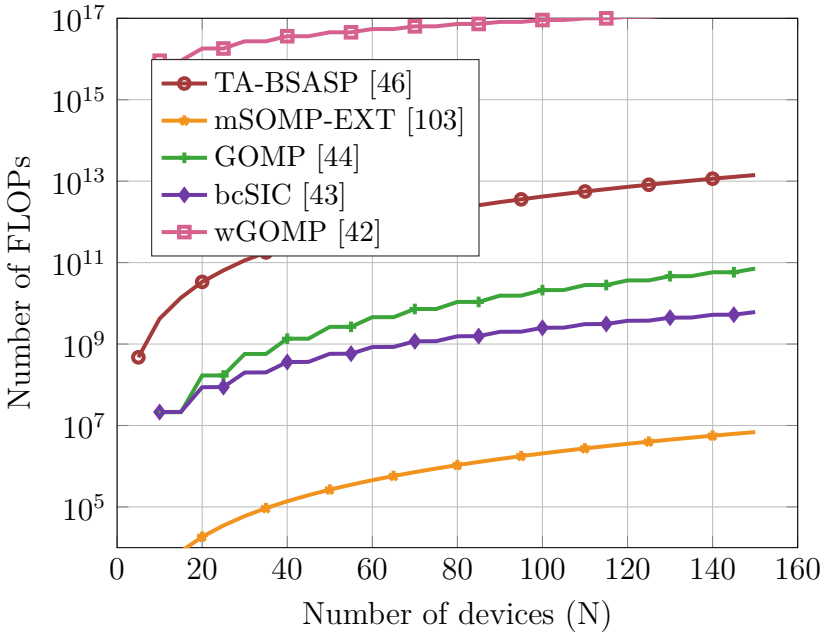


(b) Greedy algorithms for activity and data detection.

Figure 2.17: Floating-point operations of regularized and greedy algorithms vs. Number of devices. Simulation parameters: Number of receiver antennas $M$ is $N/2$ and the number of active devices $K$ is 10% of $N$. The number of symbols in each frame $\tau = 128$, $\tau_\phi = 64$, constants $c = 5$ and $c' = 10$ of GOMP, bcSIC and wGOMP, the latter, still with $N_{\text{subp}} = 8$, $\tau_{\text{seg}} = 128$ and $N_{\text{fb}} = \tau_{\text{seg}}/N_{\text{subp}}$.

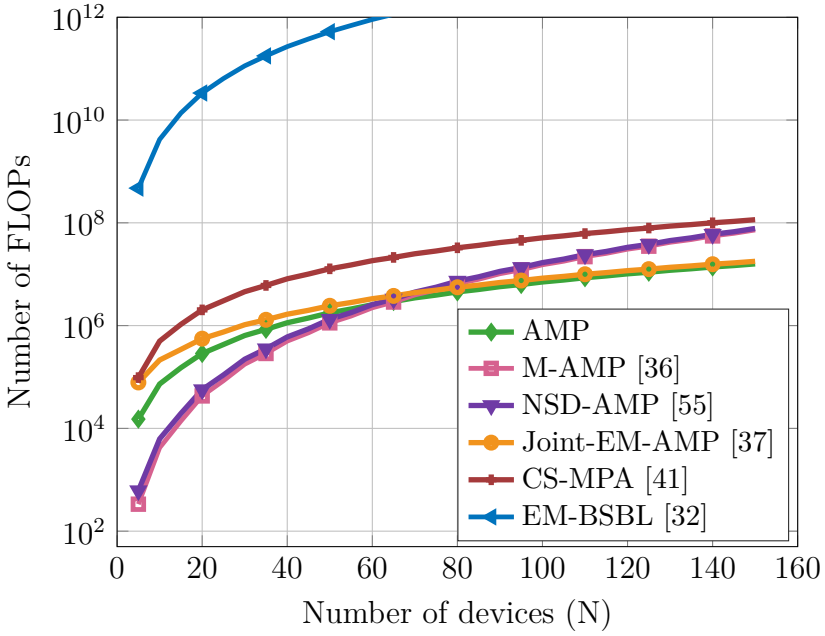


(a) Message-passing algorithms for activity and data detection.

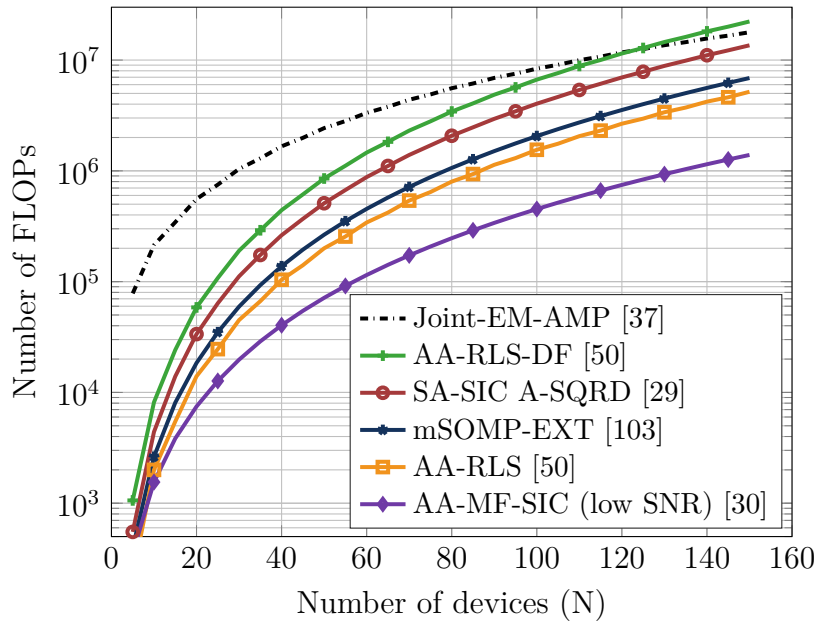


(b) Comparison of algorithms with lowest FLOPs for activity and data detection.

Figure 2.18: Floating-point operations of message-passing and best algorithms vs. Number of devices. Simulation parameters: Number of receiver antennas $M$ is $N/2$ and the number of active devices $K$ is 10% of $N$. The number of symbols in each frame $\tau = 128$, $\tau_\phi = 64$. Regarding the non-coherent approaches, the number of bits $J$ in the NSD-AMP is 2.

Table 2.2: FLOPs counting of considered techniques in detail.

| Type | Category | Algorithm | Complexity |
|---|---|---|---|
| Activity and data detection | Linear | MMSE | $2M^3+4\left(N+1\right)M^2+2\left(N^2+N+1\right)M-\left(N^2+N\right)$ |
| | Regularized | SA-SIC [27] | $\left\|\mathcal{A}_0\right\|\left(N^3+N^2+6\right)$ |
| | | SA-SIC with A-SQRD [29] | $2N^3+4\left(M+1\right)N^2+\left(M-1\right)N$ |
| | | AA-MF-SIC (high SNR) [30] | $\leq\left(1/6\right)\left(2N^3+11N^2+21N-2\right)$ |
| | | AA-MF-SIC (low SNR) [30] | $\geq\left(1/6\right)\left(2N^3+11N^2+21N-2\right)+10N^2$ |
| | | AA-RLS [50] | $\left(6M^2+10M\right)N$ |
| | | AA-RLS-DF [50] | $\sum_{i=1}^{N}\left[6\left(M+i\right)^2+10\left(M+i\right)\right]$ |
| | Greedy | TA-BSASP [46] | $5N+3N\tau+3NM\tau^2+2M\tau\left(\tau K\right)^2+\left(\tau K\right)^3$ |
| | | mSOMP-EXT [103] | $2N^3+2N^2+\left(1+2M\right)4N-2M-1$ |
| | | OMP | $\sum_{i=1}^{K}cMi^2+c'i^3$ |
| | | GOMP [44] | $\sum_{i=1}^{K}2M\left(i\tau\right)^2+c'\left(i\tau\right)^3$ |
| | | bcSIC [43] | $\sum_{i=1}^{K}K\left(cM\tau^2+c'\tau^3\right)$ |
| | | wGOMP [42] | $\sum_{u=1}^{N_{\text{fb}}K}N_{\text{fb}}N_{\text{subp}}\sum_{i=1}^{K}c\lfloor M/N_{\text{subp}}\rfloor\left(i\tau_{\text{seg}}\right)^2+c'\left(i\tau_{\text{seg}}\right)^3$ |
| | Message passing | AMP | $\tau M\left(11N+4\right)+4\left(\left\|\mathcal{A}\right\|+1\right)$ |
| | | M-AMP [36] | $N\left(M^3+7M^2+2N+2MN+1\right)$ |
| | | NSD-AMP [55] | $N\left(M^3+9M^2+12M+4MN+5\right)+2^{J+1}\left(N+1\right)$ |
| | | Joint-EM-AMP [37] | $M\tau\left(4\left\|\mathcal{A}\right\|^2+17\left\|\mathcal{A}\right\|+11N+21\right)+3\tau\left\|\mathcal{A}\right\|\left(\left\|\mathcal{A}\right\|+1\right)$ |
| | | CS-MPA [41] | $\left[T_1\left(3N-1\right)2M+T_2\left(MN\right)\right]\tau$ |
| | | EM-BSBL [32] | $(N\tau)^3+2(M\tau+3/2)(N\tau)^2+(M\tau+1)N\tau$ |
| Activity detection and channel estimation | Message passing | AMP + MMSE denoiser [52] | $\tau M\left(11N+4\right)+4\left(\left\|\mathcal{A}\right\|+1\right)$ |
| | | MP-BSBL [57] | $\left[\left(10\tau_\phi+10\right)MK+\left(7K+14\right)\tau_\phi M+N+2\right]$ |
| | | Iterative EP [59] | $\left[3N^3+\frac{5}{2}N^2+(M+1)N^2+(7M+\frac{5}{2})N-2M+15\right]$ |
| | Machine learning | BRNN [64] | $2M^3+4\left(N+1\right)M^2+2\left(N^2+N+1\right)M-\left(N^2+N\right)$ |
| | | DNN-MP-BSBL [66] | $[M(K(17\tau_\phi+16)+27\tau_\phi)+N+2]$ |

## 2.5 Chapter Summary

In this chapter, the technical background of MIMO systems has been reviewed in order to introduce the massive MTC scenario. A brief introduction of mMTC has been given, where applications, traffic features and challenges are discussed. The signal model used in the unified evaluation framework adopted has been presented, highlighting the grant-free random access model and the key performance indicators used to evaluate the efficiency of the techniques.

Subsequently, detection techniques have been presented, where relevant works were categorized as regularized, greedy and message-passing detectors, which have the objective of performing activity and data detection, were explained and discussed along with their simulation results. Moreover, activity detection and channel estimation schemes classified as message-passing and machine-learning techniques were presented and had its simulation results compared. In the discussions section, the simulation results were evaluated along with a complexity analysis of each simulated approach.

With the state-of-the-art presented, the next chapters describes the proposed approaches. Chapters 3 and 4 presents regularized solutions for joint activity detection and signal decoding that does not need explicit channel estimation. Keeping in mind the trade-off between performance and computational cost, message-passing approaches are proposed in Chapter 5 were the joint activity detection and channel estimation problem is addressed, and in Chapter 6 there is a complete solution for joint activity detection, channel estimation and signal decoding.

# 3
# Adaptive and Iterative Detection and Decoding

## 3.1
## Chapter Overview

In this chapter an adaptive detector that considers the activity and data detection task jointly in an iterative soft information framework without the need to perform explicit channel estimation is described. The problem is formulated in a signal processing fashion, where firstly it is shown the system model, followed by the proposed adaptive decision feedback structure, the detection order update procedure and the inclusion of an $l_0$-norm regularization factor in the RLS algorithm cost function. Furthermore, the proposed IDD scheme is derived, addressing the question of how channel coding and knowledge of the probability of each device activity can jointly be exploited to enhance the detection performance. The chapter ends with the performance comparison of the proposed detection and decoding scheme and the state-of-the-art solutions.

## 3.2
## System Model

Recalling the the massive uplink connectivity scenario presented in the previous Chapter where $N$ devices with a single antenna access a single base station (BS), equipped with $M$ antennas is illustrated in Fig. 3.1 is considered.

As the frame size of mMTC is typically very small (between 10 and 100 bytes) [113], it is possible to assume the devices are synchronized in time. That is, the devices are turned on or turned off in the same transmission slot, as represented in Fig. 3.1. The duration of a transmission slot ($\tau = \tau_\phi + \tau_x$) is smaller than the coherence time and coherence bandwidth of the channel. The BS has the knowledge of the metadata sequences and the time index $t$ indicates

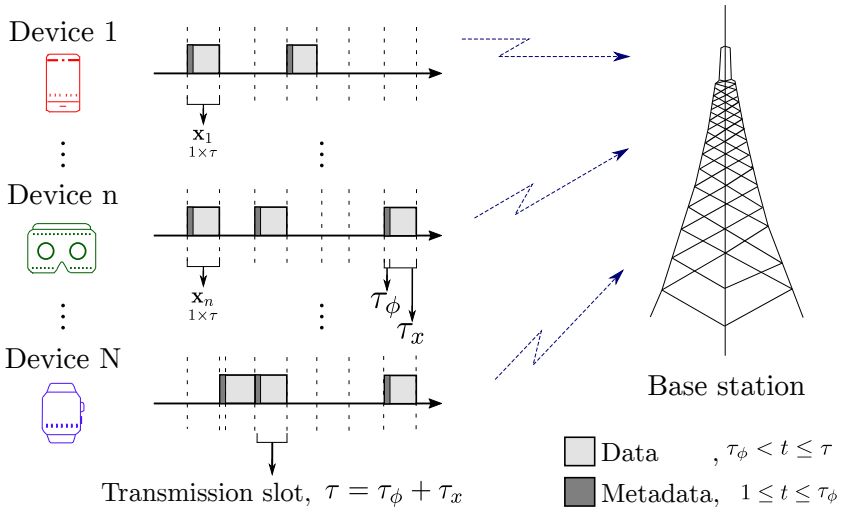


Figure 3.1: mMTC single-cell system model. When active, each device transmits $\tau_\phi$ and $\tau_x$ symbols of metadata and data, respectively, in the coherence time.

each transmitted vector in the same transmission slot. As we considered a grant-free random access model, each frame has metadata and data, in this way the time index indicates how each frame is divided.

The signal model is the same as in (2-27). Thus, the received signal $\mathbf{y}[t]$ in a given coherence time is organized in a $M \times 1$ vector that contains the transmitted metadata ($\boldsymbol{\phi}[t]$) or the data ($\mathbf{x}[t]$), as

$$\mathbf{y}[t] = \begin{cases} \mathbf{H}\sqrt{\tau_\phi}\,\mathbf{B}\,\boldsymbol{\phi}[t] + \mathbf{v}[t], & \text{if} \quad 1 \leq t \leq \tau_\phi \\ \mathbf{H}\sqrt{\tau_x}\,\mathbf{B}\,\mathbf{x}[t] + \mathbf{v}[t], & \text{if} \quad \tau_\phi < t \leq \tau \end{cases}$$

where $\mathbf{H}$ is the $M \times N$ channel matrix, $\mathbf{B}$ is the $N \times N$ transmission power diagonal matrix, $\mathbf{v}$ is the $M \times 1$ noise vector, while $\tau_\phi$ and $\tau_x$ are the number of metadata and data symbols, respectively.

Given the features of mMTC scenarios, the number of devices $N$ is larger than that of antennas $M$ at the base station, in a way that it consists of an underdetermined system. However, the transmitted symbols can be detected as their vectors have a sparse structure as the rows corresponding to the inactive users are zero. So, the activity detection problem is reduced to finding the non-zero rows of $\boldsymbol{\phi}[t]$. With the signal model presented, the proposed detector

structure is derived below.

## 3.3 Adaptive Activity-Aware Iterative Detection

Recursive least squares (RLS) is one of the most used adaptive algorithm, that recursively finds the coefficients that minimize a weighted linear least squares cost function relating to the input signals. It has the advantage of robust performance and fast convergence. In this section, a modified version of the RLS algorithm, named AA-RLS-DF, is presented. The detection scheme is illustrated in a block diagram in Fig. 3.2.

As the transmission slots are separated by metadata and data, AA-RLS-DF has two modes of operation, training mode ($1 \leq t \leq \tau_\phi$) and decision-directed mode ($\tau_\phi < t \leq \tau$). Although the same scheme is used for both cases, in the training mode the focus is to use the metadata to update the RLS algorithm, while the decision-directed mode uses the filter to detect the received data symbols. AA-RLS-DF detects each symbol at a time, per layer. The detection order is updated at each new layer, using the least squares estimation (LSE) criterion. The adaptive receive filter can be decomposed into feedforward and feedback filters. The feedforward one is updated at every new received vector by the $l_0$-norm regularized RLS algorithm. The feedback filter is a component that is concatenated to the feedforward filter in order to cancel the interference of the previously detected symbols.

In the first layer, the filter is composed by the feedforward part and obtains a soft estimate of the symbol with the received vector $\mathbf{y}[t]$. After the first detection, the LSE defines which will be the next layer, the received vector $\mathbf{y}[t]$ is concatenated with the previous detected symbol and the filter of the selected layer is concatenated with the feedback part. This procedure is repeated until the last layer. At this point, the scheme has two vectors, one with all soft estimates ($\tilde{\mathbf{d}}_\psi[t]$), the second one with the detected symbols ($\hat{\mathbf{d}}_\psi[t]$). After the reordering process, if AA-RLS-DF is in the decision-directed

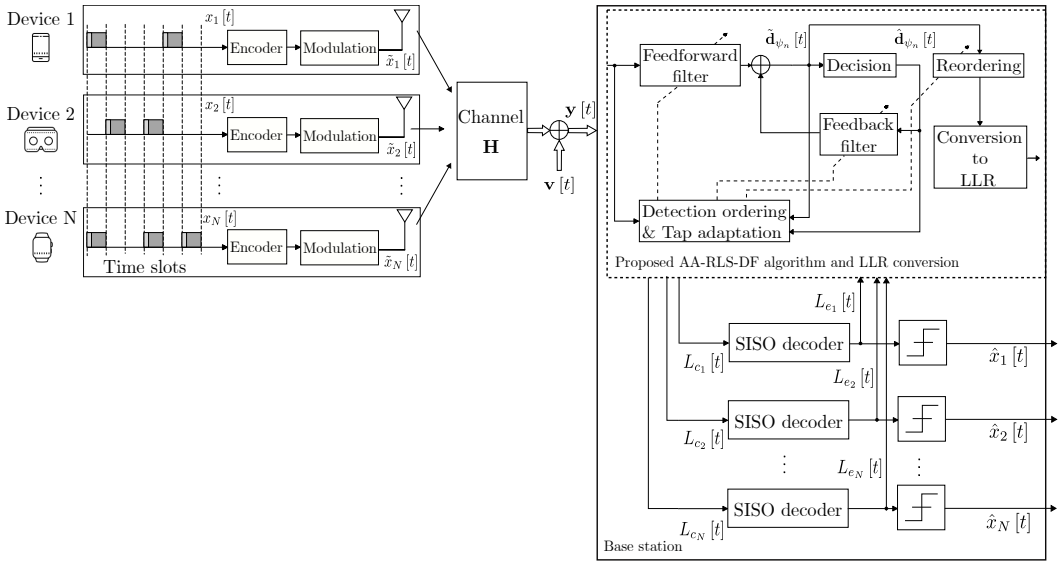


Figure 3.2: Block diagram of AA-RLS-DF with IDD structure. For more details of the scheme, the figure is in landscape format in the Appendix A.1.

mode, the reordered soft estimation vector ($\tilde{\mathbf{d}}[t]$) is converted to LLRs in order to be decoded by the iterative scheme. Otherwise, the reordered vectors of soft estimates and detected symbols ($\hat{\mathbf{d}}[t]$), are used to define the first symbol to be detected in the next received metadata vector.

The following subsections presents the proposed AA-RLS-DF detector in detail. Firstly, the adaptive decision feedback structure is explained, how the receive filters and the received vector concatenation are performed. Then, it is described the detection order update and the $l_0$-norm regularized RLS algorithm.

### 3.3.1 Adaptive Decision Feedback Structure

The main idea is to use a feedforward filter to detect the transmitted symbol and a feedback filter to cancel the interference. For each operation mode, both filters are concatenated and written as

$$\mathbf{w}_{\psi_n}[t] = \begin{cases} \mathbf{w}^f_{\psi_n}[t], & n = 1; \\ \left[\mathbf{w}^{f\ \mathrm{T}}_{\psi_n}[t], \mathbf{w}^{b\ \mathrm{T}}_{\psi_n}[t]\right]^{\mathrm{T}}, & n = 2, \ldots, N. \end{cases} \tag{3-1}$$

where $\mathbf{w}_{\psi_n}[t]$ corresponds to both filters used for the detection of the symbol of

the $n$-th device (or layer). Both filters update their weights and the detection order $\boldsymbol{\psi}$ at each new symbol detection. The received vector $\mathbf{y}\left[t\right]$ is concatenated with the vector $\hat{\mathbf{d}}_{\psi_{n-1}}\left[t\right]$ which contains the previously detected symbols as

$$\mathbf{y}_{\psi_n}\left[t\right] = \begin{cases} \mathbf{y}\left[t\right], & n = 1; \\ \left[\mathbf{y}^{\mathrm{T}}\left[t\right], \hat{\mathbf{d}}^{\mathrm{T}}_{\psi_{n-1}}\left[t\right]\right]^{\mathrm{T}}, & n = 2, \ldots, N \end{cases} \tag{3-2}$$

and each soft symbol estimate of the $n$-th device is given by

$$\tilde{d}_{\psi_n}\left[t\right] = \mathbf{w}^{\mathrm{H}}_{\psi_n}\left[t\right]\mathbf{y}_{\psi_n}\left[t\right]. \tag{3-3}$$

Thus, the filter $\mathbf{w}_{\psi_n}\left[t\right]$ and the received vector $\mathbf{y}_{\psi_n}\left[t\right]$ increases in length at each detection. In the last detection, $\mathbf{w}_{\psi_N}\left[t\right]$ and $\mathbf{y}_{\psi_N}\left[t\right]$ are a $(M+N)\times 1$ vectors, as $\mathbf{w}_N\left[t\right] = \left[w^f_{\psi_N,1}\left[t\right], \ldots, w^f_{\psi_N,M}\left[t\right], w^b_{\psi_N,M+1}\left[t\right], \ldots, w^b_{\psi_N,M+N}\left[t\right]\right]^{\mathrm{T}}$.

### 3.3.2 Detection Order Update

The metric chosen to update the detection order $\boldsymbol{\psi}$, is the minimum LSE. At each symbol detection, we compute the $l_0$-norm cost function $\mathcal{J}_j\left[t\right]$ for the symbols that were not detected yet. The set $S_j\left[t\right]$ contains the index of the remaining symbols to be detected and is updated with the output $\psi_j$ of the cost function. Thus, the index of the chosen filter is stored in the sequence of detection $\boldsymbol{\psi}$, represented as

$$\psi_j = \underset{j\in S_j}{\arg\min}\ \mathcal{J}_j\left[t\right], \tag{3-4}$$

where the indicator $j$ in (3-4) belongs to the set $S_j = \{1, 2, \ldots, N\} - \{\psi_1, \psi_2, \ldots, \psi_{n-1}\}$, which contains the index of not yet detected symbols. Hence, the output index of the cost function is removed from the set and this symbol is chosen to be detected. In the next detection, the already detected symbol does not participate in the new cost function computation. Therefore, the $l_0$-norm cost functions of each phase, are respectively given by

$$\mathcal{J}_j^{\varphi}[t] = \sum_{l=0}^{t} \lambda^{t-l} \left| \varphi_j[l] - \mathbf{w}_j^{\mathrm{H}}[t]\, \mathbf{y}_{\psi_n}[t] \right|^2 + \gamma \|\mathbf{w}_j[t]\|_0, \tag{3-5}$$

$$\mathcal{J}_j^{d}[t] = \sum_{l=\tau_\phi+1}^{t-1} \lambda^{t-1-l} \left| \hat{d}_j[l] - \mathbf{w}_j^{\mathrm{H}}[t]\, \mathbf{y}_{\psi_n}[t] \right|^2 + \gamma \|\mathbf{w}_j[t]\|_0 \tag{3-6}$$

where $\|\cdot\|_0$ denotes $l_0$-norm that counts the number of zero entries in $\mathbf{w}_j$ and $\gamma$ is a non-zero positive constant to balance the regularization and, consequently, the estimation error. Moreover, $0 < \lambda \leq 1$ is the forgetting factor which gives exponentially less weight to older error samples. $\mathcal{J}_j^{\varphi}[t]$ represents in (3-5) the cost function for the metadata mode and $\mathcal{J}_j^{d}[t]$ for the data mode.

### 3.3.3 Regularized RLS Algorithm

In order to exploit the sparse activity of devices and compute the parameters of the proposed DF detector without the need for explicit channel estimation [114], we devise an $l_0$-norm regularized RLS algorithm that minimizes the cost function. Approximating the value of the $l_0$-norm [115], the cost function in (3-5) can be rewritten as

$$\mathcal{J}_j^{\varphi}[t] = \sum_{l=0}^{t} \lambda^{t-l} \left| \varphi_j[l] - \mathbf{w}_j^{\mathrm{H}}[t]\, \mathbf{y}_{\psi_n}[t] \right|^2 + \gamma \sum_{p=1}^{2M} \left(1 - \exp\left(-\xi |w_{j,p}[t]|\right)\right), \tag{3-7}$$

where the parameter $\xi$ regulates the range of the attraction to zero on small coefficients of the filter. Thus, taking the partial derivatives for all entries $t$ of the coefficient vector $\mathbf{w}_j[t]$ in (3-7) and setting the results to zero, yields

$$\mathbf{w}_j[t] = \mathbf{w}_j[t-1] + \mathbf{k}[t]\, \epsilon_n^*[t] - \gamma\, \xi\, \mathrm{sgn}\left(w_{j,p}[t]\right) \exp\left(-\xi |w_{j,p}[t]|\right) \tag{3-8}$$

where $\mathbf{k}[t]$ is the gain vector and $\mathrm{sgn}(\cdot)$ is a component-wise sign function defined as

$$\mathrm{sgn}\left(w_{j,p}[t]\right) = \begin{cases} w_{j,p}[t] / |w_{j,p}[t]|, & w_{j,p}[t] \neq 0; \\ 0, & \text{otherwise.} \end{cases} \tag{3-9}$$

In order to reduce computational complexity in (3-8), the exponential

**Algorithm 1:** Activity-Aware Recursive Least Squares Decision-Feedback (AA-RLS-DF)

**input :** $M$, $N$, $\boldsymbol{\rho}$, $\xi$, $\gamma$, $\lambda$, $\mathbf{P}_{\psi_n} = \boldsymbol{\rho}\,\mathbf{I}_{\mathrm{M}}$
**output:** $\hat{\boldsymbol{x}}$

**begin**

For training mode

▷ *For each metadata sequence,* $\hat{\mathbf{d}}\,[t]$ *and* $\mathbf{y}_{\psi_n}\,[t]$,

$\mathbf{k}_{\psi_n}\,[t] = (\mathbf{P}_{\psi_n}\,[t]\;\mathbf{y}_{\psi_n}\,[t])/(\lambda + \mathbf{y}^{\mathrm{H}}_{\psi_n}\,[t]\;\mathbf{P}_{\psi_n}\,[t]\;\mathbf{y}_{\psi_n}\,[t])$

$\tilde{d}_{\psi_n}\,[t] = \mathbf{w}^{\mathrm{H}}_n\,[t]\;\mathbf{y}_n\,[t]$

$\epsilon_{\psi_n}\,[t] = \hat{d}_{\psi_n}\,[t] - \tilde{d}_{\psi_n}\,[t]$

Update the filters with Eq. (3-11)

$\mathbf{P}_{\psi_n}\,[t] = \lambda^{-1}\left(\mathbf{P}_{\psi_n}\,[t] - \mathbf{k}_{\psi_n}\,[t]\;\mathbf{y}^{\mathrm{H}}_{\psi_n}\,[t]\;\mathbf{P}_n\,[t]\right)$

Concatenate $\mathbf{y}_{\psi_n}\,[t]$ with $\hat{d}_{\psi_n}\,[t]$

Update the sequence of detection with Eq. (3-4)

For decision-directed mode

Compute the *a priori probability* with Eqs. (3-13) and (3-14)

Repeat steps 2 to 8

Compute $\mu_{\psi_n}\,[t]$ and $\zeta^2_{\psi_n}\,[t]$ with Eqs. (3-16) and (3-17)

Verify the likelihood function $P\left(\tilde{d}_n\,[t]\,|\overline{x}\right)$ with Eq. (3-15)

Compute the LLR value according to Eq.(3-18)

**end**

function is approximated by the first order of the Taylor series expansion, given by

$$\exp\left(-\xi\,|w_{j,p}\,[t]\,|\right) \approx \begin{cases} 1 - \xi\,|w_{j,p}\,[t]\,|, & |w_{j,p}\,[t]\,| \leq 1/\xi; \\ 0, & \text{otherwise.} \end{cases} \tag{3-10}$$

As the exponential function is positive, the approximation of (3-10) is also positive. In this way, (3-8) becomes

$$\mathbf{w}_j\,[t] = \mathbf{w}_j\,[t-1] + \mathbf{k}\,[t]\,\epsilon^*_n\,[t] - \gamma\,\xi\,\mathrm{sgn}\left(w_{j,p}\,[t]\right) f_\xi\left(w_{j,p}\,[t]\right) \tag{3-11}$$

where the function $f_\xi\left(w_{j,p}\,[t]\right)$ is given by

$$f_\xi\left(w_{j,p}\,[t]\right) = \begin{cases} \xi^2\left(w_{j,p}\,[t]\right) + \xi, & -1/\xi \leq w_{j,p}\,[t] < 0; \\ \xi^2\left(w_{j,p}\,[t]\right) - \xi, & 0 \leq w_{j,p}\,[t] \leq 1/\xi; \\ 0, & \text{otherwise.} \end{cases} \tag{3-12}$$

We notice that the function $f_\xi\left(w_{j,p}\left[t\right]\right)$ in (3-11) imposes an attraction to zero of small coefficients. So, if the value of $w_{j,p}\left[t\right]$ is not equal or in the range $[-1/\xi, 1/\xi]$, no additional attraction is exerted. Thus, the convergence rate of near-zero coefficients of parameters of devices in mMTC applications that exhibit sparsity will be increased [115]. The pseudo-code, which also considers an IDD scheme with AA-RLS-DF, is described in Algorithm 1.

### 3.3.4 Parameter Adjustment

AA-RLS-DF has three parameters that can be freely chosen, $\gamma$, $\lambda$ and $\xi$. The first one, $\gamma$ is a non-zero positive constant to balance the regularization and, consequently, the estimation error. The forgetting factor of the RLS algorithm gives exponentially less weight to older error samples and $\xi$ regulates the range of the attraction to zero on small coefficients of the filter.

For practical reasons, it was decided to keep the value suggested of $\xi = 10$ in [115] and to optimize the others. The effects of variation of $\lambda$ and $\gamma$ are shown in Figs. 3.4 and 3.3. The simulation results were obtained with the parameters of scenario which are described in section 3.5.

All results are evaluated using the symbol error rate (SER), which considers only the active devices. As a lower bound, the oracle linear mean squared error (LMMSE) which has the knowledge of the index of nonzero entries, is considered. Fig. 3.3 evaluates the effect in the SER for different values of the forgetting factor $\lambda$. As this parameter must respect $0 < \lambda \leq 1$, it was decided to start with it, keeping the value of $\gamma$ present in the literature. As shown in Fig. 3.3, the results are similar for a range of values. When choosing the value $\lambda = 0.92$, its possible to proceed to evaluate the range of values of $\gamma$, as depicted in Fig. 3.4. It is shown that for smaller values than 0.01 of $\gamma$, the best performance is achieved. The higher the value, the worse is the performance. In this way, in order to incorporate the AA-RLS-DF in the IDD scheme, the parameters chosen are $\lambda = 0.92$, $\gamma = 0.001$ and $\xi = 10$.

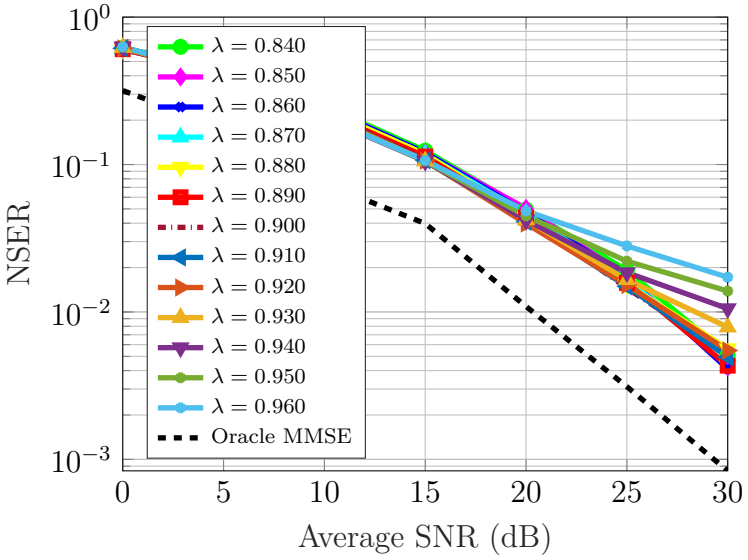


Figure 3.3: Effects of variation of $\lambda$, with $\gamma = 0.001$ and $\xi = 10$.

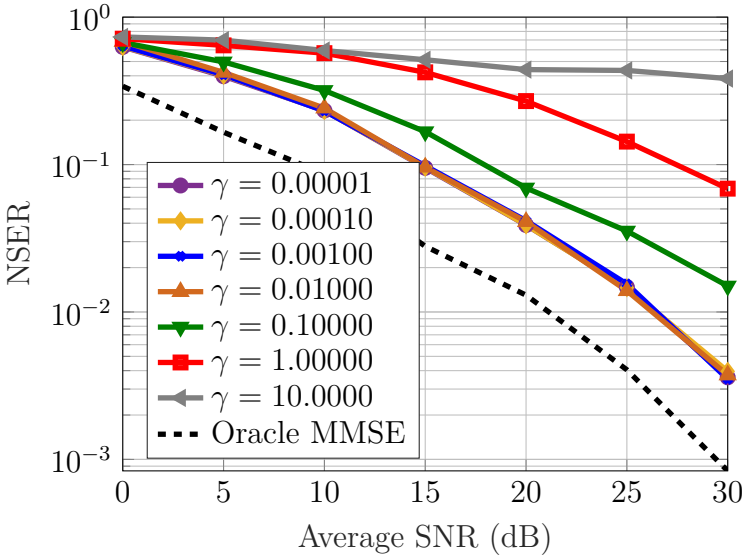


Figure 3.4: Effects of variation of $\gamma$, with $\lambda = 0.92$ and $\xi = 10$.

## 3.4 Iterative Soft Information Processing and Decoding

In order to devise an IDD scheme, we incorporate the detected symbols by AA-RLS-DF in an iterative soft information decoding scheme. Unlike existing approaches such as [116], we incorporate the probability of each device being active in the mMTC scenario in the computation of each a priori probability symbol, which avoids the need for channel estimation.

The *a priori* probabilities are computed based on the extrinsic LLRs $L_{e_n}^z[t]$, provided by the LDPC decoder. In the first iteration, all $L_{e_n}^z[t]$ are zero and, assuming the bits are statistically independent of one another, the *a priori* probabilities are calculated as

$$\Pr\left(x_n[t]=\overline{x}\right)=\sum_{\overline{x}\in\mathcal{A}_0}\overline{x}\left(\prod_{z=1}^{M_c}\left[1+\exp\left(-\overline{x}^z L_{e_n}^z[t]\right)\right]^{-1}\right), \tag{3-13}$$

where $M_c$ represents the total number of bits of symbol $\overline{x}$, the superscript $z$ indicates the $z$-th bit of symbol of $\overline{x}$, in $\overline{x}^z$ (whose value is $(+1,-1)$). As each device has a different activity probability $\rho_n$, the *a priori* probabilities should take into account, as

$$\begin{aligned}\rho_n+(1-\rho_n)\Pr\left(x_n[t]=\overline{x}\right), &\quad \text{if } (\overline{x}^1 \text{ and } \overline{x}^2)=0,\\ (1-\rho_n)\Pr\left(x_n[t]=\overline{x}\right), &\quad \text{otherwise.}\end{aligned} \tag{3-14}$$

where in the next iteration of the scheme, the new *a priori* probabilities incorporates the probability that the $n$-th device is active and the extrinsic LLR values.

As the output of the proposed receive filter has a large number of independent variables, we can approximate it as a Gaussian distribution [117]. Hence, we approximate $\tilde{d}_n[t]$ by the output of an equivalent AWGN channel with $\tilde{d}_n[t]=\mu_n[i]\,x_n[t]+b_n[t]$. Therefore, the likelihood function $P\left(\tilde{d}_n[t]\,|\,\overline{x}\right)$ is approximated by

$$P\left(\tilde{d}_n[t]\,|\,\overline{x}\right)\approx\frac{1}{\pi\,\zeta_n^2[t]}\exp\left(-\frac{1}{\zeta_n^2[t]}|\tilde{d}_n[t]-\mu_n[t]\,\overline{x}|^2\right), \tag{3-15}$$

where the mean $\mu_n[t]$ is given by

$$\begin{aligned}\mu_n[t]&=\mathbb{E}\left\{\tilde{d}_n[t]\,x_n[t]\right\}=\mathbb{E}\left\{\mathbf{w}_n^{\mathrm{H}}[t]\,\mathbf{y}_n[t]\,x_n[t]\right\}\\ &\approx\mathbf{w}_n^{\mathrm{H}}[t]\left(\sum_{p=1}^{t-1}\lambda^{t-1-p}\,\mathbf{y}_n[p]\,x_n[p]\right).\end{aligned} \tag{3-16}$$

Note that $x_n$ is the previously detected symbol. In the first case, $\mu_n[t]=$

$\mathbf{w}_n^{\mathrm{H}}[t]\,\mathbf{y}_n[t]$. Each $b_n[t]$ is a zero-mean complex Gaussian variable with variance $\zeta_n^2[t]$ as

$$\begin{aligned}\zeta_n^2[t] &= \mathrm{var}\left\{\tilde{d}_n[t]\right\} = \mathbb{E}\left\{\|\tilde{d}_n[t]\|^2\right\} - \mu_n^2[t] \\ &= \mathbf{w}_n^{\mathrm{H}}[t]\,\mathbb{E}\left\{\mathbf{y}_n[t]\,\mathbf{y}_n^{\mathrm{H}}[t]\right\}\mathbf{w}_n[t] - \mu_n^2[t] \\ &\approx \mathbf{w}_n^{\mathrm{H}}[t]\left(\sum_{p=1}^{t}\lambda^{t-p}\,\mathbf{y}_n[p]\,\mathbf{y}_n^{\mathrm{H}}[p]\right)\mathbf{w}_n[t] - \mu_n^2[i]\,.\end{aligned} \tag{3-17}$$

Then, the extrinsic LLRs computed by the AA-RLS-DF detector for the $z$-th bit ($z \in \{1,\ldots,M_c\}$) of the symbol $x_n$ transmitted by the $n$-th device are given by

$$L_{c_n}^{z}[t] = \log\frac{\sum_{\overline{x}\in\mathcal{A}_z^{+1}}\Pr\left(\tilde{d}_n[t]\,|\,\overline{x}\right)\Pr(\overline{x})}{\sum_{\overline{x}\in\mathcal{A}_z^{-1}}\Pr\left(\tilde{d}_n[t]\,|\,\overline{x}\right)\Pr(\overline{x})} - L_{e_n}^{z}[t] \tag{3-18}$$

where $\mathcal{A}_z^{+1}$ is the set of $2^{M_c-1}$ hypotheses of $\overline{x}$ for which the $z$-th bit is $+1$ (analogously for $\mathcal{A}_z^{-1}$).

## 3.5 Numerical Results

The simulation results were obtained considering an under-determinated mMTC system with $N = 128$ devices and a single-base station equipped with $M = 64$ antennas. The proposed and existing schemes experience an independent and identically-distributed (i.i.d.) random flat-fading channel model and the values are taken from complex Gaussian distribution of $\mathcal{N}_c(0,1)$. The active devices radiate QPSK symbols with the same power and the activity probabilities $\{\rho_n\}_{n=1}^{N}$ are drawn uniformly at random in $[0.1, 0.3]$. Each symbol block has 128 symbols, split in to 60 metadata and 68 data. This balance between pilots and data is suggested in [118]. All these assumptions are considered into two scenarios, uncoded and coded systems, in which numerical results are averaged over $10^5$ runs. The performance of AA-RLS-DF is compared with other relevant schemes, as the linear mean squared

error (LMMSE), unsorted SA-SIC [28], SA-SIC with A-SQRD [29], AA-MF-SIC [30] and a version of AA-RLS-DF without decision feedback, AA-RLS. As a lower bound, the Oracle LMMSE detector, which has the knowledge of the index of nonzero entries, is considered. For all algorithms that require explicit channel estimation, we considered $\hat{\mathbf{H}} = \mathbf{H} + \mathbf{E}$, where $\mathbf{H}$ represents the channel estimate and $\mathbf{E}$ is a random matrix corresponding to the error for each link. Each coefficient of the error matrix follows a Gaussian distribution, i.e., $\sim \mathcal{N}_c\,(0, \sigma_e^2)$, where $\sigma_e^2 = \sigma_v^2/5$. For uncoded systems, the average SNR is given by $10\log\left(N\,\sigma_x^2/\sigma_v^2\right)$, while for coded systems is $10\log\left(NR\,\sigma_x^2/\sigma_v^2\right)$.

Fig. 3.5a shows the symbol error rate (SER) which considers only the active devices. LMMSE exhibits poor performance since the system is underdetermined. Due to error propagation, the unsorted SA-SIC does not perform well. A-SQRD and AA-MF-SIC are effective since both consider the activity probabilities, but under imperfect CSI conditions, their performance is not so good. In contrast, as AA-RLS-DF does not need a explicit channel estimation, it is more efficient. The decision-feedback scheme provides a SER gain due to the interference cancellation. For the coded systems with IDD, Fig. 3.5b shows the BER of the already considered algorithms and the modified scheme of Wang and Poor [117]. The sparsity of mMTC approach degrades the expected efficiency of LMMSE-PIC, obtaining little variation in relation to LMMSE and SA-SIC. The hierarchy of performance of the other considered algorithms is the same as the uncoded case but with better error rate values.

In order to evaluate the activity detection of the algorithms, the false alarm rate and the missed detection rate are used. The missed detection rate (MDR) denotes the total number of symbols that have been transmitted in a specific time instant that the detector judged as zero, divided by the number of active devices. On the other hand, the false alarm rate (FAR) denotes the total number of symbols that the detector judged as different of zero, divided by the difference between the total number of devices and the number

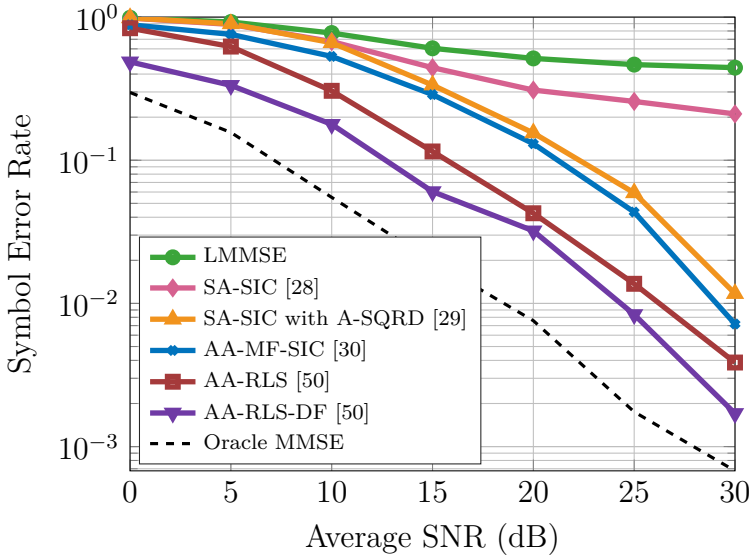


(a) Symbol error rate vs. Average SNR.

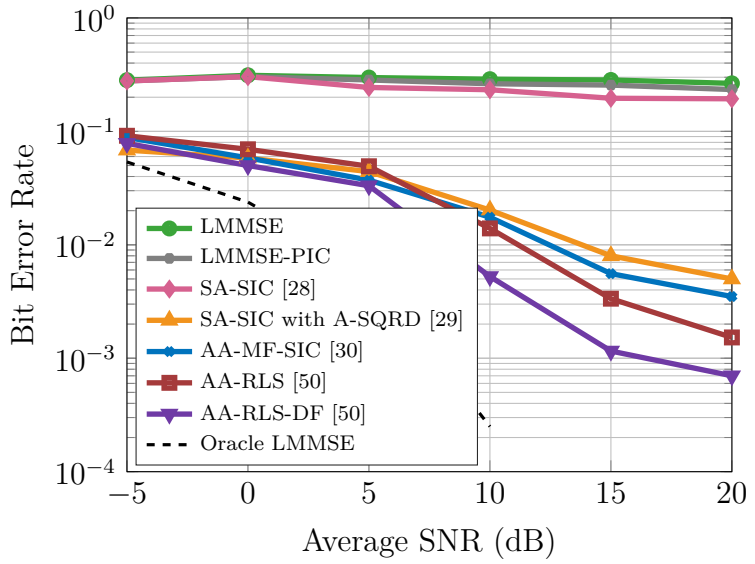


(b) Bit error rate vs. Average SNR.

Figure 3.5: Numerical results under KPI evaluation. Parameters of proposed schemes are $\lambda = 0.92$, $\gamma = 0.001$ and $\xi = 10$, other approaches consider imperfect CSI. LDPC with block length of 128, symbol rate $R = 0.5$, refined by 2 decoding iterations.

of active devices in a specific time instant. For the same scenario described before, Figs. 3.6a and 3.6b show the activity detection performance of the considered algorithms. One can see that, regarding the proposed AA-RLS-DF, the bottleneck to improve the detection is the missed detection rate, that is, there is a significant number of devices wrongly being judged as inactive.

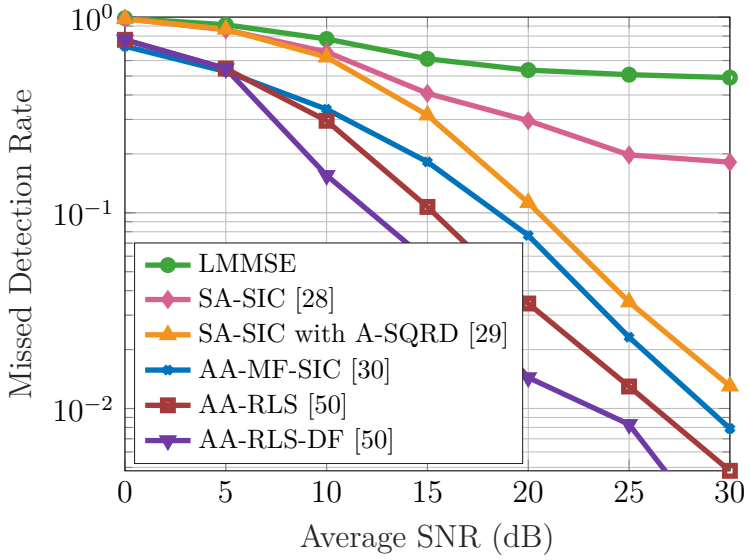


(a) Missed detection rate vs. Average SNR.

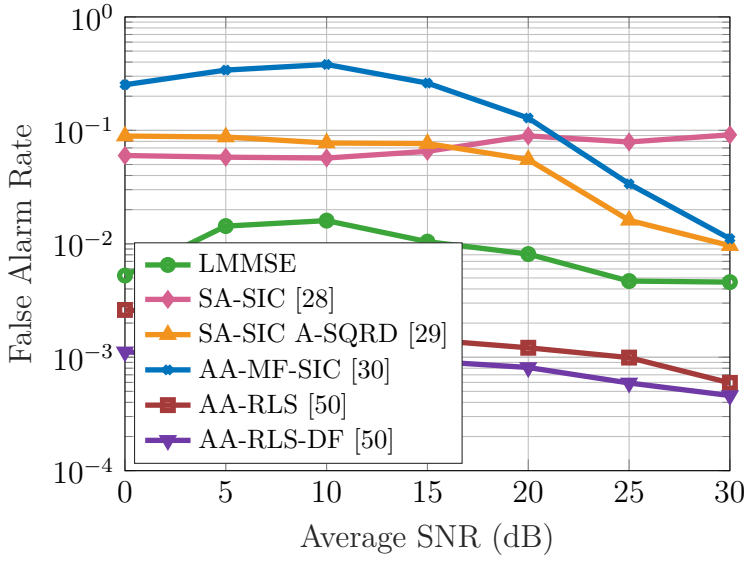


(b) False alarms rate vs. Average SNR.

Figure 3.6: Numerical results under KPI evaluation. Parameters of proposed schemes are $\lambda = 0.92$, $\gamma = 0.001$ and $\xi = 10$, other approaches consider imperfect CSI. LDPC with block length of 128, symbol rate $R = 0.5$, refined by 2 decoding iterations.

Therefore, improvements with respect to decision-making of the activity can be made.

## 3.6 Chapter Summary

In this chapter an adaptive and iterative soft processing algorithm that jointly estimate the activity and the data of MTCDs has been presented and studied. The AA-RLS-DF detector augments state-of-the-art solutions by processing soft information from a channel decoder and from an activity estimation jointly. Therefore, the AA-RLS-DF detection scheme consists of three blocks accounting for the estimation of the multiuser signal, the information bits and the activity states of the MTCDs. These blocks exchange extrinsic information and do not perform any explicit channel estimation. Hence, the information symbols from all devices, active or not, are estimated. Thus, all the key indicator performances (SER, BER, MDR and FAR) should be considered in the analysis.

# 4
# Adaptive and Iterative List Detection and Decoding

## 4.1
## Chapter Overview

The previous chapter mainly focused on the description and derivation of the AA-RLS-DF detector. As the results have shown, despite presenting a performance superior to the state-of-the-art, AA-RLS-DF has a room for improvement. Since there is a gap between the performance of the considered lower bound and the proposed algorithm, a new detection scheme, named AA-VGL-DF, exploits the the system sparsity, and refines the detection provided for the adaptive $l_0$-norm regularized RLS algorithm using two candidate-list techniques. Besides that, in order to perform the decoding, an IDD scheme based on the proposed AA-VGL-DF is also incorporated.

Furthermore, the grant-free access model is improved, where the considered traffic model is based on a 3GPP technical report. As a means of improving the performance of the AA-RLS-DF detector, we describe the two candidate-list techniques incorporated. Subsequently, the chapter provides an evaluation of AA-VGL-DF in a comprehensive way with the analysis of the computational complexity, diversity order and the derivation of uplink sum-rate expressions. The chapter ends with the performance comparison of the proposed AA-VGL-DF detector and state-of-the-art solutions in terms of SER, BER and spectral efficiency. The proposed AA-VGL-DF detection scheme is also analysed for different traffic model scenarios.

## 4.2 System Model

As networks should support many different applications with distinct requirements, naturally each device has its own activity behaviour. In order to model this scenario, the beta-binomial distribution [119] is considered to model the problem as the probability of being active $\rho_n$ is randomly drawn from a beta distribution, proposed as a traffic model by the 3GPP [120]. Considering $N$ devices with a single antenna accessing a base station (BS), the probability mass function is given by

$$p\left(K\right) = \binom{N}{K} \rho_n^K \left(1-\rho_n\right)^{N-K} \tag{4-1}$$

where $\rho_n$ is a random variable with a beta distribution that represents the probability of being active of the $n$-th device and $K$ is the number of active devices out of $N$ at the same transmission slot. The sparsity of the scenario is modified as soon as each random variable $\rho_n$ with beta distribution is modelled. Thus, each device has its own activity probability.

Hence, the probability of having K active devices within a total of N at the same transmission slot is given by

$$\begin{aligned} p\left(K \mid N, \alpha, \beta\right) = & \frac{\Gamma\left(N+1\right)}{\Gamma\left(K+1\right)\Gamma\left(N-K+1\right)} \\ & \times \frac{\Gamma\left(N+\alpha\right)\Gamma\left(N-K+\beta\right)}{\Gamma\left(N+\alpha+\beta\right)} \frac{\Gamma\left(\alpha+\beta\right)}{\Gamma\left(\alpha\right)\Gamma\left(\beta\right)} \end{aligned} \tag{4-2}$$

where $\Gamma\left(\cdot\right)$ is the gamma function, $\alpha$ and $\beta$ are real positive parameters that appear as exponents of the random variable $\rho_n$ and control the shape of the distribution. The average number of active devices is $\left(N\alpha\right)/\left(\alpha+\beta\right)$ and its variance is $\Big(N\alpha\beta\left(\alpha+\beta+N\right)\Big)\Big/\Big(\left(\alpha+\beta\right)^2\left(\alpha+\beta+1\right)\Big)$.

In most mMTC applications the devices have low probability of being active. Fig. 4.1 shows the probability of a specific number of devices to be active at the same time for different values of $\alpha$ and $\beta$ in a scenario of $N = 120$.

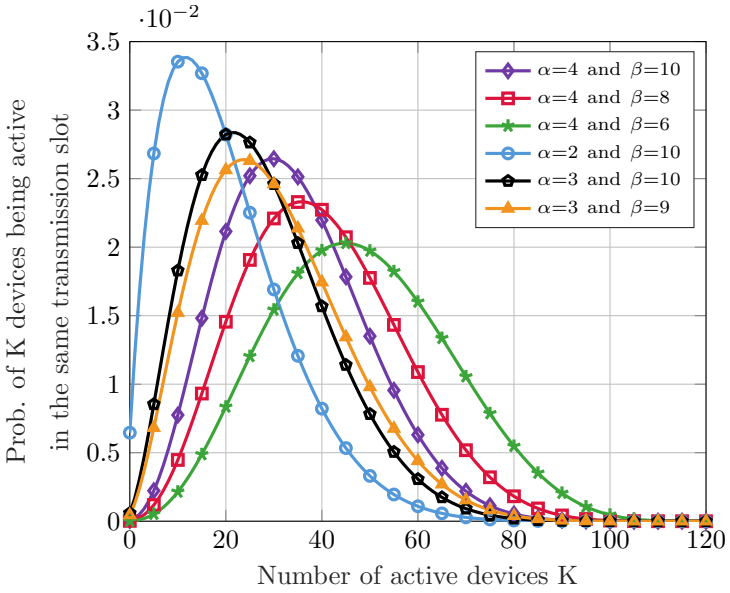


Figure 4.1: Model of probability of having $K$ active devices within a total of $N = 120$. All devices become independently active with a probability determined by the random variable $\rho_n \in [0, 0.1, \ldots, 1]$ with a beta distribution.

When adding the traffic model described here, the system model presented in the previous chapter is considered in remainder of this chapter.

## 4.3 Variable Group-List Decision Feedback Detection

For the purpose of reducing the detection error propagation of the AA-RLS-DF scheme, two candidates-list techniques are developed. In this section, the new activity-aware variable group-list decision feedback (AA-VGL-DF) detector is presented. The new detection scheme is illustrated in a block diagram in Fig. 4.2.

Following the same procedure of AA-RLS-DF, AA-VGL-DF has the same two modes of operation, training mode ($1 \leq t \leq \tau_\phi$) and decision-directed mode ($\tau_\phi < t \leq \tau$), also detecting each symbol at a time, per layer. In the step that the feedforward filter obtains a soft estimate of the symbol being detected with the received vector $\mathbf{y}[t]$, the soft estimate is analysed by the first candidates-list technique, named internal list. A criterion, named shadow area constraints (SAC), is developed in order to evaluate the reliability of the hard decision of the soft symbol estimate. The idea is that if the symbol is considered unreliable,

a list of candidates drawn from the constellation symbols is generated and the best candidate, chosen by the maximum likelihood criterion, replaces the unreliable symbol. After the first detection, the LSE defines which will be the next layer, the received vector $\mathbf{y}\,[t]$ is concatenated with the previous detected symbol and the filter of the selected layer is concatenated with the feedback part. This procedure is repeated until the last layer. At this point, the scheme has three vectors, one with all soft estimates ($\tilde{\mathbf{d}}_{\psi}\,[t]$), the second one with the detected symbols ($\hat{\mathbf{d}}_{\psi}\,[t]$) and the third one ($\boldsymbol{\vartheta}_{\psi}\,[t]$) that keeps the information about the reliability of each soft estimate. Those three vectors are reordered to the original sequence and the second list of candidates, named external list, begins. The idea of this list is to perform a group list verification of the most unreliable symbols, after the last detection. With more reliable detected vectors, a more accurate decision of the first filter to be used in the next detection will be taken. In order to define which soft estimates will be rechecked with the second list, we apply the SAC criterion again, but with a larger radius. After the reordering process, if AA-VGL-DF is in the decision-directed mode, the reordered soft estimation vector ($\tilde{\mathbf{d}}\,[t]$) is converted to LLRs in order to be decoded by the iterative scheme. Otherwise, the reordered vectors of soft estimates and detected symbols ($\hat{\mathbf{d}}\,[t]$), are used to define the first symbol to be detected in the next received metadata vector. The candidates-list techniques are detailed in the following subsections.

### 4.3.1 Internal List

In order to improve the detection performance, we include a SAC, to evaluate the reliability of the soft estimates. As shown in Fig. 4.2, with the augmented alphabet of a QAM modulation scheme, the SAC compares the distance between the soft estimate and all the possible constellation symbols with

$$r = \underset{i\,\in\,1,\cdots,(|\mathcal{A}|+1)}{\arg\min} \; \|\mathcal{A}_{0_i} - \tilde{d}_{\psi_n}\,[t]\,\|^2, \tag{4-3}$$

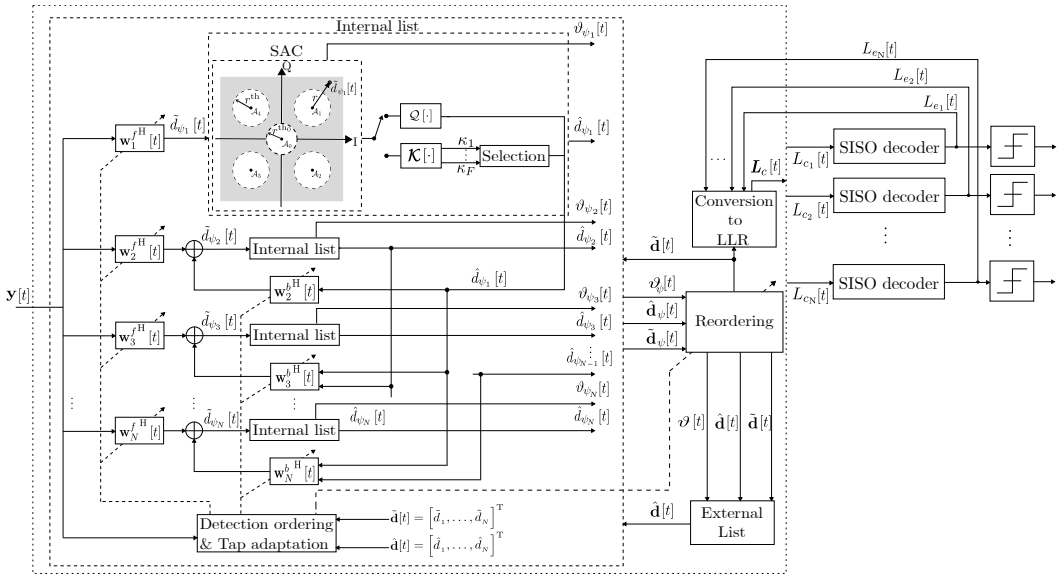


Figure 4.2: Detailed structure of the AA-VGL-DF detector and the IDD scheme. To simplify notations, just one received vector is considered in the base station. For more details of the scheme, the figure is in landscape format in the Appendix A.2.

where $|\mathcal{A}|$ is the modulation order. If the soft estimate falls into the shadow area ($r > r^{\text{th}}$ or $r > r^{\text{th}_0}$), the estimate is considered unreliable and then $\tilde{d}_{\psi_n}[t]$ proceeds to the list scheme. Otherwise, it is just quantized to the nearest symbol of the augmented constellation $\mathcal{A}_0$, as

$$\hat{d}_{\psi_n}[t] = \mathcal{Q}\left[\mathbf{w}_{\psi_n}^{\text{H}}[t]\,\mathbf{y}_{\psi_n}[t]\right]. \tag{4-4}$$

The $r^{\text{th}}$ and $r^{\text{th}_0}$ radius of each reliability region are defined by the probability of being active of each device and the radius of the region around the zero (inactive device) is the complement of the radius of the regions around the constellation symbols, $r^{\text{th}_0} = 1 - r^{\text{th}}$. This radius was chosen given the simulations results shown in Fig. 4.3. Instead of choosing a fixed radius value, use the probability of being active of each device provided a better result.

The list scheme is a verification of a list of candidates drawn from constellation symbols to the actual detection. The list $\boldsymbol{\kappa} = \left[\kappa_1 \cdots, \kappa_{(|\mathcal{A}_0|)}\right]$ is used to select the best candidate according to

$$\boldsymbol{\kappa}_{\text{opt}} = \underset{i \in 1,\cdots,(|\mathcal{A}_0|)}{\arg\min} \|\mathbf{y}[t] - \hat{\mathbf{h}}_{\psi_n}\,\kappa_i\|^2, \tag{4-5}$$

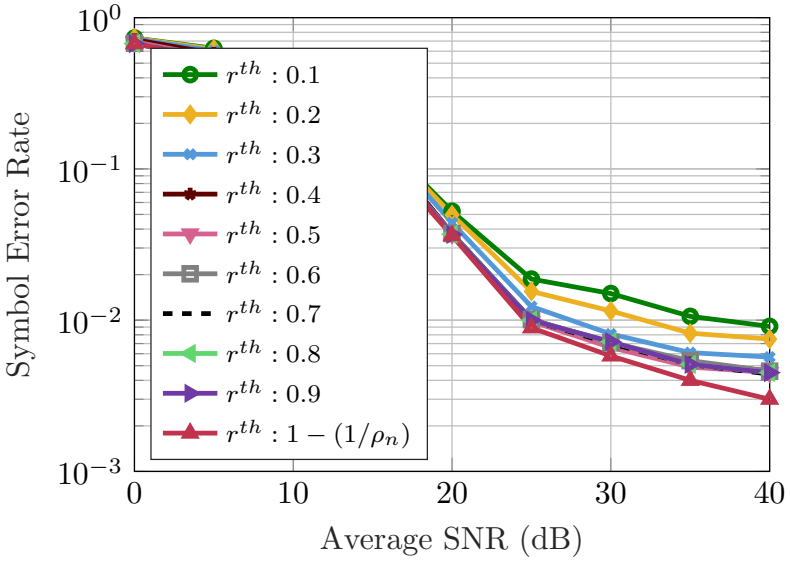


Figure 4.3: Variation of SAC radius.

where the vector $\hat{\mathbf{h}}_{\psi_n}$ contains the estimate of the channel between the device that performs symbol detection and the BS. As the channel estimation is not the focus of this work, we considered the well known linear MMSE (LMMSE) estimation. The estimate of each $\hat{\mathbf{h}}_{\psi_n}$ is detailed in Subsection 4.4.2.2.

The vector with minimum argument $\boldsymbol{\kappa}_{\text{opt}}$ indicates which candidate $\kappa$ will replace the quantized version of the unreliable soft symbol estimate $\tilde{d}_{\psi_n}[t]$.

### 4.3.2 External List

The idea of the external list is to carry out a group list verification of the most unreliable symbols, after the last detection. In the internal list block, AA-VGL-DF also keeps the information about the reliability of each soft estimate. The $N \times 1$ binary vector $\boldsymbol{\vartheta}_{\psi}[t]$ gathers this information as $\vartheta_{\psi_n}[t] = 1$ when a soft estimate falls into the shadow area and $\vartheta_{\psi_n}[t] = 0$, otherwise. After the reordering process, the external list block receives the estimated symbols $\tilde{\mathbf{d}}[t]$, the detected symbols $\hat{\mathbf{d}}[t]$ and the vector with the reliability information, $\boldsymbol{\vartheta}[t]$.

With the knowledge of which symbols had a reliable soft estimate, the external list generates all possible combinations $\mathcal{G}$ of the symbols of the considered augmented alphabet $\mathcal{A}_0$ and gathers all these vectors in an $\nu \times \mathcal{G}$

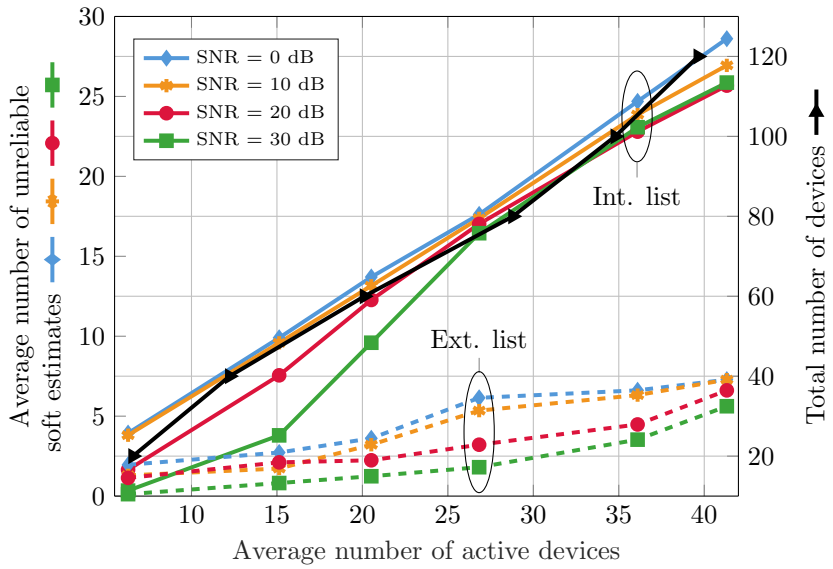


Figure 4.4: The internal list results are the continuous line while the external list values are shown in dashed lines. The probability of being active of each device is randomly drawn from a beta distribution with $\alpha = 4$ and $\beta = 8$.

matrix $\mathbf{G}$ given by

$$\mathbf{G} = \begin{bmatrix} \mathcal{A}_{0_1} & \mathcal{A}_{0_1} & \mathcal{A}_{0_1} & \cdots & \mathcal{A}_{0_3} & \cdots & \mathcal{A}_{0_{|\mathcal{A}_0|}} \\ \mathcal{A}_{0_1} & \mathcal{A}_{0_2} & \mathcal{A}_{0_1} & \cdots & \mathcal{A}_{0_1} & \cdots & \mathcal{A}_{0_{|\mathcal{A}_0|}} \\ \mathcal{A}_{0_1} & \mathcal{A}_{0_1} & \mathcal{A}_{0_2} & \cdots & \mathcal{A}_{0_2} & \cdots & \mathcal{A}_{0_{|\mathcal{A}_0|}} \\ \vdots & \vdots & \vdots & \ddots & \vdots & \ddots & \vdots \\ \mathcal{A}_{0_1} & \mathcal{A}_{0_1} & \mathcal{A}_{0_1} & \cdots & \mathcal{A}_{0_4} & \cdots & \mathcal{A}_{0_{|\mathcal{A}_0|}} \end{bmatrix}, \tag{4-6}$$

where $\nu$ is the number of soft estimates considered unreliable. With the complete candidate vector matrix, the verification of the most appropriate vector occurs as in the internal list, as follows:

$$\mathbf{g}_{\text{opt}} = \underset{i \in 1,\cdots,\mathcal{G}}{\arg\min} \left\| \mathbf{y}\,[t] - \sum_{j=1}^{\nu} \hat{\mathbf{h}}_j \, g_{j,i} \right\|^2, \tag{4-7}$$

where $\hat{\mathbf{h}}_j$ is the estimated channel of the unreliable symbol to be verified. The vector candidate $\mathbf{g}_{\text{opt}}$ is chosen and its values replace the ones considered unreliable in $\hat{\mathbf{d}}\,[t]$ in order to proceed to the detection, ordering and parameter estimation of the next received vector.

As an example, let us suppose that we have 4 unreliable estimates

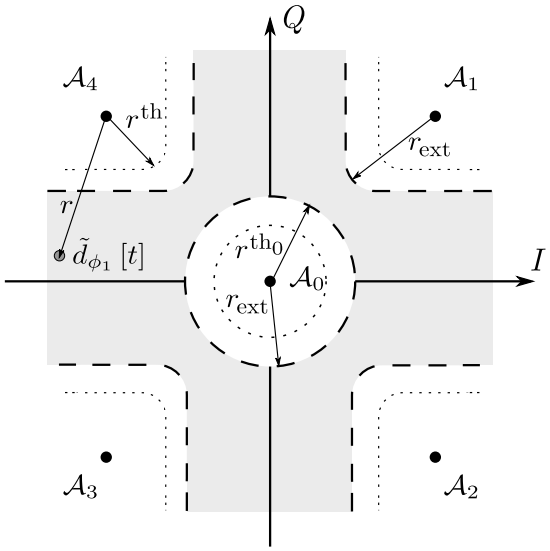


Figure 4.5: The radius $r^{\text{th}_0}$ and $r^{\text{th}}$ delimits the reliable regions for the internal list while $r_{\text{ext}}$ for the external list.

(non-zero elements) in vector $\boldsymbol{\vartheta}_{\psi}[t]$. Considering a QPSK modulation, the augmented alphabet $\mathcal{A}_0$ would have 5 elements and $\mathcal{G}$ would be a $4 \times 70$ matrix, considering all the 70 combination possibilities of 5 possible symbols in 4 unreliable estimates.

Since mMTC is a crowded scenario, building the external $\mathbf{G}$ matrix with all possible combinations would be impractical. Thus, considering the distribution of probability of being active of devices, we notice in Fig. 4.4 that just a few symbols are considered unreliable by the internal list per received vector and this number is reduced as the SNR grows. Therefore, we considered a constraint in order to reduce the computational complexity of the external list. Instead of verifying all the possibilities of all unreliable soft estimates, we check the worst cases, that is, the soft estimates considered more unreliable. Thus, we define another radius in the SAC in order to designate which unreliable symbols should be or not in the external list. As the number of unreliable estimates varies with the SNR, we choose the radius, represented in Fig. 4.5, as $r_{\text{ext}} = r^{\text{th}}\left[\left(M/\hat{K}\right) + (N\sigma_x^2/\sigma_v^2)\right]$ since it follows the increase of the average SNR value. Thus, the reliability of $\tilde{\mathbf{d}}[t]$ will be rechecked, with the new radius $r_{\text{ext}}$. As we have a $\hat{\mathbf{d}}[t]$, we have an estimation of which device is active

**Algorithm 2:** Activity-Aware Variable Group List Decision Feedback (AA-VGL-DF)

**input :** $M$, $N$, $\boldsymbol{\rho}$, $\xi$, $\gamma$, $\lambda$, $\mathbf{P}_{\psi_n} = \boldsymbol{\rho}\,\mathbf{I}_{\mathrm{M}}$
**output:** $\hat{\boldsymbol{x}}$

**begin**

For training mode

▷ *For each metadata sequence,* $\hat{\mathbf{d}}\,[t]$ *and* $\mathbf{y}_{\psi_n}\,[t]$,

$\mathbf{k}_{\psi_n}\,[t] = (\mathbf{P}_{\psi_n}\,[t]\;\mathbf{y}_{\psi_n}\,[t])/(\lambda + \mathbf{y}^{\mathrm{H}}_{\psi_n}\,[t]\;\mathbf{P}_{\psi_n}\,[t]\;\mathbf{y}_{\psi_n}\,[t])$
$\tilde{d}_{\psi_n}\,[t] = \mathbf{w}^{\mathrm{H}}_{n}\,[t]\;\mathbf{y}_{n}\,[t]$
$\epsilon_{\psi_n}\,[t] = \hat{d}_{\psi_n}\,[t] - \tilde{d}_{\psi_n}\,[t]$
Update the filters with Eq. (3-11)
$\mathbf{P}_{\psi_n}\,[t] = \lambda^{-1}\left(\mathbf{P}_{\psi_n}\,[t] - \mathbf{k}_{\psi_n}\,[t]\;\mathbf{y}^{\mathrm{H}}_{\psi_n}\,[t]\;\mathbf{P}_{n}\,[t]\right)$
Concatenate $\mathbf{y}_{\psi_n}\,[t]$ with $\hat{d}_{\psi_n}\,[t]$
Update the sequence of detection with Eq. (3-4)

For decision-directed mode

Compute the *a priori probability* with Eqs. (3-13) and (3-14)
Repeat steps 2 to 8
Evaluate the reliability of the soft estimation $\tilde{d}_{\psi_n}\,[t]$ with SAC and proceeds with the internal list if it is judged as unreliable
Update the sequence of detection with the output of 11
Proceed with the update of $\boldsymbol{\vartheta}_{\psi}\,[t]$, $\mathbf{y}_{\psi_n}\,[t]$ and $\mathbf{w}_{\psi_n}\,[t]$
After all detections, update $\hat{\mathbf{d}}\,[t]$ with the external list
Compute $\mu_{\psi_n}\,[t]$ and $\zeta^2_{\psi_n}\,[t]$ with Eqs. (3-16) and (3-17)
Verify the likelihood function $P\left(\tilde{d}_n\,[t]\,|\overline{x}\right)$ with Eq. (3-15)
Compute the LLR value according to Eq.(3-18)

**end**

or not, given by $\hat{K}$. So, the number $\nu$ of considered unreliable soft estimates is reduced as the SNR value grows, as shown in Fig. 4.4. Algorithm 2 summarizes the procedure and in the next section the AA-VGL-DF is analysed.

## 4.4 Analysis

This section analyses the AA-VGL-DF in terms of the computational complexity and both the diversity order achieved by the AA-VGL-DF detector and the achievable rate of the uplink transmission from the $n$-th user are discussed.

Table 4.1: FLOPs counting of considered techniques in detail.

| Algorithms | Required number of FLOPs |
|---|---|
| LMMSE | $2M^3 + 4\left(N+1\right)M^2 + 2\left(N^2+N+1\right)M - \left(N^2+N\right)$ |
| SA-SIC | $\left\|\mathcal{A}_0\right\|\left(N^3+N^2+6\right)$ |
| SA-SIC A-SQRD [29] | $2N^3 + 4\left(M+1\right)N^2 + \left(M-1\right)N$ |
| AA-RLS | $\left(6M^2+10M\right)N$ |
| AA-RLS (internal list) | $\left[6M^2+10M+\vartheta_n\left(2M\left\|\mathcal{A}_0\right\|\right)\right]N$ |
| AA-RLS-DF | $\sum_{i=1}^{N}\left[6\left(M+i\right)^2+10\left(M+i\right)\right]$ |
| AA-RLS-DF (internal list) | $\sum_{i=1}^{N}\left[6\left(M+i\right)^2+10\left(M+i\right)+\vartheta_n\left(2M\left\|\mathcal{A}_0\right\|\right)\right]$ |
| AA-VGL-DF | $\sum_{i=1}^{N}\left[6\left(M+i\right)^2+10\left(M+i\right)+\vartheta_n\left(2M\left\|\mathcal{A}_0\right\|\right)\right]+2M\mathcal{G}$ |

### 4.4.1 Complexity

The computational complexity of AA-VGL-DF is analyzed below by counting each required numerical operation in terms of complex FLOPs. In particular, Table 4.1 compares the number of required FLOPs, for a different number of devices $N$, receive antennas $M$ and the $\mathcal{G}$ group size. We consider both well-known algorithms as linear minimum-mean-squared-error (LMMSE) and modifications for mMTC, as SA-SIC [27], SA-SIC with A-SQRD [29] and AA-RLS-DF [50], proposed in the previous chapter.

Including the internal list technique in the AA-RLS-DF, as shown in Fig. 4.6, results in just a slight complexity increase. Recalling that $\mathcal{G}$ is the number of combinations of the unreliable soft estimates, the upper bound of AA-VGL-DF is a version where there are not constraints in the lists. As verified in Fig. 4.4, the number of unreliable soft estimates increase as the number of devices rises. The computational cost of AA-VGL-DF is comparable with a standard DF detector with an RLS algorithm. Since many other considered algorithms have a similar computational cost, AA-VGL-DF has a competitive complexity when compared with other schemes.

### 4.4.2 Uplink Sum-Rate

As seen that the mMTC has an amount of features that distinguish from the standard massive MIMO communications, we compute the uplink sum-

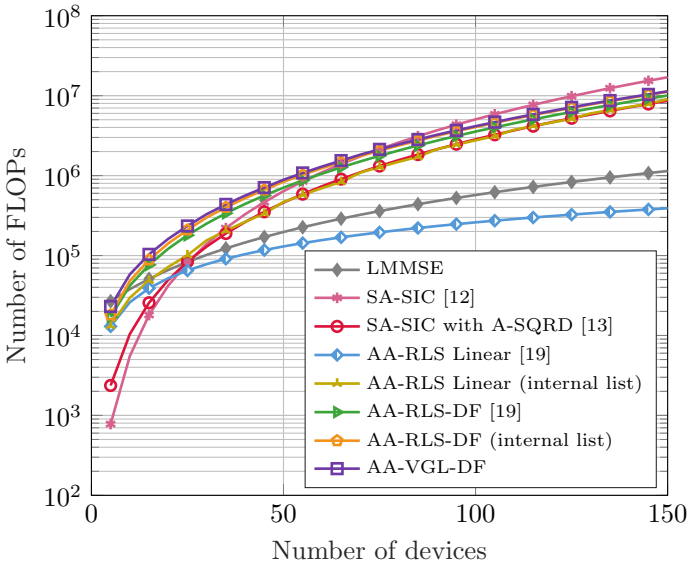


Figure 4.6: Comparison of complexity of considered algorithms. The values chosen were $M = 20$, $\tau_\phi = N/2$ and the variables related to the lists $\mathcal{G}$ reach the maximum of 5. Just 25% of $\boldsymbol{\vartheta}$ is equal to 1, following the beta-binomial distribution as $\alpha = 4$ and $\beta = 8$.

rate considering our detector. Whereas the scenario implies the consideration of a different number of active devices at the same transmission slot and the probability of collision due to reuse of metadata sequences, we compute the achievable rate of each device. We take into account all the possible contamination events from the active devices, as the number of transmission slots are large enough. Were also considered that the BS can estimate the number of active devices, as well as the average channel energy $\eta_n$. In this way, each device has the knowledge of its channel energy and is able to associate it with its rate, as both parameters are broadcast by the BS.

Differently from the literature, the expressions derived take into account, beyond the filter computed by each approach, the probability of metadata collisions, the probability of having a specific number of active devices and different features of each device, as variable activity probability, transmission power and the path loss and shadowing experienced.

*Theorem 1:* An approximation of a lower bound of the maximal achievable sum-rate (in bits per symbol) is

$$R = \sum_{K=1}^{N} p(K) K \sum_{c=0}^{K-1} p(c|K) \mathbb{E}_{\{\eta\}} \left[ \mathcal{R}(\mathcal{C}_i, K, \{\eta\}) \right] \tag{4-8}$$

where $p(K)$, given by (4-1), is the probability of having $K$ active devices in a total of $N$ and $p(c|K)$ is the probability of having $c$ devices with the same metadata sequence of the $i$-th device being observed out of $K$ active devices and $\mathcal{C}_i$ refers to a set of those contaminator devices. The expression of $p(c|K)$ is given by

$$p(c|K) = \binom{K-1}{c} \left(\frac{1}{\tau_\phi}\right)^c \left(1 - \frac{1}{\tau_\phi}\right)^{K-1-c}. \tag{4-9}$$

The procedure and the derivation of the first summations are given by [121]. $\mathbb{E}_{\{\eta\}}$ designates the expectation with respect to $\eta_j, j \in \{i, \mathcal{C}_i\}$ and $\mathcal{R}(\mathcal{C}_i, K, \{\eta\})$ is a lower bound on the maximal achievable rate of device $i$ conditioned on a collider set with indices $\mathcal{C}_i$ within $K$ active devices is given by

$$\mathcal{R}(\mathcal{C}_i, K, \{\eta\}) = \log_2 \left(1 + \mathrm{SINR}(\mathcal{C}_i, K, \{\eta\})\right). \tag{4-10}$$

#### 4.4.2.1 Perfect Channel Estimation

We first consider the case when the BS has perfect CSI, i.e., it has the perfect knowledge of $\mathbf{H}$. Therefore, the channel capacity $C$, recalling $\tilde{\mathbf{d}}[t]$ and $\mathbf{y}[t]$ in (3-3) and suppressing the time index for simplicity, is

$$\begin{aligned} C &= \max_{p_{\tilde{\mathbf{d}}}(\tilde{\mathbf{d}})} I\left(\mathbf{y}; \tilde{\mathbf{d}}\right) \\ &= \max_{p_{\tilde{\mathbf{d}}}(\tilde{\mathbf{d}})} H(\mathbf{y}) - H\left(\tilde{\mathbf{d}}|\mathbf{y}\right) = \max_{p_{\tilde{\mathbf{d}}}(\tilde{\mathbf{d}})} H\left(\mathbf{W}^{\mathrm{H}}\mathbf{y}\right) - H\left(\mathbf{W}^{\mathrm{H}}\mathbf{v}\right) \end{aligned} \tag{4-11}$$

where $H$ is the differential entropy and $I$ the mutual information. Thus, as the considered signals are Gaussian, the mutual information is given by [122]

$$I\left(\mathbf{y}; \tilde{\mathbf{d}}\right) = \log_2 \left(\det\left(\mathbb{E}\left[\mathbf{W}^{\mathrm{H}} \mathbf{y}\mathbf{y}^{\mathrm{H}} \mathbf{W}\right]\right)\right) - \log_2 \left(\det\left(\mathbb{E}\left[\mathbf{W}^{\mathrm{H}} \mathbf{v}\mathbf{v}^{\mathrm{H}} \mathbf{W}\right]\right)\right). \tag{4-12}$$

Thus, computing $\Omega = \mathbb{E}\left[\mathbf{W}^{\mathrm{H}}\,\mathbf{y}\mathbf{y}^{\mathrm{H}}\mathbf{W}\right]$, we have to rewrite the following:

$$\begin{aligned}\Omega &= \mathbb{E}\left[\sum_{j=1}^{K}\mathbf{w}_j^{\mathrm{H}}\,y_j y_j^{\mathrm{H}}\mathbf{w}_j\right] \\ &= \mathbb{E}\left[\sum_{j=1}^{K}\mathbf{w}_j^{\mathrm{H}}\,\left(\mathbf{h}_j\sqrt{b_j}\,x_j+\mathbf{v}\right)\left(\mathbf{h}_j\sqrt{b_j}\,x_j+\mathbf{v}\right)^{\mathrm{H}}\mathbf{w}_j\right] \\ &= \mathbb{E}\left[\sum_{j=1}^{K}\left(\mathbf{w}_j^{\mathrm{H}}\,\mathbf{h}_j\sqrt{b_j}\,x_j x_j^{\mathrm{H}}\sqrt{b_j}\mathbf{h}_j^{\mathrm{H}}\,\mathbf{w}_j\right)+\left(\mathbf{w}_j^{\mathrm{H}}\,\mathbf{h}_j\sqrt{b_j}\,x_j v_j^{\mathrm{H}}\mathbf{w}_j\right)+\right. \\ &\qquad\left.\left(\mathbf{w}_j^{\mathrm{H}}v_j x_j^{\mathrm{H}}\sqrt{b_j}\mathbf{h}_j^{\mathrm{H}}\,\mathbf{w}_j\right)+\left(\mathbf{w}_j^{\mathrm{H}}v_j v_j^{\mathrm{H}}\mathbf{w}_j\right)\right].\end{aligned} \tag{4-13}$$

As the main objective is to compute the maximum achievable rate of a device $i$ out of $K$ active devices in the same time instant $t$ we have,

$$\begin{aligned}\Omega &= \mathbb{E}\left[\sum_{j=1}^{K}\left(\mathbf{w}_i^{\mathrm{H}}\,\mathbf{h}_j\sqrt{b_j}\,x_j x_j^{\mathrm{H}}\sqrt{b_j}\mathbf{h}_j^{\mathrm{H}}\,\mathbf{w}_i\right)+\left(\mathbf{w}_i^{\mathrm{H}}\mathbf{v}\mathbf{v}^{\mathrm{H}}\mathbf{w}_i\right)\right] \\ &= \mathbb{E}\left[\left|\mathbf{w}_i^{\mathrm{H}}\,\mathbf{h}_i\sqrt{b_i}\,x_i\right|^2+\sum_{j=1,j\neq i}^{K}\left|\mathbf{w}_i^{\mathrm{H}}\,\mathbf{h}_j\sqrt{b_j}\,x_j\right|^2+\left|\mathbf{w}_i^{\mathrm{H}}\mathbf{v}\right|^2\right]\end{aligned} \tag{4-14}$$

where the first term is the signal of interest and the other additive terms are treated as a Gaussian noise. Thus, substituting (4-14) in (4-12), we get the expression of the signal-to-noise-plus-interference for the fixed channel realization $\mathbf{H}$, as

$$\mathrm{SINR} = \frac{\left|\mathbf{w}_i^{\mathrm{H}}\,\mathbf{h}_i\sqrt{b_i}\right|^2}{\sum\limits_{j=1,j\neq i}\left|\mathbf{w}_i^{\mathrm{H}}\,\mathbf{h}_j\sqrt{b_j}\right|^2+\|\mathbf{w}_i^{\mathrm{H}}\|^2}. \tag{4-15}$$

#### 4.4.2.2 Imperfect Channel Estimation

In practice, the channel matrix $\mathbf{H}$ has to be estimated at the BS. Thus, we define the computation of the LMMSE estimate of the channel estimate of

the $n$-th device, as

$$\begin{aligned}\mathbf{y}_n = \mathbf{Y}_\phi\,\boldsymbol{\varphi}_n^H &= \sum_{n'\in N}\left(\sqrt{\tau_\phi\, b_{n'}}\,\mathbf{h}_{n'}\,\boldsymbol{\varphi}_{n'} + \mathbf{V}_\phi\right)\boldsymbol{\varphi}_n^H,\\ &= \sqrt{\tau_\phi\, b_n}\,\mathbf{h}_n + \sum_{n'\neq n}\sqrt{\tau_\phi\, b_{n'}}\,\mathbf{h}_{n'}\,\boldsymbol{\varphi}_{n'}\boldsymbol{\varphi}_n^H + \mathbf{V}_\phi\,\boldsymbol{\varphi}_n^H \end{aligned} \tag{4-16}$$

where $\boldsymbol{\varphi}_n$ is the $1\times\tau_\phi$ metadata vector of the $n$-th device, $\mathbf{V}_\phi$ is the $M\times\tau_\phi$ noise matrix and the components of $\left(\mathbf{V}_\phi\,\boldsymbol{\varphi}_n^H\right)$ are i.i.d., as $\|\boldsymbol{\varphi}_n\|^2$. Then, the LMMSE estimate of $\mathbf{h}_n$, $\hat{\mathbf{h}}_n$ is

$$\hat{\mathbf{h}}_n = \frac{\mathbb{E}\left\{\mathbf{y}_n^H\mathbf{h}_n\right\}}{\mathbb{E}\left\{\mathbf{y}_n\mathbf{y}_n\right\}}\,\mathbf{y}_n = \frac{\eta_n\sqrt{\tau_\phi\, b_n}}{\sum_{n'\in N}\tau_\phi\, b_{n'}\,\eta_{n'}\,|\boldsymbol{\varphi}_{n'}\boldsymbol{\varphi}_n^H|^2 + \,\sigma_v^2}\,\mathbf{y}_n. \tag{4-17}$$

Thus, $\hat{\mathbf{H}}$ is the $N\times M$ matrix of channel estimate. We denote $\boldsymbol{\mathcal{E}} = \hat{\mathbf{H}} - \mathbf{H}$, where the elements of $\boldsymbol{\mathcal{E}} = [\boldsymbol{\varepsilon}_1, \boldsymbol{\varepsilon}_2, \cdots, \boldsymbol{\varepsilon}_M]$ are random variables with zero mean and variance $(\eta_i)\,/\,(b_i\eta_i + 1)$. Furthermore, owing to the properties of LMMSE estimation, $\boldsymbol{\mathcal{E}}$ is independent of $\hat{\mathbf{H}}$. Splitting (4-14) in devices with and without the same metadata sequence assigned to the $i$-th device, we have

$$\begin{aligned}\Omega = \mathbb{E}\Bigg[&\sum_{j\in\{i,\mathcal{C}_i\}}\left(\mathbf{w}_i^{\mathrm{H}}\,\mathbf{h}_j\sqrt{b_j}\,x_j x_j^{\mathrm{H}}\sqrt{b_j}\mathbf{h}_j^{\mathrm{H}}\,\mathbf{w}_i\right) + \\ &\sum_{j\notin\{i,\mathcal{C}_i\}}\left(\mathbf{w}_i^{\mathrm{H}}\,\mathbf{h}_j\sqrt{b_j}\,x_j x_j^{\mathrm{H}}\sqrt{b_j}\mathbf{h}_j^{\mathrm{H}}\,\mathbf{w}_i\right) + \left(\mathbf{w}_i^{\mathrm{H}}\mathbf{v}\mathbf{v}^{\mathrm{H}}\mathbf{w}_i\right)\Bigg],\end{aligned} \tag{4-18}$$

Recalling that $\boldsymbol{\mathcal{E}} = \hat{\mathbf{H}} - \mathbf{H}$ and considering the independence between $\boldsymbol{\mathcal{E}}$, $\hat{\mathbf{H}}$ and separating the signal of interest we obtain,

$$\begin{aligned}\Omega = \mathbb{E}\Bigg[&\left|\mathbf{w}_i^{\mathrm{H}}\,\hat{\mathbf{h}}_i\sqrt{b_i}\,x_i\right|^2 + \sum_{j\in\{\mathcal{C}_i\}}\left|\mathbf{w}_i^{\mathrm{H}}\,\hat{\mathbf{h}}_j\sqrt{b_j}\,x_j\right|^2 + \left|\mathbf{w}_i^{\mathrm{H}}\mathbf{v}\right|^2 + \\ &\sum_{j\in\{i,\mathcal{C}_i\}}\left|\mathbf{w}_i^{\mathrm{H}}\,\boldsymbol{\varepsilon}_j\sqrt{b_j}\,x_j\right|^2 + \sum_{j\notin\{i,\mathcal{C}_i\}}\left|\mathbf{w}_i^{\mathrm{H}}\,\mathbf{h}_j\sqrt{b_j}\,x_j\right|^2\Bigg]\end{aligned} \tag{4-19}$$

where the first term is the signal of interest and the other additive terms are

treated as a Gaussian noise. Thus, substituting (4-19) in (4-12), we get

$$\text{SINR} = \frac{\left|\mathbf{w}_i^{\text{H}}\,\hat{\mathbf{h}}_i\sqrt{b_i}\right|^2}{\sum\limits_{j\in\{\mathcal{C}_i\}}\left|\mathbf{w}_i^{\text{H}}\,\hat{\mathbf{h}}_j\sqrt{b_j}\right|^2+\sum\limits_{j\in\{j,\mathcal{C}_i\}}\left|\mathbf{w}_i^{\text{H}}\,\boldsymbol{\varepsilon}_j\sqrt{b_j}\right|^2+\sum\limits_{j\notin\{i,\mathcal{C}_i\}}\left|\mathbf{w}_i^{\text{H}}\,\mathbf{h}_j\sqrt{b_j}\right|^2+\|\mathbf{w}_i^{\text{H}}\|^2} \tag{4-20}$$

$$= \frac{\mathbf{w}_i^{\text{H}} b_i\left(\eta_i-\left(\left(b_j\,\eta_i^2\right)\Big/\left(\sqrt{b_j}\eta_i+\sum\limits_{j\in C_i}\eta_j+1\right)\right)\right)\mathbf{w}_i}{\mathbf{w}_i^{\text{H}}\left(\sum\limits_{j\in\{\mathcal{C}_i\}}b_j\left(\eta_i-\frac{b_j\,\eta_i^2}{\sqrt{b_j}\eta_i+\sum\limits_{j\in C_i}\eta_j+1}\right)+\sum\limits_{j\in\{j,\mathcal{C}_i\}}b_j\left(\frac{\eta_j}{b_j\eta_j+1}\right)+\sum\limits_{j\notin\{i,\mathcal{C}_i\}}b_j\eta_j\right)\mathbf{w}_i+\varrho}$$

where $\varrho=\left(\left(1-\lambda\right)^2\,\sigma_v^2\,\sigma_y^2+1\right)/\left(2-2\lambda\right)$.

### 4.4.3 Diversity Order

This section is devoted to present the diversity order achieved by the AA-VGL-DF detector. We adopt the geometrical approach presented in [123] and used in the previous work [124] in order to reach the expression. As for non-ergodic scenarios the error probability is the probability that the signal level is less than the specified value, also known as outage probability, the diversity order, that is, the asymptotic slope of the outage probability curve [125, 126], is given by

$$d \triangleq \lim_{x\to\infty}\frac{\log\left(P_r\left(R_{k,\text{span}\{\overline{k}\}}\right)\leq x\right)}{\log\left(x\right)} \tag{4-21}$$

where $R_{k,\text{span}\{\overline{k}\}} = R_{k,\text{span}\{1,2,\ldots,k-1,k+1,\ldots,K\}}$ is the squared projection height from the $k$th column vector $\mathbf{h}_K$ of $\mathbf{H}$. From the definition in [126], $R_{k,\text{span}\{\overline{k}\}} = \|\boldsymbol{\Upsilon}\,\mathbf{h}_K\|^2$ where $\boldsymbol{\Upsilon}=\mathbf{I}-\mathbf{P}\mathbf{P}^{\text{H}}$ is the projection matrix to the orthogonal space of span $\left\{\overline{k}\right\}$ and $\mathbf{P}$ is composed of any orthonormal bases of this subspace. An important point is that only the $K$ active devices are considered for the computation of the diversity order.

*Theorem 2: The diversity order achieved by the AA-VGL-DF detector is given by*

$$d_{\mathrm{VGL}} = M - K + \left(\boldsymbol{\vartheta}^{\mathrm{T}}\,\mathbf{m}_{\mathrm{ord}} + \vartheta^{0}\right) + \mathcal{G} \tag{4-22}$$

*where* $\boldsymbol{\vartheta}$ *is the* $K \times 1$ *binary vector presented in Subsection 4.3.2 that gathers the information about the reliability of the soft estimates.* $\mathbf{m}_{ord} = [|\mathcal{A}|, |\mathcal{A}|, \ldots, |\mathcal{A}|]^{T}$ *is also a* $K \times 1$ *vector but each column has the number of symbols of the considered alphabet and* $\mathcal{G}$ *is the number of all the possible combinations of the symbols of the considered augmented alphabet generated by the external list.* $\vartheta^{0}$ *is the total number of zeros in the vector* $\boldsymbol{\vartheta}$*.*

*Proof:* As the decision feedback scheme applies an interference cancellation at each detection step, as it is common in the literature [127, 128], we can make an analogy to the well-known successive interference cancellation (SIC) scheme. Assuming the channel model described in Section 3.2 and making the common assumption that there is no error propagation related to the interference cancellation [123–126], the interference nulling out can be expressed as a general matrix form given by

$$\mathbf{y}_{\perp} = \boldsymbol{\Upsilon} \cdot \mathbf{y}, \tag{4-23}$$

where (4-23) projects $\mathbf{y}$ onto the direction orthogonal to the span $\left\{\overline{k}\right\}$. Following the procedure in [123], to reach the expression of the diversity order of each step of the SIC, the idea is to rotate the set of channels $[\mathbf{h}_1, \ldots, \mathbf{h}_K]$ in a way that $\mathbf{h}_K$ becomes parallel to $\mathbf{p}_K$, one of the orthonormal basis of the subspace. Considering the detection of the first step, $\mathbf{h}_K$ is fixed and position $\mathbf{h}_{K-1}$ into the $[\mathbf{p}_{K-1}\,\mathbf{p}_K]$ plane. In this way, the received signal vector can be written as

$$\mathbf{y}_{\perp} = \sqrt{b_1 \tau_x}\, x_1 \boldsymbol{\Upsilon} \cdot \mathbf{h}_1 + \mathbf{v}, \tag{4-24}$$

where the time instants are suppressed to reduce the notation. The rotations happens until the last channel vector, $\mathbf{h}_K$, is positioned into the $[\mathbf{p}_2\,\mathbf{p}_3, \ldots, \mathbf{p}_K]$

hyper plane. In the well-known SIC scheme, the diversity order after all rotations is $(M-K+1)$, as $\mathbf{h}_{1\perp}$ has a total of $(M-K+1)$ nonzero components. On the other hand, as the AA-VGL-DF detector has an internal list at each detection step, the diversity gain can be increased.

Assuming that the first soft estimate was considered unreliable by the SAC, the internal list scheme would imply more than one possible received vector to be cancelled. Thus, designating the order of the alphabet of the chosen modulation scheme as $|\mathcal{A}|$, for the first step, the diversity order is $(M-K+|\mathcal{A}|)$. For the steps that the soft estimation is reliable, the diversity order is the same as the SIC scheme. Thereby, the result can be achieved by induction. For the $i$th step, the diversity order can be represented by

$$\begin{cases} M-K+\vartheta_i^0, & \text{if } \tilde{d}_n \text{ is reliable and} \\ M-K+\boldsymbol{\vartheta}^{\mathrm{T}}\,\mathbf{m}_{\mathrm{ord}}, & \text{if } \tilde{d}_n \text{ is unreliable,} \end{cases} \tag{4-25}$$

where $\boldsymbol{\vartheta}$ and $\mathbf{m}_{\mathrm{ord}}$ vectors are scaled as $i\times 1$ and $\vartheta_i^0$ is the total number of zeros in the vector $\boldsymbol{\vartheta}$ until the $i$th step. Therefore, for $K=5$ and $\boldsymbol{\vartheta}^{\mathrm{T}}=[1\,0\,1\,1\,0]$, we have

$$\begin{cases} \text{for } i=1, & d_{\mathrm{VGL}}=M-K+\boldsymbol{\vartheta}^{\mathrm{T}}\,\mathbf{m}_{\mathrm{ord}} \\ \text{for } i=2, & d_{\mathrm{VGL}}=M-K+\boldsymbol{\vartheta}^{\mathrm{T}}\,\mathbf{m}_{\mathrm{ord}}+1 \\ \text{for } i=3, & d_{\mathrm{VGL}}=M-K+\boldsymbol{\vartheta}^{\mathrm{T}}\,\mathbf{m}_{\mathrm{ord}}+1 \\ \text{for } i=4, & d_{\mathrm{VGL}}=M-K+\boldsymbol{\vartheta}^{\mathrm{T}}\,\mathbf{m}_{\mathrm{ord}}+1 \\ \text{for } i=5=K, & d_{\mathrm{VGL}}=M-K+\boldsymbol{\vartheta}^{\mathrm{T}}\,\mathbf{m}_{\mathrm{ord}}+2. \end{cases} \tag{4-26}$$

Thus, considering the internal list, the diversity order achieved by AA-VGL-DF is $M-K+\left(\boldsymbol{\vartheta}^{\mathrm{T}}\,\mathbf{m}_{\mathrm{ord}}+\vartheta^0\right)$,

The external list also contributes to the diversity gain. As the external list is comparable as a low complexity ML detector, the increase gain in the diversity order can follow the same idea. As the ML detector has a diversity gain of $M$ [125] and the size of the group list is variable, we consider the $\nu$ number of symbols chosen to be verified in a total of $\mathcal{G}$ possible vectors. In this way, the diversity order achieved by the AA-VGL-DF is given by (4-22).

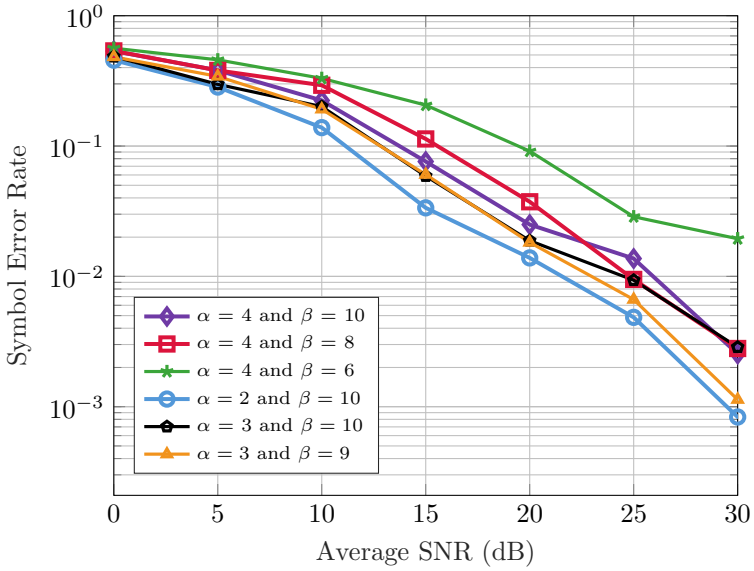


Figure 4.7: Symbol Error Rate vs. Average SNR of the AA-VGL-DF detector in different sparsity scenarios. The activity pattern of devices is determined by a random variable with beta distribution, as shown in Fig. 4.1. In the legend, are shown the $\alpha$ and $\beta$ parameters of each considered distribution, for $N = 128$ and $M = 64$.

## 4.5 Numerical Results

In this section, the performance of the AA-VGL-DF and other relevant mMTC detection schemes are evaluated. Considering an underdetermined mMTC system with $N = 128$ devices and a single base-station equipped with $M = 64$ antennas. The evaluated schemes experience an independent and identically-distributed (i.i.d.) random flat-fading channel model and the values $a_{m,n}$ of (2-26) are taken from complex Gaussian distribution of $\mathcal{N}_c(0, 1)$. The active devices radiate QPSK symbols with power values drawn uniformly at random in $[0.1, 0.3]$ and the activity probabilities are given by a beta-binomial distribution, as described in Section 4.2. Each transmission slot has 256 symbols, equally split into metadata and data. This balance between pilots and data is suggested in [118]. For systems that need explicit channel estimation, we considered the scheme described in Section 4.4.2.2.

Initially, we verify the Symbol Error Rate (SER) performance and the Spectral Efficiency of the AA-VGL-DF for the six sparsity scenarios shown

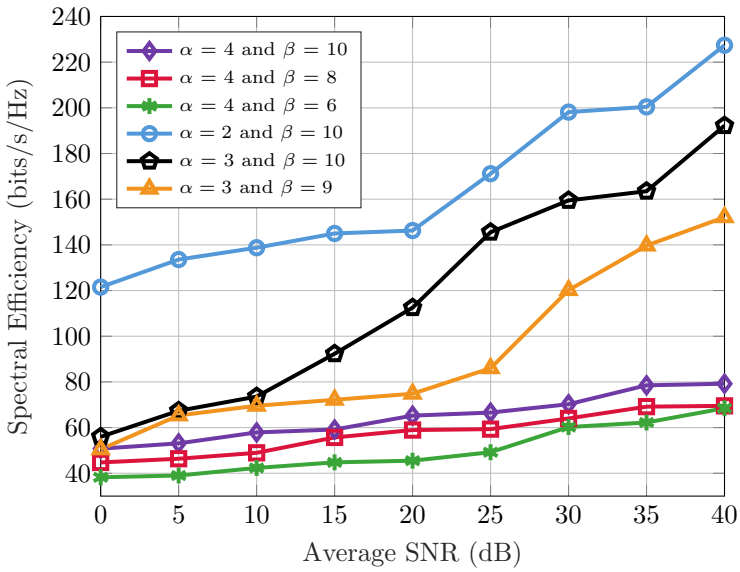


Figure 4.8: Spectral Efficiency vs. Average SNR of the AA-VGL-DF detector with imperfect CSI in different sparsity scenarios. In the legend, are shown the $\alpha$ and $\beta$ parameters of each considered distribution, for $N = 128$ and $M = 64$.

in Fig. 4.1. Fig. 4.7 shows that as lower is the activity probability of devices, better is the SER performance of AA-VGL-DF. The result of Fig. 4.8 illustrates the achievable spectral efficiency of the system with the AA-VGL-DF detector and shows that, as the sparsity increases, the spectral efficiency also increases. This is due to the reduced number of block collisions and better detection performance, thus reducing the interference. Both plots consider the average SNR as $10\log\left(N\,\sigma_x^2/\sigma_v^2\right)$.

Given the SER results of those different scenarios, we choose the beta-distribution with $\alpha = 4$ and $\beta = 8$ as it provides an intermediary sparsity, to compare the SER and Bit Error Rate (BER) performances of the AA-VGL-DF and other relevant mMTC detection schemes.

The numerical results of both uncoded and coded systems are averaged over $10^5$ runs. The performance of AA-VGL-DF is compared with other relevant schemes, as the linear mean squared error (LMMSE), unsorted SA-SIC [28], SA-SIC with A-SQRD [29], AA-RLS, AA-RLS-DF and a version of AA-RLS-DF with the internal list of this work. Besides that, we analyze a version with AA-VGL-DF with perfect activity user detection (AUD) and, as

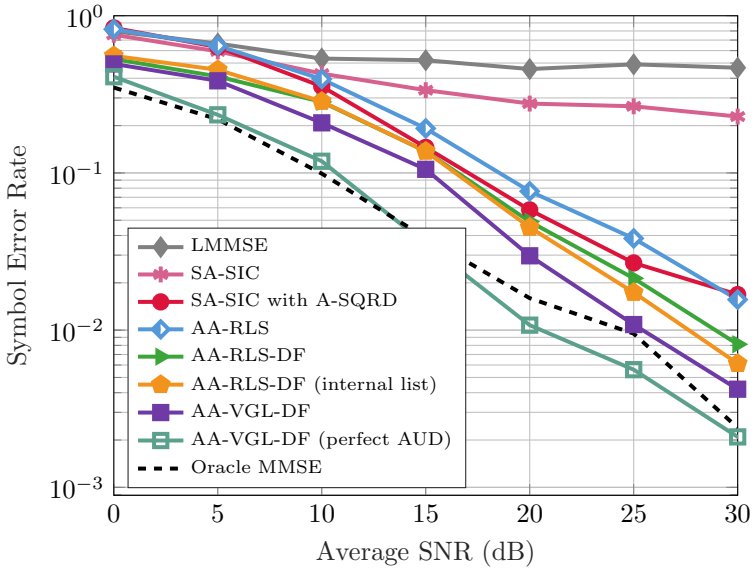


Figure 4.9: Symbol Error Rate values vs. Average SNR. Parameters of proposed schemes are $\lambda = 0.92$, $\gamma = 0.001$ and $\xi = 10$. The pattern activity of the $N = 128$ devices is modelled with a beta-binomial distribution with $\alpha = 4$ and $\beta = 8$. Imperfect CSI is considered in the approaches which depends of the channel estimation.

a lower bound, the Oracle LMMSE detector, which has the knowledge of the index of nonzero entries, is considered.

Fig. 4.9 shows the symbol error rate performance of the considered algorithms. LMMSE has a poor performance as the system is underdetermined. Due to error propagation, the unsorted SA-SIC does not perform well. SA-SIC with A-SQRD is effective since it considers the activity probabilities, but under imperfect CSI conditions, its performance is not so good. In contrast, as AA-RLS-DF does not need explicit channel estimation, it is more efficient. The decision-feedback scheme provides a SER gain due to the interference cancellation, which also happens by including the internal list. The proposed schemes with lists of candidates obtain results that outperform the other relevant schemes, approaching the lower bound. The AA-VGL-DF with perfect AUD surpasses the lower bound for high SNRs, where the filter weights are better adjusted and the list schemes are able to correct more errors.

For the coded systems with IDD, Fig. 4.10 shows the BER of the already considered algorithms under the same scenario. The LDPC matrix has 256

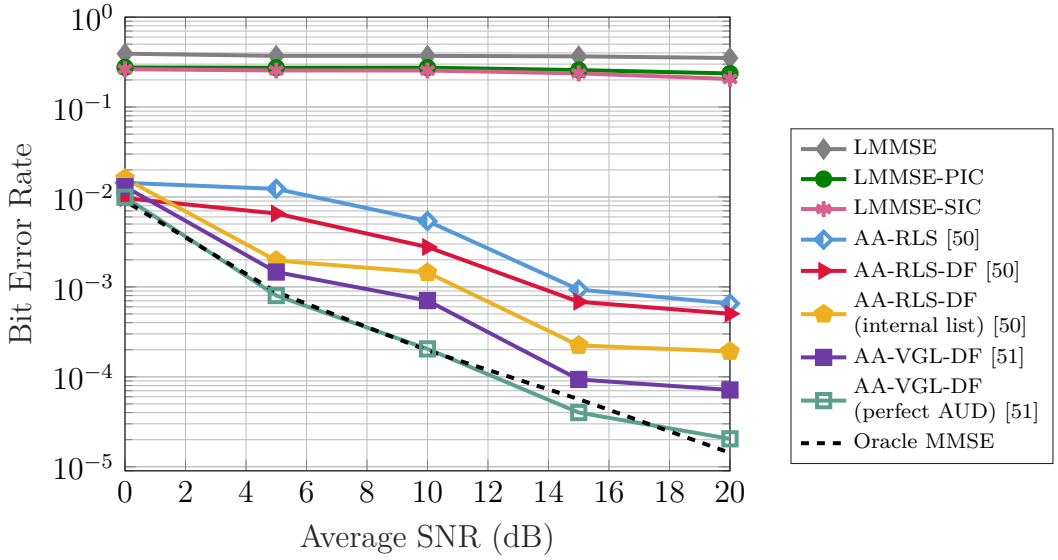


Figure 4.10: Bit Error Rate values vs. Average SNR. LDPC with block length of 128, symbol rate $R = 0.5$, refined by 2 decoding iterations for the same scenario of Fig. 4.9.

columns and 128 rows, avoiding length-4 cycles and with 6 ones per column. The Sum-Product Algorithm (SPA) decoder is used and the average SNR is $10\log\left(NR\sigma_x^2/\sigma_v^2\right)$, where $R = 1/2$ is the rate of the LDPC code. The sparsity of the mMTC approach degrades the expected efficiency of LMMSE-PIC, obtaining little variation in relation to LMMSE and LMMSE-SIC. The hierarchy of performance of the other considered algorithms is the same as the uncoded case but with better error rate values. The iterative scheme matches the results for low bit error rate values. Fig. 4.11 exhibits the spectral efficiency of the considered algorithms. The filter refinement promoted by the internal and external lists provokes a better spectral efficiency than the other detection schemes. The oracle LMMSE is the upper bound of the system.

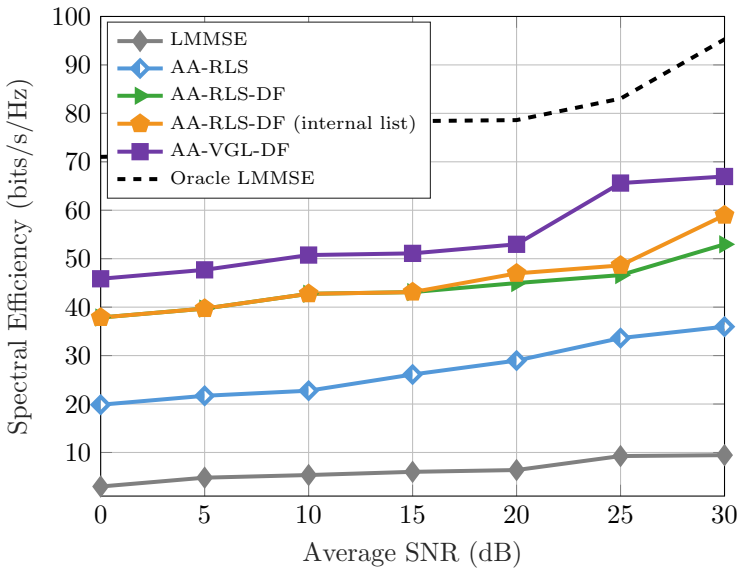


Figure 4.11: Spectral Efficiency vs. Average SNR. Parameters of proposed schemes are $\lambda = 0.92$, $\gamma = 0.001$ and $\xi = 10$. The pattern activity of the $N = 128$ devices is modelled with a beta-binomial distribution with $\alpha = 4$ and $\beta = 8$ and imperfect CSI..

## 4.6 Chapter Summary

In this chapter, an adaptive and iterative soft processing detection scheme, denoted as AA-VGL-DF, that jointly estimates activity and the data of MTCDs has been presented. The performance of AA-VGL-DF demonstrates that the two candidates-list techniques proposed successfully improved the first detector, the AA-RLS-DF. Moreover, the computational complexity has also been compared, where the AA-VGL-DF demonstrates a competitive cost. Furthermore, the derivation of the diversity order and the sum-rate expressions are also presented, which show that the proposed AA-VGL-DF detection scheme can approach the performance of the optimal detector.

# 5
# Dynamic Message-Scheduling Based on Activity-Aware Residual Belief Propagation for Channel Estimation

## 5.1
## Chapter Overview

Unlike the solutions presented in the previous chapters that do not require explicit channel estimation, the joint activity detection and channel estimation problem is studied in this chapter. In addition, we replace receive filters whose solutions require matrix inversions with computationally efficient factor graphs and message passing strategies. The chapter starts with a system model discussion where, besides the frame-level synchronized scenario previously presented, an asynchronous scenario is introduced. Exploiting the fact that the channel is given by a Gaussian function, the problem is formulated in a factor graph fashion, separated into loopy belief propagation (LBP) and a generalized approximate message-passing (GAMP) parts. After the presentation of the message-passing structure, a set of dynamic message-scheduling techniques are introduced. Each technique is based on different criteria, as instantaneous activity detection and residual belief propagation (RBP), that reduce the computational complexity and the number of iterations to reach convergence. The chapter ends with the performance comparison in terms of normalized mean squared-error (NMSE), AER and convergence analysis of the proposed solutions and the state-of-the-art. In addition, an NMSE comparison is given in order to contrast the performance of all considered solutions in a synchronous and asynchronous scenario.

## 5.2 System Model

Regarding Section 2.3, the use of GFRA in massive MIMO systems is due to the fact that mMTC traffic characteristics differ substantially from those of conventional human-based communications. As devices transmit rather short data packets sporadically, yielding bursty traffic with packet arrival times of several seconds up to minutes. Moreover, there are high requirements on energy efficiency due to power limitations of battery driven devices, and a demand for high reliability for safety-critical services with strict latency constraints [129, 130].

Despite the fact that it is the most used in the literature, considering the above aspects of mMTC, a time synchronous transmission as required by conventional OFDM systems is not the most suitable choice to facilitate an efficient transmission, as the synchronization signalling would generate a substantial overhead and increase the overall transmission latency. If massive access is further considered for mMTC, this overhead could quickly eat up the system capacity and thus limit the number of connected devices. Therefore, the support for asynchronous transmission would therefore be highly beneficial for mMTC, enabling transmissions with minimized signalling overhead and delay [131]. However, the necessary coordination between the base-station (BS) and the machine-type devices (MTCDs) in the expected massive scenario would be an issue. Most of the literature, considers a grant-free random access (GFRA) [118,132] scenario, where frame-level synchronization is assumed. The GFRA mechanism allows the MTCDs to simply transmit their packages to the BS directly, without the need to wait for a specific uplink grant from the BS.

With the massive number of MTDs requiring access without coordination, even the use of non-orthogonal preambles a time-slotted transmission would cause significant overhead. In a scenario where devices can transmit their packets only at the beginning of each time-slot, any device that fails to align its time slots properly may degrade its detection and estimation perfor-

mance. Hence, a non-time-slotted (or asynchronous) transmission would further simplify the scheduling procedure, resulting in a smaller signalling overhead, reduced transmission latency and improved energy efficiency [129]. Despite the fact that in asynchronous scenarios the preamble and data signals are superposed in a non-orthogonal manner and interfere with each other, due to the asymptotic favourable propagation in massive multiple-input multiple-output (mMIMO), their spatial subspaces are approximately mutually orthogonal [122, 133]. Thus, the BS can decode the data of MTCDs that transmitted first and then employ successive interference cancellation (SIC) to estimate channels and decode data for the following received packets [134].

Additionally, in the current LTE system, both orthogonal frequency division multiplexing (OFDM) waveforms, the cyclic prefix OFDM (CP-OFDM) and the direct fourier transform spread OFDM (DFTs-OFDM) impose strict synchronization requirements to the system. To guarantee reliable link performance, the timing inaccuracy of the receiving window needs to be kept within the range of the CP. However, in the cellular uplink, the mobility of the users yields a continuous change in the propagation delay of the users' transmission signals, and thus introduces time-variant timing offsets. In order to address such random and variable timing misalignment, a closed-loop timing advance (TA) procedure is designed in the LTE systems for the BS to keep control of each individual user device during an active RRC connection [129, 130].

In summary, there are significant reasons to study, not only the synchronous but the asynchronous uplink mMTC scenario. Thus, this chapter considers two system models, the synchronous, used in previous chapters and the asynchronous, where symbol-level synchronization is assumed but not frame-level synchronization. Since there are just a few recent works that study the asynchronous scenario for mMTC [70, 135–138], this chapter, an extended version of our recently published work [63], faces a completely open-problem.

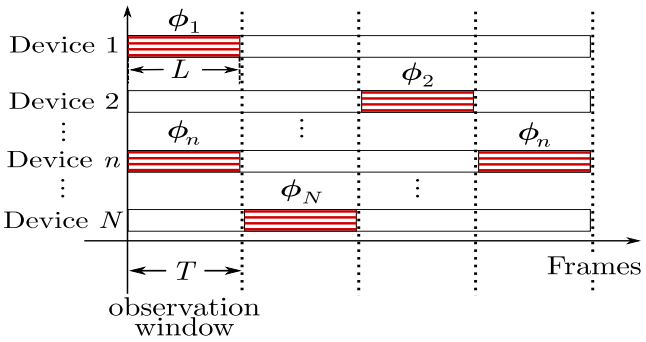


(a) Frame-level synchronization assumption.

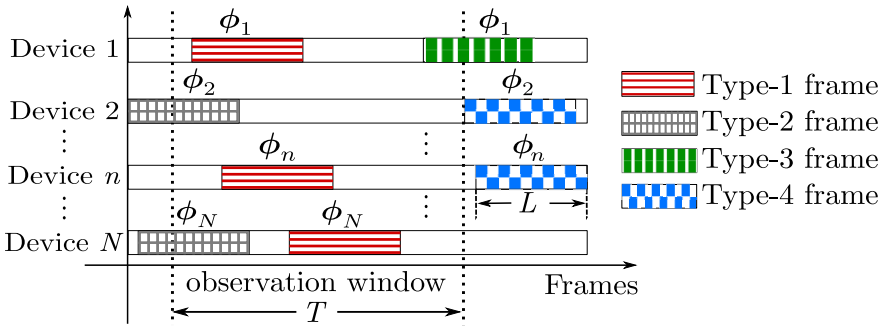


(b) Symbol-level synchronization assumption.

Figure 5.1: (a) Synchronous and (b) asynchronous frames of the uplink grant-free mMTC scenario. Type-1 frames should be detected by the BS, while the others must be re-transmitted.

### 5.2.1 Asynchronous Scenario

Differently from the synchronous scenario considered in the previous chapters, in the asynchronous scenario, a symbol-level synchronization is assumed but not frame-level synchronization. This contrast is depicted in Fig. 5.1, where at the beginning of any symbol interval, each device is allowed to transmit $L$ pilot symbols, which form a frame. As depicted in Fig. 5.1b, in the asynchronous scenario, it is possible that just part of the transmitted frame falls within the observation window. Since the problem of interest here is to jointly estimate the channels and the activity of devices, the BS is only able to deal with the type-1 frames. Thus, type-2 and type-3 frames should have their channels estimated and activity detected in another observation window. Accordingly, the BS generates a sequence of observation windows $\{t_x, t_x + T\}_{x\in\mathbb{Z}_+}$ where $t_x = 0$, if $x = 1$ and $t_x = t_{x-1} + \Delta t$, otherwise. This

sequence can be seen as a sliding window with window size $T$ and step size $\Delta t$. Since $T > L$, any consecutive observation windows have an intersection of $T - \Delta t$ symbol intervals, enabling BS to estimate the channels of all frames.

Since mMTC results in sparse systems, we designate the Boolean variable $\xi_{n,t} = 1$ that indicates the activity of the $n$-th device in the $t$-th symbol interval and $\xi_{n,t} = 0$, otherwise. Thus, considering $\rho_n$ the probability of being active of the $n$-th device, $P(\xi_{n,t} = 1) = 1 - P(\xi_{n,t} = 0) = \rho_n$, where all $\xi_{n,t}$ are considered i.i.d. in relation to $n$ and each device has its own activity probability. When an MTD is active, it transmits one of the independent pilot sequences previously provided by the BS. The frame of the $n$-th device is composed by $\boldsymbol{\phi}_n = \exp(j\pi\boldsymbol{\alpha})$, where each element of vector $\boldsymbol{\alpha} \in \mathbb{R}^L$ is drawn uniformly at random in $[-1, 1]$. Despite the intermittent pattern of transmissions, each device should wait, at least, to the guard period interval to transmit again.

Let $\mathbf{h}_t \in \mathbb{C}^{N\times 1}$ be the vector that models the channels between the BS and $N$ devices in the $t$-th symbol interval. Considering $t_n$ as the symbol interval in which the $n$-th device initiates its transmission, each component is modeled as

$$h_{n,t} = \begin{cases} \sqrt{\beta_n}\, a_{n,t}\,(t - t_n + 1)\,, \;\; \forall\; (t_n \leq t < t_n + L)\,, \\ 0, \;\; \text{otherwise.} \end{cases} \tag{5-1}$$

where $\mathbf{h}_t$ gathers independent fast fading, geometric attenuation and log-normal shadow fading. The vector $\mathbf{a}_t$ contains the fading coefficients modeled as circularly symmetric complex Gaussian random variables with zero mean and unit variance, while $\beta_n$ represents the path-loss and shadowing component of each device, which depends on the location of the devices and remains the same for all frames of the $n$-th device.

Considering the $M$ BS antennas, for an arbitrary observation window $[t_x, t_x + T)$ and omitting the subscript $t_x$ to simplify the notation, the received signals are described by the model

$$\mathbf{Y}_m = \sum_{n=1}^{N} \frac{\boldsymbol{\phi}_n}{\|\boldsymbol{\phi}_n\|}\, \mathbf{h}_{nm}^T + \mathbf{W}_m = \boldsymbol{\Phi}\, \mathbf{H}_m + \mathbf{W}_m, \qquad \forall\,(m = 1, \cdots, M) \tag{5-2}$$

where $\mathbf{W}_m \in \mathbb{C}^{L\times T}$ is the independent complex-Gaussian noise matrix with $\mathcal{N}_c\left(0,\sigma_w^2\right)$, $\mathbf{Y}_m \in \mathbb{C}^{L\times T}$ is the matrix that gathers the received signals and $\mathbf{H}_m \in \mathbb{C}^{N\times T}$ the channels. The subscript $m$ indicates which BS antenna received the signals. For each new window, the values of $\mathbf{W}_m$, $\mathbf{Y}_m$ and $\mathbf{H}_m$ change, while $\mathbf{\Phi} \in \mathbb{C}^{L\times N}$ keeps the pilot sequence of each device. As in this scenario we have a massive number of devices, the size of the window $T$ is smaller than $N$ thus, the system is overloaded. However, as seen in (5-1), $\mathbf{H}$ is sparse, which makes its recovery possible through the theory of compressed sensing (CS) [20].

In order to present the message updating rules of the MSGAMP algorithm, we introduce some statistical properties of the system model. Assuming a BS with one antenna ($M = 1$), the subscript $m$ is omitted in the following formulation.

## 5.3 Factor Graph Approach

As reported in the literature [62,139], it is possible to estimate the channels exploiting the statistical properties of the system model approximating the marginal posterior density by a product of the prior distribution of $\mathbf{h}_t$, $p\left(\mathbf{h}_t|\boldsymbol{\xi}_t\right)$, and the likelihood, $p\left(\mathbf{Y}|\mathbf{H},\boldsymbol{\xi}\right)$. Thus, the minimum MSE (MMSE) estimate of $h_{nt}$, $\hat{h}_{nt} = \mathbb{E}_{h_{nt}|\mathbf{y}}\left[h_{nt}\right] \forall\, n,t$ is

$$p\left(h_{nt}|\mathbf{Y}\right) = \int p\left(\mathbf{H},\boldsymbol{\xi}|\mathbf{Y}\right)\, \mathrm{d}\boldsymbol{\xi}\, \mathrm{d}\mathbf{H}_{\backslash nt} \tag{5-3}$$

where $\mathbf{H}_{\backslash nt}$ denotes all elements except $h_{nt}$ and the posterior distribution, denoted by $p\left(\mathbf{H},\boldsymbol{\xi}|\mathbf{Y}\right) = \frac{1}{p(\mathbf{Y})} p\left(\mathbf{Y}|\mathbf{H},\boldsymbol{\xi}\right) p\left(\mathbf{H}|\boldsymbol{\xi}\right) p\left(\boldsymbol{\xi}\right)$ given by the Bayes' rules

$$p\left(\mathbf{H},\boldsymbol{\xi}|\mathbf{Y}\right) = \\ \frac{1}{p\left(\mathbf{Y}\right)} \left[\prod_{l=1}^{L}\prod_{t=1}^{T} p\left(y_{lt}\middle|\sum_{n=1}^{N}\phi_{ln}\, h_{nt}\right)\right] \left[\prod_{n=1}^{N}\prod_{t=1}^{T} p\left(h_{nt}|\xi_{nt}\right)\right] \left[\prod_{n=1}^{N}\prod_{t=1}^{T} P\left(\xi_{nt}\right)\right], \tag{5-4}$$

where $P\left(h_{nt}|\xi_{nt}\right)$ is the conditional density for the random variable in (5-1).

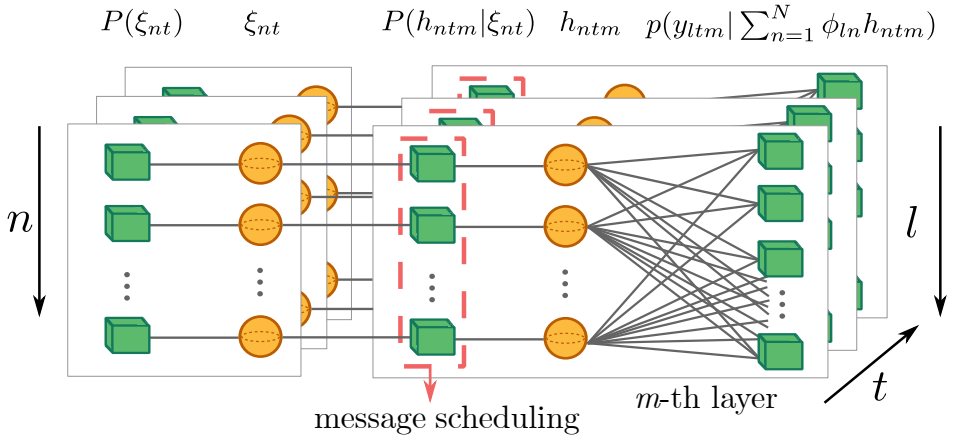


Figure 5.2: The factor graph of joint distribution $p(\mathbf{H}, \mathbf{Y}, \boldsymbol{\xi})$ where cubes denote factor nodes and spheres variable nodes.

In order to apply the proposed message scheduling techniques, the first step is to marginalize the problem. As seen in GAMP [140] and HyGAMP [139], one approach is to employ an approximation of the sum-product loopy belief propagation (BP). For each $t$-th symbol interval, the factor graph (FG) in Fig. 5.2 represents the problem, wherein factor nodes that represents the density functions, prior and likelihood, are depicted as cubes and the variable nodes $\xi_{nt}$ and $h_{nt}$ are seen as spheres. As $\mathbf{\Phi}$ is a dense matrix, the FG in Fig. 5.2 is fully connected. Computing the messages in fully connected graphs is tricky as the messages themselves are functions. Thus, a common method is to approximate the messages by prototype functions that resemble Gaussian density functions which can be described by two parameters only. So, message passing reduces to the exchange of the parameters of a function instead of the function itself. Therefore, it is possible to iteratively approximate, for a FG with cycles as in Fig. 5.2, the marginal posteriors passing messages between different nodes. Thus, we can define the messages, for all $l$s, from $p\left(y_{lt}\middle|\cdot\right)$ to $h_{nt}$ and to the opposite direction as

$$\Delta^{(i)}_{n\leftarrow lt}\left(h_{nt}\right) \propto \int p\left(y_{lt}\middle|\sum_{k=1}^{N}\phi_{lk}\,h_{kt}\right)\prod_{j\neq n}^{N}\Delta^{(i)}_{j\rightarrow lt}\left(h_{jt}\right)\,\mathrm{d}h_{jt} \tag{5-5}$$

$$\Delta^{(i+1)}_{n\rightarrow lt}\left(h_{nt}\right) \propto \Delta^{(i)}_{n\rightarrow nt}\left(h_{nt}\right)\prod_{k\neq t}^{T}\Delta^{(i)}_{n\leftarrow lk}\left(h_{nk}\right) \tag{5-6}$$

and, considering $\propto$ as proportional, the messages from $P\left(h_{nt}|\xi_{nt}\right)$ to $h_{nt}$ and

to the opposite direction are

$$\Delta_{n\leftarrow nt}^{(i)}\left(h_{nt}\right) \propto \prod_{k=1}^{T} \Delta_{n\rightarrow lk}^{(i)}\left(h_{nt}\right), \tag{5-7}$$

$$\Delta_{n\rightarrow nt}^{(i+1)}\left(h_{nt}\right) \propto \int p\left(h_{nt}|\xi_{nt}\right) \Delta_{n\rightarrow nt}^{(i)}\left(\xi_{nt}\right) \mathrm{d}\xi_{nt}. \tag{5-8}$$

Thus, the belief distribution that provides an approximation to marginal posterior distribution $p\left(h_{nt}|\mathbf{Y},\boldsymbol{\xi}\right)$ is given by

$$\Delta_{nt}^{(i+1)}\left(h_{nt}\right) = \frac{\Delta_{n\rightarrow nt}^{(i)} \prod_{s=1}^{T} \Delta_{n\leftarrow ls}^{(i)}\left(h_{ns}\right)}{\int \Delta_{n\rightarrow nt}^{(i)} \prod_{s=1}^{T} \Delta_{n\leftarrow ls}^{(i)}\left(h_{ns}\right) \mathrm{d}h_{nt}}, \tag{5-9}$$

where, defining $\mathbf{Z} = \boldsymbol{\Phi}\mathbf{H}$ and

$$p\left(h\middle|\hat{r}_{nt}^{(i)}, \nu_{nt}^{r(i)}; \hat{\rho}_{nt}^{(i)}\right) \triangleq \frac{p\left(h; \hat{\rho}_{nt}^{(i)}\right) \mathcal{N}_c\left(h|\hat{r}_{nt}^{(i)}, \nu_{nt}^{r(i)}\right)}{\int p\left(h; \hat{\rho}_{nt}^{(i)}\right) \mathcal{N}_c\left(h|\hat{r}_{nt}^{(i)}, \nu_{nt}^{r(i)}\right) \mathrm{d}h} \tag{5-10}$$

$$p\left(z\middle|p_{lt}^{(i)}, \nu_{lt}^{p(i)}\right) \triangleq \frac{p\left(y_{lt}|z_{lt}^{(i)}\right) \mathcal{N}_c\left(z|p_{lt}^{(i)}, \nu_{lt}^{p(i)}\right)}{\int p\left(y_{lt}|z_{lt}^{(i)}\right) \mathcal{N}_c\left(z|p_{lt}^{(i)}, \nu_{lt}^{p(i)}\right) \mathrm{d}z}, \tag{5-11}$$

we can compute $\mathbb{E}\left[\Delta_{nt}^{(i+1)}\left(h_{nt}\right)\right] = \hat{h}_{nt}^{(i+1)}$ and $\mathrm{Var}\left[\Delta_{nt}^{(i+1)}\left(h_{nt}\right)\right] = \nu_{nt}^{h(i+1)}$.

Specifically, each iteration of Algorithm 3 has three stages. The first one, labelled as "GAMP approximation" contains the updates of the GAMP based on expectation propagation (EP) algorithm, which treats the components $h_{nt}$ as independent with the estimated probability of being active $\hat{\rho}_{nt}$. As well as [59, 62], the EP is incorporated in the process of LBP to the relaxed belief propagation and then to GAMP. At iteration $i$, MSGAMP produces estimates $\hat{\mathbf{h}}^{(i)}$ and $\hat{\mathbf{z}}^{(i)}$ of the vectors $\mathbf{h}$ and $\mathbf{z}$. Several other intermediate vectors, $\hat{\mathbf{p}}^{(i)}$, $\hat{\mathbf{r}}^{(i)}$ and $\hat{\mathbf{s}}^{(i)}$, are also produced. Associated with each of these vectors are matrices like $\mathbf{Q}^{h(i)}$ and $\mathbf{Q}^{z(i)}$ that represent covariances. Thus, in order to reduce the complexity of $O\left(LNT\right)$ to $O\left(NT\right)$, the message in (5-5) is firstly mapped to a Gaussian distribution based on the central limit theorem and Taylor expansions. So, $\Delta_{n\leftarrow lt}^{(i)}\left(h_{nt}\right)$ is updated by the Gaussian reproduction property (GRP)[1] [62]. Following the same procedure in the messages of (5-6), (5-7) and

[1] $\mathcal{N}_c(x|a,A)\,\mathcal{N}_c(x|b,B) = \mathcal{N}_c(0|a-b,A+B)\,\mathcal{N}_c(x|c,C)$ with $C = (A^{-1}+B^{-1})^{-1}$ and $c = C(a/A + b/B)$.

(5-8), relaxed BP is obtained by combination of the approximated messages. Since many of these messages slightly differ from each other, in order to fill out those differences, new variables are produced and, ignoring the infinitesimals, GAMP based on EP is obtained.

The second stage of Algorithm 3, labelled as "sparsity-rate update", refers to the "box" part of the FG in Fig. 5.2 and updates the estimates of each probability of being active $\hat{\rho}_{ntm}$. In order to use the diversity of the antennas in the BS to refine the activity detection, from this point we include the subscript $m$ into the formulation. Computed using Gaussian approximations of likelihood functions, these estimates are then used to define the message scheduling proposed in this work. The messages in the "sparsity-rate update" stage are given by

$$\Delta^{(i+1)}_{n\leftarrow ntm}\left(\xi_{nt}\right) \propto \int p\left(h|\xi_{nt}\right) \Delta^{(i)}_{n\leftarrow ntm}\left(h\right)\, \mathrm{d}h, \tag{5-12}$$

$$\Delta^{(i)}_{n\rightarrow ntm}\left(\xi_{nt}\right) \propto P\left(\xi_{nt}\right) \prod_{k\neq t}^{T} \Delta^{(i)}_{n\leftarrow nkm}\left(\xi_{nt}\right), \tag{5-13}$$

where (5-12) refers to the message from $P\left(h_{ntm}|\xi_{nt}\right)$ to $\xi_{nt}$ while (5-13) denotes the message in opposite direction and each belief at $\xi_{nt}$ is given by $\Delta^{(i)}_{n}\left(\xi_{nt}\right) \propto P(\xi_{nt}) \prod_{t=1}^{T} \Delta^{(i)}_{n\leftarrow ntm}(\xi_{nt})$.

Defining $\mathcal{X} = R+W$ as a scalar random variable with the same density as $\mathbf{H}$, the message in (5-12) can be approximated as a likelihood function given by $\Delta^{(i)}_{n\leftarrow ntm}\left(\xi_{nt}\right) = \mathcal{N}_c\left(h_{ntm}|\hat{r}^{(i)}_{ntm}, \nu^{r(i)}_{ntm}\right)$, where $\hat{r}_{ntm}$ is a component of the AWGN corrupted version of $\mathcal{X}$, $R$, and $\nu^r$ is the variance of $\mathcal{X}$. Applying the GRP enables us to define

$$\mathrm{LLR}^{(i)}_{n\leftarrow ntm} = \log \frac{\mathcal{N}_c\left(0\middle|\hat{r}^{(i)}_{ntm}, \nu^{r(i)}_{ntm}+\beta_n\right)}{\mathcal{N}_c\left(0\middle|\hat{r}^{(i)}_{ntm}, \nu^{r(i)}_{ntm}\right)}. \tag{5-14}$$

Similarly to (5-14), we have

$$\mathrm{LLR}_{ntm} \triangleq \log \frac{\Delta^{(i)}_{n}\left(\xi_{nt}=1\right)}{\Delta^{(i)}_{n}\left(\xi_{nt}=0\right)} \qquad \text{and} \qquad \mathrm{LLR}^{(i)}_{n\rightarrow ntm} \triangleq \log \frac{\Delta^{(i)}_{n\rightarrow ntm}\left(\xi_{nt}=1\right)}{\Delta^{(i)}_{n\rightarrow ntm}\left(\xi_{nt}=0\right)}.$$

**Algorithm 3:** MSGAMP for Joint Activity User Detection and Channel Estimation

**input :** $i = 1$, $\hat{s}_{ltm}^{(0)} = \hat{r}_{ntm}^{(0)} = 0$, $\nu_{ntm}^{r(0)} = 1$, $\hat{\rho}_{ntm}^{(0)} = \rho_n$, $\mathcal{S}^{(0)} = [1, \ldots, N]$

**output:** $\hat{\boldsymbol{\rho}}^{\text{end}}$ and $\hat{\mathbf{h}}^{\text{end}}$

**begin**

GAMP approximation

**while** $(i < I \ or \ tol \ < 10^{-4})$ **do**

**for** $\left(n = 1, \ldots, |\mathcal{S}^{(i-1)}|\right) \forall n \in \mathcal{S}^{(i-1)}$ **do**

**for** $(t = 1, \ldots, T)$ **do**

**for** $(m = 1, \ldots, M)$ **do**

$\hat{h}_{ntm}^{(i)} = \mathbb{E}\left[\mathcal{X}_{ntm} \middle| \hat{r}_{ntm}^{(i-1)}, \nu_{ntm}^{r(i-1)}; \hat{\rho}_{ntm}^{(i-1)}\right]$

$\nu_{ntm}^{h(i)} = \text{Var}\left[\mathcal{X}_{ntm} \middle| \hat{r}_{ntm}^{(i-1)}, \nu_{ntm}^{r(i-1)}; \hat{\rho}_{ntm}^{(i-1)}\right]$

**for** $(l = 1, \ldots L)$ **do**

$\nu_{ltm}^{p(i)} = \sum_{n=1}^{N} |\Phi_{ln}|^2 \nu_{ntm}^{h(i)}$

$p_{ltm}^{(i)} = \sum_{n=1}^{N} \Phi_{ln} \hat{h}_{ntm}^{(i)} - \nu_{ltm}^{p(i)} \hat{s}_{ltm}^{(i-1)}$

$\tilde{z}_{ltm}^{(i)} = \left(y_{ltm} \nu_{ltm}^{p(i)} + \sigma_w^2 p_{ltm}^{(i)}\right) \Big/ \left(\nu_{ltm}^{p(i)} + \sigma_w^2\right)$

$\nu_{ltm}^{z(i)} = \left(\sigma_w^2 \nu_{ltm}^{p(i)}\right) \Big/ \left(\nu_{ltm}^{p(i)} + \sigma_w^2\right)$

$\hat{s}_{ltm}^{(i)} = \left(\tilde{z}_{ltm}^{(i)} - p_{ltm}^{(i)}\right) \Big/ \nu_{ltm}^{p(i)}$

$\nu_{ltm}^{s(i)} = \nu_{ltm}^{-p(i)} \left(1 - \frac{\nu_{ltm}^{z(i)}}{\nu_{ltm}^{p(i)}}\right)$

**end**

$\nu_{ntm}^{-r(i)} = \sum_{l=1}^{L} |\Phi_{ln}|^2 \nu_{ltm}^{s(i)}$

$r_{ntm}^{(i)} = \hat{h}_{ntm}^{(i)} + \nu_{ntm}^{r(i)} \sum_{l=1}^{L} \Phi_{ln}^* \hat{s}_{ltm}^{(i)}$

Sparsity-rate update

$$\text{LLR}_{n \leftarrow ntm}^{(i)} = \log \frac{\mathcal{N}_c\left(0 \middle| \hat{r}_{ntm}^{(i)}, \nu_{ntm}^{r(i)} + \beta_n\right)}{\mathcal{N}_c\left(0 \middle| \hat{r}_{ntm}^{(i)}, \nu_{ntm}^{r(i)}\right)}$$

$\text{LLR}_{n \to ntm}^{(i)} = \log\left(\rho_n / 1 - \rho_n\right) + \sum_{k \neq t}^{T} \text{LLR}_{n \leftarrow nkm}^{(i)}$

$\hat{\rho}_{ntm}^{(i)} \triangleq \nu_{n \to ltm}^{(i+1)} \left(\xi_{nt} = 1\right) = 1 - 1 / 1 + \exp\left(\text{LLR}_{n \to ntm}^{(i)}\right)$

**end**

**end**

MSGAMP-type technique

$\hat{\rho}_{nt}^{(i)} = \sum_{m=1}^{M} \hat{\rho}_{ntm}^{(i)} \Big/ M$

$\mathcal{S}^{(i)} = update\left[\mathcal{S}^{(i-1)}\right]$

**end**

$\text{tol} = \sum_{m=1}^{M} \frac{\|\hat{\underline{\mathbf{h}}}_{tm}^{(i)} - \hat{\underline{\mathbf{h}}}_{tm}^{(i-1)}\|}{\|\hat{\underline{\mathbf{h}}}_{tm}^{(i)}\|}$ and $i = i + 1$

**end**

**end**

Substituting (5-14) in (5-13) and in each belief, $\mathrm{LLR}_{n\to ntm}^{(i)}$ is given by

$$\mathrm{LLR}_{n\to ntm}^{(i)} = \log\left(\frac{\rho_n}{1-\rho_n}\right) + \sum_{k\neq t}^{T} \mathrm{LLR}_{n\leftarrow nkm}^{(i)}. \tag{5-15}$$

Thereby, the message in (5-6) is described by

$$\Delta_{n\to lt}^{(i+1)}\left(h_{ntm}\right) = \hat{\rho}_{ntm}^{(i)}\,\mathcal{N}_c\left(h_{ntm}|0,\beta_n\right) + \left(1-\hat{\rho}_{ntm}^{(i)}\right)\delta\left(h_{ntm}\right), \tag{5-16}$$

where

$$\hat{\rho}_{ntm}^{(i)} \triangleq \Delta_{n\to ltm}^{(i+1)}\left(\xi_{nt}=1\right) = 1 - \frac{1}{1+\exp\left(\mathrm{LLR}_{n\to ntm}^{(i)}\right)}. \tag{5-17}$$

With the message passing established, the next step is to use the estimates obtained in (5-17) in message scheduling.

## 5.4 Dynamic Message-Scheduling Strategies

Since it is expected up to $300,000$ devices per cell [4] in future mobile communication systems a technique with low computational cost is fundamental. We develop three different message scheduling criteria that reduce the computational complexity and the number of iterations to reach convergence as compared to HYGAMP.

MSGAMP determines a group of nodes $\mathcal{S}^{(i)}$ to update based on two different criterion, the AUD and the RBP. The goal is to update, at every iteration $i$, only the nodes of the group and not all of them, as in HyGAMP. MSGAMP proceeds until $i$ reaches the maximum number of iterations $I$ or $(\mathrm{tol}/M < 10^{-4})$, where tol is given by

$$\mathrm{tol} = \sum_{m=1}^{M} \frac{\|\hat{\underline{\mathbf{h}}}_{tm}^{(i)} - \hat{\underline{\mathbf{h}}}_{tm}^{(i-1)}\|}{\|\hat{\underline{\mathbf{h}}}_{tm}^{(i)}\|}, \tag{5-18}$$

where $\hat{\underline{\mathbf{h}}}_{tm}^{(i)}$ is a $|\mathcal{S}^{(i)}| \times 1$ vector that corresponds to the estimated channel gains between the $|\mathcal{S}^{(i)}|$ devices and the $m$-th BS antenna. As this stopping criterion takes into account only the devices in the group, unlike the parallel message update of HyGAMP that, in each iteration, $O(NTM)$ messages must be computed, MSGAMP needs only $O(|\mathcal{S}^{(i)}|TM)$ . Considering that we have

a crowded scenario of MTCDs in future mobile communication systems and the sporadic transmission pattern of each device, the computational cost gain using scheduling schemes is evident, since $|\mathcal{S}^{(i)}| << N$. With the stopping criterion defined, we present the first message scheduling scheme.

### 5.4.1 MSGAMP Based on Activity User Detection

The message scheduling based on activity user detection (MSGAMP-AUD) sequentially updates the messages of devices detected as active and repeats the previous values of other devices. The criterion based on AUD uses the estimates of each BS antenna, as $\hat{\rho}_{nt}^{(i)} = \sum_{m=1}^{M} \hat{\rho}_{ntm}^{(i)}/M$. If $\hat{\rho}_{nt}^{(i)}$ is higher than a threshold, the device is considered as active and is included in the set $\mathcal{S}^{(i)}$.

In the first iteration, all messages of all nodes are updated. When $i = 2$, we have the first values of $\hat{\boldsymbol{\rho}}_{tm}$, thus enabling the set $\mathcal{S}^{(i)}$. In this iteration, all messages that belong to $\mathcal{S}^{(i)}$, except for $s_1^{(i)}$ will be updated. Then, the index that refers to the messages that had been updated is removed of $\mathcal{S}^{(i)}$ as in

$$\mathcal{S}^{(i)} = \left[s_2^{(i-1)}, \ldots, s_{|\mathcal{S}^{(i-1)}|}^{(i-1)}\right]. \tag{5-19}$$

Therefore, we exclude a group of messages that belong to a specific device to be updated, one at a time. In summary, we reduce the set $\mathcal{S}^{(i)}$ that is updated in parallel until there is no message to update. When $\mathcal{S}^{(i)}$ is empty, MSGAMP updates all messages, including the ones that do not belong to the older set, i.e., the new set is $\mathcal{S}^{(i)} = [1, \ldots, N]$. In the next iteration, a new update of the set $\mathcal{S}^{(i)}$, using the new $\hat{\rho}_{ntm}$ is performed.

### 5.4.2 MSGAMP Based on Residual Belief Propagation

In this variation, MSGAMP updates the messages according to an ordering metric called residual belief propagation (RBP). A residual is the norm (defined over the message space) of the difference between the values of a message before and after an update. In our scheme, we define the residual

with the beliefs described in (5-9). Thus, the residual for the belief distribution at $h_{nt}$, is given by

$$\mathrm{Res}\left(\nu_{ntm}\left(h_{ntm}\right)\right) = \left|\left|\Delta_{ntm}^{(i+1)}\left(h_{ntm}\right) - \Delta_{ntm}^{(i)}\left(h_{ntm}\right)\right|\right|. \tag{5-20}$$

The intuitive justification of this method is that as the factor graph approach converges, the differences between the messages before and after an update diminish. Therefore, if a message has a large residual, it means that it is located in a part of the graph that has not converged yet. Thus, propagating that message first should speed up the convergence. Using the residual values computed in (5-20), we compute the set $\mathcal{S}^{(i)}$ of messages to be updated in the next iteration. Since the probability of being active of each MTD is typically around 5% [8], $\mathcal{S}^{(i)}$ has the $0.05\,N$ nodes with highest residual. The update sequence of MSGAMP-RBP is the same of MSGAMP-AUD, the difference is how both groups are formed.

**Algorithm 4:** Message-scheduling based on Group Residual Belief Propagation

**input :** $l = 1$, $N$, $\mathcal{S}^i$, $\hat{\mathbf{h}}^i$, $\hat{\mathbf{r}}^i$, $\nu^{r(i)}$, $\nu^{h(i)}$
**output:** $\mathcal{S}^{i+1}$, $\hat{\mathbf{h}}^{i+1}$, $\hat{\mathbf{r}}^{i+1}$, $\nu^{r(i+1)}$, $\nu^{h(i+1)}$

**begin**
  **if** $\left(|\mathcal{S}^{(i)}| = 0\right)$ **then**
    **for** $(n = 1, \ldots, N)$ **do**
      **if** $\left(Res\left(\nu_{nm}\left(h_{nm}\right)\right) > \textit{the first other } |\hat{\boldsymbol{\rho}}^{(i)}| \textit{residuals}\right)$ **then**
        $\mathcal{S}_l^{(i+1)} = n$
        $l = l + 1$
      **end**
    **end**
  **else**
    % Remove the first element of $\mathcal{S}^{(i)}$, that is,
    $\mathcal{S}^{(i+1)} = \left[\mathcal{S}_2^{(i)}, \ldots, \mathcal{S}_{|\mathcal{S}^{(i)}|}^{(i)}\right]$
  **end**
  $\forall \left(n \notin \mathcal{S}^{(i+1)}\right)$,
  **for** $(m = 1, \ldots, M)$ **do**
    $\hat{h}_{nm}^{(i+1)} = \hat{h}_{nm}^{(i)}$; $\quad \nu_{nm}^{h(i+1)} = \nu_{nm}^{h(i)}$
    $\hat{r}_{nm}^{(i+1)} = \hat{r}_{nm}^{(i)}$; $\quad \nu_{nm}^{r(i+1)} = \nu_{nm}^{r(i)}$
  **end**
**end**

### 5.4.3 MSGAMP Based on AUD and RBP

This dynamic scheduling strategy combines the AUD and RBP criterion. The main idea is use AUD criterion to create $\mathcal{S}^{(i)}$ and the RBP criterion to compute the updating sequence of it. MSGAMP-ARBP updates the messages of one node per iteration, starting with the one with highest residual. After the group being fully updated, MSGAMP-ARBP proceeds as in previous strategies, updating the messages of the nodes that does not belong to $\mathcal{S}^{(i)}$ and compute a new set. When a stop criterion is met, the activity detection and the channel estimation are given by lines 26 and 6 in Algorithm 3.

## 5.5 Numerical Results

In order to verify the performance of the proposed MSGAMP schemes, we simulate an mMTC system with $N = 128$ devices, $M = 2$ BS antennas, $L = 32$ symbols per frame and $T = 3\,L$ as the size of the observation window. The threshold to detect the activity of devices considered is 0.9, the average SNR is set to $1/\sigma_w^2$, while the activity probabilities $p_n$ are drawn uniformly at random in $[0.01, 0.05]$. The variations of MSGAMP are compared to the well-known generalized approximate message passing (GAMP) [140] and the state-of-the-art HyGAMP [139] algorithm. Versions of MSGAMP-ARBP and of HyGAMP with perfect activity knowledge (OMSGAMP-ARBP and OHyGAMP) are used as lower bounds. Figs. 5.3 and 5.4 show results of NMSE and AER per frame, respectively. In terms of NMSE, Fig. 5.3 shows that the message scheduling schemes have a competitive performance, where MSGAMP-AUD and MSGAMP-RBP slightly outperform HyGAMP, requiring less computational cost. MSGAMP-ARBP surpasses not only HyGAMP and the other MSGAMP algorithms but also OHyGAMP.

One can see in Fig. 5.4 that the use of the BS antennas in order to refine the activity detection improved the AER performance of MSGAMP-ARBP

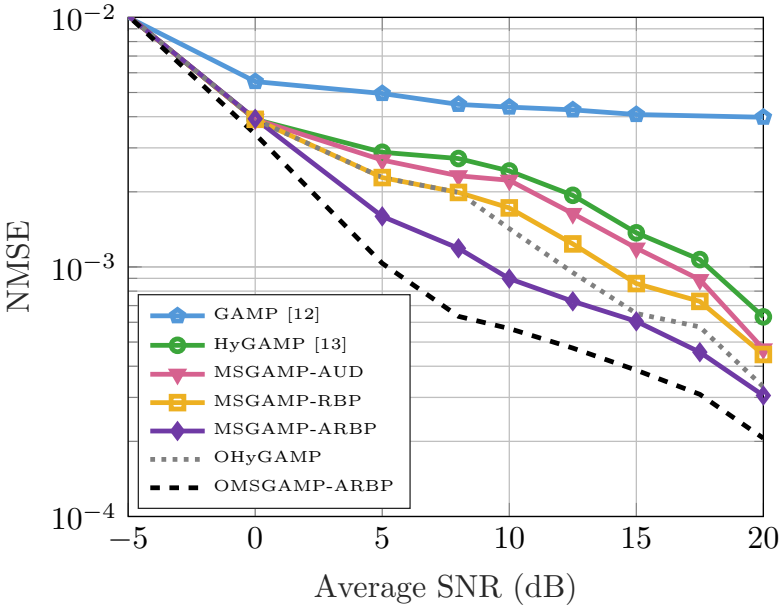


Figure 5.3: Normalized mean squared error per frame vs. Average SNR. We considered only the active devices, in the asynchronous scenario with $N = 128, M = 2$ and $L = 32$, after 10 iterations by $10^4$ Monte Carlo trials.

since the AER curves have lower values as $M$ increases. Fig. 5.5 depicts the convergence of MSGAMP-type techniques and HyGAMP. One can notice that for different values of SNR, our solutions converge faster and to lower values of NMSE than HyGAMP.

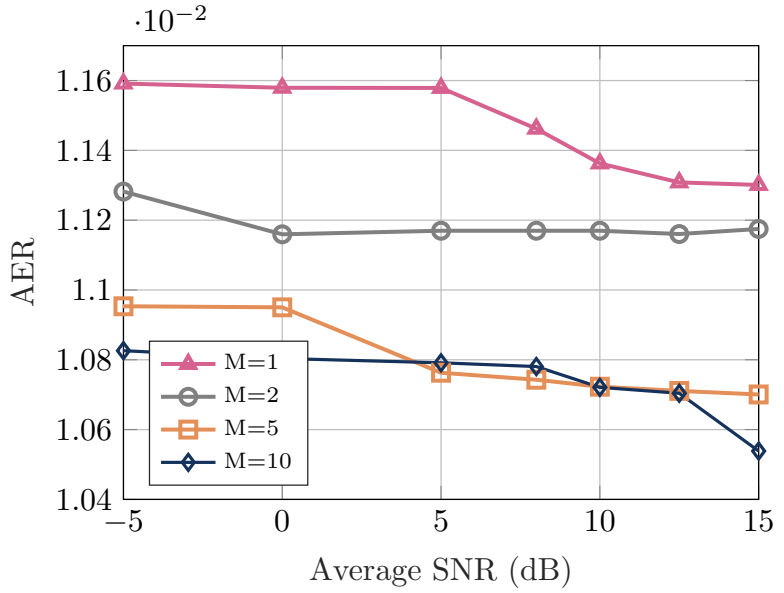


Figure 5.4: Activity error rate per symbol of MSGAMP-ARBP vs. Average SNR in the asynchronous scenario with $N = 128, M = 2$ and $L = 32$, after 10 iterations. AER is the sum of the missed detections and false alarm rates.

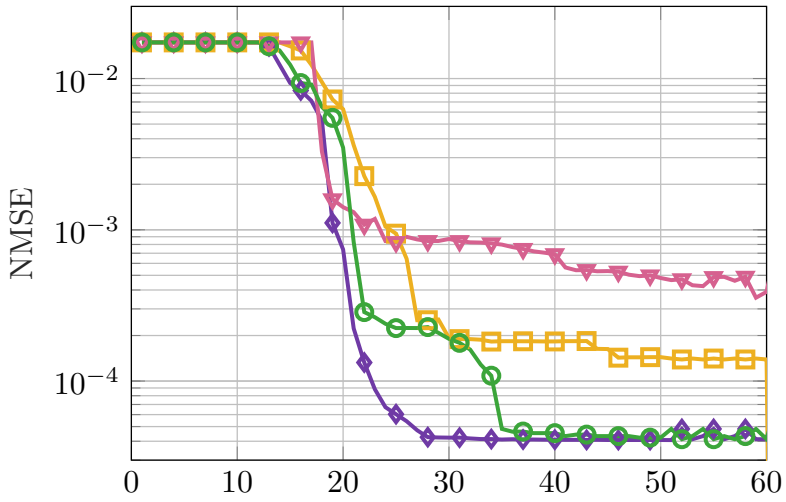


(a) SNR = 0 dB.

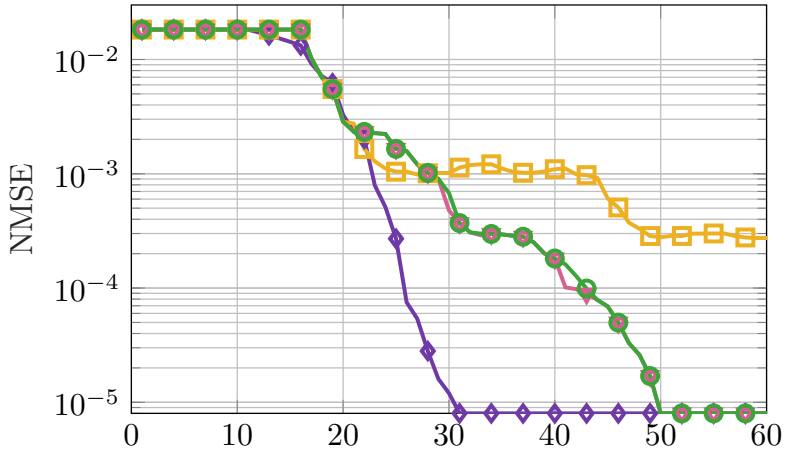


(b) SNR = 8 dB.

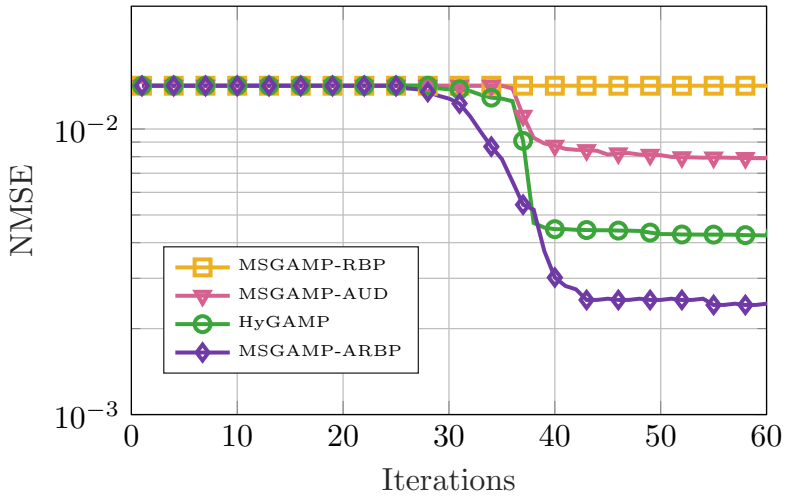


(c) SNR = 10 dB.

Figure 5.5: Convergence rate in terms of NMSE per symbol versus iterations. The NMSE considered only the active devices in the asynchronous scenario with $N = 128, M = 2$ and $L = 32$, by $10^4$ Monte Carlo trials.

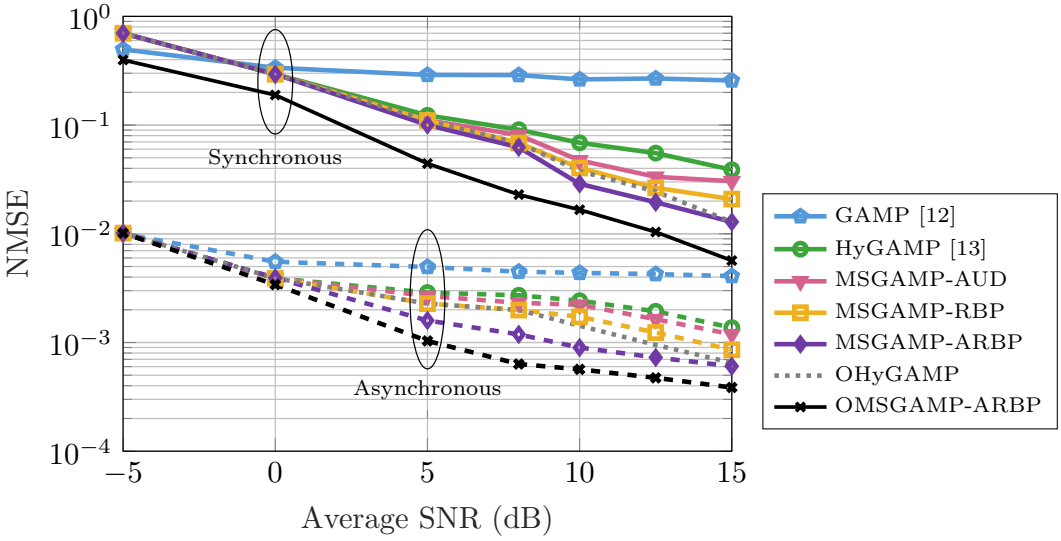


Figure 5.6: Comparison of synchronous and asynchronous scenario in terms of normalized mean squared error vs. Average SNR. The NMSE considered only the active devices with $N = 128$, $M = 2$ and $L = 32$, after 10 iterations. The activity probabilities $\rho_n$ are drawn uniformly at random in $[0.01, 0.05]$ and each SNR value was averaged over $10^4$ Monte Carlo runs.

Lastly, we compare in Fig. 5.6, GAMP, HyGAMP and our best proposed solution, MSGAMP-ARBP, for the synchronous (slotted) and asynchronous (non-slotted) scenarios, in terms of NMSE. Similarly of the previous simulations, the NMSE considered only the active devices with $N = 128$, $M = 2$ and $L = 32$, after 10 iterations. The activity probabilities $\rho_n$ are drawn uniformly at random in $[0.01, 0.05]$ and each SNR value was averaged in $10^4$ Monte Carlo runs. One can see that the performance of the asynchronous scenario is better as the channel matrix is more sparse. Since all evaluated algorithms are compressed sensing solutions, it is expected that we have better results. It is important to highlight, that, independently of the scenario, our main proposed algorithm outperforms HyGAMP in terms of NMSE.

## 5.6 Chapter Summary

In this chapter, we have addressed the joint activity detection and channel estimation problem and considered an asynchronous uplink scenario. After introducing the motivation of the study, a new signal model has been

presented, making considerations regarding the synchronous version. In order to propose a more computationally efficient solution than in previous chapters, the problem has been formulated in a factor graph fashion, which allows that we devise a message-passing solution. Splitting the factor graph in loopy belief propagation (LBP) and generalized approximate message-passing (GAMP) parts, this chapter presented a novel approach, named MSGAMP, that uses the LBP part of the factor graph to detect the activity of devices and GAMP to estimate the channels. The concept of dynamic message-scheduling has been also introduced, where three different techniques based on RBP and instantaneous AUD are applied to MSGAMP. Considering distinct criteria, each technique favors the update of specific nodes of the factor graph, thus reducing the computational complexity and the number of iterations to reach convergence, comparing to a completely-parallel update.

In order to evaluate the proposed schemes, this chapter has also presented performance comparisons in terms of NMSE and AER. Comparing the MSGAMP-type solutions to GAMP and HyGAMP, one can see that the proposed algorithms exhibit a competitive performance, where the efficiency of MSGAMP-AUD and MSGAMP-RBP is comparable to HyGAMP but requires less computational cost. On the other hand, MSGAMP-ARBP outperforms not only HyGAMP and the other MSGAMP algorithms but also a version of HyGAMP with perfect activity detection. The chapter has also provided a convergence analysis where the intuitive idea that the RBP criterion speeds the convergence is confirmed. In addition, an NMSE comparison that contrasts the performance of all considered solutions in a synchronous and asynchronous scenario has been provided. Besides the fact that the performance hierarchy of algorithms remain, the synchronous scenario reduces the sparsity-level of each symbol interval. Thus, under our assumptions, we can conclude that the use of the asynchronous scenario should be an interesting way to increase the joint activity detection and channel estimation performance.

# 6
# Joint Channel Estimation, Activity Detection and Data Decoding Based on Dynamic Message-Scheduling Strategies

## 6.1
## Chapter Overview

With the knowledge acquired in the previous chapter, this chapter devises a joint channel estimation, activity detection and data decoding scheme. By including the channel and the *a priori* activity factor in the factor graph, this chapter presents the bilinear message-scheduling GAMP (BiMSGAMP), a message-passing solution that uses the channel decoder beliefs to refine the activity detection and data decoding. Considered one of the promising features of 5G/B5G channel coding techniques, the fact that the decoding of the Low-Density Parity-Check (LDPC) codes is also based on message-passing is exploited. Since the dynamic message-scheduling techniques described in the last chapter exhibit excellent performance, they have been incorporated in BiMSGAMP as part of the proposed solution.

After presenting the main steps of the proposed BiMSGAMP algorithm, an analysis of the convergence of BiMSGAMP along with a study of its computational complexity based on required floating-point operations (FLOPs) is carried out. In order to assess the BiMSGAMP performance, the chapter ends with numerical results that highlight the performance of the proposed BiMSGAMP and other algorithms, the gains achieved by using the dynamic scheduling strategies over the state-of-the-art in the literature and the effects of the channel decoding part in the system.

## 6.2 System Model and Problem Formulation

Although the formulation of the asynchronous case is straightforward, in order to facilitate the reading and understanding of the proposed technique, in this chapter it is considered a synchronous uplink single-cell GFRA system model. Therefore, the system model of this chapter is briefly explained, since most of it was already described in other chapters.

In order to represent the sparse mMTC scenario as in Fig. 5.1a, for the synchronous scenario, at the beginning of of any observation window, each device is allowed to transmit $L$ symbols, which we denote here as a frame. We then designate the Boolean variable $\gamma_n = 1$ that indicates that the $n$-th device is active in the observation window and $\gamma_n = 0$, otherwise. Thus, considering $\rho_n$ the probability of being active of the $n$-th device, $P(\gamma_n = 1) = 1 - P(\gamma_n = 0) = \rho_n$, where all activity indicators $\gamma_n$ are considered i.i.d. and each device has its own activity probability. For an arbitrary observation window, the received signals are given by

$$\mathbf{Y} = \mathbf{H}\,\mathbf{X} + \mathbf{W}, \tag{6-1}$$

where $\mathbf{W} \in \mathbb{C}^{M \times L}$ is the independent complex Gaussian noise matrix with $\mathcal{N}_c(0, \sigma_w^2)$, $\mathbf{H} \in \mathbb{C}^{M \times N}$ represents the channels and $\mathbf{Y} \in \mathbb{C}^{M \times L}$ is the matrix that gathers the received signals. To estimate the channels and the user data, the transmitting matrix is divided into $L_P$ pilots and $L_D$ data, i.e., $\mathbf{X} = \left[\mathbf{X}^P, \mathbf{X}^D\right]$ such that $L = L_P + L_D$. Therefore, after the encoding of the information bits, the data symbol matrix $\mathbf{X}^D \in \mathbb{C}^{N \times L_D}$ is composed by symbols of a modulation alphabet $\mathcal{A}$, such as quadrature phase shift keying (QPSK).

As discussed in the previous chapter, in order to eliminate the need for round-trip signaling, firstly the BS broadcasts a set of non-orthogonal pilot sequences and each activated device directly transmits frames without

previous scheduling [15]. Although 3GPP's technical specification for 5G TS38.211 [141, 142] consider Zadoff-Chu, $m$ and Gold sequences for the pilots, as discussed in the previous chapter, assigning orthogonal sequences to the MTDs would be impractical. On the other hand, recent works consider pilot sequences generated by ideal i.i.d. Gaussian matrices. Since it is still in discussion, in order to satisfy the GFRA system model and consider non-orthogonal sequences, the pilot part of the frame of the $n$-th device assumed is the same as in Chapter 5, composed by

$$\mathbf{x}_n^P = \frac{\exp\left(j\pi\boldsymbol{\alpha}\right)}{\|\exp\left(j\pi\boldsymbol{\alpha}\right)\|} \tag{6-2}$$

where each element of vector $\boldsymbol{\alpha} \in \mathbb{R}^{1\times L}$ is drawn according to a uniform distribution in the interval $[-1, 1]$.

Regarding the realizations of the channel matrix $\mathbf{H} \in \mathbb{C}^{M\times N}$, here it is assumed that the channel matrix is constant over a transmission frame duration and changes independently from frame to frame. As before, the channel matrix gathers independent fast fading, geometric attenuation and log-normal shadow fading within the observation window. Thus, given the vector $\boldsymbol{\gamma}$, the components of the channel matrix are given by

$$h_{mn} = \begin{cases} \sqrt{\beta_n}\, a_{mn}, & \text{if } \gamma_n = 1, \\ 0, & \text{otherwise.} \end{cases} \tag{6-3}$$

## 6.3 Problem formulation

In order to facilitate the exposition, we formulate the problem for the synchronous scenario, but the use in the asynchronous form is straightforward. To address the goal of the joint activity, data and channel estimation, we treat the problem under the framework of Bayesian inferences, which provides optimal estimation in the MSE sense, named minimum mean square error (MMSE) estimator. The MMSE estimates of $\mathbf{X}_D$ and $\mathbf{H}$ are respectively given by

$$\begin{aligned} \forall\, n, l \in L_D: \quad \hat{x}_{nl} &= \mathbb{E}\left[x_{nl}|\mathbf{y}\right] \\ \forall\, m, n: \quad \hat{h}_{mn} &= \mathbb{E}\left[h_{mn}|\mathbf{y}\right] \end{aligned} \tag{6-4}$$

where the expectations are taken over $p_{\mathbf{x}_{nl}|\mathbf{y}}(x_{nl}|\mathbf{y})$ and $p_{\mathbf{h}_{mn}|\mathbf{y}}(h_{mn}|\mathbf{y})$ both of which are marginalization of $p_{\mathbf{H},\mathbf{X},\boldsymbol{\Gamma}|\mathbf{Y}}(\mathbf{H},\mathbf{X},\boldsymbol{\gamma}|\mathbf{Y})$ from the joint distribution $p_{\mathbf{H},\mathbf{X},\boldsymbol{\Gamma},\mathbf{Y}}(\mathbf{H},\mathbf{X},\boldsymbol{\gamma},\mathbf{Y})$ given by

$$\begin{aligned} &p_{\mathbf{H},\mathbf{X},\boldsymbol{\Gamma}|\mathbf{Y}}(\mathbf{H},\mathbf{X},\boldsymbol{\gamma}|\mathbf{Y}) \\ &\quad= p_{\mathbf{Y}|\mathbf{H},\mathbf{X},\boldsymbol{\Gamma}}(\mathbf{Y}|\mathbf{H},\mathbf{X},\boldsymbol{\gamma})\, p_{\mathbf{X}}(\mathbf{X})\, p_{\mathbf{H}}(\mathbf{H})\, p_{\boldsymbol{\Gamma}}(\boldsymbol{\gamma})\, / p_{\mathbf{Y}}(\mathbf{Y}) \\ &\quad\propto p_{\mathbf{Y}|\mathbf{Z}}(\mathbf{Y}|\mathbf{H}\mathbf{X})\, p_{\mathbf{X}}(\mathbf{X})\, p_{\mathbf{H}}(\mathbf{H})\, p_{\boldsymbol{\Gamma}}(\boldsymbol{\gamma}) \\ &\quad= \prod_{m=1}^{M}\prod_{l=1}^{L} p_{\mathbf{y}_{ml}|\mathbf{z}_{ml}}\left(y_{ml}\middle|\sum_{n=1}^{N} h_{mn}x_{nl}\right)\prod_{n=1}^{N}\prod_{l=1}^{L} p_{\mathbf{x}_{nl}}(x_{nl}) \\ &\qquad\qquad\times \prod_{m=1}^{M}\prod_{n=1}^{N} p_{\mathbf{h}_{mn}|\gamma_n}(h_{mn}|\gamma_n)\prod_{n=1}^{N} p_{\gamma_n}(\gamma_n)\,, \end{aligned} \tag{6-5}$$

where the normalization to a unit area is omitted. Moreover, the transition distribution are separable as $\mathbf{z}_{ml} = \sum_{n=1}^{N} \mathbf{h}_{mn}\mathbf{x}_{nl}$ with $\mathbf{Z} = \mathbf{H}\mathbf{X}$. Since one of the goals is to decode the data signals, the transmitted part also depends on the encoded symbols $\mathbf{c}$ and on the $\mathbf{s}$ activity variables, as given by

$$p_{\mathbf{X}}\left(\mathbf{X}\right) = \prod_{n=1}^{N}\prod_{l\in L_P} p_{\mathbf{x}_P}\left(x_{nl}\right)\sum_{s_{nl}}\sum_{c_{nl}}\prod_{n=1}^{N}\prod_{l\in L_D} p_{\mathbf{x}_D}\left(x_{nl}, c_{nl}, s_{nl}\right), \tag{6-6}$$

where $c_{nl}$ and $s_{nl} \in \{0,1\}$. Accordingly, the MSE of those MMSE estimators are presented by $\text{MSE}\left(\mathbf{X}_D\right) = \left(1/NL_D\right)\mathbb{E}\left[\|\hat{\mathbf{X}}_D - \mathbf{X}_D\|_{\text{F}}^2\right]$ and $\text{MSE}\left(\mathbf{H}\right) = \left(1/MN\right)\mathbb{E}\left[\|\hat{\mathbf{H}} - \mathbf{H}\|_{\text{F}}^2\right]$. Besides, the activity of the $n$-th device is decided by the log-likelihood ratio (LLR) as given by

$$\text{LLR}(s_n) = \ln\frac{p_{\boldsymbol{\gamma}_n|\mathbf{Y}}\left(\gamma_n = 1|\mathbf{Y}\right)}{p_{\boldsymbol{\gamma}_n|\mathbf{Y}}\left(\gamma_n = 0|\mathbf{Y}\right)} \underset{H_1}{\overset{H_0}{\lessgtr}} 0, \tag{6-7}$$

where $p_{\boldsymbol{\gamma}_n|\mathbf{Y}}\left(\gamma_n|\mathbf{Y}\right)$ is marginalization of $p_{\mathbf{H},\mathbf{X},\boldsymbol{\Gamma}|\mathbf{Y}}(\mathbf{H},\mathbf{X},\boldsymbol{\gamma}|\mathbf{Y})$ and the hypothesis $H_0$ and $H_1$ are about the $n$-th device activity.

Since the MMSE estimators in (6-4) and the hypothesis test in (6-7) involve multi-dimensional integrals due to the marginalization of posterior distribution. Exact message passing based on the sum-product rule is too com-

plicated to implement, while the computational cost is impractical for the massive scenario. To this end, we propose an efficient algorithm that incorporates the channel coding into the message-passing approach and uses specific message-scheduling schemes that dramatically reduce the computational cost.

## 6.4 Proposed BiMSGAMP Structure

To compute the *a posteriori* densities within such a graph messages between function and variable nodes have to be exchanged. Drawing inspiration from [140] and [143], the problem is divided in three parts, the activity prior, where the LBP described in the previous chapter is considered, the channel estimation and symbol detector block, where the message scheduling is applied, and the decoder and activity detector block, as depicted in Fig. 6.1.

In the factor graph (FG), rectangles denote factor nodes while spheres are the variable nodes. The belief propagation (BP) framework consists of $L$ multiuser detectors granting probabilistic information about the symbols $x_n$ in the vectors $\mathbf{x}_l$. This information is exchanged between the $L$ multiuser detectors and processed within the detector and decoder blocks. Naturally, the function nodes $f_{nl}$ with the variables $c_{nl}$ and $s_{nl}$[1] are the connecting points for the channel decoder and the symbol detector block.

### 6.4.1 Channel estimation, activity and data detection

The channel estimation and symbol detector block is based on the well-known GAMP [140] algorithm so that, without considering the message-scheduling, both are performed as in GAMP. The main advantages of this procedure is that the messages are approximated by Gaussian distributions, which allows us to update only mean and variances. Another point is that since GAMP computes the messages on each node (instead of on each edge),

[1]Despite the fact that the joint distribution in (6-5) explicit the activity indicators $\gamma_n$, since the algorithm have any previous knowledge of it, this quantity is estimated by the variable $s_{nl}$.

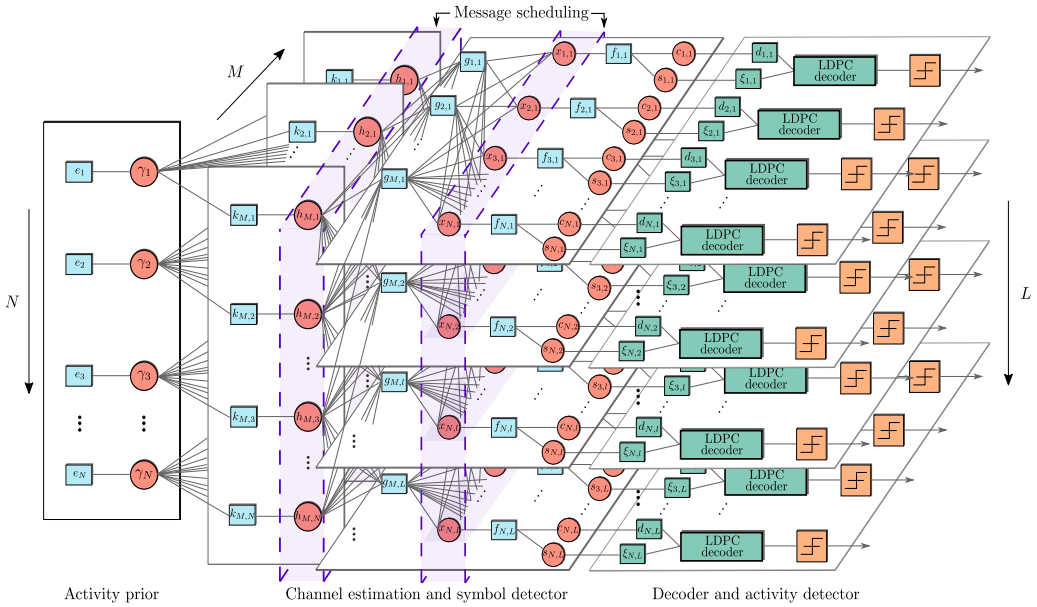


Figure 6.1: Factor graph of the problem. Rectangles represents factor nodes while spheres are the variable nodes.

the number of messages computed in the algorithm is significantly reduced. Thus, in order to introduce the activity detection and data decoding part, we outline the first steps, omitting detailed derivations for brevity. The complete derivations are in Appendices B.1 and B.2.

In order to compute the *a posteriori* densities within such a graph, messages between function and variable nodes have to be exchanged. By applying the sum-product algorithm [58] to the FG, the underlying iterative update equations at the $i-$th iteration summarize the messages from functions to variable nodes as given by

$$\begin{aligned}&\Delta^{i+1}_{g_{ml}\to h_{mn}}\left(h_{mn}\right)\\&=\int_{\{h_{mr}\}_{r\neq n},\{x_{kl}\}_{k=1}^{N}} g_{ml}\left(y_{ml}|z_{ml}\right)\prod_{k=1}^{N}\Delta^{i}_{x_{kl}\to g_{ml}}\left(x_{kl}\right)\prod_{r\neq n}\Delta^{i}_{h_{mr}\to g_{ml}}\left(h_{mr}\right)\end{aligned}\quad(6\text{-}8)$$

and

$$\begin{aligned}&\Delta^{i+1}_{g_{ml}\to x_{nl}}\left(x_{nl}\right)\\&=\int_{\{h_{mk}\}_{k=1}^{N},\{x_{rl}\}_{r\neq n}} g_{ml}\left(y_{ml}|z_{ml}\right)\prod_{r\neq n}\Delta^{i}_{x_{rl}\to g_{ml}}\left(x_{rl}\right)\prod_{k=1}^{N}\Delta^{i}_{h_{mk}\to g_{ml}}\left(h_{mk}\right),\end{aligned}\quad(6\text{-}9)$$

Table 6.1: Message definitions at $i$-th iteration.

| | |
|---|---|
| $\Delta^i_{k_{nm}\to h_{mn}}(h_{nm})$ | Message from node $P(h_{mn}\|\gamma_n)$ to node $h_{nm}$ |
| $\Delta^i_{h_{nm}\to g_{ml}}(h_{nm})$ | Message from node $h_{nm}$ to node $P(y_{ml}\|z_{ml})$ |
| $\Delta^i_{g_{ml}\to x_{nl}}(x_{nl})$ | Message from node $P(y_{ml}\|z_{ml})$ to node $x_{nl}$ |
| $\Delta^i_{x_{nl}\to f_{nl}}(x_{nl})$ | Message from node $x_{nl}$ to node $f_{nl}$ |
| $\Delta^i_{f_{nl}\to d_{nl}}(c_{nl})$ | Message from node $f_{nl}$ to node $d_{nl}$ |
| $\Delta^i_{f_{nl}\to \xi_{nl}}(s_{nl})$ | Message from node $f_{nl}$ to node $\xi_{nl}$ |

where $g_{ml}\left(y_{ml}|z_{ml}\right) = p_{\mathbf{y}_{ml}|\mathbf{z}_{ml}}\Big(y_{ml}\Big|\sum_{k=1}^{N} h_{mk}x_{kl}\Big)$ and the messages from variable to factor nodes are given by

$$\Delta^{i+1}_{h_{mn}\to g_{ml}}\left(h_{mn}\right) = \underbrace{k_{mn}\left(h_{mn}, e_n\right)}_{\Delta_{k_{mn}\to h_{mn}(h_{mn})}} \prod_{p\neq l} \Delta^{i}_{g_{mp}\to h_{mn}}\left(h_{mn}\right) \tag{6-10}$$

$$\Delta^{i+1}_{x_{nl}\to g_{ml}}\left(x_{nl}\right) = \underbrace{f_{nl}\left(x_{nl}, c_{nl}, s_{nl}\right)}_{\Delta_{f_{nl}\to x_{nl}(x_{nl})}} \prod_{p\neq m} \Delta^{i}_{g_{pl}\to x_{nl}}\left(x_{nl}\right). \tag{6-11}$$

Regarding the linear model, $z_{ml} = \sum_{n=1}^{N} h_{mn}x_{nl}$, the messages of $y_{ml}$ are accumulated to obtain an estimate of $z_{ml}$. With the "Onsager" correction applied, the messages in (6-9), in the form of means $\hat{p}^i_{ml}$ and variances $\nu^{pi}_{ml}$, for all $l$, are computed as in [140],

$$\nu^{pi}_{ml} \triangleq \sum_{k=1}^{N} |\hat{h}^i_{mn}|^2\, \nu^{xi}_{nl} + \nu^{hi}_{nl}\, |\hat{x}^i_{nl}|^2 + \nu^{hi}_{nl}\, \nu^{xi}_{nl}, \tag{6-12}$$

$$\hat{p}^i_{ml} \triangleq \sum_{k=1}^{N} \hat{h}^i_{mn}\, \hat{x}^i_{nl} - \hat{s}^{i-1}_{ml}\left(|\hat{h}^i_{mn}|^2\, \nu^{xi}_{nl} + \nu^{hi}_{nl}\, |\hat{x}^i_{nl}|^2\right), \tag{6-13}$$

where initially, $\hat{s}^0_{ml} = 0, \forall l$. Then, the means $\hat{z}^i_{ml}$ and variances $\nu^{zi}_{ml}$ are computed as given by

$$\nu^{zi}_{ml} = \mathrm{VAR}\left\{\mathbf{z}_{ml}|\mathbf{p}_{ml} = \hat{p}^i_{ml}, \nu^{pi}_{ml}\right\}, \tag{6-14}$$

$$\hat{z}^i_{ml} = \mathbb{E}\left\{\mathbf{z}_{ml}|\mathbf{p}_{ml} = \hat{p}^i_{ml}, \nu^{pi}_{ml}\right\}, \tag{6-15}$$

where the mean and variance operations are taken with respect to the *a posteriori* distribution of $z_{ml}$ given the *a priori* distribution $z_{ml} \sim \mathcal{N}_c\left(\hat{p}^i_{ml}, \nu^{pi}_{ml}\right)$. Lastly, the residual $\hat{s}^i_{ml}$ and the inverse-residual-variances $\nu^{si}_{ml}$ are computed by

$$\nu_{ml}^{si} = \left(\frac{1-\nu_{ml}^{zi}}{\nu_{ml}^{pi}}\right)\frac{1}{\nu_{ml}^{pi}}, \qquad (6\text{-}16) \qquad \hat{s}_{ml}^{i} = \frac{(\hat{z}_{ml}^{i} - \hat{p}_{ml}^{i})}{\nu_{ml}^{pi}}. \qquad (6\text{-}17)$$

With the quantities $\hat{s}_{ml}^{i}$ and $\nu_{ml}^{si}$ computed, the means and variances derived from the messages $\Delta_{h_{mn}\to g_{ml}}^{i+1}(h_{mn})$ used to estimate the channels are given by

$$\nu_{mn}^{h\,i+1} = \text{VAR}\left\{\mathbf{h}_{mn}|\mathbf{q}_{mn} = \hat{q}_{mn}^{i}, \nu_{mn}^{qi}\right\} \qquad (6\text{-}18)$$

$$\hat{h}_{mn}^{i+1} = \mathbb{E}\left\{\mathbf{h}_{mn}|\mathbf{q}_{mn} = \hat{q}_{mn}^{i}, \nu_{mn}^{qi}; \gamma_n\right\} \qquad (6\text{-}19)$$

where the variance $\nu_{mn}^{qi}$ is given by

$$\nu_{mn}^{qi} = \left[\nu_{ml}^{si}\left(\sum_{l\in L_P}|x_{nl}|^2 + \sum_{l\in L_D}|\hat{x}_{nl}^{i}|^2\right)\right]^{-1}, \qquad (6\text{-}20)$$

and the mean $\hat{q}_{mn}^{i}$ is

$$\hat{q}_{mn}^{i} = \hat{h}_{mn}^{i}\left(1 - \nu_{mn}^{qi}\sum_{l\in L_D}\nu_{nl}^{xi}\,\nu_{ml}^{si}\right) + \nu_{mn}^{qi}\left(\sum_{l\in L_P}x_{nl}^{i*}\,\hat{s}_{ml}^{i} + \sum_{l\in L_D}\hat{x}_{nl}^{i*}\,\hat{s}_{ml}^{i}\right). \qquad (6\text{-}21)$$

Similarly, for the data we have

$$\nu_{nl}^{x\,i+1} = \text{VAR}\left\{\mathbf{x}_{nl}|\mathbf{r}_{nl} = \hat{r}_{nl}^{i},\, \nu_{nl}^{ri}\right\} \qquad (6\text{-}22)$$

$$\hat{x}_{nl}^{i+1} = \mathbb{E}\left\{\mathbf{x}_{nl}|\mathbf{r}_{nl} = \hat{r}_{nl}^{i},\, \nu_{nl}^{ri}\right\} \qquad (6\text{-}23)$$

where $\nu_{nl}^{ri}$ is given by

$$\nu_{nl}^{ri} = \left(\sum_{m=1}^{M}\hat{h}_{mn}^{i^2}\nu_{ml}^{si}\right)^{-1}, \qquad (6\text{-}24)$$

and the mean $\hat{r}_{nl}^{i}$ is

$$\hat{r}_{nl}^{i} = \hat{x}_{nl}^{i}\left(1 - \nu_{nl}^{ri}\sum_{m=1}^{M}\nu_{mn}^{hi}\,\nu_{ml}^{si}\right) + \nu_{nl}^{ri}\sum_{m=1}^{M}\hat{h}_{mn}^{i*}\,\hat{s}_{ml}^{i}. \qquad (6\text{-}25)$$

Naturally, these means and variances are approximated values, derived in Appendices B.1 and B.2. With the messages based on the GAMP algorithm defined, we describe the messages from the factor node $f_{n,l}$ to the decoder and activity estimator part. For a BPSK scenario, we have from (6-11) [143],

$$f_{nl}\left(x_{nl}, c_{nl}, s_{nl}\right) = s_{nl}\left[\, c_{nl}\,\delta\left(x_{nl}-1\right) + \left(1-c_{nl}\right)\delta\left(x_{nl}+1\right)\right] + \left(1-s_{nl}\right)\delta\left(x_{nl}\right). \quad (6\text{-}26)$$

The function $f_{nl}\left(x_{nl}, c_{nl}, s_{nl}\right)$ in (6-26) summarizes the connection between variables $\{x_{nl}, c_{nl}, s_{nl}\}$, explicit their probabilistic dependencies and can be seen as a check node that is zero for any invalid combination of the variables involved. For the BPSK example and considering $\rho_n$ as the probability of being active of the $n$-th device, for the prior probability of $x_n$ we have $s_n = \rho_n$ and $c_n = 0.5$, then the function node is given by

$$f_n\left(x_n\right) = \left(\rho_n/2\right)\left[\delta\left(x_n-1\right) + \delta\left(x_n+1\right)\right] + \left(1-\rho_n\right)\delta(x_n).$$

To process the encoded bits $c_{nl}$ and the activity variable $s_{nl}$, we define two new function nodes that correspond to the decoder ($d_{nl}$) and activity detector ($\xi_{nl}$). Since that channel code and activity states are node specific, the branch corresponding to one node connects to one function $d_{nl}$ and $\xi_{nl}$ only.

### 6.4.2 Decoder and activity estimator

Following the sum-update rules, the corresponding beliefs have to be multiplied point-wise and marginalized. However, seeing that the variables $c_{nl}$ and $s_{nl}$ have only two connections, the output message equals the input message. Thus, we can directly give the message from the multiuser detector to the decoder as given by

$$\Delta^{i+1}_{f_{nl}\to d_{nl}}\left(c_{nl}\right) \propto \sum_{x_{nl}, s_{nl}} f_{nl}\left(x_{nl}, c_{nl}, s_{nl}\right)\Delta^{i}_{\xi_{nl}\to f_{nl}}\left(s_{nl}\right)\prod_{m=1}^{M}\Delta^{i}_{g_{m,l}\to x_{nl}}\left(x_{nl}\right) \quad (6\text{-}27)$$

where one can see that the message to the decoder already contains information from the activity detector and from the likelihood function. Similarly, the

message from the multiuser detector to the activity detector can be directly devised as

$$\Delta^{i+1}_{f_{nl}\to\xi_{nl}}(s_{nl}) \propto \sum_{x_{nl},c_{nl}} f_{nl}(x_{nl},c_{nl},s_{nl})\,\Delta^{i}_{d_{nl}\to f_{nl}}(c_{nl}) \prod_{m=1}^{M} \Delta^{i}_{g_{m,l}\to x_{nl}}(x_{nl})\,. \quad (6\text{-}28)$$

Accordingly, we can formulate the message from the function node $f_{nl}$ to the likelihood factor $g_{ml}$. Using the sum-product update rules where the messages from the activity detector $\Delta_{\xi_{nl}\to f_{nl}}(x_{nl})$ and the message from the channel decoder $\Delta_{d_{nl}\to f_{nl}}(x_{nl})$ are point-wise multiplied, the extrinsic information from the channel decoder and the activity detector is incorporate as given by

$$\Delta^{i+1}_{f_{nl}\to g_{ml}}(x_{nl}) \propto \sum_{c_{nl},s_{nl}} f_{nl}(x_{nl},c_{nl},s_{nl})\,\Delta^{i}_{d_{nl}\to f_{nl}}(c_{nl})\,\Delta^{i}_{\xi_{nl}\to f_{nl}}(s_{nl}) \prod_{p\neq m} \Delta^{i}_{g_{p,l}\to x_{nl}}(x_{nl})\,. \quad (6\text{-}29)$$

### 6.4.3 LLR conversion

In order to detect the activity of devices and decode the transmitted data, the idea is to convert the messages from $f_{nl}$ to $d_{nl}$ and to $\xi_{nl}$ into LLRs. The idea is to study how the beliefs exchanged between the multiuser detector, decoder and activity detector influence each other. It is expected that the beliefs from the multiuser detector to the decoder exhibit low magnitude if the activity detector has a high belief toward inactivity. Additionally, the beliefs from the multiuser detector to the activity detector are also influenced by the beliefs from the decoder about the encoded symbols.

Starting with the message from the multiuser detector to the decoder in combination with the definition of the function node $f_{nl}$, we have

$$\begin{aligned}\Delta^{i+1}_{f_{nl}\to d_{nl}}(c_{nl}) &\propto \sum_{x_{nl},s_{nl}} f_{nl}(x_{nl},c_{nl},s_{nl})\,\Delta^{i}_{\xi_{nl}\to f_{nl}}(s_{nl})\,\Delta^{i}_{x_{nl}\to f_{nl}}(x_{nl})\\ &\propto \Delta^{i}_{\xi_{nl}\to f_{nl}}(s_{nl}=0)\,\Delta^{i}_{x_{nl}\to f_{nl}}(x_{nl}=0)\\ &\quad+(1-c_{nl})\,\Delta^{i}_{\xi_{nl}\to f_{nl}}(s_{nl}=1)\,\Delta^{i}_{x_{nl}\to f_{nl}}(x_{nl}=-1)\\ &\quad+c_{nl}\,\Delta^{i}_{\xi_{nl}\to f_{nl}}(s_{nl}=1)\,\Delta^{i}_{x_{nl}\to f_{nl}}(x_{nl}=1)\end{aligned}\tag{6-30}$$

where $\Delta^{i}_{x_{nl}\to f_{nl}}(x_{nl}) = \prod_{m=1}^{M}\Delta^{i}_{g_{ml}\to x_{nl}}(x_{nl})$ and messages are functions reflecting probabilities. In this case, we can summarize the message as encoded symbol LLR by computing

$$\begin{aligned}&L^{i+1}_{f_{nl}\to d_{nl}}(c_{nl})\\ &:=\log\frac{\Delta^{i}_{f_{nl}\to d_{nl}}(c_{nl}=1)}{\Delta^{i}_{f_{nl}\to d_{nl}}(c_{nl}=0)}\\ &:=\log\frac{\Delta^{i}_{\xi_{nl}\to f_{nl}}(s_{nl}=0)\,\Delta^{i}_{x_{nl}\to f_{nl}}(x_{nl}=0)+\Delta^{i}_{\xi_{nl}\to f_{nl}}(s_{nl}=1)\,\Delta^{i}_{x_{nl}\to f_{nl}}(x_{nl}=1)}{\Delta^{i}_{\xi_{nl}\to f_{nl}}(s_{nl}=0)\,\Delta_{x_{nl}\to f_{nl}}(x_{nl}=0)+\Delta^{i}_{\xi_{nl}\to f_{nl}}(s_{nl}=1)\,\Delta^{i}_{x_{nl}\to f_{nl}}(x_{nl}=-1)},\end{aligned}\tag{6-31}$$

what expresses the belief of the multiuser detector about the $n,l$-th code symbol as a code symbol LLR.

Regarding the activity detection, we study the influence of the decoder beliefs into the activity LLRs from the multiuser detector to the activity detector. This message is composed of the beliefs given by the likelihood factors and the beliefs from the decoder. This message reads as

$$\Delta^{i+1}_{f_{nl}\to\xi_{nl}}(s_{nl}) \propto \sum_{x_{nl},c_{nl}} f_{nl}(x_{nl},c_{nl},s_{nl})\,\Delta^{i}_{d_{nl}\to f_{nl}}(c_{nl})\,\Delta^{i}_{x_{nl}\to f_{nl}}(x_{nl}),\tag{6-32}$$

which can be also written as an LLR using the definition of the function node $f_{nl}$, as given by

$$\begin{aligned}&L^{i+1}_{f_{nl}\to\xi_{nl}}(s_{nl})\\ &:=\log\frac{\Delta^{i}_{f_{nl}\to\xi_{nl}}(s_{nl}=0)}{\Delta^{i}_{f_{nl}\to\xi_{nl}}(s_{nl}=1)}\\ &:=\log\frac{\Delta^{i}_{x_{nl}\to f_{nl}}(x_{nl}=0)}{\Delta^{i}_{d_{nl}\to f_{nl}}(c_{nl}=0)\,\Delta^{i}_{x_{nl}\to f_{nl}}(x_{nl}=-1)+\Delta^{i}_{d_{nl}\to f_{nl}}(c_{nl}=1)\,\Delta^{i}_{x_{nl}\to f_{nl}}(x_{nl}=1)}.\end{aligned}\tag{6-33}$$

**Algorithm 5:** Bilinear Message-Scheduling GAMP - BiMSGAMP

**input :** $i=1$, $\mathcal{S}^{(1)}=[1,\ldots,N]$,
$\forall\, m,n,l : \hat{\rho}_{nml}^{(0)}=\rho_n, \hat{u}_{lm}^{(0)}=\hat{r}_{nm}^{(0)}=\mathbf{L}^{\mathrm{dec}}=0,\ \nu_{nm}^{r(0)}=1$
**output:** $\hat{\boldsymbol{\rho}}^{\mathrm{end}}$, $\mathbf{L}^{\mathrm{dec}}$

**begin**

Adapted BiG-AMP approximation

**while** ($i<I$ *or* $tol<10^{-4}$) **do**

$\nu_{ml}^{pi}=\sum_n^{|\mathcal{S}^{(i)}|}|\hat{h}_{mn}^{i}|^2\,\nu_{nl}^{x}+\nu_{nl}^{hi}\,|x_{nl}|^2+\nu_{nl}^{hi}\,\nu_{nl}^{x}$ $\quad\forall\, m$ and $l\in\mathcal{L}_P$

$\hat{p}_{ml}^{i}=\sum_n^{|\mathcal{S}^{(i)}|}\hat{h}_{mn}^{i}\,x_{nl}-\hat{s}_{ml}^{i-1}\,\nu_{ml}^{pi}$ $\quad\forall\, m$ and $l\in\mathcal{L}_P$

$\nu_{ml}^{pi}=\sum_n^{|\mathcal{S}^{(i)}|}|\hat{h}_{mn}^{i}|^2\,\nu_{nl}^{xi}+\nu_{nl}^{hi}\,|\hat{x}_{nl}^{i}|^2+\nu_{nl}^{hi}\,\nu_{nl}^{xi}$ $\quad\forall\, m$ and $l\in\mathcal{L}_D$

$\hat{p}_{ml}^{i}=\sum_n^{|\mathcal{S}^{(i)}|}\hat{h}_{mn}^{i}\,\hat{x}_{nl}^{i}-\hat{s}_{ml}^{i-1}\nu_{ml}^{pi}$ $\quad\forall\, m$ and $l\in\mathcal{L}_D$

$\nu_{ml}^{zi}=\mathrm{VAR}\left\{\mathbf{z}_{ml}|\mathbf{p}_{ml}=\hat{p}_{ml}^{i};\nu_{ml}^{pi}\right\}$ $\quad\forall\, m$ and $l$

$\hat{z}_{ml}^{i}=\mathbb{E}\left\{\mathbf{z}_{ml}|\mathbf{p}_{ml}=\hat{p}_{ml}^{i};\nu_{ml}^{pi}\right\}$ $\quad\forall\, m$ and $l$

$\nu_{ml}^{si}=\left(\left(1-\nu_{ml}^{zi}\right)/\nu_{ml}^{pi}\right)/\nu_{ml}^{pi}$ $\quad\forall\, m$ and $l$

$\hat{s}_{ml}^{i}=\left(\hat{z}_{ml}^{i}-\hat{p}_{ml}^{i}\right)/\nu_{ml}^{pi}$ $\quad\forall\, m$ and $l$

$\nu_{mn}^{qi}=\left[\nu_{ml}^{si}\left(\sum_{l\in L_P}|x_{nl}|^2+\sum_{l\in L_D}|\hat{x}_{nl}^{i}|^2\right)\right]^{-1}$ $\quad\forall\, m$ and $n\in|\mathcal{S}^{(i)}|$

$\hat{q}_{mn}^{i}=\hat{h}_{mn}^{i}\left(1-\nu_{mn}^{qi}\sum_{l\in L_D}\nu_{nl}^{xi}\,\nu_{ml}^{si}\right)$ $\quad\forall\, m$ and $n\in|\mathcal{S}^{(i)}|$
$\quad+\nu_{mn}^{qi}\left(\sum_{l\in L_P}x_{nl}^{*}\,\hat{s}_{ml}^{i}+\sum_{l\in L_D}\hat{x}_{nl}^{i*}\,\hat{s}_{ml}^{i}\right)$

$\nu_{mn}^{h\,i+1}=\mathrm{VAR}\left\{\mathbf{h}_{mn}|\mathbf{q}_{mn}=\hat{q}_{mn}^{i},\nu_{mn}^{qi}\right\}$ $\quad\forall\, m$ and $n\in|\mathcal{S}^{(i)}|$

$\hat{h}_{mn}^{i+1}=\mathbb{E}\left\{\mathbf{h}_{mn}|\mathbf{q}_{mn}=\hat{q}_{mn}^{i},\nu_{mn}^{qi};\gamma_n\right\}$ $\quad\forall\, m$ and $n\in|\mathcal{S}^{(i)}|$

$\nu_{nl}^{ri}=\left(\sum_{m=1}^{M}\hat{h}_{mn}^{i^2}\nu_{ml}^{si}\right)^{-1}$ $\quad\forall\, l\in\mathcal{L}_D$ and $n\in|\mathcal{S}^{(i)}|$

$\hat{r}_{nl}^{i}=\hat{x}_{nl}^{i}\left(1-\nu_{nl}^{ri}\sum_{m=1}^{M}\nu_{mn}^{hi}\,\nu_{ml}^{si}\right)$ $\quad\forall\, l\in\mathcal{L}_D$ and $n\in|\mathcal{S}^{(i)}|$
$\quad+\nu_{nl}^{ri}\sum_{m=1}^{M}\hat{h}_{mn}^{i*}\,\hat{s}_{ml}^{i}$

$\nu_{nl}^{x\,i+1}=\mathrm{VAR}\left\{\mathbf{x}_{nl}|\mathbf{r}_{nl}=\hat{r}_{nl}^{i},\,\nu_{nl}^{ri}\right\}$ $\quad\forall\, l\in\mathcal{L}_D$ and $n\in|\mathcal{S}^{(i)}|$

$\hat{x}_{nl}^{i+1}=\mathbb{E}\left\{\mathbf{x}_{nl}|\mathbf{r}_{nl}=\hat{r}_{nl}^{i},\,\nu_{nl}^{ri}\right\}$ $\quad\forall\, l\in\mathcal{L}_D$ and $n\in|\mathcal{S}^{(i)}|$

Joint activity detection and LDPC decoding

Compute $L_{mn}^{i}$ with (5-15) and
(5-16), and $\hat{\rho}_{mn}^{i+1}$ with (5-17) $\quad\forall\, l\in\mathcal{L}_P$ and $n\in|\mathcal{S}^{(i)}|$

Compute $L_{f_{nl}\to d_{nl}}^{i}(c_{nl})$ with (6-16),
(6-17), (6-19), (6-23) and (6-31) $\quad\forall\, l\in\mathcal{L}_D$ and $n\in|\mathcal{S}^{(i)}|$

$\hat{\rho}_{nl}^{i}=1\Big/\left(1+\exp\left\{L_{f_{nl}\to\xi_{nl}}^{i+1}(s_{nl})\right\}\right)$ $\quad\forall\, l\in\mathcal{L}_D$ and $n\in|\mathcal{S}^{(i)}|$

$L_{nl}^{\mathrm{dec}}=\mathrm{Decode}\left[L_{f_{nl}\to d_{nl}}^{i}(c_{nl})-L_{f_{nl}\to d_{nl}}^{i-1}(c_{nl})\right]$

$L_{f_{nl}\to d_{nl}}^{i+1}(c_{nl})=L_{nl}^{\mathrm{dec}}-L_{f_{nl}\to d_{nl}}^{i}(c_{nl})$ $\quad\forall\, l\in\mathcal{L}_D$ and $n\in|\mathcal{S}^{(i)}|$

$\hat{\rho}_{nl}^{i+1}=\mathbb{E}\left[L_{nl}^{\mathrm{dec}},\hat{\rho}_{nl}^{i}\right]$ $\quad\forall\, l\in\mathcal{L}_D$ and $n\in|\mathcal{S}^{(i)}|$

Message-scheduling update

$\mathcal{S}^{(i)}=\mathrm{Update}\left[\mathcal{S}^{(i-1)}\right]$ with chosen MSGAMP-type technique

Update tol with (6-40) and $i=i+1$

**end**

**end**

One can see that the information provided by the decoder does not make difference, at this point, into the activity detection. Thus, since at this moment we already have the means and variances of $\hat{x}$, that is, $\hat{r}$ and $\nu^r$, we can approximate $L^{i+1}_{f_{nl}\to\xi_{nl}}(s_{nl})$ as given by

$$L^{i+1}_{f_{nl}\to\xi_{nl}}(s_{nl}) := \log \frac{\mathcal{N}_c(0|\hat{r}_{nl}, \nu^r_{nl})}{\mathcal{N}_c(0|\hat{r}_{nl}, \nu^r_{nl} + \sigma^2_x)}. \tag{6-34}$$

With the LLRs computed, we use (6-31) for decoding and (6-34) as *a priori* activity probability LLRs into a logarithmic LDPC decoder, as described in [144]. Regarding the activity detection, when the evaluated symbol is a pilot, that is, $l \in [1, \ldots, L_P]$, BiMSGAMP uses the activity prior described in the last Chapter, with (5-15), (5-16) and (5-17). For data, BiMSGAMP uses the extrinsic LLRs provided by the LDPC decoder to refine the probability of being active of each device, as given by

$$\hat{\rho}^i_{nl} = 1 \Big/ \left(1 + \exp\left\{L^{i+1}_{f_{nl}\to\xi_{nl}}(s_{nl})\right\}\right). \tag{6-35}$$

Using the previous LLR values, we have, similarly to the idea in Chapters 3 and 4,

$$L^{\text{dec}}_{nl} = \text{Decode}\left[L^{i}_{f_{nl}\to d_{nl}}(c_{nl}) - L^{i-1}_{f_{nl}\to d_{nl}}(c_{nl})\right], \tag{6-36}$$

$$L^{i+1}_{f_{nl}\to d_{nl}}(c_{nl}) = L^{\text{dec}}_{nl} - L^{i}_{f_{nl}\to d_{nl}}(c_{nl}), \tag{6-37}$$

$$\hat{\rho}^{i+1}_{nl} = \mathbb{E}\left[L^{\text{dec}}_{nl}, \hat{\rho}^i_{nl}\right], \tag{6-38}$$

where $L^{\text{dec}}_{nl}$ is the LLR output of the LDPC decoder and $\hat{\rho}^{i+1}_{nl} = \Delta^i_{\xi_{nl}\to f_{nl}}(s_{nl} = 1)$ which closes the loop.

Since the LDPC decoder decides for bit zero or one, an all-zero frame corresponds to an inactive device. Thus, for a bit matrix $\mathbf{B}$, the final activity detection after the hard decision procedure in $\mathbf{L}^{\text{dec}}$, for the $n$-th device,

$$\begin{cases} \hat{\gamma}_n = 0, & \text{if } \mathbf{b}_n = \mathbf{0} \text{ and} \\ \hat{\gamma}_n = 1, & \text{otherwise.} \end{cases} \tag{6-39}$$

The whole procedure, summarized in Algorithm 5, iterates until a predefined threshold condition is satisfied or the iteration marker $i$ reaches the maximum number of iterations $I$. In this work, we consider the threshold given by

$$\text{tol} = \left( \frac{\|\hat{\mathbf{x}}_l^{(i)} - \hat{\mathbf{x}}_l^{(i-1)}\|}{\|\hat{\mathbf{x}}_l^{(i)}\|} \right) < 10^{-4}, \tag{6-40}$$

that is, if tol reaches a value equal or larger than $10^{-4}$ and/or $i < I$, BiMSGAMP stops.

## 6.5 Analysis

This section analyses the BiMSGAMP-type schemes in terms of the computational complexity and the convergence in terms of NMSE regarding the activity and data detection, and the channel estimation. All results are discussed and compared with state-of-the-art solutions.

### 6.5.1 Complexity

The computational cost of BiMSGAMP-type schemes is analyzed below by counting each required numerical operation in terms of complex FLOPs. In particular, to provide a more precise comparison, Table 6.2 separates the number of operations in three groups, since the number of required FLOPs is different, depending of the operation type. Thus, for a different number of devices $N$, receive antennas $M$ and the number of pilots $L_P$ and data symbols $L_D$ per frame, the previous algorithms are compared. In the case of joint activity and data detection algorithms, in order to try to provide a fair comparison, a separate channel estimation part has been considered, where an adapted version of the same solution is considered. This approach has also been used in order to verify the performance of each solution.

As it is clearly shown in Fig. 6.2, a key benefit of using message-scheduling approaches is the computational cost saving. As explained before, while the state-of-the-art algorithms as BiGAMP [112] and HyGAMP [139]

Table 6.2: Operations counting of considering techniques per iteration. Approaches that originally considered just the joint activity and signal detection have a separate channel estimation part, adapted using the same solution considered.

| Algorithm | Additions, Subtractions and Multiplications | Divisions and Square roots | Sine, exp, and log |
|---|---|---|---|
| AMP [34] | $L\left(6M-2N+12MN\right)$ | $L\left(2+M\right)$ | N/A |
| Joint-EM-AMP [37] | $M\left(8L_D+3L_P\right)$ $+N\left[\left(27+3\lvert\mathcal{A}\rvert\right)L_D-L_P\right]$ | $M\left(2L_D+L_P\right)$ $+4NL_P+2L_P$ | N/A |
| BiGAMP [112] | $L\left(12M+11N\right)$ | $3L\left(M+N\right)$ | N/A |
| HyGAMP [139] | $L\left(12M+17N+4\right)$ | $3L\left(M+N\right)$ | $L\left(5N\right)$ |
| BiMSGAMP | $L\left(12M+17\lvert\mathcal{S}\rvert+4\right)$ | $3L\left(M+\lvert\mathcal{S}\rvert\right)$ | $L\left(5\lvert\mathcal{S}\rvert\right)$ |

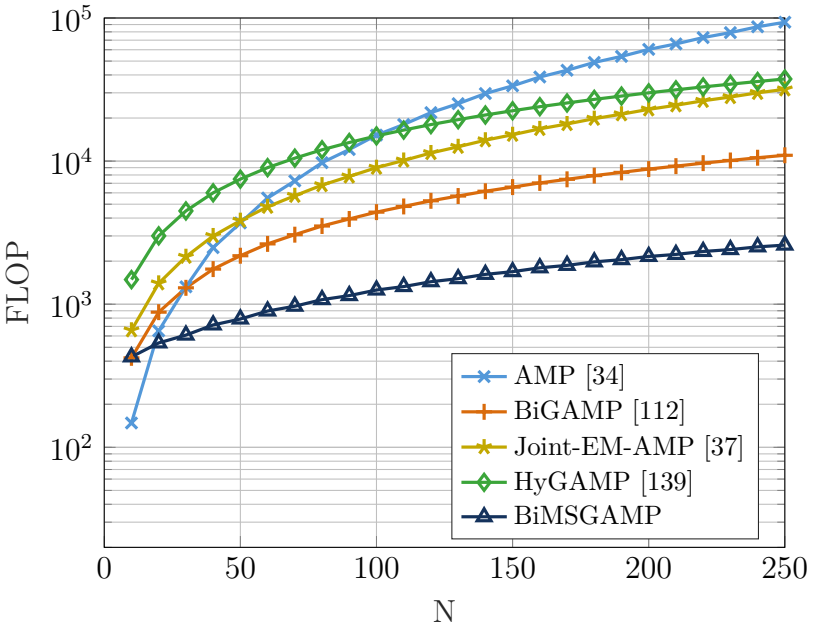


Figure 6.2: Floating-point operation (FLOP) counting per iteration. Each operation has an weight as defined in the Lightspeed MATLAB toolbox [3].

have $O(MN)$ messages to be computed, BiMSGAMP-type schemes demands only $O(M|\mathcal{S}^{(i)}|)$. With the prediction that the mMTC scenario need to handle up to $300,000$ devices per cell [7], the gain of BiMSGAMP is evident since $|\mathcal{S}^{(i)}| << N$. In order to highlight this benefit, Table 6.2 provides the number of operations needed for each state-of-the-art algorithm in terms of $N$ devices, $M$ BS antennas and $L = L_P + L_D$ frame size. Considering $N = [10, 250]$, $M = N/4$ and $L_P = L_D = 128$, Fig. 6.2 depicts that BiMSGAMP-type schemes require less computational cost than other approaches.

### 6.5.2 Convergence

In order to analyze the convergence behaviour of BiMSGAMP-type schemes, the NMSE of the channel estimation, activity and data detection is depicted in Figs. 6.3, 6.4 and 6.5. Since the BiGAMP algorithm does not exhibit a competitive performance in terms of NMSE, as shown in Fig. 6.6a, and FER, as shown in Fig. 6.6b, HyGAMP is chosen for comparison. Another important point is that these results considered the components of all devices, including active and inactive ones.

Starting with the channel estimation, it is interesting to see in Figs. 6.3a, 6.3b and 6.3c that the residual-based metric displays jumps on the convergence, due to the group update. Apparently, the neglected nodes had a considerable influence in low-SNRs scenarios, as when the set $\mathcal{S}$ is empty, all nodes are updated, which fits with the "jumps" on iterations. We remark that for the convergence analysis all the channels are considered and notice that HyGAMP's and BiMSGAMP-AUD's performances are almost the same. Regarding the activity detection, the jumping behaviour of BiMSGAMP disappears since it is computed only after the procedure. Furthermore, although for SNR values $< 5$ dB, the convergence behaviour of HyGAMP and BiMSGAMP-AUD is quite similar, from SNR $= 10$ dB, BiMSGAMP-AUD exhibits better values up to SNR $= 20$ dB, where all schemes perform equally. With respect to the convergence, the performance of the channel NMSE repeats, but the "jumpings" of BiMSGAMP-RBP vanishes from SNR $= 10$ dB.

In spite of most of the scenarios the BiMSGAMP-type solutions converge equally/later than HyGAMP, it is important to say that the performance is achieved with a considerable computational cost saving. Even if it is needed more iterations to reach convergence, using BiMSGAMP-RBP with the expected massive number of devices requiring connection, the advantage of using dynamic scheduling approaches outperforms algorithms with message passing in parallel.

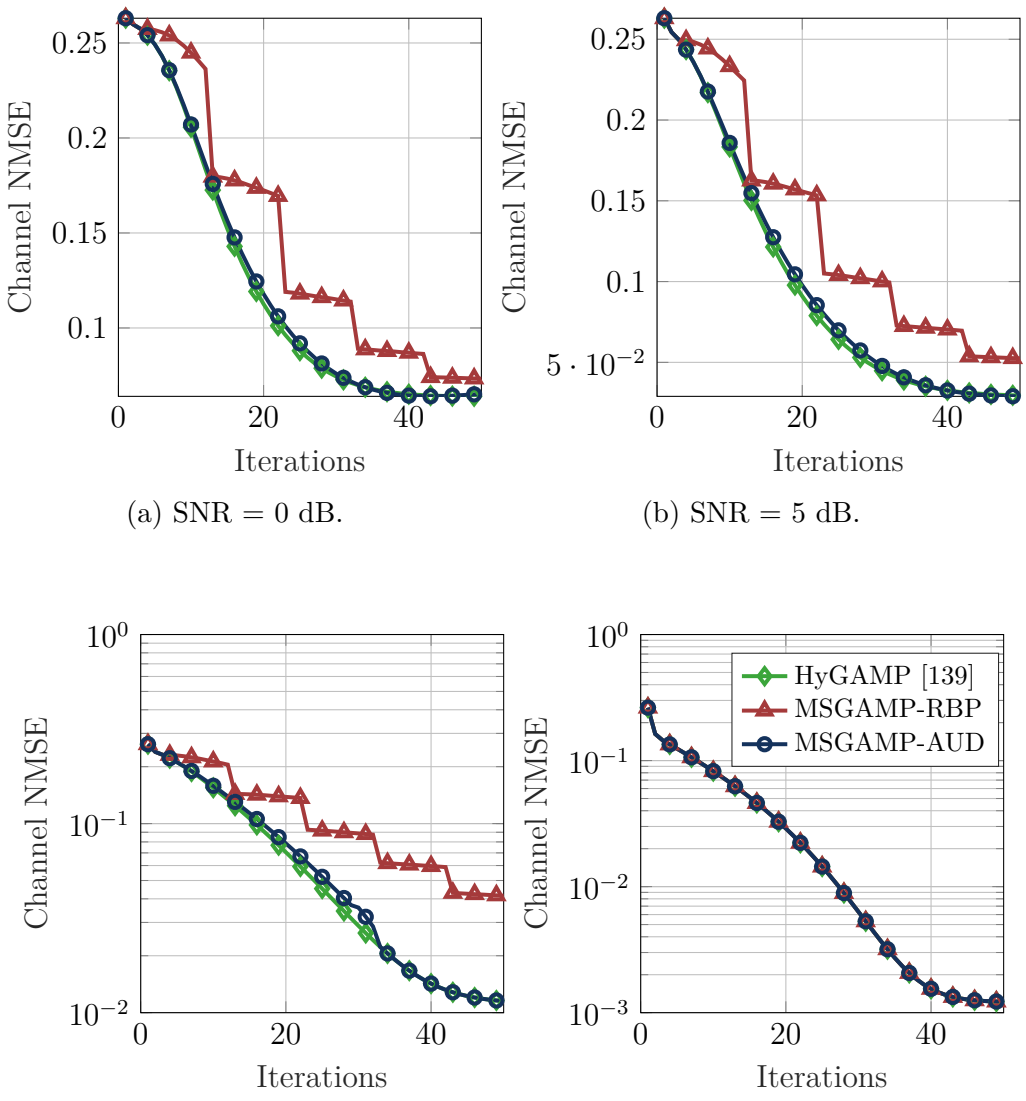


(a) SNR = 0 dB.

(b) SNR = 5 dB.

(c) SNR = 10 dB.

(d) SNR = 20 dB.

Figure 6.3: Convergence of channel estimation in terms of NMSE for different SNR values.

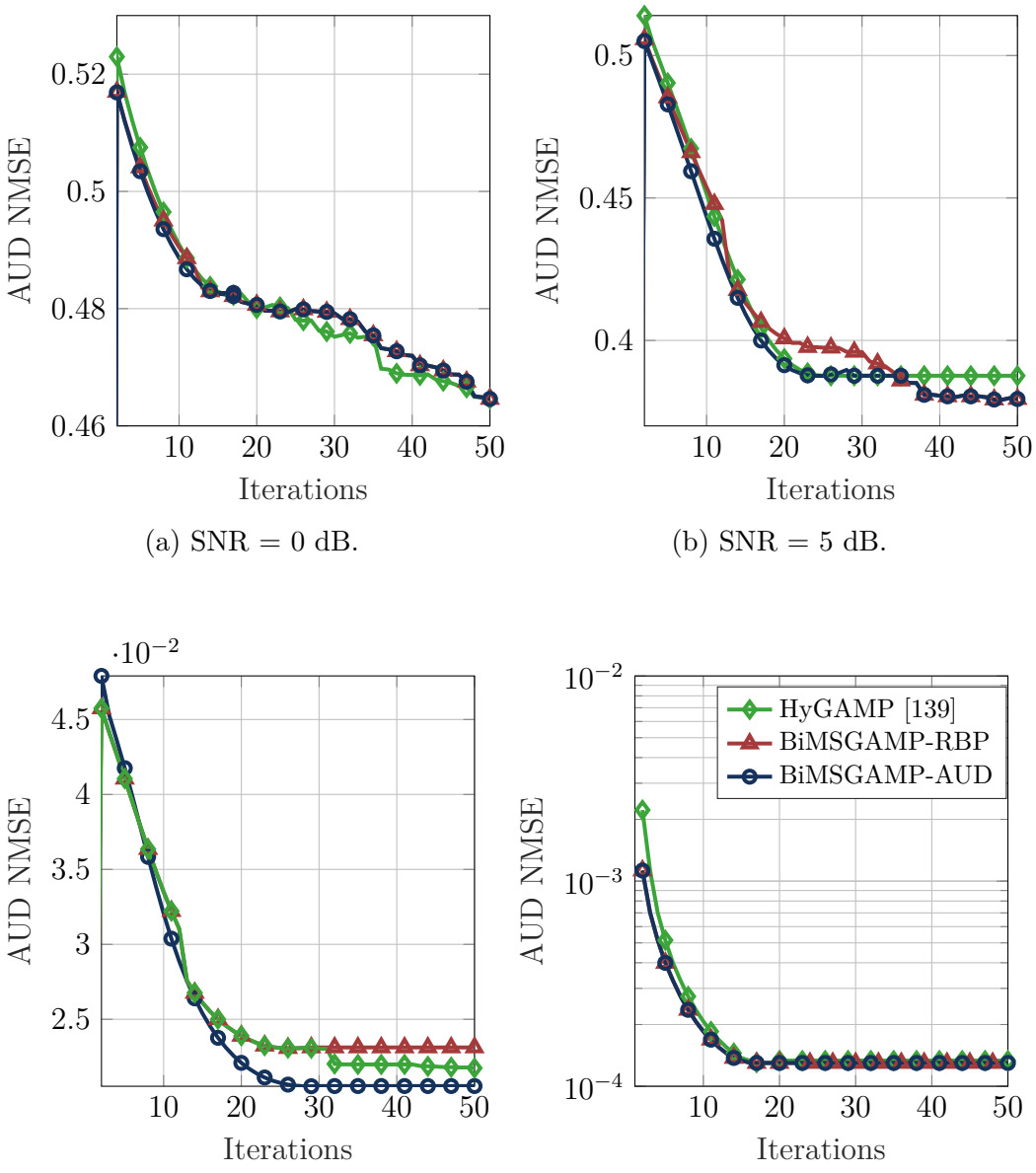


(a) SNR = 0 dB.

(b) SNR = 5 dB.

(c) SNR = 10 dB.

(d) SNR = 20 dB.

Figure 6.4: Convergence of activity detection in terms of NMSE for different SNR values.

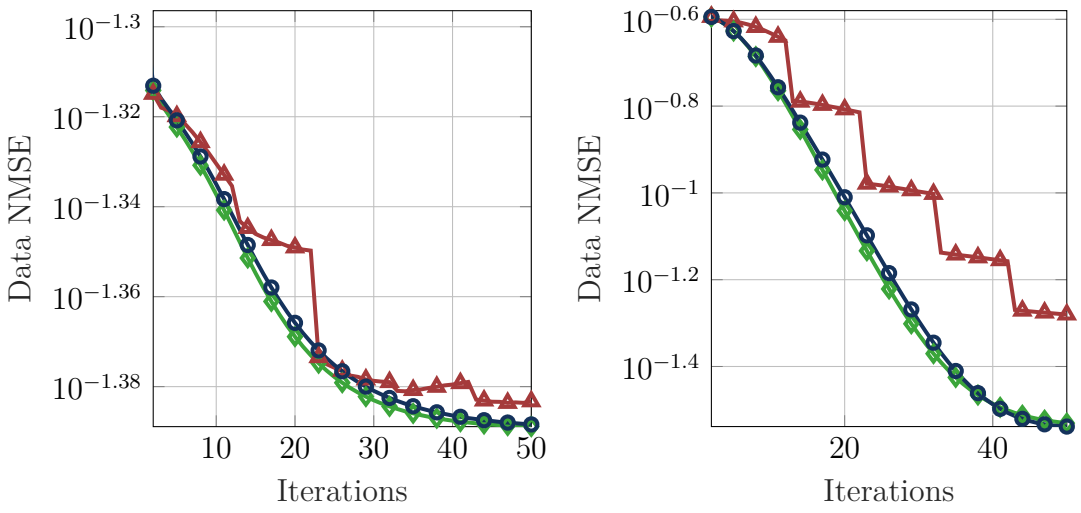


(a) SNR = 0 dB. (b) SNR = 5 dB.

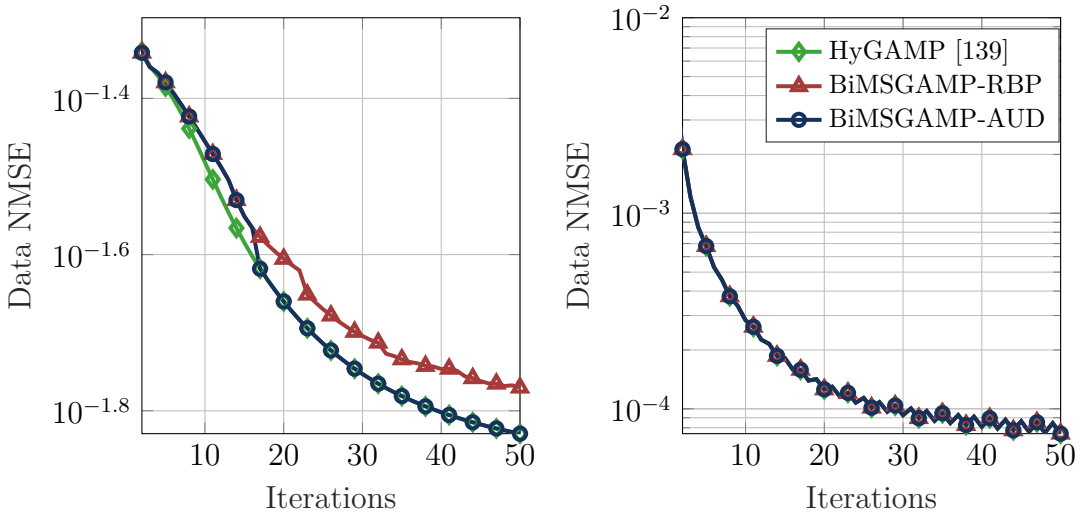


(c) SNR = 10 dB. (d) SNR = 20 dB.

Figure 6.5: Convergence of data detection in terms of NMSE for different SNR values.

## 6.6 Numerical Results

In order to assess the proposed schemes, the well-known approximate message passing (AMP) [34], and state-of-the-art solutions as the joint expectation-maximization AMP (Joint-EM-AMP) [37], a bilinear version of AMP [112] and the HyGAMP [139] are used for comparison. HyGAMP includes a loopy belief propagation (LBP) part for user activity detection before the GAMPs factor graph, refining the AUD. The Joint-EM-AMP uses expectation maximization (EM) algorithm to perform the activity detection, while the means and variances for signal detection are provided by AMP. As a lower bound, we consider the oracle HyGAMP (OHyGAMP), a version of HyGAMP with perfect activity detection.

Averaging the results over $10^4$ runs, it is considered an uplink underdetermined mMTC system with $N = 100$ devices with a single antenna each transmitting to a BS equipped with $M = 32$ antennas. All the simulated schemes experience a block-fading channel model as described in (6-3). In each observation window, the number of active devices vary, but this number is limited by 10% of $N$. The channel coding considered is LDPC with rate 1/2 and the modulation scheme is QPSK. Following Chapter 4, the balance between pilots and data is $L_P = L_D = 128$, where the pilots are given by (6-2) and the symbols are modulated after channel coding with block length of 256 bits. The average SNR is given by $10\log\left(NR\sigma_x^2/\sigma_v^2\right)$.

Since there are not many works in the literature that perform joint channel estimation, activity detection and signal decoding in the mMTC scenario, the algorithms that do not consider the channel estimation part (AMP, Joint-EM-AMP and HyGAMP), have a separate channel estimation stage, which is adapted using the same solution considered. Additionally, in order to give a fair comparison, all evaluated algorithms used the LLR conversion presented in Section 6.4.3. The maximum number of iterations considered for AMP and Joint-EM-AMP is $N/2$ while 30 for BiGAMP,

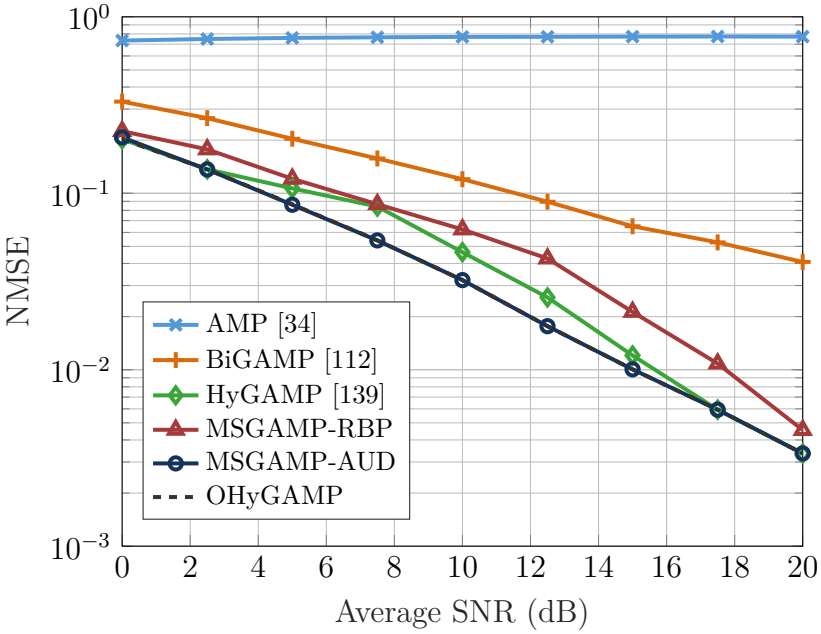


(a) Normalized mean squared error rate vs. Average SNR (dB).

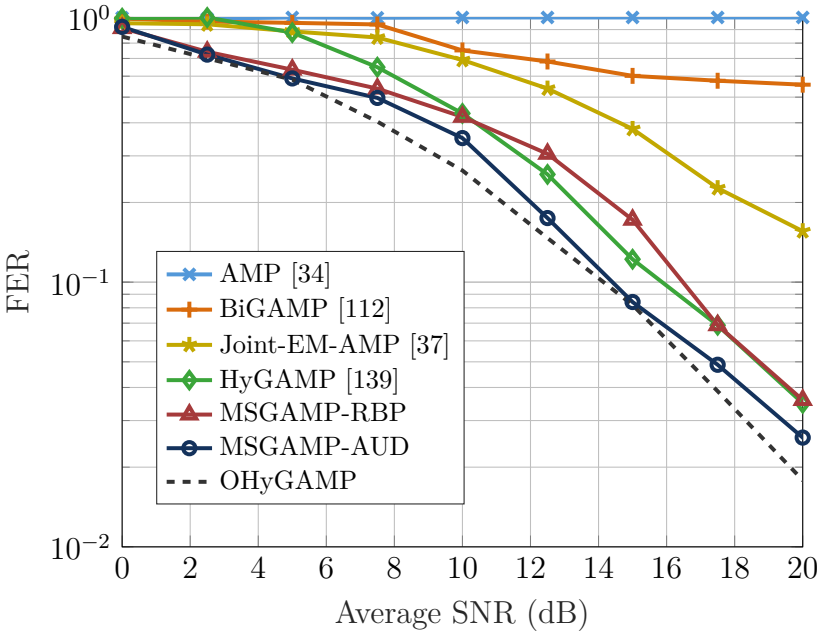


(b) Frame error rate vs. Average SNR (dB).

Figure 6.6: NMSE and FER in an mMTC scenario with $N = 100$, $M = 32$ and $L = 256$, by $10^4$ Monte Carlo trials.

HyGAMP and BiMSGAMP-type schemes.

Fig. 6.6a depicts the NMSE versus different signal-to-noise ratio values. It is noticed that in this new scenario the metric that considers the activity detection as message-scheduling, BiMSGAMP-AUD, reached the oracle

HyGAMP performance, outperforming all other approaches. It is a good indication that the use of the channel decoding LLRs to refine the AUD improves not only the data detection, but also the channel estimation. Nevertheless, the HyGAMP outperforms the residual-based solution, for SNR values $> 7.5$ dB. Since BiMSGAMP-RBP updates all nodes in the end of the set procedure, is possible that the neglected nodes had a considerable influence in this scenario. This point is further discussed in the analysis section. Besides that, the well-known AMP exhibits an poor performance, even though requiring more iterations. This channel estimation is used for the AMP and the Joint-EM-AMP schemes in the data decoding part. Since BiGAMP has any previous knowledge of the sparsity of the scenario as HyGAMP and it jointly performs the AUD, CE and data decoding (using the proposed scheme), it clearly losses performance. Probably an adaptive dumping and/or a channel estimation initialization should be considered to improve its efficiency specifically for the mMTC scenario. Another hypothesis is that the mMTC system is not sparse enough for it, since the number of active devices vary from 1 to 10% of $N$.

Using the channel estimation depicted in Fig. 6.6a, the frame error rate (FER) performance of the schemes is shown in Fig. 6.6b. Firstly, it is interesting to observe that for low SNR values ($<$ 10 dB), we can notice that the BiMSGAMP-type solutions outperforms other approaches, getting even closer to the lower bound. For larger SNR values, BiMSGAMP-RBP and HyGAMP exhibits almost the same performance. The loss of performance of BiMSGAMP-RBP in SNRs between 10 and 18 dB, is due to the fact that the channel estimation was not as efficient. On the other hand, as cited before, the approach of the LLRs used in BiMSGAMP-AUD proved to be efficient for data decoding. Despite the fact that, as seen in Figs. 6.7a and 6.7b, BiGAMP and Joint-EM-AMP provide a satisfactory MDR and FAR values, their means and variances estimates that are the base of the LLRs for signal detection seems not to be as accurate as HyGAMP and BiMSGAMP.

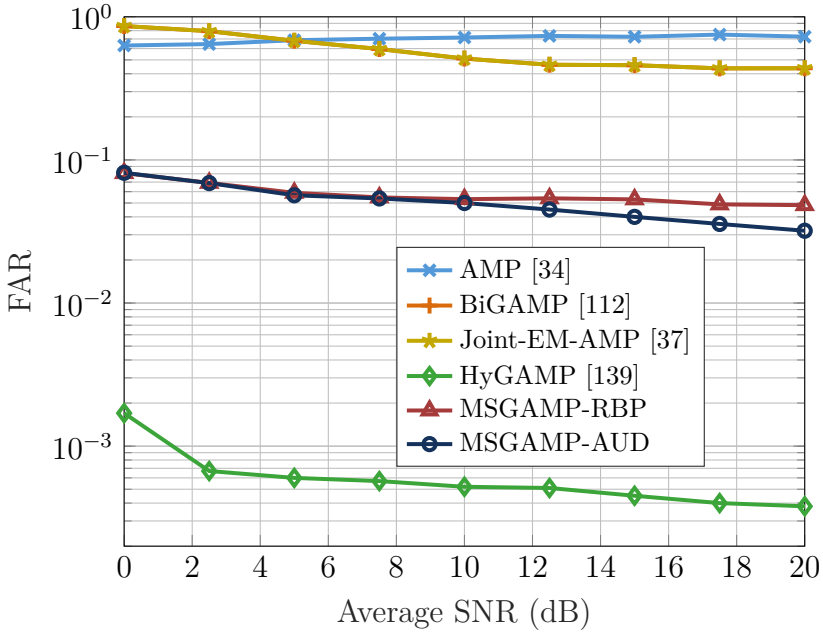


(a) False alarm rate vs. Average SNR (dB).

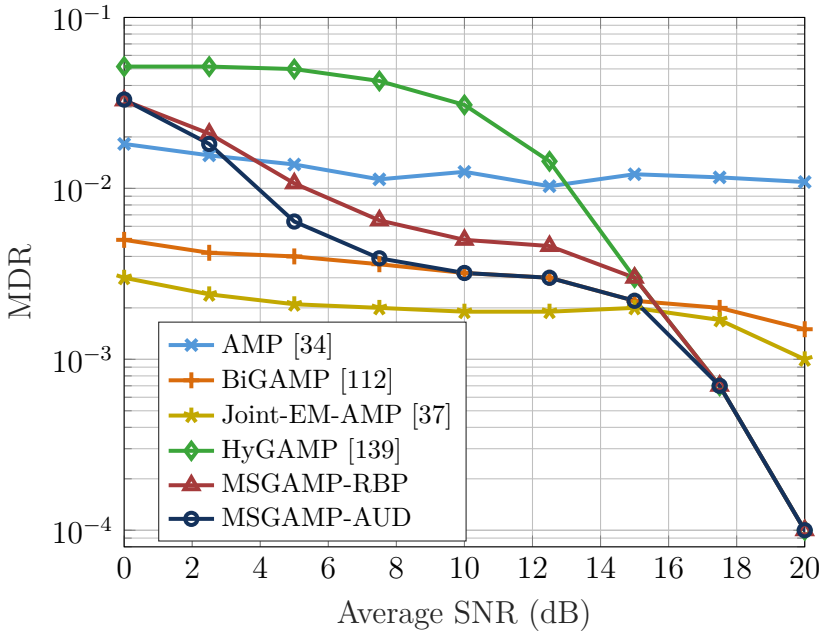


(b) Missed detection rate vs. Average SNR (dB).

Figure 6.7: Activity error rates per symbol in an mMTC scenario with $N = 100, M = 32$ and $L = 256$, by $10^4$ Monte Carlo trials.

As a crucial part of the analysis, the activity error rates are shown in Figs 6.7a and 6.7b. Evidently, there is a trade-off regarding the false alarm and missed detection rates. Since most of the approaches in the literature use the means to detect the activity, the threshold considered by all of them is 0.5,

while for BiMSGAMP-type schemes, that considers LLRs (for each symbol), is 0.95. Thus, it is possible to see that for lower MDR values, the detector benefits in terms of FER since we have interest in the active devices. Naturally, the activity threshold is a parameter that depends on the system designer.

## 6.7 Chapter Summary

In this chapter, a joint channel estimation, activity detection and data decoding solution is presented. Under the synchronous signal model the complete computationally efficient message-passing solution BiMSGAMP has been developed. Formulating a new factor graph, divided in three blocks: activity prior, channel estimation and symbol detector, and decoder and activity estimation. After formulating the problem, the chapter introduces the proposed BiMSGAMP algorithm, where the message-passing approach is detailed along with the LLR conversion for use with the LDPC decoder.

After presenting the BiMSGAMP algorithm procedure, numerical results in terms of NMSE, AER and FER that highlights the performance gains of BiMSGAMP over other state-of-the-art algorithms are provided. The usage of message-scheduling techniques is discussed as well as the effects of the joint solution. An analysis of the convergence of BiMSGAMP that studies its behaviour along a computational complexity based on required floating-point operations (FLOP) is carried out, that demonstrates the huge computational cost saving by using message-scheduling approaches without loss of performance.

# 7
# Conclusions and Future Work

## 7.1
## Conclusions

Covering numerous new applications, massive machine-type communications will increasingly become part of future networks. Designed for specific applications, mMTC devices (MTCDs) exhibit a sporadic data traffic, where small packets are transmitted at low rates. Since most MTCDs are battery operated, they are drastically energy-constrained. These unique aspects of mMTC impose new demands and challenges to the random access (RA) design. Despite the fact that detection techniques have been investigated for more than 50 years, at each new emerging application, novel schemes are required. Thus, this thesis aims to present and discuss novel channel estimation, activity detection and signal decoding techniques for mMTC.

In **Chapter 2**, a technical background on this thesis is provided. Firstly, basic concepts of multiuser MIMO are presented, which includes channel estimation, multiuser detection and channel capacity. After this part, the mMTC scenario is introduced, where its as traffic, medium access and challenges are presented and discussed. In order to provide a comprehensive overview of the main detection techniques designed specifically for mMTC, Chapter 2 also presents not only a list of the main state-of-the-art approaches, but a performance evaluation of them in the same evaluation framework.

Motivated by the need to develop novel detection schemes for mMTC, **Chapter 3** presents the AA-RLS-DF scheme that jointly detects the activity and signal of devices without the need to perform explicit channel estimation using a regularized version of the adaptive RLS algorithm. An iterative

soft information processing and decoding scheme has been devised specifically for mMTC, which is incorporated along with the AA-RLS-DF scheme. As demonstrated by simulation results, AA-RLS-DF outperforms other regularized approaches, in terms of SER, FAR, MDR and BER.

Since there still a gap between the AA-RLS-DF and the lower bound, **Chapter 4** presents two candidate-list detection schemes for mMTC that employ the regularized version of the adaptive RLS algorithm to adjust the receive filter parameters. Numerical results show the excellent performance of the proposed AA-VGL-DF scheme as compared to existing approaches. In order to understand the scenario and provide a deeper explanation of the proposed solution, **Chapter 4** also presents a complexity and diversity analysis and devises uplink sum-rate expressions.

As the solutions on previous chapters do not require explicit channel estimation, **Chapter 5** studies the joint active device detection and channel estimation problem. In order to devise a low complexity solution, this chapter formulates the problem as a framework based on factor graphs. Given the aforementioned mMTC characteristics, two different scenarios are studied, synchronous and asynchronous uplink transmissions. After a discussion, a message-scheduling GAMP (MSGAMP) algorithm that uses a factor graph approach has been devised with three different message-scheduling techniques. Based on the RBP and instantaneous AUD, simulation results of NMSE, AER and a convergence analysis shows that dynamic message-scheduling techniques dramatically reduce the complexity cost with no loss of performance.

Lastly, in order to provide a complete solution, **Chapter 6** presents the bilinear message-scheduling GAMP (BiMSGAMP) scheme, that jointly performs active device detection, channel estimation and data decoding. Considered one of the promising 5G/B5G channel coding techniques, the fact that the decoding of LDPC codes is also based on message-passing has been exploited. Using part of the dynamic message-scheduling techniques described in Chapter

5, numerical results highlight the performance of the proposed BiMSGAMP algorithm against existing algorithms, where the gains achieved by the dynamic scheduling strategies over the state-of-the-art in the literature are significant. Due to a convergence and complexity analysis, it is possible to observe that the performance of MSGAMP-type schemes is excellent while it considerably saves computational cost. Even though message-scheduling approaches need more iterations to reach convergence they still outperform parallel message-passing solutions.

## 7.2 Future Works

- As discussed in Chapters 2 and 5, a time synchronous transmission as required by conventional OFDM systems is not the most suitable choice to facilitate an efficient transmission, as the synchronization signalling would generate a substantial overhead and increase the overall transmission latency. Thus, with the gap in the literature and the initial study realized in Chapter 5, a framework that considers frame collisions in the asynchronous scenario would be interesting.
- Besides the three message-scheduling strategies proposed, there is room for improvement. A study of different criteria and a development of a steady-state analysis can indicate even better solutions. The use of message-scheduling strategies in the LDPC decoder [145], can also improve the data decoding and, consequently, the activity detection in the proposed solutions could also be considered.
- As seen in Chapter 2, an almost unexplored approach in the literature is the non-coherent transmission scenario. Despite the problems previously described, the fact that the transmitted data bits can be embedded in the index of the transmitted pilot sequence of each active device is promising. A solution that could successfully deal with the disadvantage of non-

orthogonal pilot sequences would fit appropriately to the small frame mMTC scenario.

- Although it seems clear that it is impractical the use of orthogonal pilots, this point deserves further study. The latest 3GPP technical report [142] recommends the use of Zadoff-Chu and Gold sequences and there are a few recent works that study if the increase of the number of non-orthogonal preambles could result in worse performance under certain conditions although it can reduce the probability of preamble collision [146]. Additionally, there are a few other works that study the effects of high correlated preambles in channel estimation [147]. Thus, this topic can be considered for further investigation.

# Bibliography


[1] MARZETTA, T. L., **Massive MIMO: An Introduction**, Bell Labs Technical Journal, vol. 20, pp. 11–22, 2015.

[2] DE LAMARE, R. C., **Massive mimo systems: Signal processing challenges and future trends**, URSI Radio Science Bulletin, vol. 2013, no. 347, pp. 8–20, 2013.

[3] MINKA, T., **Lightspeed MATLAB toolbox**, GitHub, access: 2021-05-15.

[4] CISCO, **Cisco Annual Internet Report (2018–2023)**, White Paper 1, 35p., Cisco, 2020.

[5] POPOVSKI, P.; ET AL., **5G Wireless Network Slicing for eMBB, URLLC, and mMTC: A Communication-Theoretic View**, IEEE Access, vol. 6, pp. 55765–55779, 2018.

[6] ZHENG, K.; OU, S.; ALONSO-ZARATE, J.; DOHLER, M.; LIU, F. ; ZHU, H., **Challenges of massive access in highly dense LTE-advanced networks with machine-to-machine communications**, IEEE Wireless Communications, vol. 21, no. 3, pp. 12–18, 2014.

[7] 3GPP, **Study on provision of low-cost Machine-Type Communications (MTC) UEs based on LTE**, Technical Specification TS 36.888 1, 3rd Generation Partnership Project (3GPP), 2013.

[8] DI RENNA, R. B.; BOCKELMANN, C.; DE LAMARE, R. C. ; DEKORSY, A., **Detection techniques for massive machine-type communi-**

**cations: Challenges and solutions**, IEEE Access, vol. 8, pp. 180928–180954, 2020.

[9] INT. TELECOMMUN. UNION, **IMT vision—Framework and overall objectives of the future development of IMT for 2020 and beyond**, ITU-Recommendation M.2083-0 1, Int. Telecommun. Union, Geneva, Switzerland, 2015.

[10] A. OSSEIRAN, J. F. MONSERRAT AND P. MARSCH, *5G Mobile and Wireless Communications Technology*, Cambridge University Press, Cambridge, 2nd edition, 2016.

[11] MADUENÕ, G. C.; STEFANOVIC, C. ; POPOVSKI, P., **How many smart meters can be deployed in a GSM cell?**, In: 2013 IEEE INTERNATIONAL CONFERENCE ON COMMUNICATIONS WORKSHOPS (ICC), pp. 1263–1268, 2013.

[12] 3GPP, **Narrowband Internet of Things**, LTE Release 13 1, 3rd Generation Partnership Project (3GPP), 2016.

[13] DUAN, S.; SHAH-MANSOURI, V.; WANG, Z. ; WONG, V. W. S., **D-ACB: Adaptive congestion control algorithm for bursty M2M traffic in LTE networks**, IEEE Transactions on Vehicular Technology, vol. 65, no. 12, pp. 9847–9861, 2016.

[14] CENTENARO, M.; VANGELISTA, L.; SAUR, S.; WEBER, A. ; BRAUN, V., **Comparison of Collision-Free and Contention-Based Radio Access Protocols for the Internet of Things**, IEEE Transactions on Communications, vol. 65, no. 9, pp. 3832–3846, 2017.

[15] BOCKELMANN, C.; ET AL., **Towards Massive Connectivity Support for Scalable mMTC Communications in 5G Networks**, IEEE Access, vol. 6, pp. 28969–28992, 2018.

[16] SALAM, T.; REHMAN, W. U. ; TAO, X., **Data Aggregation in Massive Machine Type Communication: Challenges and Solutions**, IEEE Access, vol. 7, pp. 41921–41946, 2019.

[17] SCHLEGEL, C.; KEMPTER, R. ; KOTA, P., **A novel random wireless packet multiple access method using CDMA**, IEEE Transactions on Wireless Communications, vol. 5, no. 6, pp. 1362–1370, 2006.

[18] SCHEPKER, H. F.; BOCKELMANN, C. ; DEKORSY, A., **Exploiting Sparsity in Channel and Data Estimation for Sporadic Multi-User Communication**, In: ISWCS 2013; THE TENTH INTERNATIONAL SYMPOSIUM ON WIRELESS COMMUNICATION SYSTEMS, pp. 1–5, Ilmenau, Germany, 2013.

[19] WUNDER, G.; STEFANOVIC, C.; POPOVSKI, P. ; THIELE, L., **Compressive coded random access for massive MTC traffic in 5G systems**, In: 2015 49TH ASILOMAR CONFERENCE ON SIGNALS, SYSTEMS AND COMPUTERS, pp. 13–17, Pacific Grove, CA, 2015.

[20] CHOI, J., **Two-Stage Multiple Access for Many Devices of Unique Identifications Over Frequency-Selective Fading Channels**, IEEE Internet of Things Journal, vol. 4, no. 1, pp. 162–171, 2017.

[21] CHOI, J.; LEE, K. ; YU, N. Y., **Compressive Random Access Using Multiple Resource Blocks for MTC**, In: 2016 IEEE GLOBECOM WORKSHOPS (GC WKSHPS), pp. 1–5, 2016.

[22] CHOI, J.; YU, N. Y., **Compressive Channel Division Multiple Access for MTC Under Frequency-Selective Fading**, IEEE Transactions on Communications, vol. 65, no. 6, pp. 2715–2725, 2017.

[23] DING, J.; QU, D.; JIANG, H. ; JIANG, T., **Success Probability of Grant-Free Random Access With Massive MIMO**, IEEE Internet of Things Journal, vol. 6, no. 1, pp. 506–516, 2019.

[24] DING, J.; QU, D. ; JIANG, H., **Optimal Preamble Length for Spectral Efficiency in Grant-Free RA with Massive MIMO**, In: 2019 INTERNATIONAL CONFERENCE ON ELECTRONICS, INFORMATION, AND COMMUNICATION (ICEIC), pp. 1–5, Barcelona, Spain, 2019.

[25] CHOI, J. W. E. A., **Compressed sensing for wireless communications: Useful tips and tricks**, IEEE Commun. Surveys & Tut., vol. 19, no. 3, pp. 1527–1550, 2017.

[26] ZHU, H.; GIANNAKIS, G. B., **Exploiting Sparse User Activity in Multiuser Detection**, IEEE Transactions on Communications, vol. 59, no. 2, pp. 454–465, 2011.

[27] KNOOP, B.; MONSEES, F.; BOCKELMANN, C.; WUEBBEN, D.; PAUL, S. ; DEKORSY, A., **Sparsity-Aware Successive Interference Cancellation with Practical Constraints**, In: WSA 2013; 17TH INTERNATIONAL ITG WORKSHOP ON SMART ANTENNAS, pp. 1–8, Stuttgart, Germany, 2013.

[28] KNOOP, B.; MONSEES, F.; BOCKELMANN, C.; PETERS-DROLSHAGEN, D.; PAUL, S. ; DEKORSY, A., **Compressed sensing K-best detection for sparse multi-user communications**, In: 2014 22ND EUROPEAN SIGNAL PROCESSING CONFERENCE (EUSIPCO), pp. 1726–1730, Lisboa, Portugal, 2014.

[29] AHN, J.; SHIM, B. ; LEE, K. B., **Sparsity-Aware Ordered Successive Interference Cancellation for Massive Machine-Type Communications**, IEEE Wireless Communications Letters, vol. 7, no. 1, pp. 134–137, 2018.

[30] DI RENNA, R. B.; LAMARE, R. C. D., **Activity-Aware Multiple Feedback SIC for Massive Machine-Type Communications**, In:

SCC 2019; 12TH INTERNATIONAL ITG CONFERENCE ON SYSTEMS, COMMUNICATIONS AND CODING, pp. 1–6, Rostock, Germany, 2019.

[31] CIRIK, A. C.; MYSORE BALASUBRAMANYA, N. ; LAMPE, L., **Multi-User Detection Using ADMM-Based Compressive Sensing for Uplink Grant-Free NOMA**, IEEE Wireless Communications Letters, vol. 7, no. 1, pp. 46–49, 2018.

[32] ZHANG, X.; LIANG, Y.-C. ; FANG, J., **Novel Bayesian Inference Algorithms for Multiuser Detection in M2M Communications**, IEEE Transactions on Vehicular Technology, vol. 66, no. 9, pp. 7833–7848, 2017.

[33] ZHANG, X.; LABEAU, F.; LIANG, Y.-C. ; FANG, J., **Compressive Sensing-Based Multiuser Detection via Iterative Reweighed Approach in M2M Communications**, IEEE Wireless Communications Letters, vol. 7, no. 5, pp. 764–767, 2018.

[34] DONOHO, D.; MALEKI, A. ; MONTANARI, A., **Message-passing algorithms for compressed sensing**, Proc. Nat. Acad. Sci. USA, vol. 106, no. 45, pp. 18914–18919, 2009.

[35] CHEN, Z.; SOHRABI, F. ; YU, W., **Multi-Cell Sparse Activity Detection for Massive Random Access: Massive MIMO Versus Cooperative MIMO**, IEEE Transactions on Wireless Communications, vol. 18, no. 8, pp. 4060–4074, 2019.

[36] SENEL, K.; LARSSON, E. G., **Grant-Free Massive MTC-Enabled Massive MIMO: A Compressive Sensing Approach**, IEEE Transactions on Communications, vol. 66, no. 12, pp. 6164–6175, 2018.

[37] WEI, C.; LIU, H.; ZHANG, Z.; DANG, J. ; WU, L., **Approximate Message Passing-Based Joint User Activity and Data Detection**

**for NOMA**, IEEE Communications Letters, vol. 21, no. 3, pp. 640–643, 2017.

[38] TROPP, J. A.; GILBERT, A. C., **Signal Recovery From Random Measurements Via Orthogonal Matching Pursuit**, IEEE Transactions on Information Theory, vol. 53, no. 12, pp. 4655–4666, 2007.

[39] CHEN, S.; BILLINGS, S. A. ; LUO, W., **Orthogonal least squares methods and their application to non-linear system identification**, Int. J. Control, vol. 50, no. 5, pp. 1873–1896, 1989.

[40] SCHEPKER, H. F.; DEKORSY, A., **Sparse Multi-User Detection for CDMA transmission using greedy algorithms**, In: 2011 8TH INTERNATIONAL SYMPOSIUM ON WIRELESS COMMUNICATION SYSTEMS, pp. 291–295, 2011.

[41] WANG, B.; DAI, L.; YUAN, Y. ; WANG, Z., **Compressive Sensing Based Multi-User Detection for Uplink Grant-Free Non-Orthogonal Multiple Access**, In: 2015 IEEE 82ND VEHICULAR TECHNOLOGY CONFERENCE (VTC2015-FALL), pp. 1–5, 2015.

[42] SCHEPKER, H. F.; BOCKELMANN, C. ; DEKORSY, A., **Improving Greedy Compressive Sensing Based Multi-User Detection with Iterative Feedback**, In: 2013 IEEE 78TH VEHICULAR TECHNOLOGY CONFERENCE (VTC FALL), pp. 1–5, 2013.

[43] SCHEPKER, H. F.; BOCKELMANN, C. ; DEKORSY, A., **Efficient Detectors for Joint Compressed Sensing Detection and Channel Decoding**, IEEE Transactions on Communications, vol. 63, no. 6, pp. 2249–2260, 2015.

[44] MAJUNDAR, A.; WARD, R. K., **Fast Group Sparse Classification**, Canadian Journal of Electrical and Computer Engineering, vol. 34, no. 4, pp. 2249–2260, 2009.

[45] LIU, J.; WU, G.; LI, S. ; TIRKKONEN, O., **Blind detection of uplink grant-free SCMA with unknown user sparsity**, In: 2017 IEEE INTERNATIONAL CONFERENCE ON COMMUNICATIONS (ICC), pp. 1–6, 2017.

[46] Y. DU AND C. CHENG AND B. DONG AND Z. CHEN AND X. WANG AND J. FANG AND S. LI, **Block-Sparsity-Based Multiuser Detection for Uplink Grant-Free NOMA**, IEEE Transactions on Wireless Communications, vol. 17, no. 12, pp. 7894–7909, 2018.

[47] SCHEPKER, H. F.; DEKORSY, A., **Compressive Sensing Multi-User Detection with Block-Wise Orthogonal Least Squares**, In: 2012 IEEE 75TH VEHICULAR TECHNOLOGY CONFERENCE (VTC SPRING), pp. 1–5, 2012.

[48] BOCKELMANN, C., **Iterative Soft Interference Cancellation for Sparse BPSK Signals**, IEEE Communications Letters, vol. 19, no. 5, pp. 855–858, 2015.

[49] DU, Y.; CHENG, C.; DONG, B.; CHEN, Z.; WANG, X.; FANG, J. ; LI, S., **Block-Sparsity-Based Multiuser Detection for Uplink Grant-Free NOMA**, IEEE Transactions on Wireless Communications, vol. 17, no. 12, pp. 7894–7909, 2018.

[50] DI RENNA, R. B.; DE LAMARE, R. C., **Adaptive Activity-Aware Iterative Detection for Massive Machine-Type Communications**, IEEE Wireless Communications Letters, vol. 8, no. 6, pp. 1631–1634, 2019.

[51] DI RENNA, R. B.; DE LAMARE, R. C., **Iterative List Detection and Decoding for Massive Machine-Type Communications**, IEEE Transactions on Communications, vol. -, no. -, pp. –, 2020.

[52] LIU, L.; YU, W., **Massive Connectivity With Massive MIMO—Part I: Device Activity Detection and Channel Es-**

**timation**, IEEE Transactions on Signal Processing, vol. 66, no. 11, pp. 2933–2946, 2018.

[53] SUN, Z.; WEI, Z.; YANG, L.; YUAN, J.; CHENG, X. ; WAN, L., **Exploiting Transmission Control for Joint User Identification and Channel Estimation in Massive Connectivity**, IEEE Transactions on Communications, vol. 67, no. 9, pp. 6311–6326, 2019.

[54] DAI, W.; WEI, H.; ZHOU, J. ; ZHOU, W., **An Efficient Message Passing Algorithm for Active User Detection and Channel Estimation in NOMA**, In: 2019 IEEE 90TH VEHICULAR TECHNOLOGY CONFERENCE (VTC2019-FALL), pp. 1–6, 2019.

[55] TANG, Z.; WANG, J. ; SONG, J., **Device Activity Detection and Non-Coherent Information Transmission for Massive Machine-Type Communications**, IEEE Access, vol. 8, pp. 41452–41465, 2020.

[56] WEI, F.; CHEN, W.; WU, Y.; MA, J. ; TSIFTSIS, T. A., **Message-Passing Receiver Design for Joint Channel Estimation and Data Decoding in Uplink Grant-Free SCMA Systems**, IEEE Transactions on Wireless Communications, vol. 18, no. 1, pp. 167–181, 2019.

[57] ZHANG, Y.; GUO, Q.; WANG, Z.; XI, J. ; WU, N., **Block Sparse Bayesian Learning Based Joint User Activity Detection and Channel Estimation for Grant-Free NOMA Systems**, IEEE Transactions on Vehicular Technology, vol. 67, no. 10, pp. 9631–9640, 2018.

[58] KSCHISCHANG, F. R.; FREY, B. J. ; LOELIGER, H. ., **Factor graphs and the sum-product algorithm**, IEEE Transactions on Information Theory, vol. 47, no. 2, pp. 498–519, 2001.

[59] AHN, J.; SHIM, B. ; LEE, K. B., **EP-Based Joint Active User Detection and Channel Estimation for Massive Machine-Type**

**Communications**, IEEE Transactions on Communications, vol. 67, no. 7, pp. 5178–5189, 2019.

[60] LEHMANN, F., **Joint User Activity Detection, Channel Estimation, and Decoding for Multiuser/Multiantenna OFDM Systems**, IEEE Transactions on Vehicular Technology, vol. 67, no. 9, pp. 8263–8275, 2018.

[61] WUNDER, G.; ROTH, I.; FRITSCHEK, R. ; EISERT, J., **HiHTP: A custom-tailored hierarchical sparse detector for massive MTC**, In: 2017 51ST ASILOMAR CONFERENCE ON SIGNALS, SYSTEMS, AND COMPUTERS, pp. 1929–1934, 2017.

[62] ZOU, Q. E. A., **Message passing based joint channel and user activity estimation for uplink grant-free massive mimo systems with low-precision adcs**, IEEE Signal Processing Letters, vol. 27, pp. 506–510, 2020.

[63] DI RENNA, R. B.; DE LAMARE, R. C., **Dynamic message scheduling based on activity-aware residual belief propagation for asynchronous mmtc**, IEEE Wireless Communications Letters, pp. 1–1, 2021.

[64] BAI, Y.; AI, B. ; CHEN, W., **Deep Learning Based Fast Multiuser Detection for Massive Machine-Type Communication**, In: 2019 IEEE 90TH VEHICULAR TECHNOLOGY CONFERENCE (VTC2019-FALL), pp. 1–5, 2019.

[65] GUI, G.; HUANG, H.; SONG, Y. ; SARI, H., **Deep Learning for an Effective Nonorthogonal Multiple Access Scheme**, IEEE Transactions on Vehicular Technology, vol. 67, no. 9, 2018.

[66] ZHANG, Z.; LI, Y.; HUANG, C.; GUO, Q.; YUEN, C. ; GUAN, Y. L., **DNN-Aided Block Sparse Bayesian Learning for User Activity Detection and Channel Estimation in Grant-Free Non-Orthogonal**

**Random Access**, IEEE Transactions on Vehicular Technology, vol. 68, no. 12, pp. 12000–12012, 2019.

[67] ZHU, W.; TAO, M.; YUAN, X. ; GUAN, Y., **Deep-learned approximate message passing for asynchronous massive connectivity**, IEEE Transactions on Wireless Communications, pp. 1–1, 2021.

[68] CUI, Y.; LI, S. ; ZHANG, W., **Jointly sparse signal recovery and support recovery via deep learning with applications in mimo-based grant-free random access**, IEEE Journal on Selected Areas in Communications, vol. 39, no. 3, pp. 788–803, 2021.

[69] WEI, F.; CHEN, W.; WU, Y.; MA, J. ; TSIFTSIS, T. A., **Message-Passing Receiver Design for Joint Channel Estimation and Data Decoding in Uplink Grant-Free SCMA Systems**, IEEE Transactions on Wireless Communications, vol. 18, no. 1, pp. 167–181, 2019.

[70] DING, T.; YUAN, X. ; LIEW, S. C., **Sparsity Learning-Based Multiuser Detection in Grant-Free Massive-Device Multiple Access**, IEEE Transactions on Wireless Communications, vol. 18, no. 7, pp. 3569–3582, 2019.

[71] KUAI, X.; ET AL., **Double-sparsity learning-based channel-and-signal estimation in massive mimo with generalized spatial modulation**, IEEE Transactions on Communications, vol. 68, no. 5, pp. 2863–2877, 2020.

[72] ZOU, Q.; ZHANG, H.; CAI, D. ; YANG, H., **A low-complexity joint user activity, channel and data estimation for grant-free massive mimo systems**, IEEE Signal Processing Letters, vol. 27, pp. 1290–1294, 2020.

[73] JIANG, S.; ET AL., **Joint user identification, channel estimation, and signal detection for grant-free noma**, IEEE Transactions on Wireless Communications, vol. 19, no. 10, pp. 6960–6976, 2020.

[74] ZHANG, Y.; YUAN, Z.; GUO, Q.; WANG, Z.; XI, J. ; LI, Y., **Bayesian Receiver Design for Grant-Free NOMA With Message Passing Based Structured Signal Estimation**, IEEE Transactions on Vehicular Technology, vol. 69, no. 8, pp. 8643–8656, 2020.

[75] TELATAR, E., **Capacity of multi-antenna gaussian channels**, European Transactions on Telecommunications, vol. 10, no. 6, pp. 585–595, 1999.

[76] FOSCHINI, G.; CHIZHIK, D.; GANS, M.; PAPADIAS, C. ; VALENZUELA, R., **Analysis and performance of some basic space-time architectures**, IEEE Journal on Selected Areas in Communications, vol. 21, no. 3, pp. 303–320, 2003.

[77] BIGLIERI, E. T., *MIMO wireless communications*, Cambridge University Press, 2nd edition, 2007.

[78] GOLDSMITH, A.; JAFAR, S.; JINDAL, N. ; VISHWANATH, S., **Capacity limits of mimo channels**, IEEE Journal on Selected Areas in Communications, vol. 21, no. 5, pp. 684–702, 2003.

[79] FOSCHINI, G. J., **Layered space-time architecture for wireless communication in a fading environment when using multi-element antennas**, Bell Labs Technical Journal, vol. 1, no. 2, pp. 41–59, 1996.

[80] LATHI, B. P.; DING, Z., *Modern Digital and Analog Communication*, Oxford University Press, 5th edition, 2018.

[81] BJÖRNSON, E.; HOYDIS, J. ; SANGUINETTI, L., **Massive MIMO networks: Spectral, energy, and hardware efficiency**, Foundations and Trends® in Signal Processing, vol. 11, no. 3-4, pp. 154–655, 2017.

[82] GOLDSMITH, A., **Wireless communications**, 2005.

[83] SHANNON, C. E., **A mathematical theory of communication**, Bell System Technical Journal, vol. 20, pp. 379–423, 1948.

[84] SHNIDMAN, D. A., **A generalized Nyquist criterion and an optimum linear receiver for a pulse modulation system**, Bell System Technical Journal, vol. 46, no. 9, pp. 2163–2177, 1967.

[85] TUFTS, D., **Nyquist's problem - The joint optimization of transmitter and receiver in pulse amplitude modulation**, Proceedings of the IEEE, vol. 53, no. 3, pp. 248–259, 1965.

[86] YANG, S.; HANZO, L., **Fifty years of mimo detection: The road to large-scale mimos**, IEEE Communications Surveys Tutorials, vol. 17, no. 4, pp. 1941–1988, 2015.

[87] WOLNIANSKY, P. W.; FOSCHINI, G. J.; GOLDEN, G. D. ; VALENZUELA, R. A., **V-BLAST: An architecture for realizing very high data rates over the rich-scattering wireless channel**, In: PROCEEEDINGS URSI ISSSE), pp. 295–300, 1998.

[88] GOLDEN, G. D.; FOSCHINI, G. J.; VALENZUELA, R. A. ; WOLNIANSKY, P. W., **Detection algorithm and initial laboratory results using V-BLAST space-time communication architecture**, Eletronics Letters, vol. 35, no. 1, pp. 14–16, 1999.

[89] VITERBI, A. J., **Very low rate convolution codes for maximum theoretical performance of spread-spectrum multiple-access channels**, IEEE J. Sel. Areas Commun., vol. 8, no. 4, pp. 641–649, 1990.

[90] YOON, Y.; KOHNO, R. ; IMAI, H., **A spread-spectrum multiaccess system with cochannel interference cancellation for multipath fading channels**, IEEE Journal on Selected Areas in Communications, vol. 11, no. 7, pp. 1067–1075, 1993.

[91] DIVSALAR, D.; SIMON, M. ; RAPHAELI, D., **Improved parallel interference cancellation for cdma**, IEEE Transactions on Communications, vol. 46, no. 2, pp. 258–268, 1998.

[92] LUO, Z.; ZHAO, M.; LIU, S. ; LIU, Y., **Generalized parallel interference cancellation with near-optimal detection performance**, IEEE Transactions on Signal Processing, vol. 56, no. 1, pp. 304–312, 2008.

[93] DE LAMARE, R. C.; SAMPAIO-NETO, R., **Minimum Mean-Squared Error Iterative Successive Parallel Arbitrated Decision Feedback Detectors for DS-CDMA Systems**, IEEE Transactions on Communications, vol. 56, no. 5, pp. 778–789, 2008.

[94] GHAVIMI, F.; CHEN, H.-H., **M2M communications in 3GPP LTE/LTE-A networks: Architectures, service requirements, challenges, and applications**, IEEE Communications Surveys & Tutorials, vol. 17, no. 2, pp. 525–549, 2015.

[95] SALEEM, Y.; CRESPI, N.; REHMANI, M. H. ; COPELAND, R., **Internet of Things-Aided Smart Grid: Technologies, Architectures, Applications, Prototypes, and Future Research Directions**, IEEE Access, vol. 7, pp. 62962–63003, 2019.

[96] SOLTANMOHAMMADI, E.; GHAVAMI, K. ; NARAGHI-POUR, M., **A Survey of Traffic Issues in Machine-to-Machine Communications Over LTE**, IEEE Internet of Things Journal, vol. 3, no. 6, pp. 865–884, 2016.

[97] SHAFIQ, M. Z.; JI, L.; LIU, A. X.; PANG, J. ; WANG, J., **Large-Scale Measurement and Characterization of Cellular Machine-to-Machine Traffic**, IEEE/ACM Transactions on Networking, vol. 21, no. 6, pp. 1960–1973, 2013.

[98] RAPPAPORT, T. S., *Wireless Communications: Principles and Practice*, Prentice Hall PTR, Upper Saddle River, 1nd edition, 2002.

[99] BJORCK, A., **Numerics of gram-schmidt orthogonalization**, Linear Algebra Appl., vol. 197–198, pp. 297–316, 1994.

[100] LI, P.; DE LAMARE, R. C. ; FA, R., **Multiple Feedback Successive Interference Cancellation Detection for Multiuser MIMO Systems**, IEEE Transactions on Wireless Communications, vol. 10, no. 8, pp. 2434–2439, 2011.

[101] TROPP, J. A.; GILBERT, A. C. ; STRAUSS, M. J., **Algorithms for simultaneous sparse approximation. Part I: Greedy pursuit**, Signal Processing, vol. 86, no. 3, pp. 572–588, 2006.

[102] YU, N. Y., **A Fast and Noise-Robust Algorithm for Joint Sparse Recovery Through Information Transfer**, IEEE Access, vol. 7, pp. 37735–37748, 2019.

[103] YU, N. Y., **Multiuser Activity and Data Detection via Sparsity-Blind Greedy Recovery for Uplink Grant-Free NOMA**, IEEE Communications Letters, vol. 23, no. 11, pp. 2082–2085, 2019.

[104] DONOHO, D. L.; MALEKI, A. ; MONTANARI, A., **Message passing algorithms for compressed sensing: I. motivation and construction**, In: 2010 IEEE INFORMATION THEORY WORKSHOP ON INFORMATION THEORY (ITW 2010, CAIRO), pp. 1–5, 2010.

[105] DONOHO, D. L.; MALEKI, A. ; MONTANARI, A., **Message passing algorithms for compressed sensing: II. analysis and validation**,

In: 2010 IEEE INFORMATION THEORY WORKSHOP ON INFORMATION THEORY (ITW 2010, CAIRO), pp. 1–5, 2010.

[106] BERTHIER, R.; MONTANARI, A. ; NGUYEN, P.-M., **State Evolution for Approximate Message Passing with Non-Separable Functions**, 2017.

[107] ZHANG, Z.; RAO, B. D., **Sparse Signal Recovery With Temporally Correlated Source Vectors Using Sparse Bayesian Learning**, IEEE Journal of Selected Topics in Signal Processing, vol. 5, no. 5, pp. 912–926, 2011.

[108] NEEDELL, D.; TROPP, J. A., **CoSaMP: Iterative signal recovery from incomplete and inaccurate samples**, Applied and Computational Harmonic Analysis, vol. 26, no. 3, pp. 301–321, 2009.

[109] ELDAR, Y. C.; KUPPINGER, P. ; BOLCSKEI, H., **Block-Sparse Signals: Uncertainty Relations and Efficient Recovery**, IEEE Transactions on Signal Processing, vol. 58, no. 6, pp. 3042–3054, 2010.

[110] G. E. HINTON, S. OSINDERO, AND Y. W. THE, **A fast learning algorithm for deep belief nets**, Neural Comput., vol. 18, pp. 1527–1554, 2006.

[111] WANG, B.; DAI, L.; MIR, T. ; WANG, Z., **Joint User Activity and Data Detection Based on Structured Compressive Sensing for NOMA**, IEEE Communications Letters, vol. 20, no. 7, pp. 1473–1476, 2016.

[112] PARKER, J. T.; SCHNITER, P. ; CEVHER, V., **Bilinear Generalized Approximate Message Passing—Part I: Derivation**, IEEE Transactions on Signal Processing, vol. 62, no. 22, pp. 5839–5853, 2014.

[113] SALAM, T.; REHMAN, W. U. ; TAO, X., **Data Aggregation in Massive Machine Type Communication: Challenges and Solutions**, IEEE Access, vol. 7, pp. 41921–41946, 2019.

[114] DE LAMARE, R. C.; SAMPAIO-NETO, R., **Adaptive reduced-rank processing based on joint and iterative interpolation, decimation, and filtering**, IEEE Transactions on Signal Processing, vol. 57, no. 7, pp. 2503–2514, 2009.

[115] BRADLEY, P. S., **Feature selection via concave minimization and support vector machines**, In: PROC. 13TH ICML, pp. 82–90, 1998.

[116] UCHOA, A. G. D.; HEALY, C. T. ; DE LAMARE, R. C., **Iterative Detection and Decoding Algorithms for MIMO Systems in Block-Fading Channels Using LDPC Codes**, IEEE Transactions on Vehicular Technology, vol. 65, no. 4, pp. 2735–2741, 2016.

[117] WANG, X.; POOR, H. V., **Iterative (turbo) soft interference cancellation and decoding for coded CDMA**, IEEE Transactions on Communications, vol. 47, no. 7, pp. 1046–1061, 1999.

[118] LIU, L.; LARSSON, E. G.; YU, W.; POPOVSKI, P.; STEFANOVIC, C. ; CARVALHO, E. D., **Sparse Signal Processing for Grant-Free Massive Connectivity: A Future Paradigm for Random Access Protocols in the Internet of Things**, IEEE Signal Processing Magazine, vol. 35, no. 5, pp. 88–99, 2018.

[119] SKELLAM, J. G. A., **A probability distribution derived from the binomial distribution by regarding the probability of success as variable between the sets of trials**, Journal of Royal Statistical Society, vol. Series B, 1948.

[120] 3GPP, **Study on RAN Improvements for Machine-type Communications; (Release 10**, Technical Report TR 37.868 1, 3rd Generation Partnership Project (3GPP), 2014.

[121] DE CARVALHO, E.; BJÖRNSON, E.; SØRENSEN, J. H.; LARSSON, E. G. ; POPOVSKI, P., **Random Pilot and Data Access in Massive MIMO for Machine-Type Communications**, IEEE Transactions on Wireless Communications, vol. 16, no. 12, pp. 7703–7717, 2017.

[122] TSE, D.; VISWANATH, P., *Fundamentals of Wireless Communications*, Cambridge University Press, Cambridge, 1st edition, 2005.

[123] LOYKA, S.; GAGNON, F., **Performance analysis of the V-BLAST algorithm: an analytical approach**, IEEE Transactions on Wireless Communications, vol. 3, no. 4, pp. 1326–1337, 2004.

[124] DE LAMARE, R. C., **Adaptive and Iterative Multi-Branch MMSE Decision Feedback Detection Algorithms for Multi-Antenna Systems**, IEEE Transactions on Wireless Communications, vol. 12, no. 10, pp. 5294–5308, 2013.

[125] ZHENG, L.; TSE, D. N. C., **Diversity and multiplexing: a fundamental tradeoff in multiple-antenna channels**, IEEE Transactions on Information Theory, vol. 49, no. 5, pp. 1073–1096, 2003.

[126] ZHANG, H.; DAI, H. ; HUGHES, B. L., **Analysis on the diversity-multiplexing tradeoff for ordered MIMO SIC receivers**, IEEE Transactions on Communications, vol. 57, no. 1, pp. 125–133, 2009.

[127] VARANASI, M. K., **Decision feedback multiuser detection: a systematic approach**, IEEE Transactions on Information Theory, vol. 45, no. 1, pp. 219–240, 1999.

[128] RONTOGIANNIS, A. A.; KEKATOS, V. ; BERBERIDIS, K., **A square-root adaptive V-BLAST algorithm for fast time-varying MIMO**

**channels**, IEEE Signal Processing Letters, vol. 13, no. 5, pp. 265–268, 2006.

[129] FANTASTIC-5G, *Preliminary Results for Multi-Service Support in Link Solution Adaptation*, document 3.1, 2016.

[130] FANTASTIC-5G, *Final Report on the Holistic Link Solution Adaptation*, document 3.2, 2016.

[131] WUNDER, G.; JUNG, P.; KASPARICK, M.; WILD, T.; SCHAICH, F.; CHEN, Y.; BRINK, S. T.; GASPAR, I.; MICHAILOW, N.; FESTAG, A.; MENDES, L.; CASSIAU, N.; KTENAS, D.; DRYJANSKI, M.; PIETRZYK, S.; EGED, B.; VAGO, P. ; WIEDMANN, F., **5gnow: non-orthogonal, asynchronous waveforms for future mobile applications**, IEEE Communications Magazine, vol. 52, no. 2, pp. 97–105, 2014.

[132] DAI, L.; WANG, B.; YUAN, Y.; HAN, S.; CHIH-LIN, I. ; WANG, Z., **Non-orthogonal multiple access for 5g: solutions, challenges, opportunities, and future research trends**, IEEE Communications Magazine, vol. 53, no. 9, pp. 74–81, 2015.

[133] LU, L.; LI, G. Y.; SWINDLEHURST, A. L.; ASHIKHMIN, A. ; ZHANG, R., **An overview of massive mimo: Benefits and challenges**, IEEE Journal of Selected Topics in Signal Processing, vol. 8, no. 5, pp. 742–758, 2014.

[134] DING, J.; CHOI, J., **Triangular Non-Orthogonal Random Access in mMIMO Systems**, IEEE Transactions on Communications, vol. 68, no. 11, pp. 6918–6931, 2020.

[135] ZHU, W.; TAO, M.; YUAN, X. ; GUAN, Y., **Asynchronous massive connectivity with deep-learned approximate message passing**, In: ICC 2020 - 2020 IEEE INTERNATIONAL CONFERENCE ON COMMUNICATIONS (ICC), pp. 1–6, 2020.

[136] KIM, S.; KIM, H.; NOH, H.; KIM, Y. ; HONG, D., **Novel transceiver architecture for an asynchronous grant-free idma system**, IEEE Transactions on Wireless Communications, vol. 18, no. 9, pp. 4491–4504, 2019.

[137] FU, J.; WU, G.; ZHANG, Y.; DENG, L. ; FANG, S., **Active user identification based on asynchronous sparse bayesian learning with svm**, IEEE Access, vol. 7, pp. 108116–108124, 2019.

[138] ABEBE, A. T.; KANG, C. G., **Comprehensive grant-free random access for massive low latency communication**, In: 2017 IEEE INTERNATIONAL CONFERENCE ON COMMUNICATIONS (ICC), pp. 1–6, 2017.

[139] RANGAN, S.; *ET AL.*, **Hybrid Approximate Message Passing**, IEEE Transactions on Signal Processing, vol. 65, no. 17, pp. 4577–4592, 2017.

[140] RANGAN, S., **Generalized approximate message passing for estimation with random linear mixing**, In: IEEE ISIT, St. Petersburg, Russia, 2011.

[141] 3GPP, **NR; Physical channels and modulation**, Technical Specification TS 38.211 15.3.0, 3rd Generation Partnership Project (3GPP), 2018.

[142] 3GPP, **NR; Physical channels and modulation (Release 16)**, Technical Specification TS 38.211 16.5.0, 3rd Generation Partnership Project (3GPP), 2021.

[143] MONSEES, F., *Signal Processing for Compressed Sensing Multiuser Detection*, PhD thesis, Uni. Bremen, Bremen, Germany, Nov 2017.

[144] MOREIRA, J. C.; FARRELL, P. G., *Essentials of Error-Control Coding*, John Wiley & Sons, Ltd, 2006.

[145] CASADO, A. I. V.; GRIOT, M. ; WESEL, R. D., **LDPC Decoders with Informed Dynamic Scheduling**, IEEE Transactions on Communications, vol. 58, no. 12, pp. 3470–3479, 2010.

[146] DING, J.; QU, D. ; CHOI, J., **Analysis of non-orthogonal sequences for grant-free ra with massive mimo**, IEEE Transactions on Communications, vol. 68, no. 1, pp. 150–160, 2020.

[147] CUI, Y.; XU, W.; WANG, Y.; LIN, J. ; LU, L., **Side-information aided compressed multi-user detection for up-link grant-free noma**, IEEE Transactions on Wireless Communications, vol. 19, no. 11, pp. 7720–7731, 2020.

[148] RANGAN, S., **Generalized Approximate Message Passing for Estimation with Random Linear Mixing**, Retrieved August 13, 2012, from the arXiv database., 2012.

# A
# Algorithms scheme in detail

## A.1
## Block diagram of AA-RLS-DF with IDD

## A.2
## Block diagram of AA-VGL-DF with IDD

## A.3
## Factor graph approach of the mMTC problem

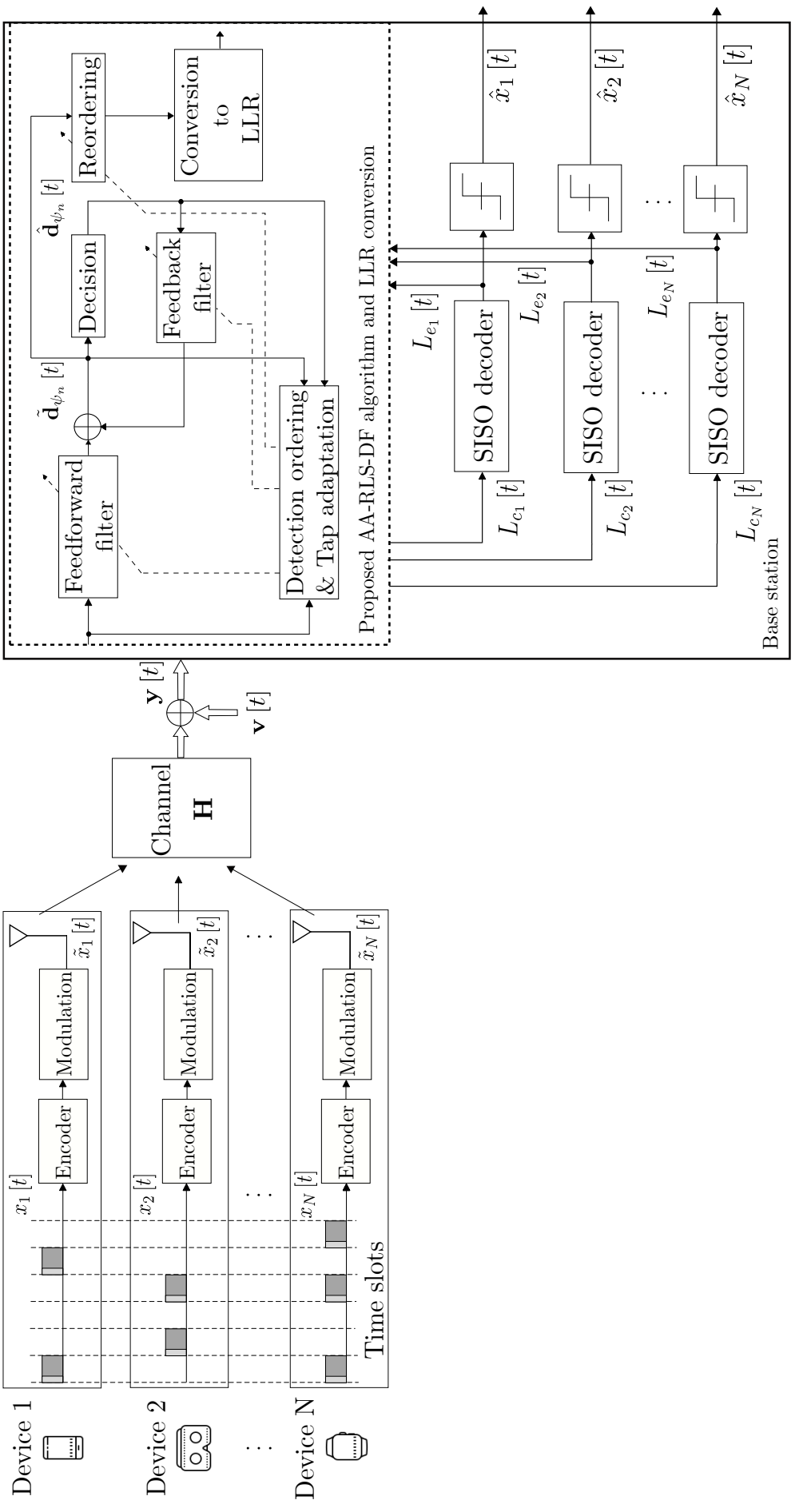


Figure A.1: Landscape format of Fig. 3.2 of the block diagram of AA-RLS-DF with IDD structure.

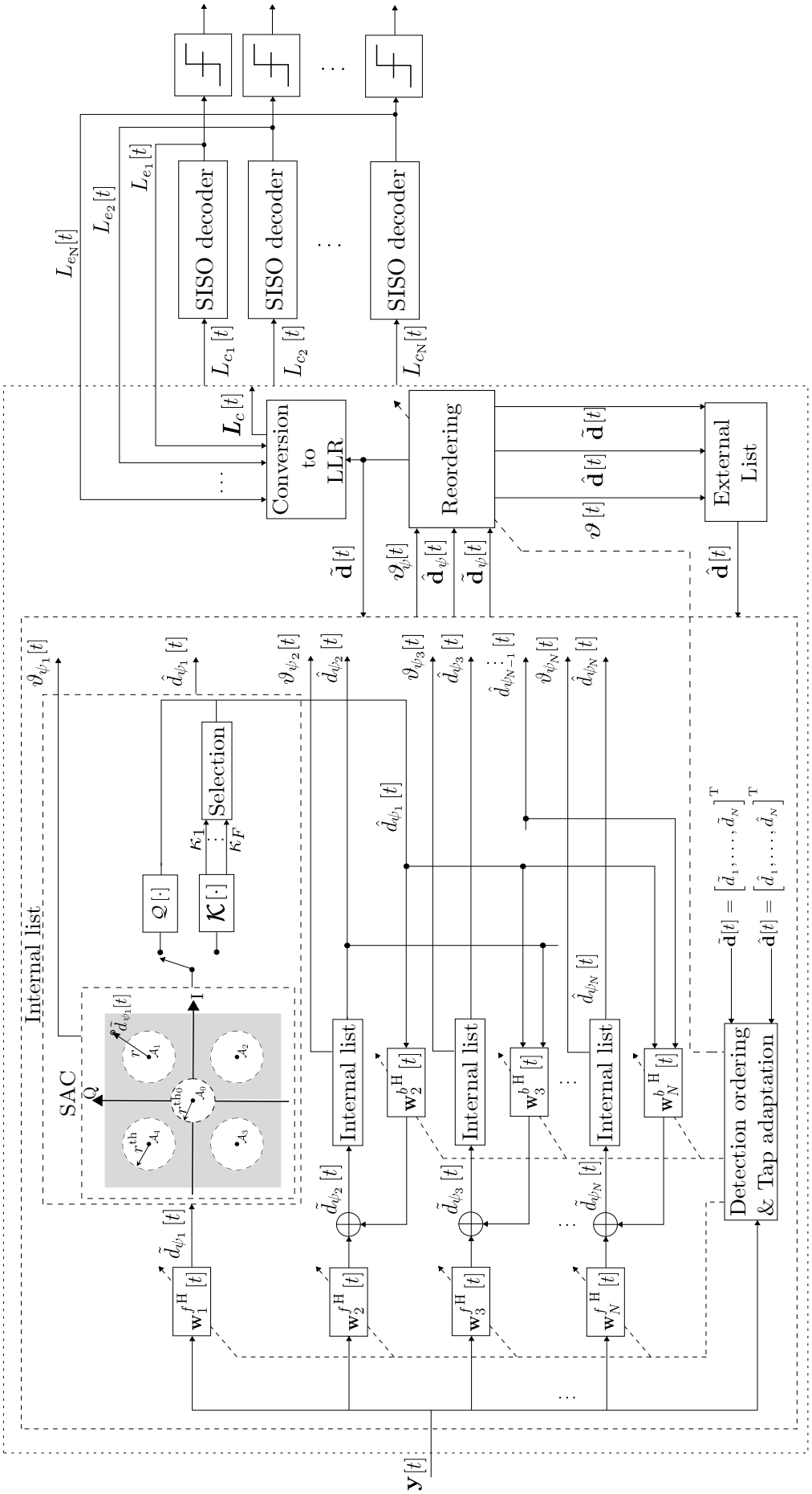


Figure A.2: Landscape format of Fig. 4.2 of the AA-VGL-DF detector and the IDD scheme. To simplify notations, just one received vector is considered in the base station.

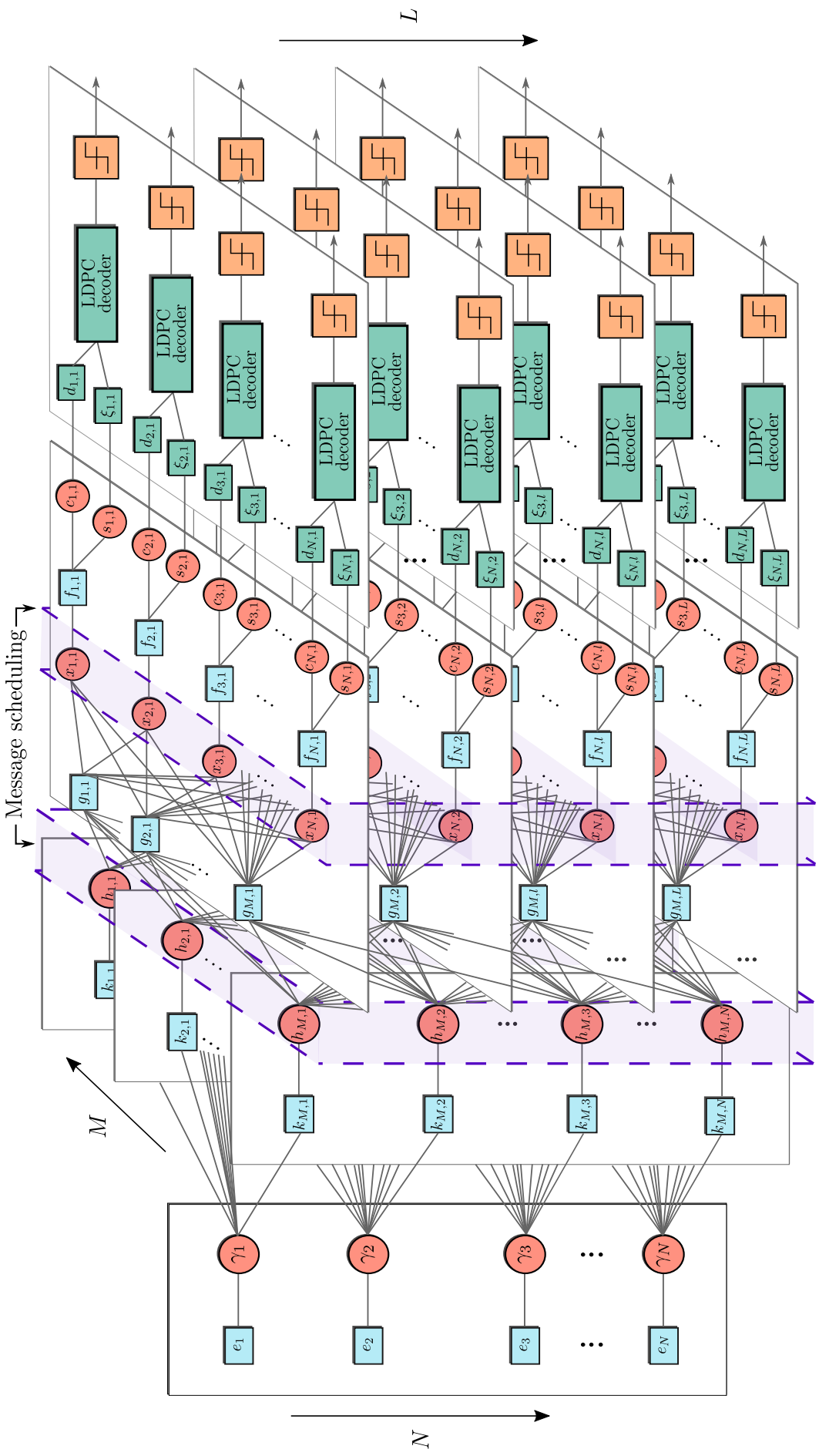


Figure A.3: Landscape format of Fig. 6.1 of the factor graph considered in Chapter 6.

# B
# Derivation of messages from factor graph approach

## B.1
## Derivation of messages from factor to variable nodes

In order to achieve the approximations as in the GAMP [140] algorithm, we convert the messages to the form of ln-pdfs with arbitrary constant offsets, that we omit for brevity.

Recalling that $z_{ml} = \sum_{k=1}^{N} h_{mk} x_{kl}$, we approximate the message in (6-9) as given by

$$
\begin{aligned}
&\Delta^{i+1}_{g_{ml}\to x_{nl}}(x_{nl}) \\
&\quad = \ln \int_{\{h_{mk}\}_{k=1}^{N},\{x_{rl}\}_{r\neq n}} p_{\mathbf{y}_{ml}|\mathbf{z}_{ml}}\left(y_{ml}\middle|\sum_{k=1}^{N} h_{mk}x_{kl}\right) \\
&\qquad \times \prod_{r\neq n} \exp\left(\Delta^{i}_{x_{rl}\to g_{ml}}(x_{rl})\right) \prod_{k=1}^{N} \exp\left(\Delta^{i}_{h_{mk}\to g_{ml}}(h_{mk})\right) \\
&\quad = \ln \int_{\{h_{mk}\}_{k=1}^{N},\{x_{rl}\}_{r\neq n}} p_{\mathbf{y}_{ml}|\mathbf{z}_{ml}}\Bigg(y_{ml}\Bigg|\underbrace{h_{mn}x_{nl} + \sum_{k\neq n}^{N} h_{mk}x_{kl}}_{z_{ml}}\Bigg) \\
&\qquad \times \prod_{r\neq n} \exp\left(\Delta^{i}_{x_{rl}\to g_{ml}}(x_{rl})\right) \prod_{k=1}^{N} \exp\left(\Delta^{i}_{h_{mk}\to g_{ml}}(h_{mk})\right)
\end{aligned}
\tag{B-1}
$$

For a large $N$, the central-limit-theorem (CLT) motivates the treatment of $\mathbf{z}_{ml}$, the random variable associated with the $z_{ml}$ identified in (B-1), conditioned on $\mathbf{x}_{nl} = x_{nl}$, as Gaussian, which is completely characterized by a (conditional) mean and variance. Defining the zero-mean r.v.s. $\tilde{\mathbf{h}}_{l,mn} \triangleq \mathbf{h}_{mn} - \hat{h}^{i}_{l,mn}$, where $\mathbf{h}_{mn} \sim (1/C)\,\Delta^{i+1}_{g_{ml}\to h_{mn}}(h_{mn})$ and $\mathbf{x}_{nl} \sim (1/C)\,\Delta^{i+1}_{g_{ml}\to x_{nl}}(x_{nl})$, we can write

$$\begin{aligned}\mathbf{z}_{ml} &= \left(\hat{h}^i_{l,mn} + \tilde{\mathbf{h}}_{l,mn}\right)\mathbf{x}_{nl} + \sum_{k\neq n}\left(\hat{h}^i_{l,mn} + \tilde{\mathbf{h}}_{l,mn}\right)\mathbf{x}_{nl} \qquad \text{(B-2)}\\ &= \left(\hat{h}^i_{l,mn} + \tilde{\mathbf{h}}_{l,mn}\right)\mathbf{x}_{nl} + \sum_{k\neq n}\left(\hat{h}^i_{l,mn} + \tilde{\mathbf{h}}_{l,mn}\right)\left(\hat{h}^i_{m,nl} + \tilde{\mathbf{x}}_{m,nl}\right)\\ &= \left(\hat{h}^i_{l,mn} + \tilde{\mathbf{h}}_{l,mn}\right)\mathbf{x}_{nl} + \sum_{k\neq n}\hat{h}^i_{l,mn}\hat{x}^i_{m,kl} + \hat{h}^i_{l,mn}\tilde{\mathbf{x}}_{m,kl} + \tilde{\mathbf{h}}_{l,mn}\hat{x}^i_{m,kl} + \tilde{\mathbf{h}}_{l,mn}\tilde{\mathbf{x}}_{m,kl}\end{aligned}$$

and after which it is straightforward to see that

$$\mathbb{E}\left\{\mathbf{z}_{ml}|\mathbf{x}_{nl} = x_{nl}\right\} = \hat{h}^i_{l,mn}x_{nl} + \hat{p}^i_{n,ml} \qquad \text{(B-3)}$$

$$\text{VAR}\left\{\mathbf{z}_{ml}|\mathbf{x}_{nl} = x_{nl}\right\} = \nu^{hi}_{l,mn}x^2_{nl} + \nu^{pi}_{n,ml} \qquad \text{(B-4)}$$

for $\hat{p}^i_{n,ml} \triangleq \sum_{k\neq n}\hat{h}^i_{l,mk}\,\hat{x}^i_{m,kl}$ and $\nu^{pi}_{n,ml} \triangleq \sum_{k\neq n}\hat{h}^{i^2}_{l,mk}\,\nu^{xi}_{m,kl} + \nu^{hi}_{l,mk}\,\hat{x}^{i^2}_{m,kl} + \nu^{hi}_{l,mk}\,\nu^{xi}_{m,kl}$. With this conditional-Gaussian approximation, (6-9) becomes

$$\begin{aligned}&\Delta^{i+1}_{g_{ml}\to x_{nl}}(x_{nl})\\ &\quad\approx \ln\int_{z_{ml}} p_{\mathbf{y}_{ml}|\mathbf{z}_{ml}}\left(y_{ml}\middle|z_{ml}\right)\mathcal{N}_c\left(z_{ml};\hat{h}^i_{l,mn}\,x_{ml} + \hat{p}^i_{n,ml}, \nu^{hi}_{l,mn}\,x^2_{nl} + \nu^{pi}_{n,ml}\right)\\ &\quad= H_{ml}\left(\hat{h}^i_{l,mn}\,x_{nl} + \hat{p}^i_{n,ml}, \nu^{hi}_{l,mn}x^2_{nl} + \nu^{pi}_{n,ml}; y_{ml}\right) \qquad \text{(B-5)}\end{aligned}$$

in terms of the function

$$H_{ml}\left(\hat{q}, \nu^q; y\right) \triangleq \ln\int_z p_{\mathbf{y}_{ml}|\mathbf{z}_{ml}}\left(y|z\right)\mathcal{N}_c\left(z;\hat{q},\nu^q\right). \qquad \text{(B-6)}$$

Unlike the original message in (6-9), the approximation (B-5) requires only a single integration. Still, additional simplifications are possible. First, notice that $\hat{p}^i_{n,ml}$ and $\nu^{pi}_{n,ml}$ differ from the corresponding n-invariant quantities

$$\hat{p}^i_{ml} \triangleq \sum_{k=1}^{N}\hat{h}^i_{l,mk}\,\hat{x}^i_{m,kl} \qquad \text{(B-7)}$$

$$\nu^{pi}_{ml} \triangleq \sum_{k=1}^{N}\hat{h}^i_{l,mk}\,\nu^{xi}_{m,kl} + \nu^{hi}_{l,mk}\,\hat{x}^{i^2}_{m,kl} + \nu^{hi}_{l,mk}\,\nu^{xi}_{m,kl} \qquad \text{(B-8)}$$

by one term. In this sequel, we will assume that $\hat{p}^i_{ml}$ and $\nu^{pi}_{ml}$ are $O(1)$ since these quantities can be recognized as the mean and variance, respectively, of an estimate of $\mathbf{z}_{ml}$, which is $O(1)$. Writing the $H_{ml}$ term in (B-5) using (B-7)

and (B-8),

$$
\begin{aligned}
&H_{ml}\left(\hat{h}^{i}_{l,mn}\, x_{nl} + \hat{p}^{i}_{n,ml},\, \nu^{hi}_{l,mn}\, x^{2}_{nl} + \nu^{pi}_{n,ml}; y_{ml}\right) \\
&\quad = H_{ml}\left(\hat{h}^{i}_{l,mn}\left(x_{nl} - \hat{x}^{i}_{m,nl}\right) + \hat{p}^{i}_{n,ml},\, \nu^{hi}_{l,mn}\left(x^{2}_{nl} - \hat{x}^{i^2}_{nl}\right)\right. \\
&\qquad\qquad \left. -\hat{h}^{i^2}_{l,mn}\,\nu^{xi}_{m,nl} - \nu^{hi}_{l,mn}\,\nu^{xi}_{m,nl} + \nu^{pi}_{ml}; y_{ml}\right) \\
&\quad = H_{ml}\left(\hat{h}^{i}_{l,mn}\left(x_{nl} - \hat{x}^{i}_{m,nl}\right) + \hat{p}^{i}_{n,ml} + O\left(1/N\right),\right. \\
&\qquad\qquad \left. \nu^{hi}_{l,mn}\left(x^{2}_{nl} - \hat{x}^{i^2}_{nl}\right) + \nu^{pi}_{n,ml} + O\left(1/N\right); y_{ml}\right) \qquad \text{(B-9)}
\end{aligned}
$$

where in (B-9) we used the facts that $\hat{h}^{i}_{l,mn}\left(x_{nl} - \hat{x}^{i}_{m,nl}\right)$ and $\nu^{hi}_{l,mn}\left(x^{2}_{nl} - \hat{x}^{i^2}_{nl}\right) - \hat{x}^{i^2}_{l,mn}\nu^{xi}_{m,nl} - \nu^{hi}_{l,mn}\nu^{xi}_{m,nl}$ are both $O(1/N)$.

Rewriting (B-5) using a Taylor series expansion in $x_{nl}$ about the point $\hat{x}^{i}_{nl}$, we get

$$
\begin{aligned}
&\Delta^{i+1}_{g_{ml}\to x_{nl}}\left(x_{nl}\right) \qquad \text{(B-10)} \\
&\quad \approx H_{ml}\left(\hat{p}^{i}_{ml} + O\left(1/N\right), \nu^{pi}_{ml} + O\left(1/N\right); y_{ml}\right) + \hat{h}^{i}_{l,mn}\left(x_{nl} - \hat{x}^{i}_{nl}\right) \\
&\qquad \times H'_{ml}\left(\hat{p}^{i}_{ml} + O\left(1/N\right), \nu^{pi}_{ml} + O\left(1/N\right); y_{ml}\right) + 2\,\nu^{hi}_{l,mn}\,\hat{x}^{i}_{nl}\left(x_{nl} - \hat{x}^{i}_{nl}\right) \\
&\qquad \times \mathring{H}_{ml}\left(\hat{p}^{i}_{ml} + O\left(1/N\right), \nu^{pi}_{ml} + O\left(1/N\right); y_{ml}\right) + \nu^{hi}_{l,mn}\left(x_{nl} - \hat{x}^{i}_{nl}\right)^{2} \\
&\qquad \times \mathring{H}_{ml}\left(\hat{p}^{i}_{ml} + O\left(1/N\right), \nu^{pi}_{ml} + O\left(1/N\right); y_{ml}\right) + \left(1/2\right)\hat{h}^{i^2}_{l,mn}\left(x_{nl} - \hat{x}^{i}_{nl}\right)^{2} \\
&\qquad \times H''_{ml}\left(\hat{p}^{i}_{ml} + O\left(1/N\right), \nu^{pi}_{ml} + O\left(1/N\right); y_{ml}\right) + O\left(1/N^{3/2}\right),
\end{aligned}
$$

where $H'_{ml}$ and $H''_{ml}$ are the first two derivatives of $H_{ml}$ w.r.t. its first argument and $\mathring{H}_{ml}$ is the first derivative w.r.t. its second argument. Considering the large-system unit, we can neglect the terms of their scaling dependence on $N$. In this way, we can approximate (B-10) by dropping terms that vanish, relative to the second-to-last in (B-10), as $N \to \infty$. Since this second-to-last term is $O(1/N)$ due to the scaling of $\hat{h}^{i^2}_{l,mn}$, $\hat{p}^{i}_{ml}$ and $\nu^{pi}_{ml}$, we drop terms that are of order $O(1/N^{3/2})$, such as the last term. We also replace $\nu^{hi}_{l,mn}$ with $\nu^{hi}_{ml}$, and $\hat{h}^{i^2}_{l,mn}$ with $\hat{h}^{i^2}_{mn}$, since in both cases the difference is $O(1/N^{3/2})$. Finally, we drop the $O(1/N)$ terms inside the $H_{ml}$ derivatives, which can be justified by taking a Taylor series expansion of these with respect to the $O(1/N)$ perturbations and

verifying that the higher-order terms in this latter expansion are $O(1/N^{3/2})$. All of these approximations are analogous to those made in previous AMP observations [34, 148]. Applying these approximations to (B-10) and dropping $x_{nl}$ invariant terms, we obtain

$$\begin{aligned}
&\Delta^{i+1}_{g_{ml}\to x_{nl}}(x_{nl}) \\
&\quad\approx H_{ml}\left(\hat{p}^i_{ml},\nu^{pi}_{ml};y_{ml}\right)+\hat{h}^i_{l,mn}\left(x_{nl}-\hat{x}^i_{nl}\right)H'_{ml}\left(\hat{p}^i_{ml},\nu^{pi}_{ml};y_{ml}\right) \\
&\qquad+2\,\nu^{hi}_{l,mn}\,\hat{x}^i_{nl}\left(x_{nl}-\hat{x}^i_{nl}\right)\mathring{H}_{ml}\left(\hat{p}^i_{ml},\nu^{pi}_{ml};y_{ml}\right) \\
&\qquad+\nu^{hi}_{l,mn}\left(x_{nl}-\hat{x}^i_{nl}\right)^2\mathring{H}_{ml}\left(\hat{p}^i_{ml},\nu^{pi}_{ml};y_{ml}\right) \\
&\qquad+(1/2)\,\hat{x}^{i^2}_{l,mn}\left(x_{nl}-\hat{x}^i_{nl}\right)^2H''_{ml}\left(\hat{p}^i_{ml},\nu^{pi}_{ml};y_{ml}\right).
\end{aligned} \tag{B-11}$$

Knowing that

$$\mathring{H}_{ml}(\hat{p}^i_{ml},\nu^{pi}_{ml};y_{ml}) \;=\; (1/2)\left[\left(H'_{ml}\left(\hat{p}^i_{ml},\nu^{pi}_{ml};y_{ml}\right)\right)^2+H''_{ml}\left(\hat{p}^i_{ml},\nu^{pi}_{ml};y_{ml}\right)\right], \tag{B-12}$$

we have

$$\begin{aligned}
&\Delta^{i+1}_{g_{ml}\to x_{nl}}(x_{nl}) \\
&\quad\approx\hat{h}^i_{l,mn}\left(x_{nl}-\hat{x}^i_{nl}\right)H'\left(\hat{p}^i_{ml},\nu^{pi}_{ml};y_{ml}\right)+\nu^{hi}_{l,mn}\left(x_{nl}-\hat{x}^i_{nl}\right)^2 \\
&\qquad\times(1/2)\left[{H'}^2_{ml}\left(\hat{p}^i_{ml},\nu^{pi}_{ml};y_{ml}\right)+H''_{ml}\left(\hat{p}^i_{ml},\nu^{pi}_{ml};y_{ml}\right)\right]+2\,\nu^{hi}_{l,mn}\,\hat{x}^i_{nl}\left(x_{nl}-\hat{x}^i_{nl}\right) \\
&\qquad\times(1/2)\left[{H'}^2_{ml}\left(\hat{p}^i_{ml},\nu^{pi}_{ml};y_{ml}\right)+H''_{ml}\left(\hat{p}^i_{ml},\nu^{pi}_{ml};y_{ml}\right)\right] \\
&\qquad+(1/2)\,\hat{h}^{i^2}_{l,mn}\left(x_{nl}-\hat{x}^i_{nl}\right)^2H''_{ml}\left(\hat{p}^i_{ml},\nu^{pi}_{ml};y_{ml}\right)
\end{aligned} \tag{B-13}$$

Computing the functions $H'_{ml}(\hat{p}^i_{ml},\nu^{pi}_{ml};y_{ml})$ and $H''_{ml}(\hat{p}^i_{ml},\nu^{pi}_{ml};y_{ml})$, we

have

$$
\begin{aligned}
&H'(\hat{p}_{ml}^{i}, \nu_{ml}^{pi}; y_{ml}) \\
&= \frac{\partial}{\partial \hat{p}_{ml}^{i}} \ln \int p_{\mathbf{y}_{ml}|\mathbf{z}_{ml}}\,(y_{ml}|z_{ml}) \left(\frac{1}{\sqrt{2\pi\nu_{ml}^{pi}}}\right) \exp\left(-\frac{1}{2\nu_{ml}^{pi}}\left(z_{ml}-\hat{p}_{ml}^{i}\right)^{2}\right) dz_{ml} \\
&= \frac{\partial}{\partial \hat{p}_{ml}^{i}} \ln \int p_{\mathbf{y}_{ml}|\mathbf{z}_{ml}}\,(y_{ml}|z_{ml}) \left(\frac{1}{\sqrt{2\pi\nu_{ml}^{pi}}}\right) \\
&\qquad\qquad \times \exp\left(\frac{z_{ml}\,\hat{p}_{ml}^{i}}{\nu_{ml}^{pi}} - \frac{z_{ml}^{2}}{2\nu_{ml}^{pi}}\right) \exp\left(\frac{-\hat{p}_{ml}^{i^2}}{2\nu_{ml}^{pi}}\right) dz_{ml} \\
&= \frac{\partial}{\partial \hat{p}_{ml}^{i}} \Bigg\{ \ln\left(\exp\left(-\frac{\hat{p}_{ml}^{i^2}}{2\nu_{ml}^{pi}}\right)\right) + \ln\left(\frac{z_{ml}}{\sqrt{2\pi\nu_{ml}^{pi}}}\right) \\
&\qquad\qquad + \ln \int \exp\left(\ln p_{\mathbf{y}_{ml}|\mathbf{z}_{ml}}\,(y_{ml}|z_{ml}) - \frac{z_{ml}^{2}}{2\nu_{ml}^{pi}} + \frac{z_{ml}\,\hat{p}_{ml}^{i}}{\nu_{ml}^{pi}}\right) dz_{ml} \Bigg\} \\
&= -\frac{\hat{p}_{ml}^{i}}{\nu_{ml}^{pi}} + \frac{\partial}{\partial \hat{p}_{ml}^{i}} \ln \int \exp\left(\ln p_{\mathbf{y}_{ml}|\mathbf{z}_{ml}}\,(y_{ml}|z_{ml}) - \frac{z_{ml}^{2}}{2\nu_{ml}^{pi}} + \frac{z_{ml}\,\hat{p}_{ml}^{i}}{\nu_{ml}^{pi}}\right) dz_{ml}.
\end{aligned}
\tag{B-14}
$$

Defining $u \triangleq z_{ml}/\nu_{ml}^{pi}$ and choosing an appropriate function $\phi(\cdot)$, we have $p_{\mathbf{u}|\mathbf{p}}\,(u|\hat{p}_{ml}^{i}) \triangleq Z(\hat{p}_{ml}^{i})^{-1} \exp\left(\phi(u) + \hat{p}_{ml}^{i} u\right)$ with $Z(\hat{p}_{ml}^{i}) \triangleq \int \exp\left(\phi(u) + \hat{p}_{ml}^{i} u\right) du$, then

$$
H'(\hat{p}_{ml}^{i}, \nu_{ml}^{pi}; y_{ml}) = -\frac{\hat{p}_{ml}^{i}}{\nu_{ml}^{pi}} + \frac{\partial}{\partial \hat{p}_{ml}^{i}} \ln \int \exp\left(\phi(u) + u\,\hat{p}_{ml}^{i}\right) \nu_{ml}^{pi}\, du. \tag{B-15}
$$

Since the mean and variance are $\frac{\partial}{\partial \hat{p}_{ml}^{i}} \ln Z(\hat{p}_{ml}^{i}) = \mathbb{E}\{\mathbf{u}|\mathbf{p} = \hat{p}_{ml}^{i}\}$ and $\frac{\partial^2}{\partial \hat{p}_{ml}^{i^2}} \ln Z(\hat{p}_{ml}^{i}) = \textsc{var}\{\mathbf{u}|\mathbf{p} = \hat{p}_{ml}^{i}\}$, we have

$$
\begin{aligned}
&H'(\hat{p}^i_{ml}, \nu^{pi}_{ml}; y_{ml}) \\
&\quad = -\frac{\hat{p}^i_{ml}}{\nu^{pi}_{ml}} + \int u \, \frac{\exp\left(\phi(u) + u\,\hat{p}^i_{ml}\right)}{Z(\hat{p}^i_{ml})} \, \nu^{pi}_{ml} \, du \\
&\quad = -\frac{\hat{p}^i_{ml}}{\nu^{pi}_{ml}} + \int \frac{z_{ml}}{\hat{p}^i_{ml}} \, \frac{\exp\left(\ln p_{\mathbf{y}_{ml}|\mathbf{z}_{ml}}\left(y_{ml}|z_{ml}\right) - \frac{z^2_{ml}}{2\nu^{pi}_{ml}} + \frac{z_{ml}\,\hat{p}^i_{ml}}{\nu^{pi}_{ml}}\right)}{Z(\hat{p}^i_{ml})} \, dz_{ml} \\
&\quad = -\frac{\hat{p}^i_{ml}}{\nu^{pi}_{ml}} + \frac{1}{\hat{p}^i_{ml}} \int z_{ml} \, \underbrace{\frac{p_{\mathbf{y}_{ml}|\mathbf{z}_{ml}}\left(y_{ml}|z_{ml}\right) \mathcal{N}_c\left(z_{ml};\, \hat{p}^i_{ml}, \nu^{pi}_{ml}\right)}{\int p_{\mathbf{y}_{ml}|\mathbf{z}_{ml}}\left(y_{ml}|z\right) \mathcal{N}_c\left(z;\, \hat{p}^i_{ml}, \nu^{pi}_{ml}\right) dz}}_{p_{\mathbf{z}_{ml}|\mathbf{p}_{ml}}\left(z_{ml}|\hat{p}^i_{ml};\nu^{pi}_{ml}\right)} \, dz_{ml}.
\end{aligned}
\tag{B-16}
$$

Similarly, the second derivative is given by

$$
\begin{aligned}
&-H''(\hat{p}^i_{ml}, \nu^{pi}_{ml}; y_{ml}) \\
&\quad = \frac{\partial}{\partial \hat{p}^i_{ml}} \left\{ \frac{\hat{p}^i_{ml}}{\nu^{pi}_{ml}} - \frac{\partial}{\partial \hat{p}^i_{ml}} \ln Z\left(\hat{p}^i_{ml}\right) \right\} = \frac{1}{\nu^{pi}_{ml}} - \textsc{var}\{\mathbf{u}|\mathbf{p} = \hat{p}^i_{ml}\} \\
&\quad = \frac{1}{\nu^{pi}_{ml}} - \int \left(u - \mathbb{E}\left\{\mathbf{u}|\mathbf{p} = \hat{p}^i_{ml}\right\}\right) \frac{2\,\exp\left(\phi(u) + u\,\hat{p}^i_{ml}\right)}{Z(\hat{p}^i_{ml})} \, du \\
&\quad = \frac{1}{\nu^{pi}_{ml}} - \frac{1}{\hat{p}^{i2}_{ml}} \int \left(z_{ml} - \hat{z}_{ml}\right)^2 \frac{p_{\mathbf{y}_{ml}|\mathbf{z}_{ml}}\left(y_{ml}|z_{ml}\right) \mathcal{N}_c\left(z_{ml};\, \hat{p}^i_{ml}, \nu^{pi}_{ml}\right)}{\int p_{\mathbf{y}_{ml}|\mathbf{z}_{ml}}\left(y_{ml}|z\right) \mathcal{N}_c\left(z;\, \hat{p}^i_{ml}, \nu^{pi}_{ml}\right) dz} \, dz_{ml},
\end{aligned}
\tag{B-17}
$$

where $\hat{z}$ is computed in (6-15). Now, we can go back to the message in (B-13). Defining $\hat{s}^i_{ml}$ and $\nu^{si}_{ml}$ that are given by

$$
\hat{s}^i_{ml} \triangleq H'_{ml}(\hat{p}^i_{ml}, \nu^{pi}_{ml}; y_{ml}) \tag{B-18}
$$

$$
\nu^{si}_{ml} \triangleq -H''_{ml}(\hat{p}^i_{ml}, \nu^{pi}_{ml}; y_{ml}), \tag{B-19}
$$

we can substitute (B-18) and (B-19) in (B-13),

$$
\begin{aligned}
&\Delta^{i+1}_{g_{ml}\to x_{nl}}\left(x_{nl}\right) \\
&\quad \approx \hat{h}^i_{l,mn}\left(x_{nl} - \hat{x}^i_{nl}\right)\hat{s}^i_{ml} + \nu^{hi}_{mn}\left(x_{nl} - \hat{x}^i_{nl}\right)^2 (1/2)\left[\hat{s}^i_{ml} + \nu^{hi}_{mn}\right] \\
&\qquad + 2\,\nu^{hi}_{mn}\,\hat{x}^i_{nl}\left(x_{nl} - \hat{x}^i_{nl}\right)(1/2)\left[\hat{s}^{i2}_{ml} + \nu^{hi}_{mn}\right] - (1/2)\,\hat{h}^{i2}_{l,mn}\left(x_{nl} - \hat{x}^i_{nl}\right)^2 \nu^{si}_{ml}.
\end{aligned}
\tag{B-20}
$$

Replacing $\nu_{l,mn}^{hi}$ by $\nu_{mn}^{hi}$ and $\hat{h}_{l,mn}^{i^2}$ by $\hat{h}_{mn}^{i^2}$, as stated before, we obtain

$$\begin{aligned}
&\Delta_{g_{ml}\to x_{nl}}^{i+1}(x_{nl}) \qquad \text{(B-21)}\\
&\quad\approx \hat{h}_{l,mn}^{i}\left(x_{nl}-\hat{x}_{nl}^{i}\right)\hat{s}_{ml}^{i}+\nu_{mn}^{hi}\left(x_{nl}-\hat{x}_{nl}^{i}\right)^{2}(1/2)\left[\hat{s}_{ml}^{i}+\nu_{ml}^{si}\right]\\
&\qquad+\nu_{mn}^{hi}\,\hat{x}_{nl}^{i}\left(x_{nl}-\hat{x}_{nl}^{i}\right)\left[\hat{s}_{mn}^{i^2}+\nu_{ml}^{si}\right]-(1/2)\,\hat{h}_{l,mn}^{i^2}\left(x_{nl}-\hat{x}_{nl}^{i}\right)^{2}\nu_{ml}^{si}\\
&\quad\approx\left[\hat{s}_{ml}^{i}\,\hat{h}_{l,mn}^{i}+\nu_{ml}^{si}\,\hat{h}_{mn}^{i^2}\,\hat{x}_{nl}^{i}\right]x_{nl}-(1/2)\left[\nu_{ml}^{si}\,\hat{h}_{mn}^{i^2}-\nu_{mn}^{hi}\left(\hat{s}_{mn}^{i^2}-\nu_{ml}^{si}\right)\right]x_{nl}^{2}.
\end{aligned}$$

In fact, $p_{\mathbf{z}_{ml}|\mathbf{p}_{ml}}(z_{ml}|\cdot)$ in (B-16) is the $i$-th iteration approximation of the algorithm to the true marginal posterior $p_{\mathbf{z}_{ml}|\mathbf{Y}}(\cdot|\mathbf{Y})$. We note that $p_{\mathbf{z}_{ml}|\mathbf{p}_{ml}}(z_{ml}|\cdot)$ can also be interpreted as the exact posterior pdf for $\mathbf{z}_{ml}$ given the likelihood $p_{\mathbf{y}_{ml}|\mathbf{z}_{ml}}(y_{ml}|\cdot)$ from the beginning and the prior $\mathbf{z}_{ml}\sim\mathcal{N}_c(\hat{p}_{ml}^{i},\nu_{ml}^{pi})$ that is implicitly assumed by $i$-th iteration of the algorithm.

Since $\mathbf{Z}^{\mathrm{T}}=\mathbf{X}^{\mathrm{T}}\mathbf{H}^{\mathrm{T}}$, the derivation of the approximation of $\Delta_{g_{ml}\to h_{nm}}^{i+1}(h_{nm})$ follows the same idea before, thus,

$$\begin{aligned}
&\Delta_{g_{ml}\to h_{nm}}^{i+1}(h_{nm}) \qquad \text{(B-22)}\\
&\quad\approx\left[\hat{s}_{ml}^{i}\,\hat{x}_{m,nl}^{i}+\nu_{ml}^{si}\,\hat{x}_{nl}^{i^2}\,\hat{h}_{mn}^{i}\right]h_{mn}-(1/2)\left[\nu_{ml}^{si}\,\hat{x}_{nl}^{i^2}-\nu_{mn}^{xi}\left(\hat{s}_{ml}^{i^2}-\nu_{ml}^{si}\right)\right]h_{nl}^{2}.
\end{aligned}$$

## B.2
## Derivation of means and variances of interest from variable to factor nodes messages

We show the approximation of the messages from variable nodes to factor nodes. Recalling (6-10), converting the messages to the form of log-pdf and

substituting (B-22), we obtain

$$\begin{aligned}
&\Delta^{i+1}_{h_{mn}\to g_{ml}}\left(h_{mn}\right) \\
&\quad\approx \Delta_{k_{mn}\to h_{mn}(h_{mn})}\prod_{p\neq l}\Delta^{i}_{g_{mp}\to h_{mn}}\left(h_{mn}\right) \\
&\quad= \ln\left(p_{\mathbf{h}_{mn}|\boldsymbol{\gamma}_n}\left(h_{mn}|\gamma_n\right)p_{\boldsymbol{\gamma}_n}\left(h_{mn}|\gamma_n\right)\right)+\sum_{p\neq l}\Delta^{i}_{g_{mp}\to h_{mn}}\left(h_{mn}\right) \\
&\quad= \ln\left(p_{\mathbf{h}_{mn}|\boldsymbol{\gamma}_n}\left(h_{mn}|\gamma_n\right)p_{\boldsymbol{\gamma}_n}\left(h_{mn}|\gamma_n\right)\right) \qquad \text{(B-23)} \\
&\qquad+\sum_{p\neq l}\left[\hat{s}^{i}_{ml}\,\hat{x}^{i}_{m,nl}+\nu^{si}_{ml}\,\hat{x}^{i^2}_{nl}\,\hat{h}^{i}_{mn}\right]h_{mn}-(1/2)\left[\nu^{si}_{ml}\,\hat{x}^{i^2}_{nl}-\nu^{xi}_{mn}\,\left(\hat{s}^{i^2}_{ml}-\nu^{si}_{ml}\right)\right]h^2_{nl}
\end{aligned}$$

Since in our system model $x$ depends only on $n$ and $l$ and $h$ only on $m$ and $n$, we ignore the components of $x$ that mathematically depends on $m$ and the ones of $h$ that depends on $l$, following the same idea of [140] and ignoring the terms $< O(1/N)$. This approximation on (B-23) leads to

$$\begin{aligned}
&\Delta^{i+1}_{h_{mn}\to g_{ml}}\left(h_{mn}\right) \qquad \text{(B-24)} \\
&\quad\approx \ln\left(p_{\mathbf{h}_{mn}|\boldsymbol{\gamma}_n}\left(h_{mn}|\gamma_n\right)p_{\boldsymbol{\gamma}_n}\left(\gamma_n\right)\right)-\frac{\left(h_{mn}-\hat{q}^{i}_{mn}\right)^2}{2\,\nu^{qi}_{mn}} \\
&\quad= \ln\left(p_{\mathbf{h}_{mn}|\boldsymbol{\gamma}_n}\left(h_{mn}|\gamma_n\right)p_{\boldsymbol{\gamma}_n}\left(\gamma_n\right)\mathcal{N}_c\left(h_{mn};\hat{q}^{i}_{mn},\nu^{qi}_{mn}\right)\right),
\end{aligned}$$

for

$$\nu^{qi}_{mn}\approx\left(\sum_{l=1}^{L}\hat{x}^{i^2}_{nl}\nu^{si}_{ml}\right)^{-1} \qquad \text{(B-25)}$$

$$\hat{q}^{i}_{mn}\approx\hat{h}^{i}_{mn}\left(1-\nu^{qi}_{mn}\sum_{l=1}^{L}\nu^{xi}_{nl}\,\nu^{si}_{ml}\right)+\nu^{qi}_{mn}\sum_{l=1}^{L}\hat{x}^{i*}_{nl}\,\hat{s}^{i}_{ml}. \qquad \text{(B-26)}$$

Therefore, the corresponding means of interest are then further approximated as

$$\hat{h}^{i+1}_{mn}\triangleq\underbrace{\frac{\int_h h\,p_{\mathbf{h}_{mn}|\boldsymbol{\gamma}_n}\left(h|\gamma\right)p_{\boldsymbol{\gamma}_n}\left(\gamma\right)\mathcal{N}_c\left(h;\hat{q},\nu^q\right)}{\int_h p_{\mathbf{h}_{mn}|\boldsymbol{\gamma}_n}\left(h|\gamma\right)p_{\boldsymbol{\gamma}_n}\left(\gamma\right)\mathcal{N}_c\left(h;\hat{q},\nu^q\right)}}_{b_{h_{mn}(\hat{q},\nu^q)}} \qquad \text{(B-27)}$$

and the variances as given by

$$\nu_{mn}^{h\,i+1} \triangleq \nu_{mn}^{hi}\, b'_{h_{mn}}\left(\hat{q}_{mn}^{i}, \nu_{mn}^{qi}\right) \tag{B-28}$$

where $b'_{h_{mn}}$ is the first derivative of $b_{h_{mn}}$ in (B-27). Similarly, following the same steps and using 6-6), $\Delta_{x_{nl}\to g_{ml}}^{i+1}(x_{nl})$, the means and variances of interest for the problem are given by

$$\begin{aligned}
&\Delta_{x_{nl}\to g_{ml}}^{i+1}(x_{nl}) \\
&\quad \approx \ln\left(p_{\mathbf{x}_{nl}}\,\mathcal{N}_c\left(x_{nl}; \hat{r}_{nl}^{i}, \nu_{nl}^{ri}\right)\right) \\
&\quad = \ln\left(p_{\mathbf{x}_{P_{nl}}}(x_{nl}) \sum_{s_{nl}} \sum_{c_{nl}} p_{\mathbf{x}_{D_{nl}}}(x_{nl}, c_{nl}, s_{nl})\,\mathcal{N}_c\left(x_{nl}; \hat{r}_{nl}^{i}, \nu_{nl}^{ri}\right)\right),
\end{aligned} \tag{B-29}$$

where the means and variances are

$$\nu_{nl}^{ri} \approx \left(\sum_{m=1}^{M} \hat{h}_{mn}^{i^2} \nu_{ml}^{si}\right)^{-1} \tag{B-30}$$

$$\hat{r}_{nl}^{i} \approx \hat{x}_{nl}^{i}\left(1 - \nu_{nl}^{ri} \sum_{m=1}^{M} \nu_{mn}^{hi}\,\nu_{ml}^{si}\right) + \nu_{nl}^{ri} \sum_{m=1}^{M} \hat{h}_{mn}^{i*}\,\hat{s}_{ml}^{i} \tag{B-31}$$

with the mean and the variance to compute the data estimates given by

$$\hat{x}_{mn}^{i+1} \triangleq \frac{\int_x x\, p_{\mathbf{x}_{P_{nl}}}(x) \sum_s \sum_c p_{\mathbf{x}_{D_{nl}}}(x, c, s)\,\mathcal{N}_c(x; \hat{r}, \nu^r)}{\int_x p_{\mathbf{x}_{P_{nl}}}(x) \sum_s \sum_c p_{\mathbf{x}_{D_{nl}}}(x, c, s)\,\mathcal{N}_c(x; \hat{r}, \nu^r)} \tag{B-32}$$

$$\nu_{nl}^{x\,i+1} \triangleq \nu_{nl}^{xi}\, b'_{x_{nl}}\left(\hat{x}_{nl}^{i}, \nu_{nl}^{ri}\right) \tag{B-33}$$

as well as for the channel, the left part of (B-32) is $b_{x_{nl}}(\hat{r}, \nu^r)$ and $b'_{x_{nl}}$ in (B-33) is its first derivative.